

THESIS

ESTIMATION OF UNGAUGED RAINFALL FROM  
MEASURED STREAMFLOW FOR THE SIMULATION  
OF A COLORADO FRONT RANGE FLOOD EVENT

Submitted by

Matthew Garcia, M.S.

Department of Civil Engineering

In partial fulfillment of the requirements

for the Degree of Master of Science

Colorado State University

Fort Collins, Colorado

Fall 2003

Copyright ©2003 by Matthew Garcia

All rights reserved.

COLORADO STATE UNIVERSITY

October 24, 2003

WE HEREBY RECOMMEND THAT THE THESIS PREPARED UNDER OUR SUPERVISION BY MATTHEW GARCIA ENTITLED "ESTIMATION OF UNGAUGED RAINFALL FROM MEASURED STREAMFLOW FOR THE SIMULATION OF A COLORADO FRONT RANGE FLOOD EVENT" BE ACCEPTED AS FULFILLING IN PART REQUIREMENTS FOR THE DEGREE OF MASTER OF SCIENCE.

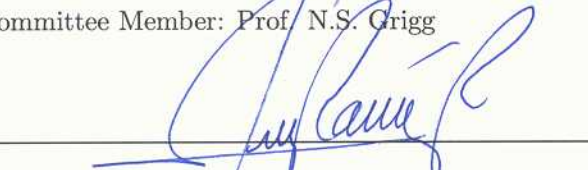
Committee on Graduate Work



Outside Committee Member: Prof. R.H. Johnson



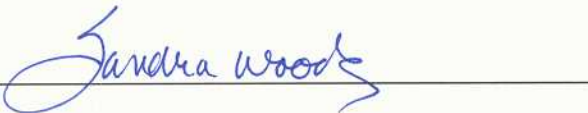
Committee Member: Prof. N.S. Grigg



Committee Member: Prof. J.A. Ramirez



Advisor: Prof. L.A. Roesner



Department Head: Prof. S.L. Woods

## ABSTRACT OF THESIS

### ESTIMATION OF UNGAUGED RAINFALL FROM MEASURED STREAMFLOW FOR THE SIMULATION OF A COLORADO FRONT RANGE FLOOD EVENT

A major flood event in the vicinity of Colorado Springs, Colorado, during April 28–May 2, 1999, was examined from a hydrometeorological perspective. The storms that contributed to this event combined with moist antecedent conditions in the affected regions to produce flash-flood conditions in several locations along the Colorado Front Range. An analysis of the spatial and temporal distributions of rainfall during the event was enhanced with a hydrological modeling study of rainfall–runoff processes in the Monument and Fountain Creek watersheds. Available rainfall records were supplemented with postulated rainfall data in areas of sparse gauge coverage in an effort to simulate, as accurately as possible, observed USGS stream discharge records at several locations.

A distributed hydrological model of the Monument and upper Fountain Creek watersheds was constructed from existing and derived data for the purposes of storm event simulation. Watershed sub-basins and stream segments were represented using the EPA Storm Water Management Model (SWMM v4.4h). Hourly and daily rainfall data for the period of the storm event, obtained from the National Weather Service and additional city-operated gauges, were employed as input to the rainfall–runoff model. Established methods of data interpolation were applied for the disaggregation of daily rainfall totals at several gauges in order to obtain hourly rainfall records. It is shown here that these existing rainfall records were insufficient for the accurate simulation of stream discharge records at several USGS gauge locations along Monument and Fountain Creeks and their tributaries.

Definition of the spatial distribution of rainfall was enhanced by the determination of supplemental rainfall data for the affected watersheds. This technique led to marked improvements in the accuracy of stream discharge simulations. This technique sought more accurate representation of the spatial variability of rainfall by the specification of “virtual” gauges, at which rainfall records were interpolated from data at existing gauges in the surrounding area. It is shown here that traditional methods of spatial interpolation, within the limits of climatological and event-based rainfall totals, were insufficient for the simulation of observed discharge records. Greater rainfall totals at these supplemental gauges, found by an iterative solution method, produced a high degree of accuracy in the simulation of available stream discharge records at USGS gauge locations.

The largest accumulations of rainfall for orographically-forced storm events in this region are often found to occur at higher elevations along the Front Range. The observed and supplemental hourly rainfall records at several locations in the modeled watersheds are consistent with this observation and demonstrate the occurrence and motion of convective cells within the storm event. These findings suggest a hybrid storm morphology composed of strong convection and locally heavy rainfall embedded within a larger forced stratiform system with characteristically moderate rainfall rates.

This work is intended to provide guidance in dealing with the complexity of hydrologic prediction in ungauged regions and to demonstrate a method by which missing or unobserved rainfall and stream discharge records may be determined. The findings presented here are also intended to enhance our understanding of a flash-flood-producing storm archetype that is seemingly common along the Colorado Front Range.

Matthew Garcia  
Department of Civil Engineering  
Colorado State University  
Fort Collins, Colorado 80523-1372  
Fall 2003

## ACKNOWLEDGEMENTS

I would most like to thank my wife Zoe Ann, for her patience and support during “all these years” of school, and our daughter Sharon, who gave me an excuse to play on the floor again. I also thank my family and friends, including fellow students in the Harold H. Short Lab, for their support and encouragement. Particular thanks go to Jorge Gironà for his assistance during construction of the hydrologic model. Finally, many thanks to Professor Larry Roesner for his continued support of my work and to my graduate committee members, Professors Neil Grigg and Jorge Ramírez (Department of Civil Engineering) and Richard Johnson (Department of Atmospheric Science), for their service.

This thesis is derived in part from contract work by the author during 2002–2003 for the City Attorney for Colorado Springs, Colorado, regarding El Paso County District Court case no. 01CV1290. I am grateful to Allen Leonard (Senior Litigation Specialist) and Shane White (Senior Litigation Attorney) for documents, information and support provided during the project period. Additional support, including computer equipment, was provided by the Harold H. Short Foundation, the Department of Civil Engineering, and Engineering Network Services at Colorado State University.

This thesis was produced with  $\text{\LaTeX}2\epsilon$  using `thesis.cls`, provided by J.P. Weiss (CU–Boulder) and modified by M. Parker (CSU) and the present author, and  $\text{\MiKTeX}$  v2.3.

“...and they knew nothing about what would happen until the flood came and took them all away.”

Matthew 24:39 (NIV)

# CONTENTS

<b>1 Introduction</b>	<b>1</b>
1.1 Region and Watershed Description . . . . .	2
1.2 Data Sources . . . . .	6
1.3 Plan of Thesis . . . . .	7
<b>2 Analysis of the April 28–May 2, 1999, Event</b>	<b>11</b>
2.1 Rainfall Climatology at Colorado Springs, Colorado . . . . .	11
2.1.1 Historical Rainfall . . . . .	11
2.1.2 Intensity–Duration–Frequency (IDF) Analysis . . . . .	12
2.1.3 Influence of the El Niño/Southern Oscillation (ENSO) cycle . . . . .	15
2.1.4 Regional and Local Influences of the Rocky Mountains . . . . .	16
2.1.5 Climatological Precipitation Patterns . . . . .	18
2.2 Relevant Principles of Synoptic Meteorological Analysis . . . . .	21
2.3 The April 28-May 2, 1999, Event . . . . .	25
2.3.1 Antecedent Conditions . . . . .	25
2.3.2 Eta Model and Surface Analyses . . . . .	27
2.3.3 Surface Observations . . . . .	33
2.3.4 Analysis and Comparison with Historical Events . . . . .	38
2.4 Discussion . . . . .	42
<b>3 Event Modeling</b>	<b>44</b>
3.1 Modeling Methodology . . . . .	44
3.1.1 Aggregated Models . . . . .	45
3.1.2 Statistical Methods . . . . .	46
3.1.3 Distributed Physical Hydrology . . . . .	47
3.2 Watershed Model . . . . .	51
3.2.1 RUNOFF Formulation and Procedure . . . . .	51
3.2.2 RUNOFF Data Requirements . . . . .	55
3.2.3 Sub-basin Parameters . . . . .	56
3.2.4 Routing Network Formulation . . . . .	65
3.2.5 Routing Network Diagnostics . . . . .	78
3.2.6 Application of Recorded Rainfall Data . . . . .	83
3.2.7 Formulation of Supplemental Rainfall Records . . . . .	88
3.2.8 Derivation of Mean Areal Precipitation (MAP) . . . . .	103
3.3 Hydrograph Evaluation Methods . . . . .	104
3.3.1 Preserved Hydrograph Statistics . . . . .	104
3.3.2 Relative Error Measures . . . . .	106
3.3.3 Absolute Error Measures . . . . .	107

<b>4 Simulation of the April 28–May 2, 1999, Event</b>	<b>109</b>
4.1 H $x$ Simulations . . . . .	110
4.1.1 H1 Experiment . . . . .	110
4.1.2 H2 Experiment . . . . .	111
4.1.3 H3 Experiment . . . . .	115
4.2 HD $x$ Simulations . . . . .	115
4.2.1 HD1 Experiment . . . . .	117
4.2.2 HD2 Experiment . . . . .	117
4.3 Application of Derived Supplemental Rainfall Records . . . . .	120
4.3.1 HDSa Simulation . . . . .	121
4.3.2 HDSb Simulation . . . . .	124
4.3.3 HDSc Simulation . . . . .	124
4.4 HDSd Simulations . . . . .	126
4.4.1 Hyetograph 15 (USGS gauge 07104000) . . . . .	128
4.4.2 Hyetograph 16 (USGS gauge 07105490) . . . . .	131
4.4.3 Hyetograph 17 (USGS gauge 07105500) . . . . .	136
4.4.4 Hyetograph 18 (USGS gauge 07105530) . . . . .	138
4.4.5 Overall Results . . . . .	141
4.4.6 Reconstructed Stream Gauge Records . . . . .	148
4.4.7 Results for the Templeton Gap/Shooks Run Region . . . . .	148
<b>5 Summary and Conclusions</b>	<b>155</b>
5.1 Summary Discussion . . . . .	155
5.2 Conclusions . . . . .	160
5.3 Future Work . . . . .	163
<b>References</b>	<b>165</b>
<b>Appendix</b>	
<b>A Rainfall Records</b>	<b>171</b>
<b>B USGS Discharge Records</b>	<b>184</b>
<b>C SWMM RUNOFF Simulation Files</b>	<b>196</b>
<b>D U.S.–Metric Conversion Factors</b>	<b>197</b>

## FIGURES

1.1	Counties and major urban areas along the Colorado Front Range. . . . .	3
2.1	Annual total rainfall at Colorado Springs, Colorado, for 1948–2002. . . . .	12
2.2	IDF curves for Colorado Springs, Colorado. . . . .	14
2.3	Reference map of the Monument and Fountain Creek watersheds. . . . .	20
2.4	Map of April + May (1961–1990) PRISM-derived total precipitation. . . . .	22
2.5	Schematic diagram of meteorological features. . . . .	23
2.6	Total liquid-equivalent precipitation during April 1–27, 1999. . . . .	26
2.7	Surface analysis for 00 UTC on April 27 (5 pm LST on April 26), 1999. . . . .	29
2.8	Eta model analysis for 12 UTC (5 am LST) on April 27, 1999. . . . .	29
2.9	Surface analysis for 12 UTC (5 am LST) on April 28, 1999. . . . .	30
2.10a	Surface analysis for 00 UTC on April 29 (5 pm LST on April 28), 1999. . . . .	31
2.10b	Eta model analysis for 00 UTC on April 29 (5 pm LST on April 28), 1999. . . . .	31
2.11a	Surface analysis for 00 UTC on April 30 (5 pm LST on April 29), 1999. . . . .	32
2.11b	Eta model analysis for 00 UTC on April 30 (5 pm LST on April 29), 1999. . . . .	32
2.12a	Surface analysis for 12 UTC (5 am LST) on April 30, 1999. . . . .	34
2.12b	Eta model analysis for 12 UTC (5 am LST) on April 30, 1999. . . . .	34
2.13a	Surface analysis for 12 UTC (5 am LST) on May 1, 1999. . . . .	35
2.13b	Eta model analysis for 12 UTC (5 am LST) on May 1, 1999. . . . .	35
2.14	Surface analysis for 00 UTC on May 2 (5 pm LST on May 1), 1999. . . . .	36
2.15	Eta model analysis for 12 UTC (5 am LST) on May 2, 1999. . . . .	36
2.16	Rainfall at hourly gauges during April 28–May 2, 1999. . . . .	37
2.17	Recorded total rainfall during April 28–May 2, 1999. . . . .	39
2.18	Figure 2 from Doswell (1980). . . . .	40
2.19	Figure 1 from Maddox et al. (1980). . . . .	41
3.1	Locations of USGS stream gauges in the modeled watersheds. . . . .	50
3.2	Schematic diagram of SWMM RUNOFF sub-basin representation. . . . .	52
3.3	Schematic diagram of non-linear reservoir model for sub-basin areas. . . . .	53
3.4a	Stream discharge (red) and base flow (green) at USGS gauge 07104000. . . . .	63
3.4b	Stream discharge (red) and base flow (green) at USGS gauge 07105490. . . . .	63
3.4c	Stream discharge (red) and base flow (green) at USGS gauge 07105500. . . . .	64
3.4d	Stream discharge (red) and base flow (green) at USGS gauge 07105530. . . . .	64
3.5	Overall plan of constructed watershed network. . . . .	66
3.6a	Northwest area of constructed watershed network. . . . .	67
3.6b	Northeast area of constructed watershed network. . . . .	68
3.6c	East area of constructed watershed network. . . . .	69
3.6d	Central area of constructed watershed network. . . . .	70
3.6e	West area of constructed watershed network. . . . .	71

3.6f	Southwest area of constructed watershed network. . . . .	72
3.6g	Southeast area of constructed watershed network. . . . .	73
3.7a	Plot of network channel distance from and elevation above outlet. . . . .	74
3.7b	Plot of network channel distance from outlet vs. total drainage area. . . . .	75
3.7c	Plot of network channel elevation above outlet vs. total drainage area. . . . .	75
3.8	Example application of modified Strahler scheme to network channels. . . . .	77
3.9	Determination of Horton bifurcation ratio by fitted linear function. . . . .	81
3.10	Determination of Horton length ratio by fitted linear function. . . . .	81
3.11	Determination of Horton area ratio by fitted linear function. . . . .	82
3.12a	Thiessen polygons for existing hourly rainfall gauges (nos. 1–6). . . . .	84
3.12b	Thiessen polygons for all existing rainfall gauges (nos. 1–14). . . . .	85
3.13	Disaggregated hourly rainfall at daily gauges for April 28–May 2, 1999. . . . .	90
3.14	Thiessen polygons for all existing and supplemental rainfall gauges. . . . .	92
3.15	Rainfall at supplemental gauges derived from existing hourly gauges. . . . .	94
3.16	Rainfall at supplemental gauges derived from all existing gauges. . . . .	96
3.17	Rainfall gauge elevation and normal April + May total precipitation. . . . .	98
3.18	Rainfall at supplemental gauges derived by characteristics method. . . . .	100
4.1	Results for simulation H1 at USGS stream gauge locations. . . . .	112
4.2	Results for simulation H2 at USGS stream gauge locations. . . . .	114
4.3	Results for simulation H3 at USGS stream gauge locations. . . . .	116
4.4	Results for simulation HD1 at USGS stream gauge locations. . . . .	118
4.5	Results for simulation HD2 at USGS stream gauge locations. . . . .	119
4.6	Results for simulation HDSa at USGS stream gauge locations. . . . .	122
4.7	Results for simulation HDSb at USGS stream gauge locations. . . . .	125
4.8	Results for simulation HDSc at USGS stream gauge locations. . . . .	127
4.9	Modeled sub-basins affected by hyetograph 15. . . . .	130
4.10a	Results of partial hydrograph simulation at USGS gauge 07104000. . . . .	132
4.10b	Results of partial model simulation at USGS gauge 07104000. . . . .	132
4.11	Modeled sub-basins affected by hyetograph 16. . . . .	134
4.12a	Results of partial hydrograph simulation at USGS gauge 07105490. . . . .	135
4.12b	Results of partial model simulation at USGS gauge 07105490. . . . .	135
4.13	Modeled sub-basins affected by hyetograph 17. . . . .	137
4.14a	Results of partial hydrograph simulation at USGS gauge 07105500. . . . .	139
4.14b	Results of partial model simulation at USGS gauge 07105500. . . . .	139
4.15	Modeled sub-basins affected by hyetograph 18. . . . .	140
4.16a	Results of partial hydrograph simulation at USGS gauge 07105530. . . . .	142
4.16b	Results of partial model simulation at USGS gauge 07105530. . . . .	142
4.17	Rainfall at supplemental gauges derived by hydrograph-fitting method. . . . .	143
4.18	Interpolated total rainfall during April 28–May 2, 1999. . . . .	144
4.19	Correlations between storm and event total rainfall and gauge elevation. . . . .	145
4.20a	Results of full model simulation at USGS gauge 07104000. . . . .	146
4.20b	Results of full model simulation at USGS gauge 07105490. . . . .	146
4.20c	Results of full model simulation at USGS gauge 07105500. . . . .	147
4.20d	Results of full model simulation at USGS gauge 07105530. . . . .	147
4.21a	Reconstructed stream gauge records for the modeled watershed. . . . .	149
4.21b	Reconstructed stream gauge records for the modeled watershed. . . . .	150
4.22a	Pre-development drainage network in the Shooks Run area. . . . .	151

4.22b	Post-development drainage network in the Shooks Run area. . . . .	152
4.23	Results of simulations at the mouth of Shooks Run. . . . .	153
5.1	Subjective analysis of rainfall totals during April 28–May 2, 1999. . . . .	159

## TABLES

1.1	Populations and growth of Metropolitan Statistical Areas (MSAs), as defined by the United States Census Bureau, and counties along the Colorado Front Range. . . . .	4
2.1	Climatological monthly mean and extreme rainfall during 1948-2000, and monthly total rainfall observations during 1999 at the Colorado Springs NWS station. . . . .	13
2.2	Names and locations of precipitation gauges in and near the Monument and Fountain Creek watersheds. . . . .	19
3.1	Names and locations of USGS stream gauges along Monument and Fountain Creeks and various tributaries. . . . .	49
3.2	Listing of SWMM RUNOFF input parameters. . . . .	56
3.3	Example calculations of sub-basin directly connected impervious area. . . .	60
3.4	Horton infiltration parameters, after UDFCD USDCM Table RO-7. . . . .	60
3.5	Summary of observed hydrograph statistics at selected USGS gauge locations. . . . .	65
3.6	Calculation of Horton bifurcation ratio for constructed channel network. . .	80
3.7	Calculation of Horton length ratio for constructed channel network. . . . .	80
3.8	Calculation of Horton area ratio for constructed channel network. . . . .	80
3.9	Daily (April 28–May 2, 1999) and event total rainfall at precipitation gauges in and near the Monument and Fountain Creek watersheds. . . . .	87
3.10	Precipitation gauge distances for disaggregation of daily total rainfall to hourly intervals. . . . .	89
3.11	Precipitation gauge weights for disaggregation of daily total rainfall to hourly intervals. . . . .	89
3.12	Gauge weights for derivation of rainfall at supplemental locations using only hourly gauges. . . . .	94
3.13	Gauge weights for derivation of rainfall at supplemental locations using all existing gauges. . . . .	95
3.14	PRISM-derived mean April + May precipitation at all gauge locations for the period 1961–1990. . . . .	97
3.15	Climate-based gauge characteristics for derivation of rainfall at supplemental locations using all existing gauges. . . . .	99
3.16	Daily (April 28–May 2, 1999) and event total rainfall at supplemental gauges as determined by various interpolation methods. . . . .	101
4.1	Summary of hydrologic model calibration results. . . . .	113
4.2	Summary of flood event hydrologic simulation results. . . . .	123
4.3	Summary of HDSd zone-based hydrologic simulation results. . . . .	133

4.4	Summary of Shooks Run development-based hydrologic simulation results. .	153
A.1	Observed hourly rainfall records at existing gauges (nos. 1–6). . . . .	171
A.2	Disaggregated hourly rainfall records at existing daily gauges (nos. 7–14). .	175
A.3	Derived hourly rainfall records for simulations HDSa and HDSb at supple- mental gauges (nos. 15–18). . . . .	178
A.4	Derived hourly rainfall records for simulations HDSc and HDSD at supple- mental gauges (nos. 15–18). . . . .	181
B.1	Discharge records for April 28–May 2, 1999, at USGS gauge 07104000. . . .	184
B.2	Discharge records for April 28–May 2, 1999, at USGS gauge 07105490. . . .	187
B.3	Discharge records for April 28–May 2, 1999, at USGS gauge 07105500. . . .	190
B.4	Discharge records for April 28–May 2, 1999, at USGS gauge 07105530. . . .	193
D.1	Factors for conversion from U.S. Customary units to Metric units. . . . .	197

## Chapter 1

### INTRODUCTION

Flash flood events are a common hazard to life and property along the Colorado Front Range. The National Weather Service (NWS) Glossary of Hydrologic Terms<sup>1</sup> specifies that a flash flood “follows within a few hours (usually less than 6 hours) of heavy or excessive rainfall.” The inherent difficulties in the forecasting and observation of heavy rainfall events in mountainous terrain only add to the problems of flash flood warning and damage mitigation. Such events may occur in this region under widely varied meteorological and hydrological conditions during the period March–November each year.

The storm and flood event examined here affected much of the Colorado Front Range during April 28–May 2, 1999. The thesis presented here encompasses a meteorological and hydrological investigation of this storm and flood event, much of which is derived from original work by the author for the City Attorney for Colorado Springs. The heaviest recorded rainfall exceeded 9.3 inches over 80 hours and was concentrated within the area of the City of Colorado Springs in El Paso County, Colorado. The greatest reported damage to property and crops, estimated in excess of \$25M, occurred along Fountain Creek downstream of the City of Colorado Springs. The evolution of this event will be discussed, and it will be demonstrated that the storms that comprised this event occurred in a meteorological environment that has been identified previously for its potential to produce heavy rainfall and flash floods in this region.

Certain aspects of the modeling methodology employed here resulted from the re-

---

<sup>1</sup> <http://www.crh.noaa.gov/hsd/hydeff.html>.

quirements of the author's work for the City Attorney for Colorado Springs. Specifically, the effects on discharge hydrographs and total flow volumes in Fountain Creek from alternative scenarios of land use within the City of Colorado Springs were determined. It will be shown that other aspects of this methodology resulted from sparse rainfall gauge coverage of the modeled watersheds. This thesis concentrates on the development and application of this latter portion of the modeling methodology, though some aspects of the effects of urbanization are explored for their contribution to the validity of the model itself.

It is intended that the methods and results presented here will contribute in several ways toward our understanding of and planning for similar Colorado Front Range storm and flood events. A technique for the determination of area-average rainfall in ungauged regions and for the reconstruction of stream discharge hydrographs at inoperable or otherwise ungauged locations is presented by way of a distributed hydrological modeling approach. The results of such an approach can assist in the diagnosis of spatial and temporal distributions of rainfall in regions of varied topography and during orographically-influenced storm events. In a more integrated sense, these methods and results may eventually contribute to efforts at forecasting of, and dissemination of public warnings for, flood and flash flood events, especially in urban areas. The potential also exists for the eventual application of these methods to the planning of municipal stormwater management systems.

## **1.1 Region and Watershed Description**

The Front Range corridor in Colorado is one of the fastest-growing urban areas in the United States. According to the U.S. Census Bureau, the four metropolitan statistical areas (MSAs) that comprise this urban corridor experienced a total population growth of nearly 30% in the 1990–2000 intercensal period (see Table 1.1). As of this writing, nearly 4,000,000 residents in eighteen counties along the Colorado Front Range (see Figure 1.1) are subject to the threat of heavy rainfall and flash flood events for nine months of the year. According to data obtained from the NWS and the National Climatic Data Center

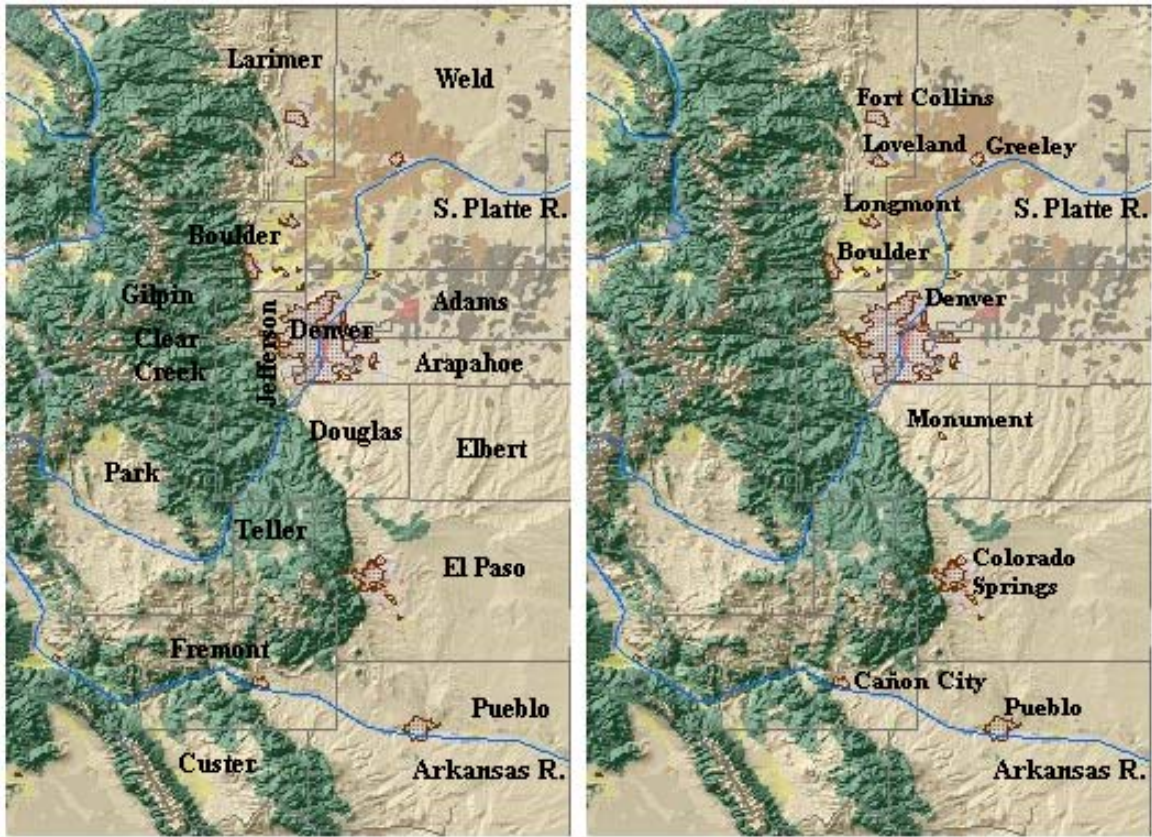


Figure 1.1: Counties (left) and major urban areas (right) along the Colorado Front Range. These maps were assembled by the author using data from the USGS Seamless Data Distribution System (<http://edcnts14.cr.usgs.gov/Website/store/index.htm>).

(NCDC), flash floods and river flooding have contributed to 12 fatalities, 11 injuries and nearly \$475M in damage to property and crops in this region during 1950–2002.

The City of Colorado Springs, Colorado, is located directly east of Pike’s Peak at the southern end of the Rampart Range, a subgroup of the Rocky Mountain Front Range, at the confluence of Monument and Fountain Creeks. Upstream of Pueblo, Colorado, the drainage basin of Fountain Creek occupies a total area of approximately 930 mi<sup>2</sup> spanning the Rocky Mountain Front Range and the Colorado Piedmont. Elevations in the basin range from the summit of Pike’s Peak at 14,110 feet MSL to the confluence of Fountain Creek with the Arkansas River in Pueblo at approximately 4,650 feet MSL. A brief description of the Fountain Creek basin can be found in U.S. Geological Survey (USGS) Water Resources

Table 1.1: Populations and growth of Metropolitan Statistical Areas (MSAs), as defined by the United States Census Bureau, and counties along the Colorado Front Range. MSA census data were obtained from <http://www.census.gov/population/www/cen2000/phc-t3.html>. County census data for 1990 were obtained from <http://govinfo.kerr.orst.edu/stateis.html>. County census data for 2000 and estimated population data for 2002 were obtained from <http://eire.census.gov/popest/data/counties.php>. \*Broomfield County was formally established on November 15, 2001, from portions of Adams, Boulder, Jefferson and Weld Counties and as such has no individual census data prior to that time. Information regarding the history of Broomfield (City and County) was obtained at <http://www.ci.broomfield.co.us/community.shtml>.

Metropolitan Statistical Area	1990 Census population	2000 Census population	1990-2000 Growth
Fort Collins–Loveland	186,136	251,494	35.11%
Denver–Boulder–Greeley	1,980,140	2,581,506	30.37%
Colorado Springs	397,014	516,929	30.20%
Pueblo	123,051	141,472	14.97%
<b>4 MSAs</b>	<b>2,686,341</b>	<b>3,491,401</b>	<b>29.97%</b>

County	1990 Census population	2000 Census population	1990-2000 Growth	2002 population (estimated)
Larimer	186,136	251,494	35.1%	264,605
Weld	131,821	180,936	37.3%	205,014
Boulder	225,339	291,288	29.3%	279,197
Broomfield*	N/A	N/A	N/A	40,823
Gilpin	3,070	4,757	55.0%	4,893
Clear Creek	7,619	9,322	22.4%	9,447
Jefferson	438,430	527,056	20.2%	531,723
Denver	467,610	554,636	18.6%	560,415
Adams	265,038	363,857	37.3%	374,099
Arapahoe	391,511	487,967	24.6%	510,136
Douglas	60,391	175,766	191.0%	211,091
Elbert	9,646	19,872	106.0%	21,959
Park	7,174	14,523	102.4%	15,993
Teller	12,468	20,555	64.9%	21,586
El Paso	397,014	516,929	30.2%	543,818
Fremont	32,273	46,145	43.0%	47,423
Custer	1,926	3,503	81.9%	3,648
Pueblo	123,051	14,1472	15.0%	146,880
<b>18 counties</b>	<b>2,760,517</b>	<b>3,610,078</b>	<b>30.8%</b>	<b>3,849,388</b>

Investigation Report No. 88-4136 and is summarized briefly here.

Monument Creek, a major tributary to Fountain Creek, is a perennial stream that flows generally eastward from its headwaters in the Rampart Range to Monument Lake, west of the Town of Monument, and then southward to its confluence with Fountain Creek in Colorado Springs. Monument Creek is actively eroding the underlying soils in most locations. Upstream of its confluence with Cottonwood Creek in the northern portion of Colorado Springs, Monument Creek is classified as a meandering pool-and-riffle stream with sand, gravel and cobble bed materials. Downstream of this confluence, within the City of Colorado Springs, Monument Creek is classified as a braided stream with primarily sand and gravel bed materials. The reader is referred to Knighton (1998) for detailed explanations of these and other stream classifications. As Monument Creek joins Fountain Creek in Colorado Springs, its contributing watershed area is more than 235 mi<sup>2</sup>.

Fountain Creek originates on the northern slopes of Pike's Peak near Woodland Park, Colorado, and flows generally southeastward through an incised canyon to Manitou Springs, Colorado, and then through a terraced alluvial plain to its confluence with Monument Creek. Upstream of Manitou Springs, Fountain Creek is classified as a meandering pool-and-riffle stream with sand, gravel, cobble and intermittent boulder bed materials. Through the alluvial terraces downstream of Manitou Springs, Fountain Creek is classified as a meandering pool-and-riffle stream with varied bed materials. As Fountain Creek joins Monument Creek in Colorado Springs, its contributing watershed area is nearly 120 mi<sup>2</sup>.

Downstream of its confluence with Monument Creek, Fountain Creek flows generally southeastward through and out of Colorado Springs toward Pueblo, Colorado. As Fountain Creek leaves Colorado Springs, its contributing watershed area is nearly 500 mi<sup>2</sup>. The character of Fountain Creek along the reach between Colorado Springs and Pueblo varies from meandering to braided configurations with similarly variable bed materials. Active bank erosion has been observed at most locations along this reach of Fountain Creek downstream of Colorado Springs.

## 1.2 Data Sources

Numerous and varied sources of data were employed for the analysis and modeling effort presented in this thesis. In addition to the references provided at the end of this work, extensive information was obtained from the following locations, agencies and organizations:

- Denver Urban Drainage and Flood Control District (UDFCD; <http://www.udfcd.org>): Urban Storm Drainage Criteria Manual (USDCM), Volume I.
- U.S. Geological Survey (USGS; <http://www.usgs.gov>): topographic maps; requested data from the National Water Information System Database.
- U.S. Department of Commerce, National Oceanic and Atmospheric Administration (NOAA), National Weather Service (NWS) and National Climatic Data Center (NCDC; <http://wlf.ncdc.noaa.gov/oa/ncdc.html>): hourly and daily rainfall data; daily surface observations.
- Unisys Weather (<http://weather.unisys.com>): satellite photographs (visible and infrared channels); Eta model analyses (4-panel charts); surface analyses.
- City Attorney for Colorado Springs, Colorado: Drainage Criteria Manual adopted by the City of Colorado Springs and El Paso County, Colorado (dated 1990/1991, amended 1994); Fountain Creek Drainage Basin Planning Study (including maps), prepared for the City of Colorado Springs, Colorado, by Muller Engineering Company, Inc. (dated 1994); Monument Creek Drainage Basin Planning Study (including maps), prepared for the City of Colorado Springs, Colorado, by CH2M HILL, Inc. (dated 1994); hourly and daily precipitation data at sites operated/maintained by the Colorado Springs Utilities Department; certified copies of NCDC hourly and daily rainfall data and daily surface observations.

- Western Regional Climate Center (<http://www.wrcc.dri.edu>): climatological monthly total rainfall data.
- University of Wyoming, College of Engineering, Department of Atmospheric Science (<http://weather.uwyo.edu>): upper-air sounding data.
- United States Weather Pages (<http://www.uswx.com>): local regular (hourly) and special weather observations.
- Spatial Climate Analysis Service (SCAS; <http://www.ocs.orst.edu/prism>): digital maps of PRISM-derived monthly (April and May, 1961–1990) mean liquid-equivalent precipitation totals for Colorado at a spatial resolution of 2.5 arc-minutes ( $\sim 3.6$  km).
- U.S. Department of Agriculture, Soil Conservation Service (SCS) and Natural Resources Conservation Service (NRCS): maps of soil types.

### 1.3 Plan of Thesis

Chapter 2 of this thesis describes the long-term rainfall climatology of the Colorado Springs region and the general meteorological environment of that region for the month preceding the storm event addressed here. The evolution and behavior of the storm and flood event that occurred in the vicinity of Colorado Springs during April 28–May 2, 1999, is examined using surface meteorological analyses and widely-available output from a numerical weather prediction model. The observed rainfall records from this event are also presented. This storm event is compared with other historical events along the Colorado Front Range, specifically the Big Thompson flood in 1976 and the Spring Creek (Fort Collins) flood in 1997. It is shown that the meteorological patterns surrounding this storm event conformed with those for established archetypes of flood-producing events in the western and High

Plains regions of the United States.

Chapter 3 describes the methodology and application of the modeling effort that is the focus of this thesis. General ideas surrounding the selection of a distributed, physically-based hydrological modeling approach are discussed, and details of the formulation of the selected modeling environment are presented. Specific parameters of the modeled hydrology are addressed for clarity of formulation and for ease of later discussion. A SWMM RUNOFF model of the Monument and Fountain Creek watersheds in the vicinity of Colorado Springs, Colorado, is described, and various diagnostic measures of this model are evaluated.

The method by which recorded rainfall records are applied to the modeled region is also addressed in Chapter 3. The formulation employed for the determination of missing data is presented, and the method by which daily total rainfall is disaggregated to hourly intervals is also described. Using a technique developed independently here, supplemental “virtual” rainfall gauges are established in data-sparse portions of the modeled region. The formulation of rainfall records for these supplemental gauges by various methods, including reliance on climatological monthly total rainfall data, is described as in the formulation of the NWS River Forecast System (NWSRFS).

Chapter 4 presents the results of simulations using the distributed hydrologic model and rainfall records presented in the previous chapter. Hourly rainfall records from existing hourly and daily gauges in and near the modeled watersheds are employed for the calibration of infiltration parameters throughout the modeled region in order to account for antecedent moisture conditions. Supplemental rainfall records are then employed in an effort to improve the simulation of observed USGS stream discharge records at four locations in the modeled watersheds. It is found that existing rainfall data and records derived by traditional methods at supplemental gauge locations are inadequate for the accurate simulation of these stream

discharge records.

Also described in Chapter 4 is the performance of a highly accurate simulation of observed discharge records at four USGS stream gauge locations in the modeled watersheds. The iterative process by which this accuracy was achieved is described in detail, and the resulting hydrographs are compared with their corresponding USGS discharge records by various visual and statistical methods. This technique leads to the determination of extreme rainfall totals for this storm and flood event in orographically-influenced regions of the storm area.

Chapter 5 summarizes the work presented in this thesis and lists several conclusions relevant to our understanding of the evolution and behavior of orographically-influenced storm and flood events, especially along the Colorado Front Range. Some of these conclusions arise from the utility of the supplemental rainfall data and hydrograph-fitting methods applied here. The intended applications of these methods and results are also discussed in Chapter 5, and various opportunities for extension of this work are considered.

References other than the sources of data listed above are given near the end of this thesis. Several appendices are given after the references:

- Appendix A includes the tabulated hourly rainfall data, employed in simulations using SWMM RUNOFF as described in Chapters 3 and 4, for hourly total rainfall observations at six gauges, disaggregated daily total rainfall observations at eight gauges, and derived hourly total rainfall depths for four simulation experiments using four supplemental gauges.
- Appendix B includes the original USGS National Water Information System data that were requested by the author from the Pueblo office of the USGS for four USGS stream gauge locations in the Monument and Fountain Creek watersheds.

- Appendix C contains a description of the author's archive of SWMM RUNOFF input and output files for this work that are available to researchers upon request.
- Appendix D includes a table of factors for conversion from the various U.S. customary units employed in this work to metric units as the reader desires.

## Chapter 2

### ANALYSIS OF THE APRIL 28–MAY 2, 1999, EVENT

The flash flood event that occurred on April 28–May 2, 1999, in and near the City of Colorado Springs is examined in several contexts. An analysis of climatological factors suggests the low likelihood of this event, though regional factors such as topography can become favorable on the basis of meteorological circumstance. The evolution and chronology of this event is analyzed using meteorological observations of large-scale weather patterns and local rainfall records, and supports previous observations regarding the composition and morphology of such hybrid storm events along the Colorado Front Range.

#### **2.1 Rainfall Climatology at Colorado Springs, Colorado**

##### *2.1.1 Historical Rainfall*

Annual total rainfall observed at the National Weather Service (NWS) station at Colorado Springs Municipal Airport for 1948–2002 is shown in Figure 2.1. During this period, the mean annual rainfall was 16.51 inches. A maximum of 25.21 inches was observed in 1999 and thus included the event studied here, and a minimum of 4.89 inches was measured in 2002. The monthly mean and extreme rainfall totals observed at the same location for the period 1948–2000 have been compiled by the Western Regional Climate Center and are shown in Table 2.1. The monthly total rainfall observed during April and May, 1999, are

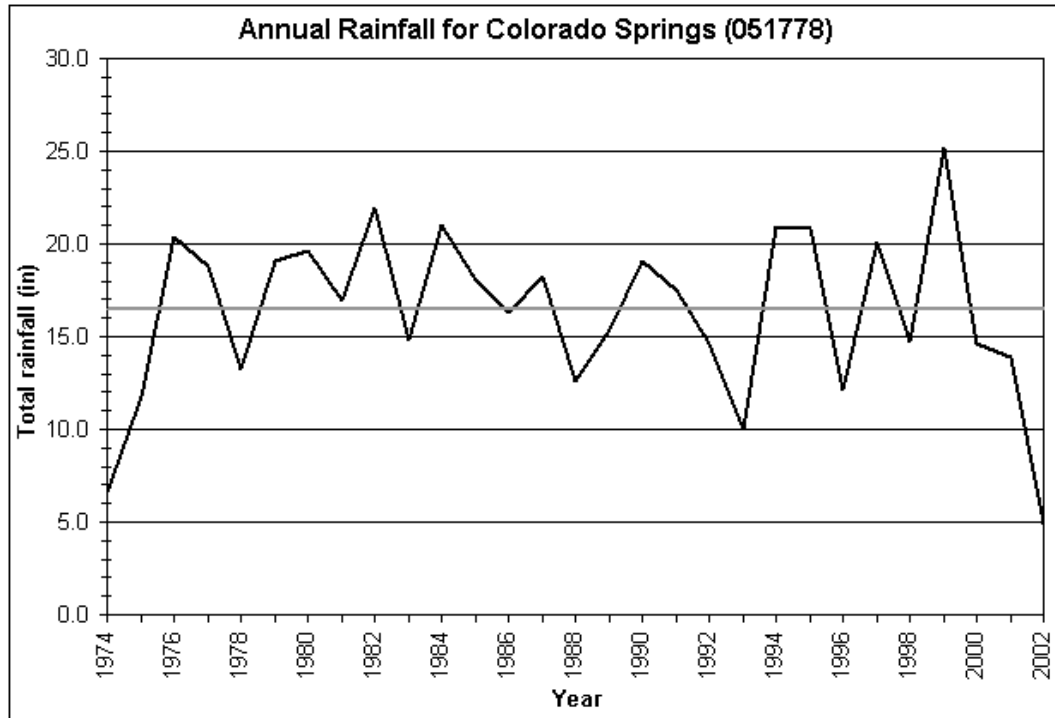


Figure 2.1: Annual total rainfall at Colorado Springs, Colorado, for 1948–2002. The mean annual rainfall during that period is shown by the gray line.

also listed there. It should be noted that the rainfall recorded on April 30, 1999, contributed 35% of the total rainfall for the entire month and that the total rainfall during April 1999 was more than 4.5 standard deviations above the climatological mean for April.

### 2.1.2 Intensity–Duration–Frequency (IDF) Analysis

A common method by which historical rainfall events are evaluated for planning purposes (e.g. stormwater management) is the intensity–duration–frequency (IDF) analysis. First, an uninterrupted record of hourly rainfall is scanned for all events of a chosen duration (e.g. 1 hour, 12 hours, etc.). Such events may contain periods of zero rainfall, in which case only those dry periods longer than a chosen duration (e.g. 6 hours) would define the end of a preceding event. For example, if one wishes to list all historical 12-hour rainfall events, it may be found that some of those events contain a 12-hour period of measured

Table 2.1: Climatological monthly mean and extreme rainfall during 1948-2000, and monthly total rainfall observations during 1999 at the Colorado Springs NWS station. Climatological data were compiled by the Western Regional Climate Center (<http://www.wrcc.dri.edu>). Liquid equivalent precipitation is indicated, for which trace amounts are excluded.

Month	Mean (1948-2000)	Standard deviation	Maximum monthly total	Maximum single day	1999 monthly total
April	1.37 in	1.34 in	7.50 in (1999)	2.63 in (4/30/1999)	7.50 in
May	2.28 in	1.44 in	5.67 in (1957)	2.23 in (5/18/1955)	3.57 in

rainfall, while others contain two short periods of measured rainfall separated by a 5-hour dry period.

Once a list of  $N$  occurrences is compiled for a particular event duration of  $H$  hours, the occurrences are ranked according to their total rainfall over the event duration found by

$$P = \sum_{h=1}^H p_h, \quad (2.1)$$

where  $p_h$  is an individual hourly rainfall total within the event. The mean hourly rainfall during the event is thus found by

$$\overline{p_h} = \frac{P}{H}. \quad (2.2)$$

The probability of exceedance can be determined for each ranked event using such expressions as

$$f_i = \frac{i - 0.4}{N + 0.2}, \quad (2.3)$$

after Cunnane (1978), where  $f_i$  is the estimated quantile (frequency) and  $i$  is the event rank in a sample ordered from largest to smallest events ( $i = 1, \dots, N$ ). The probability of exceedance  $f_i$  can then be translated to an expected recurrence interval  $T_i$  for an event of similar magnitude by

$$T_i = \frac{1}{f_i}. \quad (2.4)$$

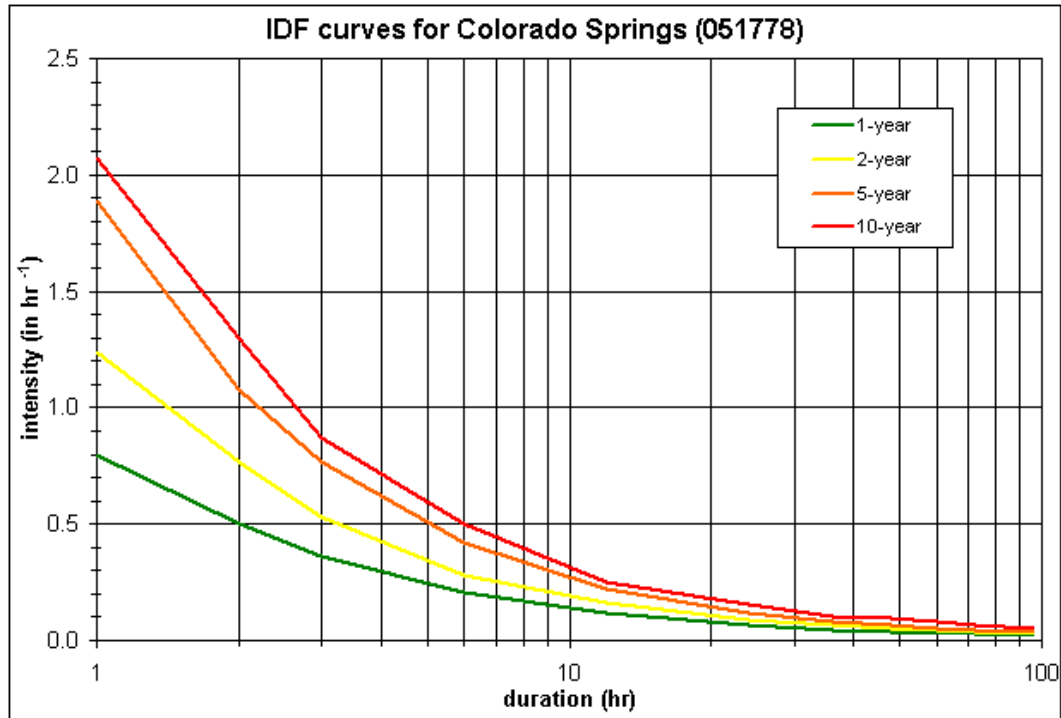


Figure 2.2: IDF curves for Colorado Springs, Colorado.

The IDF analysis shown here was performed using the RainMaster event parsing and ranking program by Mitch Heineman of Camp Dresser & McKee Inc. This analysis employed an interevent time of 6 hours and a minimum total rainfall of  $P = 0.1$  inches in the definition of events. The resulting IDF curves are shown in Figure 2.2. The reader should note that these curves are plotted on a logarithmic ordinate scale and against the mean hourly rainfall during the event of specified duration on the abscissa. Only those curves for analyzed events up to 10 years in recurrence interval are plotted here: IDF curves for events of greater recurrence interval would occur above that of the 10-year event but could not be determined on the basis of the available period of record ( $\sim 29$  years).

It was found by this analysis that the largest continuous event occurred over 54 hours beginning on April 28, 1999, with a total rainfall of 4.77 inches and a peak 1-hour rainfall of 0.57 inches. However, this event ranked no higher than 2<sup>nd</sup> in total rainfall for any of

the durations specified in the analysis (1, 2, 3, 6, 12, 24, 36, 48, 60, 72, and 96 hours), and in those cases was exceeded in total rainfall only by an event beginning on August 3, 1999. That event was also examined by the present author in previous work, though not to the level of detail presented here. With regard to the curves presented in Figure 2.2, the highest rank attained by the event beginning April 28, 1999, was 8<sup>th</sup> for  $H = 24$  hours, with  $P = 3.3$  inches and thus  $\overline{p_h} \cong 0.14$  inches. For the available period of record, these results translate to an expected return period for an event of this magnitude of approximately  $T = 8$  years.

### 2.1.3 *Influence of the El Niño/Southern Oscillation (ENSO) cycle*

The El Niño/Southern Oscillation (ENSO) cycle, observed in the eastern equatorial Pacific Ocean, produces large-scale patterns that exert a strong influence on climate and weather over the western United States during the Northern Hemisphere winter and spring seasons. Ropelewski and Halpert (1986) discussed the effects of ENSO on rainfall patterns in various regions of North America. Many studies of ENSO refer only to the warm (El Niño) period of the multi-year climate cycle and the extra-tropical effects of that warm eastern equatorial Pacific Ocean water. However, during the event examined here, cold (La Niña) conditions persisted in the Pacific Ocean and influenced the major weather patterns over central Colorado. The La Niña period of the cycle is, in general, less well understood.

According to the NOAA Climate Prediction Center, general La Niña (cold) conditions were observed from the July–August–September (JAS) period of 1998 through the April–May–June (AMJ) period of 2000. Bell et al. (1999) presented details regarding the progression of this La Niña event across the equatorial Pacific Ocean. During the January–February–March (JFM) period of 1999, immediately prior to the events examined here, a strong La Niña condition was observed. The NOAA–CIRES Climate Diagnostic Center

(<http://www.cdc.noaa.gov>) has reported that moderate-to-dry seasonal precipitation extremes would be expected in the Arkansas River basin during such episodes. According to available data, dry conditions during the March–April–May (MAM) period are several times more likely than wet conditions following a strong La Niña during the December–January–February (DJF) period.

#### 2.1.4 *Regional and Local Influences of the Rocky Mountains*

On regional and local scales, the Rocky Mountains may alter wind and weather patterns to the effect of enhanced or diminished rainfall in particular, generally predictable locations. The Rampart Range, a subgroup of the Rocky Mountain Front Range, lies immediately to the west of Colorado Springs and forms the western boundaries of the Fountain and Monument Creek watersheds. The Palmer Divide is a relatively low ridge that extends eastward from the Front Range and provides the northern boundary of the Monument Creek watershed. The interactions between passing weather systems, at all levels of the atmosphere, and these topographic features are complex. However, it may be possible to classify two primary effects of the Rocky Mountains on the initiation and evolution of weather events.

The primary mechanical influence of the Rocky Mountains is the *upward forcing of near-surface winds* (Houze 1993), which can lead to large-scale areas of clouds and sometimes to sustained rainfall on the eastern slopes of the Front Range. In the vicinity of Colorado Springs, this effect requires near-surface winds from the east/southeast that are forced upward by the Rampart Range and, to a lesser degree, by the Palmer Divide. Houze described two of the primary orographic precipitation mechanisms that were likely important during the major event examined here: (1) upslope condensation, as from the upward

forcing of moist stable air, and (2) upslope or upstream triggering of convection, as by the upward forcing of moist air to a level of convective instability. When the wind direction at higher levels is generally from the west, such a flow pattern may produce long-lived storms (e.g. Garcia 1999) as moist easterly air, forced upward from near the surface, forms cumulonimbus that are then pushed back toward the east, producing rain over densely populated areas along the Front Range.

Correlations of observed rainfall with elevation and wind direction under such circumstances have been examined by numerous authors, e.g. Spreen (1947), Oki et al. (1991), Alpert and Shafrir (1991) and Weston and Roy (1994). The reliability of these correlations is such that they have been applied to the estimation of mean areal precipitation in mountainous regions by geostatistical methods, e.g. Chua and Bras (1980, 1982) and Kyriakidis et al. (2001). On an event basis, the effects of topography on various types of surface fronts and their precipitation patterns in the vicinity of the Olympic Mountains in northwestern Washington has been studied by Parsons and Hobbs (1983). Such studies often require high-resolution observations, both spatially and temporally, for an extended period in order to obtain an accurate picture of the event morphology and resulting precipitation patterns. Such an effort would naturally lend itself to events that are more easily forecast, such as frontal passages on the Pacific coast, than Rocky Mountain Front Range upslope storm events.

The primary thermodynamical influence of the Rocky Mountains results from *solar heating of the land surface in a highly variable pattern*, which often leads to abrupt changes in wind speed and direction over short distances. Such patterns of convergent winds near the surface force air upward to form clouds and, possibly, thunderstorms. Preferential heating of peaks and ridgelines can lead to thermal triggering of convection and the devel-

opment of orographic precipitation, as described by Houze (1993). The occurrence of such thunderstorms on an almost daily basis during the summer has been found to favor specific topographically-influenced regions, such as the Rampart Range, by Karr and Wooten (1976) and Banta and Schaaf (1987). In a more regular pattern, near-surface winds may behave as drainage (gravity-driven) flows in response to nightly cooling of the ground surface. Toth and Johnson (1985) found that a cooling-induced reversal of winds along the eastern slopes of the Colorado Front Range in otherwise calm weather conditions can lead to common summer thunderstorm events at lower elevations and some distance from the highest peaks and ridgelines. However, the evolution of such mountain–valley circulations is a complex process and its diagnosis is often best performed in otherwise calm synoptic conditions, unlike those of the event discussed below.

### *2.1.5 Climatological Precipitation Patterns*

Portions of the following analyses rely on precipitation data from various locations in and near the Monument and Fountain Creek watersheds. Locations and other relevant data for these stations are listed in Table 2.2. A reference map of these locations is provided in Figure 2.4.

Gridded data sets of mean monthly and annual precipitation for the period 1961–1990 at a spatial resolution of  $\sim 3.6$  km have been produced for the entire United States by the PRISM methodology (Daly et al. 1994) and are available on-line from the Spatial Climate Analysis Service (SCAS; <http://www.ocs.orst.edu/prism/>). Contours of the long-term PRISM-derived mean precipitation in the vicinity of Colorado Springs for the months of April and May, corresponding to the specific period during which this flood event occurred, are shown in Figure 2.4. Regarding the regional climatological precipitation patterns shown

Table 2.2: Names and locations of precipitation gauges in and near the Monument and Fountain Creek watersheds. Map locations, as shown in Figure 2.4, are given in feet north and east of the confluence of Monument and Fountain Creeks in Colorado Springs, Colorado. Operating agencies are listed as the National Weather Service (NWS) and the City of Colorado Springs Utilities Department (CSU). National Weather Service “low-res” hourly gauges record precipitation in intervals of 0.1 inches (2.54 mm); NWS “high-res” hourly gauges record precipitation in intervals of 0.01 inches (0.254 mm). \*Estimated gauge elevation, based on available data.

Gauge Number	Gauge Name	Record Type	Operating Agency	Map Location		Elevation (ft ASL)
				X (ft)	Y (ft)	
1	Woodland Park 8 NNW	hourly low-res	NWS	-77250	99275	7758
2	Manitou Springs	hourly low-res	NWS	-24000	8000	6628
3	Colorado College	hourly	CSU	3000	5000	6012
4	Colorado Springs	hourly high-res	NWS	37500	-10000	6180
5	Greenland 9 SE	hourly low-res	NWS	38000	103200	7478
6	Pinello Ranch	hourly	CSU	18000	-30000	5730
7	(Town of) Monument	daily	NWS	-10000	100000	7078
8	Ruxton Park	daily	NWS	-36000	2000	9048
9	Fort Carson Butts AAF	daily	NWS	7000	-26000	5840
10	Old Farm	daily	CSU	28000	26000	6800*
11	Monument Valley Park	daily	CSU	3000	11000	6060*
12	Quail Lake	daily	CSU	7500	-14000	5940*
13	Water Operations	daily	CSU	-6000	16000	6410*
14	4-Diamond Sports Complex	daily	CSU	8000	22000	6330*
15	Monument Creek West	supplemental (hourly)	—	-20000	70000	8000*
16	Fountain Creek South	supplemental (hourly)	—	-18000	-10000	9000*
17	Fountain Creek North	supplemental (hourly)	—	-34000	16000	7800*
18	Downtown Colo. Springs	supplemental (hourly)	—	13000	7000	6080*

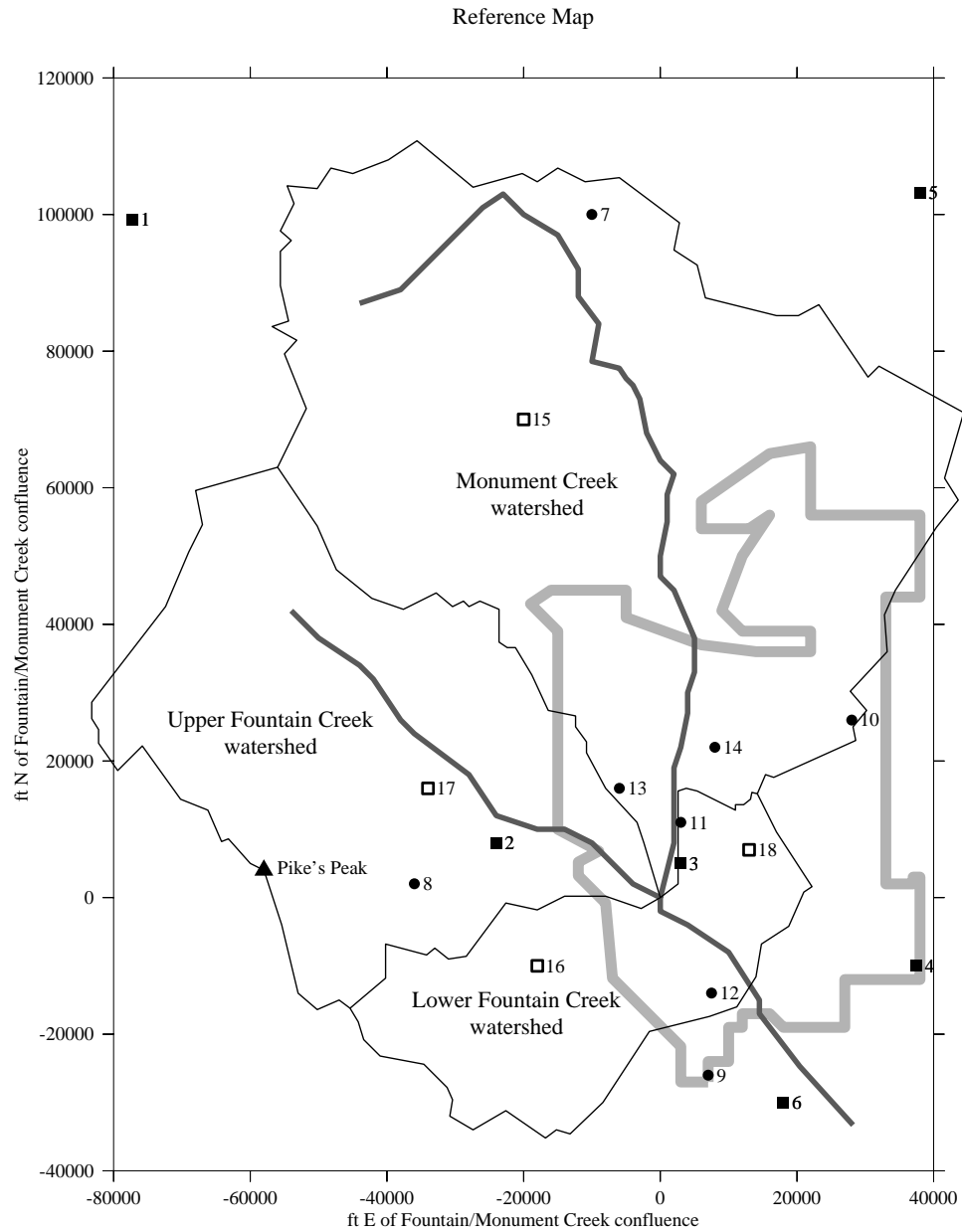


Figure 2.3: Reference map of the Monument and Fountain Creek watersheds. The approximate boundaries of the City of Colorado Springs are shown in light gray, and the location of Pike's PEak is indicated for reference. Locations for hourly (filled boxes), daily (filled circles) and supplemental (empty boxes) rainfall gauges and other relevant data are listed in Table 2.2.

there, the influences of the Rampart Range are evident in the gradient of total precipitation along a northwest–southeast axis across the City of Colorado Springs. The influences of extreme topographic variation in the southwestern part of this region, in the vicinity of Pike’s Peak, are distinguished by a concentration of climatological total precipitation exceeding 5.5 inches for the months of April and May.

The northwestern portion of the region shown in Figure 2.4 gives some indication of the local effects that may be produced at locations partially protected from upslope storms. The precipitation station located there would, in the event of an upslope storm on the eastern side of the Front Range, be shielded by the Rampart Range in an area of predominantly downslope wind patterns. A similar climatological “rain shadow” has been found on the eastern slopes of the Sierra Nevada in California by Lee (1911) and to the east of the Olympic Mountains in northwestern Washington by Mass and Ferber (1990). In a study of climatological rainfall patterns in the Great Basin (the areas of Nevada and western Utah), Houghton (1979) found the primary influences on orographic rainfall to be (1) elevation change (but not necessarily surface slope) with respect to the prevailing wind direction, (2) proximity to moisture sources (primarily the Pacific Ocean in that study), and (3) elevation of surrounding (primarily upwind) barriers. These influences can be restated in a meteorological sense as, respectively, (1) upslope forcing, (2) availability of moisture for the production of precipitation, and (3) potential for rain shadow effects.

## **2.2 Relevant Principles of Synoptic Meteorological Analysis**

In addition to local contributions from topography to storm initiation and sustained rainfall events, as discussed above, some general principles of large-scale weather patterns should be taken into consideration when reading the account presented below. For the

Climatological April + May (1961-1990) total precipitation

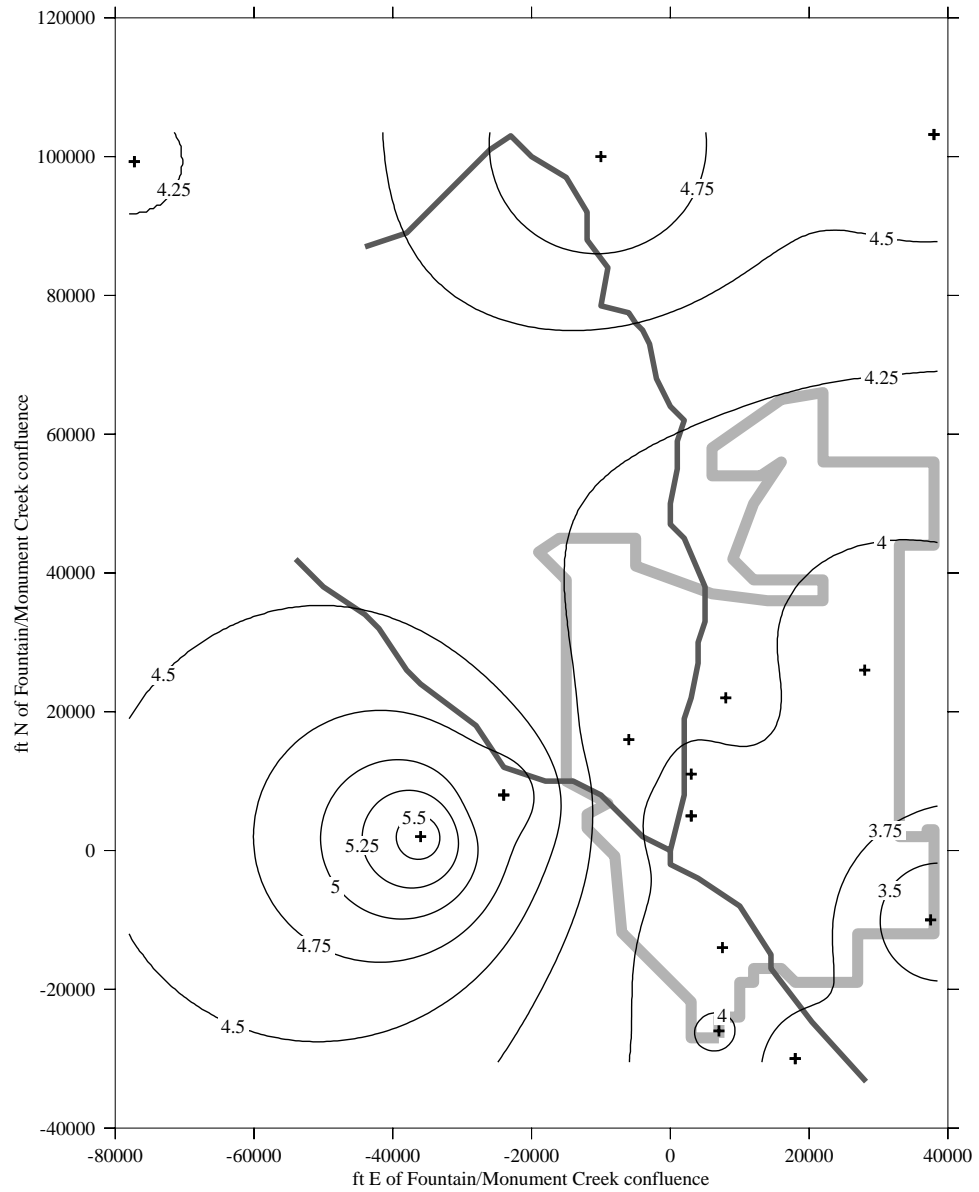


Figure 2.4: Map of April + May (1961–1990) PRISM-derived total precipitation. The approximate boundaries of the City of Colorado Springs are shown in light gray. Precipitation totals are contoured in inches.

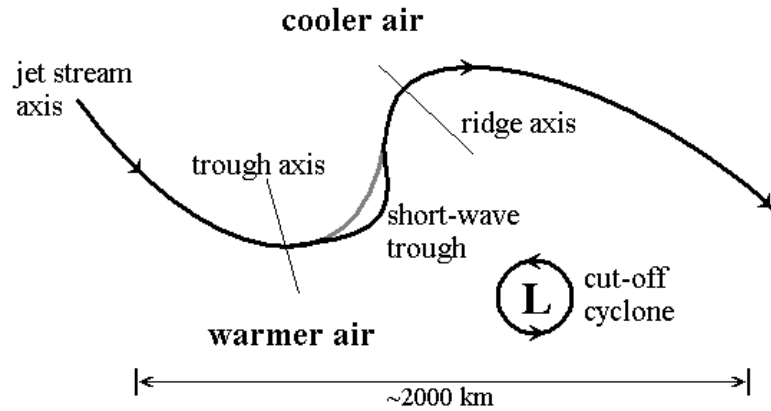


Figure 2.5: Schematic diagram of meteorological features.

reader's benefit, a schematic diagram of several meteorological features discussed here are shown in Figure 2.5. The reader should refer to this schematic for the purposes of identifying many of these features mentioned during the analysis of this event in Section 2.3.2.

- The upper-level “jet stream” is characterized by a band of strong winds at an altitude near 40,000–45,000 feet ( $\sim 8$  miles) in middle latitudes. The polar jet stream marks a boundary between relatively cool polar air and relatively warm equatorial air. This boundary can cause significant changes in weather, including the development of storms and the production of rainfall.
- During the winter and spring seasons, the westerly polar jet stream dominates the occurrence and passage of weather systems over the continental U.S.
- On weather maps, a “trough” is often indicated where the polar jet stream tends toward the equator, whereas a “ridge” indicates that the polar jet stream is far from the equator.
- In the Northern Hemisphere and as viewed from above, air flows counter-clockwise around a low-pressure center (“low” or “cyclone”) or the axis of a trough, and

clockwise around a high-pressure center (“high” or “anticyclone”) or the axis of a ridge. Where strong local curvature of the wind field is found, troughs and ridges are sometimes indicated in regions away from the polar jet stream.

- Destabilization of the atmosphere, and thus the greatest potential for storm events, typically occurs on the east side of an upper-level trough. The development of surface weather features, such as cold fronts, often occurs directly beneath and immediately ahead of this area.
- Upper-level troughs, and their associated fronts near the surface, tend to initiate storm development, whereas ridges tend to suppress convective development.
- A “short-wave” trough is a “bump” in the jet stream where particularly strong destabilization can occur, with consequently abrupt weather changes near the surface.
- A “cut-off low” or “cut-off cyclone” is a nearly circular region of strong winds at high altitudes that has separated from the polar jet stream. These systems can last for long periods before they rejoin the polar jet stream and, in the meantime, can cause major weather changes near the surface in the vicinity of their passing.
- While weather patterns over the continental U.S. generally move from west to east, along with the winds of the polar jet stream, under certain circumstances they may remain relatively stationary for long periods and may, in some cases, move from east to west. Winds and individual storms often behave quite differently from this pattern in the vicinity of the Rocky Mountains.

## 2.3 The April 28-May 2, 1999, Event

The following event analysis relies primarily on maps of Eta weather model initialization output and surface observations provided by Unisys Weather (see Section 1.4 for website). Archives of these data include products at 12-hour intervals, issued for 00 UTC<sup>1</sup> (5 pm LST<sup>2</sup> on the previous date) and 12 UTC (5 am LST on the same date). It should be noted that these times do not account for Daylight Saving Time. Additional observations (e.g. surface observations, upper-air observations, etc.) have been obtained from other sources listed in Section 1.4 and are included where appropriate.

### 2.3.1 *Antecedent Conditions*

Records obtained from the National Climatic Data Center (NCDC) indicate several snow and rain events during the four weeks prior to the storm event described below. During April 1–2, 1999, a storm produced rain and then 8–16 inches of snow in western El Paso County and along the Rampart Range, and 6 inches of snow was reported in Monument during April 4–5. During April 14–15, 11–15 inches of snow was reported in Monument and Palmer Lake. Finally, during April 21–23, 8–10 inches of snow was reported in Woodland Park and 6–8 inches of snow was reported along the Rampart Range and in Monument. During this event, as much as 6 inches of snow was reported in the northern and western areas of Colorado Springs.

Overall, the NCDC records show that a total of 1.86 inches of liquid-equivalent precipitation (rain and melted snow) occurred at the Colorado Springs NWS station in the four weeks prior to the storm event described below. A contour map of the total observed precipitation in the vicinity of Colorado Springs, including the Fountain and Monument Creek

---

<sup>1</sup> UTC: Universal Coordinated Time, an equivalent of Greenwich Mean Time (GMT).

<sup>2</sup> LST: Local Standard Time. Note that Local Daylight Time (LDT) = LST + 1 hour.

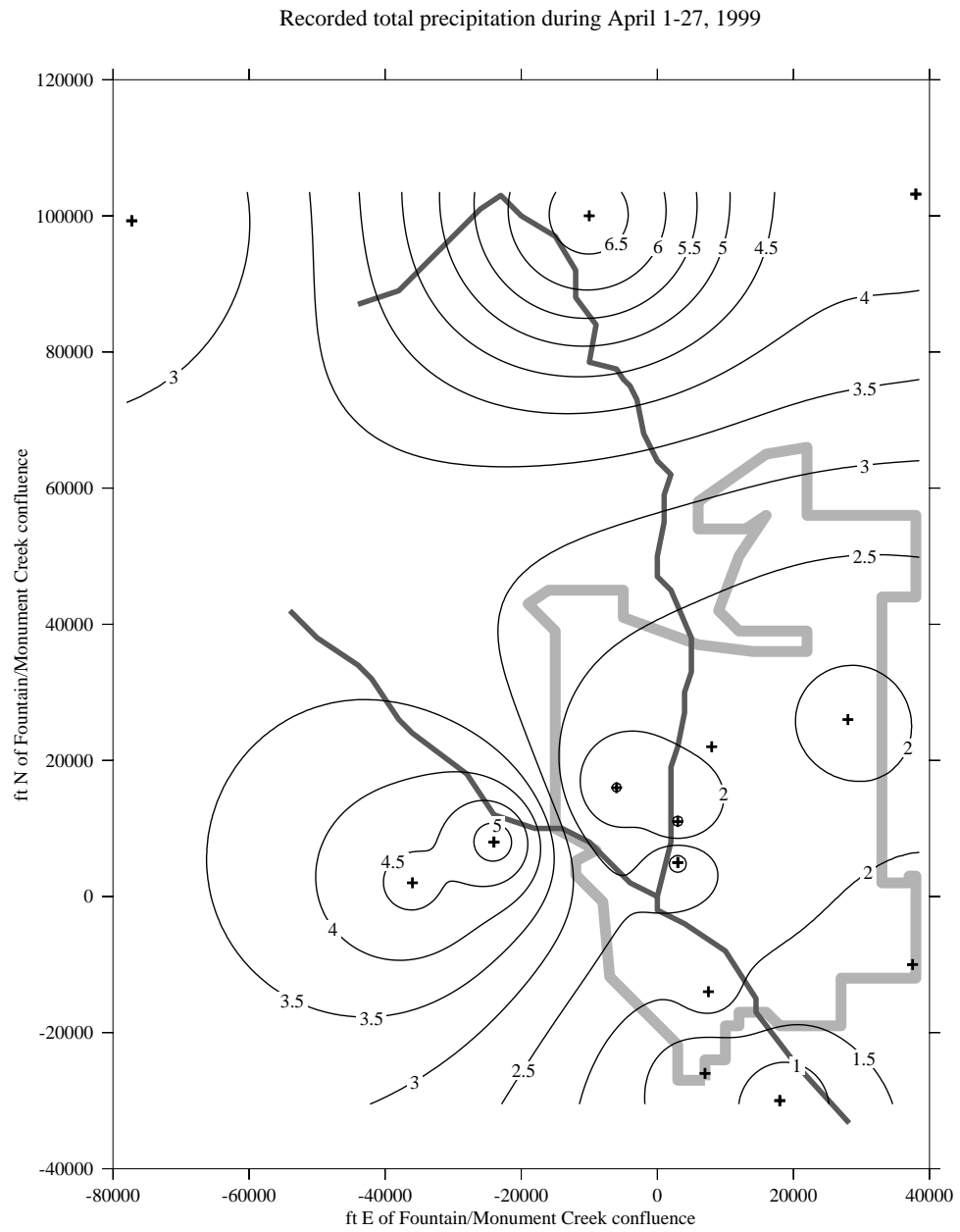


Figure 2.6: Total liquid-equivalent precipitation during April 1–27, 1999. The approximate boundaries of the City of Colorado Springs are shown in light gray. Contoured values are liquid-equivalent total precipitation in inches, with trace amounts excluded.

watersheds, for the period April 1–27, 1999, is shown in Figure 2.6. As discussed above, a rain shadow is evident in the northwestern portion of the region and can be attributed to barrier effects of the Rampart Range during upslope storm events. Large values of total precipitation in the southwestern part of the region, along the eastern ridgeline of Pike’s Peak, may be attributed to storms with northerly cold frontal passages and prevailing winds during this period. Large values of total precipitation in the northern part of the region, on the southern slopes of the Palmer Lake Divide, may be attributed to storms with moist southerly winds leading to upslope patterns in that area. Observations at the Colorado Springs NWS station indicate that any accumulated snow had melted by April 28, 1999.

### *2.3.2 Eta Model and Surface Analyses*

The reader is referred to products of the National Centers for Environmental Prediction (NCEP; <http://www.ncep.noaa.gov>) for more information regarding the operation and utility of the Eta model for numerical weather prediction. Numerous features are included in the 4-panel figures derived from Eta model initialization analyses that are shown here. The upper left panel of these figures shows temperatures (colored contours, in °C) and heights (line contours, in meters) of the 850 hPa surface. The upper right panel shows wind speeds (colored contours, in knots) and heights (line contours, in meters) of the 300 hPa surface. The lower left panel shows sea level pressure (blue contours, in hPa). The lower right panel shows relative humidity in the 850–500 hPa layer (colored contours, in %) and the lifted index, a measure of the potential for development of convective storms (line contours, in °C).

Other features are shown on surface analysis figures included here. These include contours of sea level pressure (thin purple lines) with analyzed high- and low-pressure

centers, analyzed cold (blue), warm (red), stationary (striped blue and red) and occluded (pink) fronts, and analyzed surface troughs (dashed yellow). These analyses also include national mosaic Nexrad radar reflectivity intensities (shaded green) and individual station reports. The surface station reports may indicate numerous observations, including sky (cloud) cover (center circle), wind direction and speed (wind barb and flags), temperature and dew point temperature (upper left and lower left, respectively), sea level pressure (upper right), and the occurrence of significant weather (middle left).

The movement and development of large-scale weather patterns during the days prior to April 28, 1999, can be characterized as typical of middle latitude spring conditions. The formation of a strong surface cyclone to the east of the Rocky Mountains by the afternoon of April 26 (see Figure 2.7) was associated with the slow passage of an upper-level cyclone over the central Rocky Mountains during the previous two days. It was this system that produced the last of the snow events listed in Section 2.3.1. By April 27, high surface pressures were re-established over Colorado associated with a weak upper-level ridge over the Four Corners region, and another upper-level trough was beginning to move into the Pacific Northwest region (see Figure 2.8). The low-level high weakened considerably by the evening of April 27, and by the next morning (see Figure 2.9) a large surface trough was established over the intermountain region including western Colorado. In the upper levels, the trough over the Pacific Northwest strengthened and moved slightly southward over the same period.

This flood-producing event was composed of three distinct episodes over a period of approximately 3.5 days. The first episode of this event began at approximately 00 UTC on April 29 (5 pm LST on April 28; see Figure 2.10a), and can be associated with the development of a surface cyclone over western Colorado beneath a short wave in the upper-



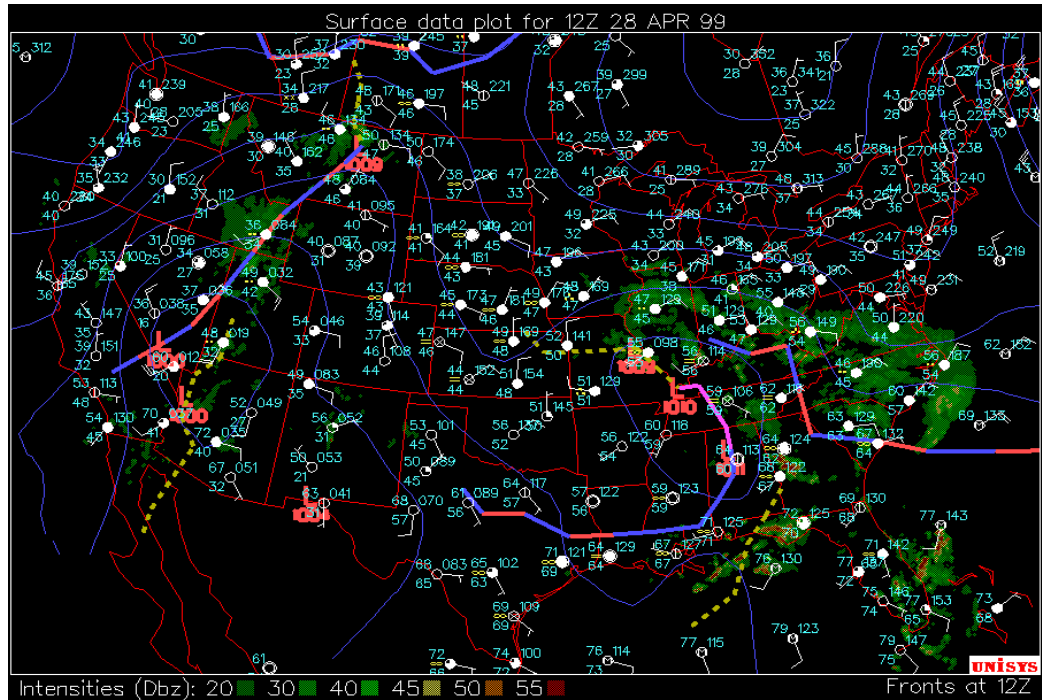


Figure 2.9: Surface analysis for 12 UTC (5 am LST) on April 28, 1999. Features of this plot are described in Section 2.3.2 of the text.

level trough over the western U.S. (see Figure 2.10b). The combination of upslope flows, drawn into eastern Colorado by the surface cyclone, and high relative humidity over the Great Plains led to the development of strong thunderstorms with heavy rainfall around this time. By the next morning, the region of heavy rainfall over central Colorado had moved to the east along with its associated major weather features.

The second episode of this event began around 5 pm LST on April 29. By 00 UTC on April 30 (5 pm LST on April 29; see Figure 2.11a), a low-level trough had developed over the Four Corners region in association with a cut-off cyclone in the upper levels over northwestern Arizona (see Figure 2.11b), a pattern that induced east-southeasterly flows over southeastern Colorado. High relative humidity and moderate rainfall persisted through the next observation time at 12 UTC (5 am LST) on April 30 (see Figure 2.12a). These conditions were supported by continued upslope flows and a slight northward movement

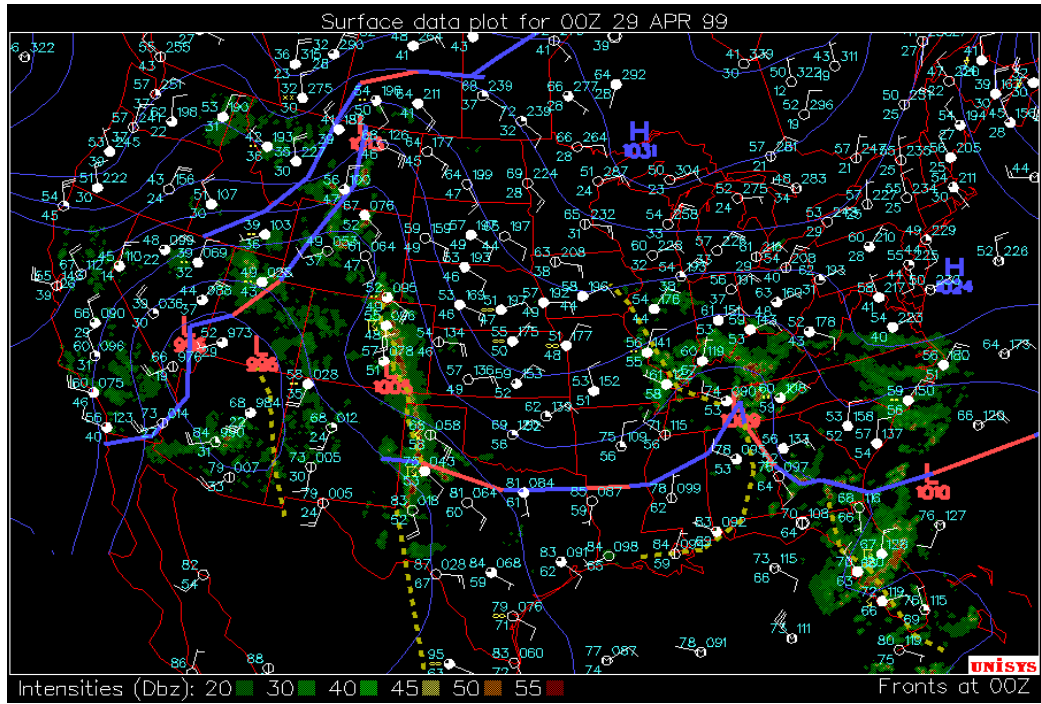


Figure 2.10a: Surface analysis for 00 UTC on April 29 (5 pm LST on April 28), 1999. Features of this plot are described in Section 2.3.2 of the text.

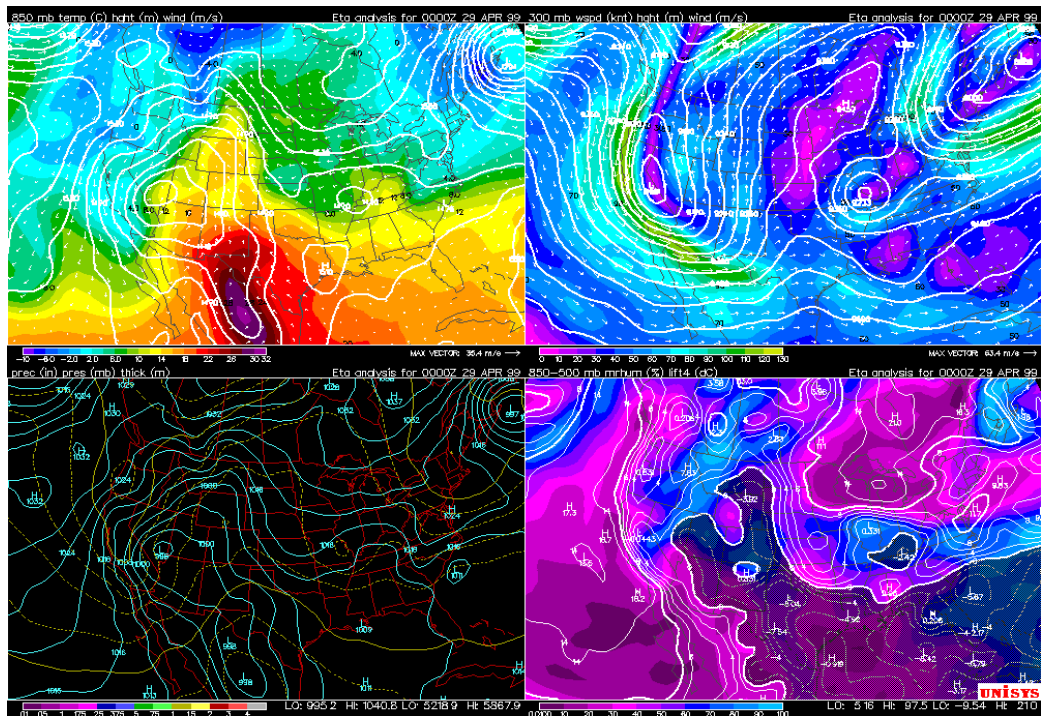


Figure 2.10b: Eta model analysis for 00 UTC on April 29 (5 pm LST on April 28), 1999. Features of these plots are described in Section 2.3.2 of the text.

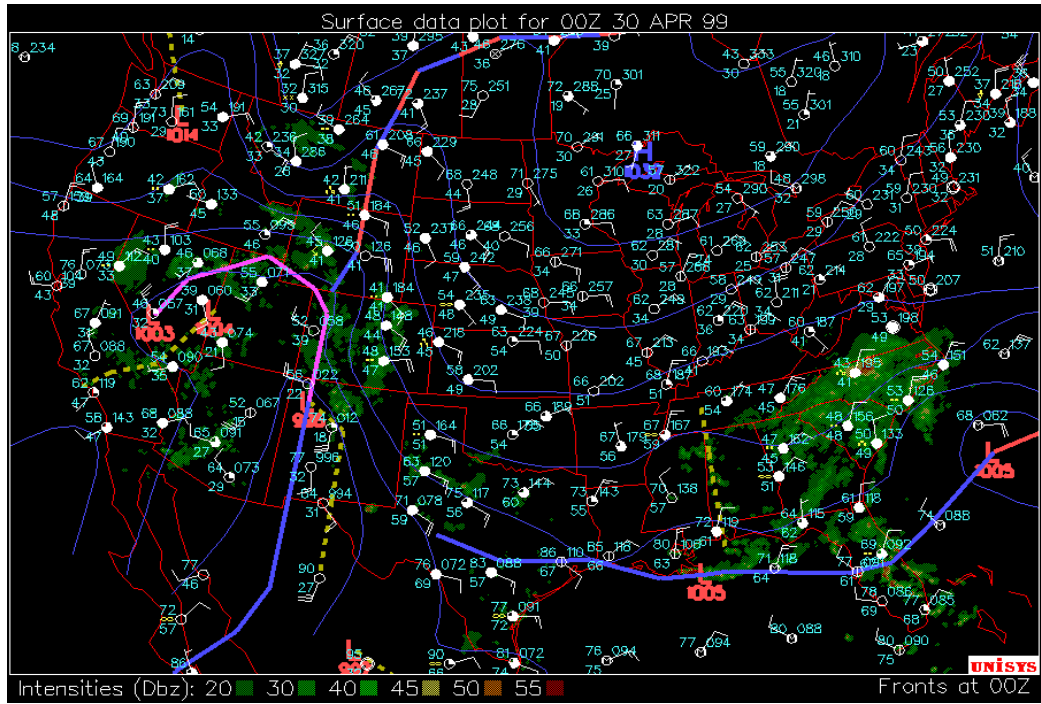


Figure 2.11a: Surface analysis for 00 UTC on April 30 (5 pm LST on April 29), 1999. Features of this plot are described in Section 2.3.2 of the text.

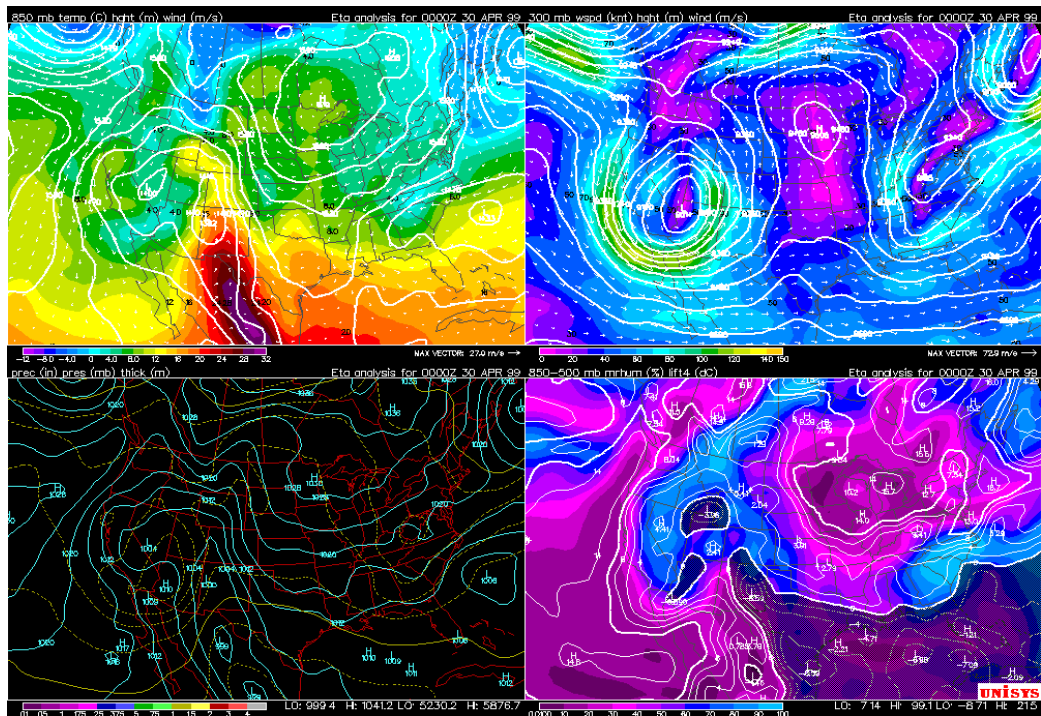


Figure 2.11b: Eta model analysis for 00 UTC on April 30 (5 pm LST on April 29), 1999. Features of these plots are described in Section 2.3.2 of the text.

of the upper-level cyclone (see Figure 2.12b). By that afternoon, however, the upper-level cyclone and its associated low-level trough had moved significantly northeastward, out of the positions most favorable for upslope flows along the Colorado Front Range.

The third episode of this event developed slowly through 12 UTC (5 am LST) on May 1 (see Figure 2.13a), and can be associated with a weakening upper-level cyclone and short wave trough over Arizona and a weak surface trough over New Mexico (see Figure 2.13b). By 00 UTC on May 2 (5 pm LST on May 1; see Figure 2.14), weak surface lows had formed over western Colorado and extreme northern Texas. Though this pattern favors weak upslope flows and sustained rainfall in southeastern Colorado, the major weather features moved out of this position by the next morning. By 12 UTC (5 am LST) on May 2 (see Figure 2.15), the weakening upper-level cut-off cyclone had dissipated, and a surface cyclone had formed over eastern Wyoming that was supported by an upper-level trough over the northern Great Plains.

### *2.3.3 Surface Observations*

Histograms of hourly rainfall at gauges listed in Table 2.2 for the period April 28–May 2, 1999, are shown in Figure 2.16. Specifically, hourly rainfall records for the Woodland Park, Manitou Springs, Colorado Springs, and Greenland 9 SE National Weather Service (NWS) stations are shown in the top two rows of Figure 2.18. Hourly rainfall records for gauges operated by the Colorado Springs Department of Utilities at Colorado College and Pinello Ranch are shown in the bottom row of Figure 2.16.

The hourly rainfall observations at these stations demonstrated a clear distinction between the three episodes that comprised this event, as discussed above. For the purposes of later analysis, using the semi-daily synoptic indicators and hourly rainfall data presented

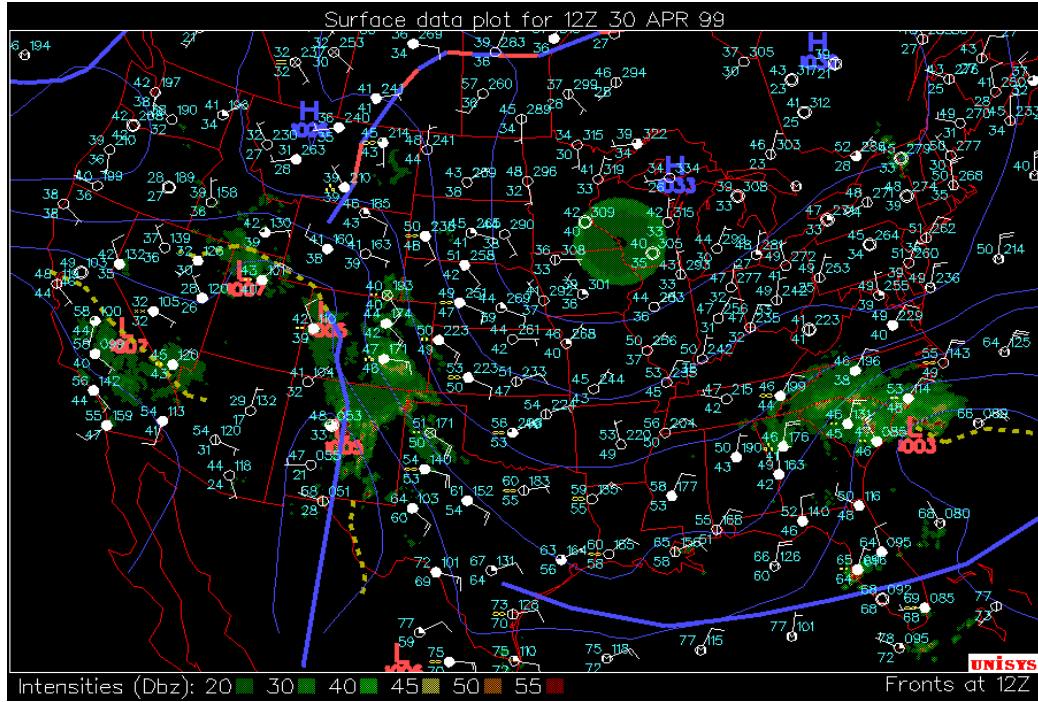


Figure 2.12a: Surface analysis for 12 UTC (5 am LST) on April 30, 1999. Features of this plot are described in Section 2.3.2 of the text.

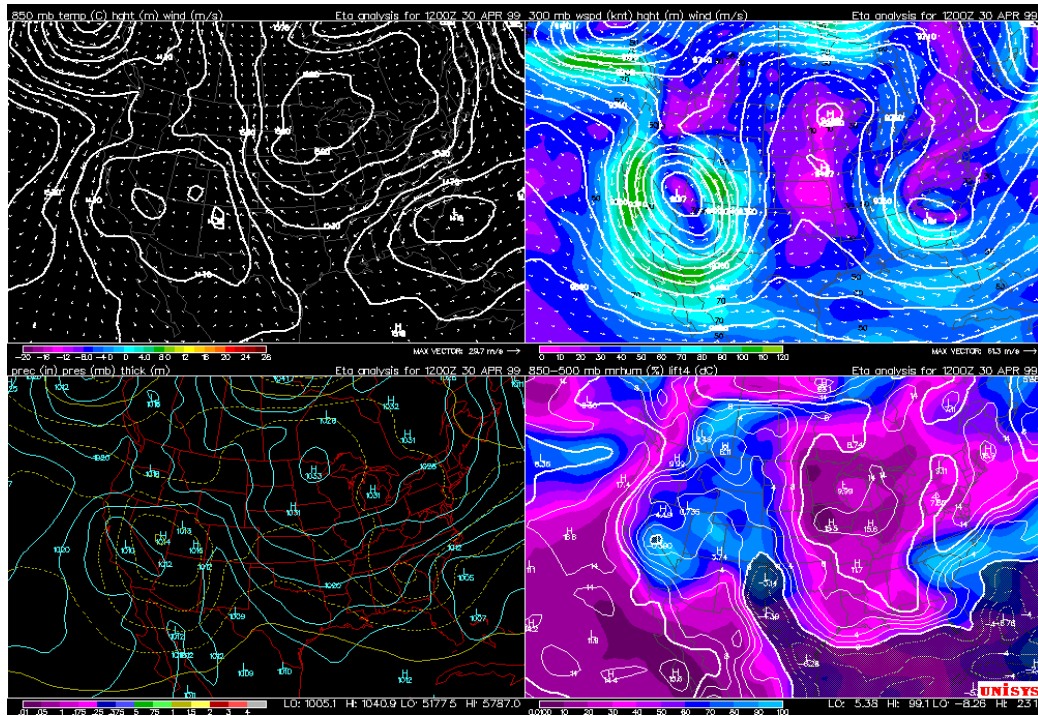


Figure 2.12b: Eta model analysis for 12 UTC (5 am LST) on April 30, 1999. Features of these plots are described in Section 2.3.2 of the text.

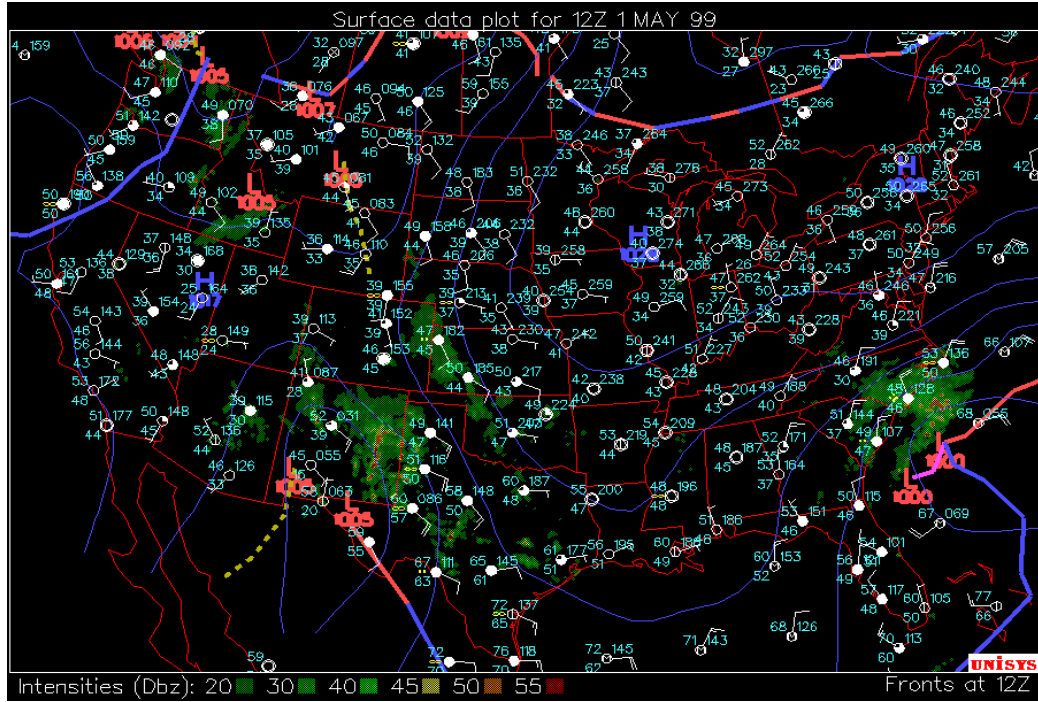


Figure 2.13a: Surface analysis for 12 UTC (5 am LST) on May 1, 1999. Features of this plot are described in Section 2.3.2 of the text.

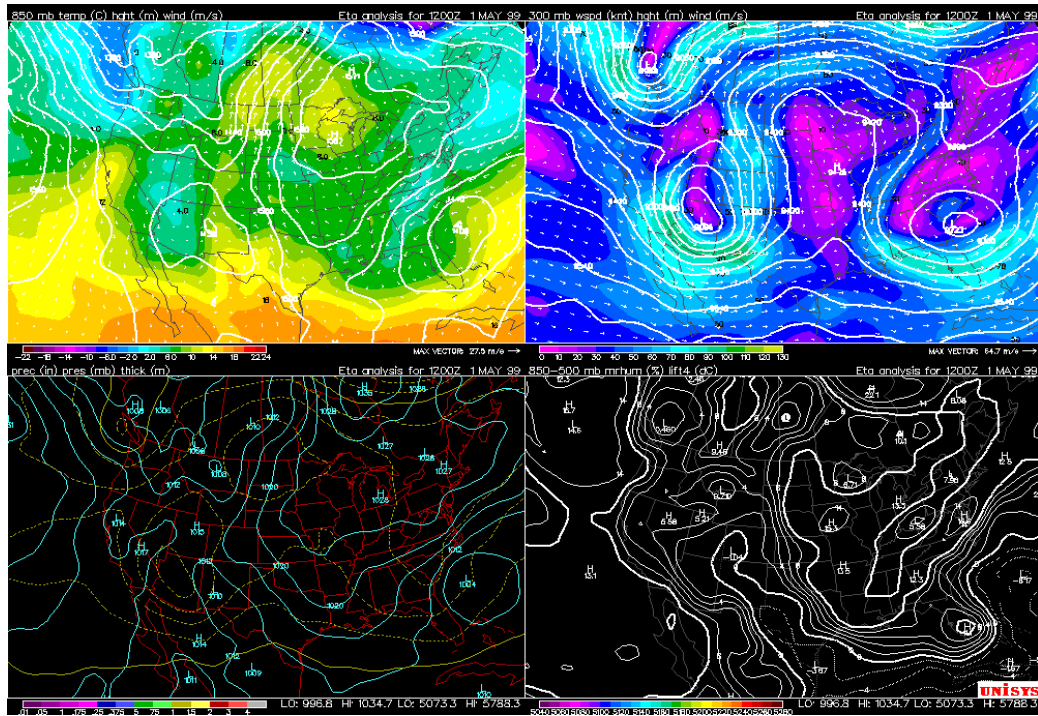


Figure 2.13b: Eta model analysis for 12 UTC (5 am LST) on May 1, 1999. Features of these plots are described in Section 2.3.2 of the text.

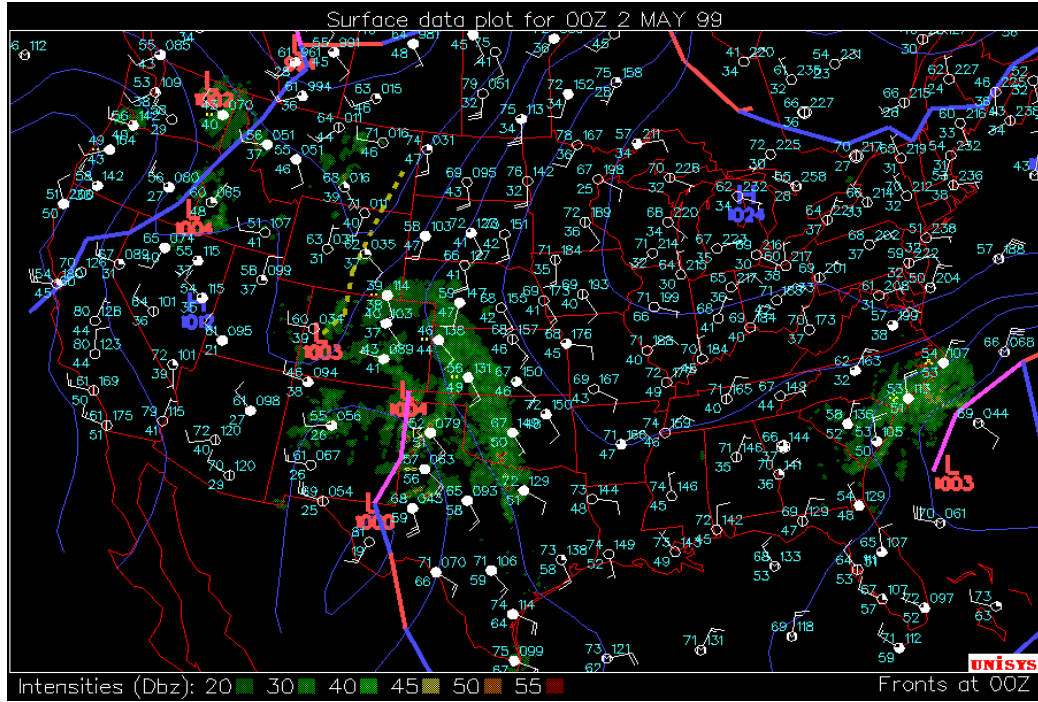


Figure 2.14: Surface analysis for 00 UTC on May 2 (5 pm LST on May 1), 1999. Features of this plot are described in Section 2.3.2 of the text.

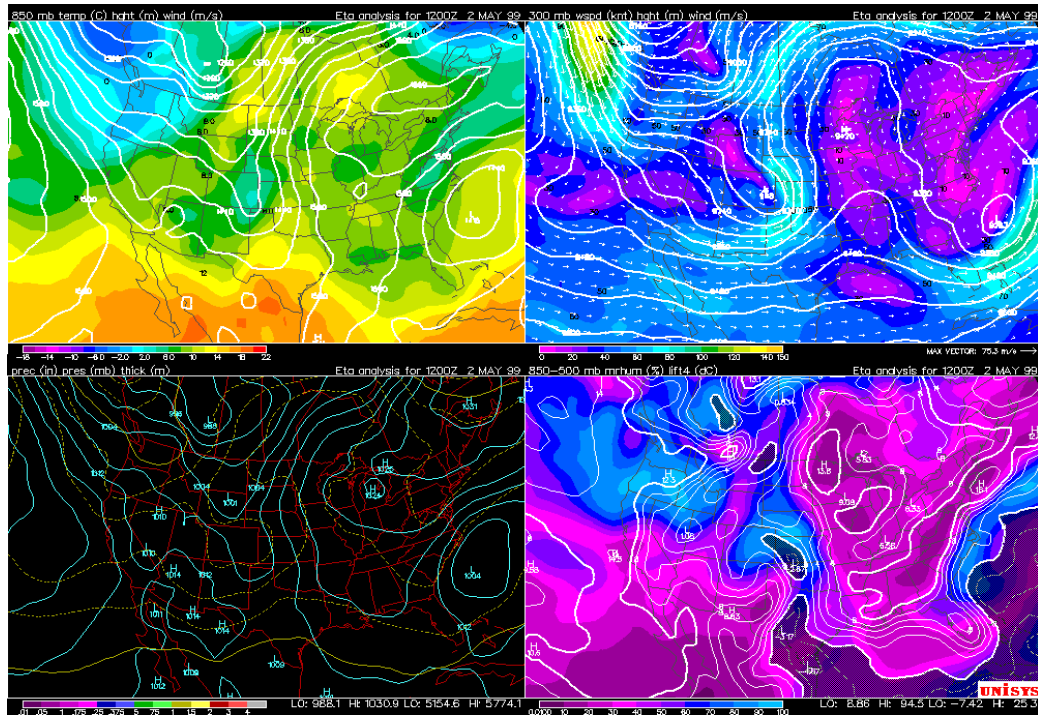


Figure 2.15: Eta model analysis for 12 UTC (5 am LST) on May 2, 1999. Features of these plots are described in Section 2.3.2 of the text.

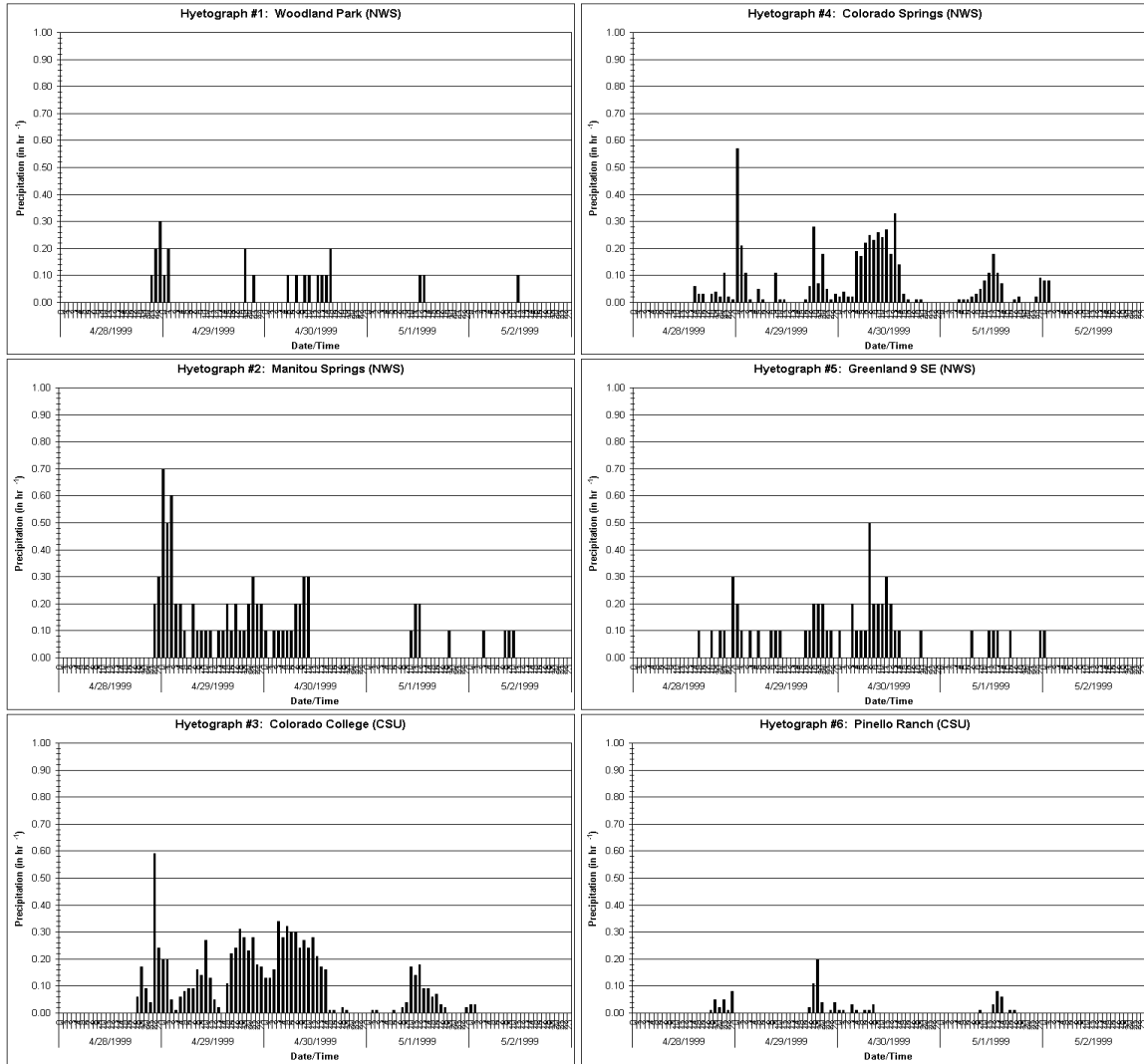


Figure 2.16: Rainfall at hourly gauges during April 28–May 2, 1999. Gauge names and locations are listed in Table 2.2.

here, we have designated the period 14 LST April 28–04 LST April 29 as Storm 1 ( $H_1 = 14$  hrs), 04 LST April 29–03 LST May 1 as Storm 2 ( $H_2 = 47$  hrs), and 03 LST May 1–04 LST May 2 as Storm 3 ( $H_3 = 25$  hrs). As noted in Table 2.1, the 2.63 inches of rainfall recorded at the Colorado Springs NWS station on April 30, during Storm 2, was the largest daily precipitation amount during April on record for that location.

A regional contour map of recorded total rainfall during April 28–May 2, 1999, for this storm event is shown Figure 2.17. It should be noted that the largest observed rainfall totals occurred over the City of Colorado Springs and were concentrated in the area immediately north of the confluence of Monument and Fountain Creeks. A rain shadow is evident in the northwestern part of the region and can again be attributed to barrier effects of the Rampart Range during upslope portions of this event. Contrary to the climatological pattern presented in Figure 2.4, a minimum in total event rainfall is evident in the southwestern part of the region and may be considered a rain shadow. The local circulation effects that may have led to this rainfall pattern will be discussed further in Chapter 5.

#### *2.3.4 Analysis and Comparison with Historical Events*

Southeasterly near-surface winds and high humidity were indicated over southeastern Colorado, western Kansas and northern Texas for the duration of this event. This near-surface flow pattern drew moisture from the area around the Gulf of Mexico, approached the Front Range and was forced upward. Sustained convection with moderate rainfall rates occurred over much of central Colorado between April 29 and May 1. The influence of upslope flows on Front Range precipitation events is widely recognized in weather forecasts and post-storm analyses, and has been cited as a contributory cause of flood events in the Big Thompson Canyon (July 31, 1976; Maddox et al. 1978) and Fort Collins (July 28–29,

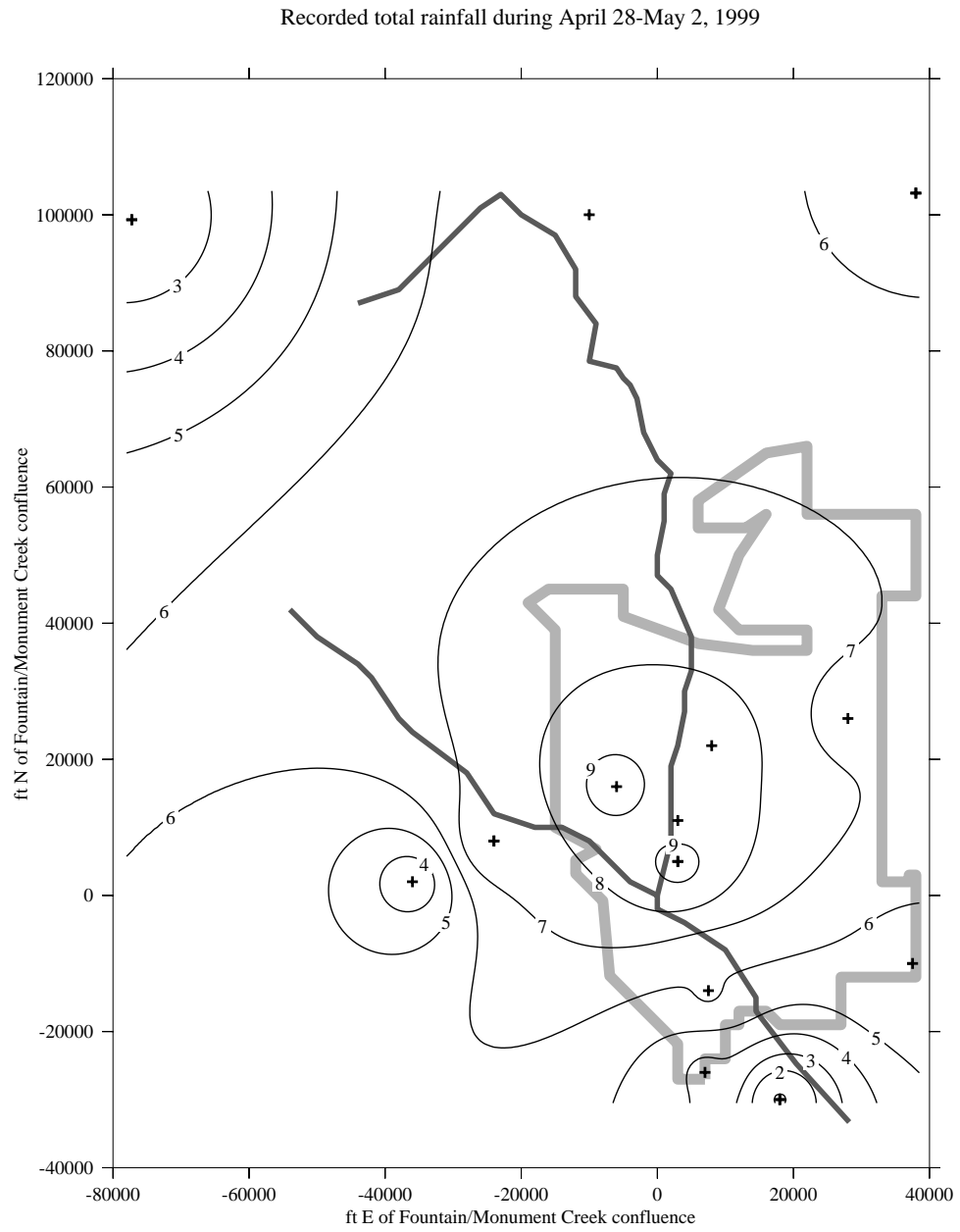


Figure 2.17: Recorded total rainfall during April 28–May 2, 1999. The approximate boundaries of the City of Colorado Springs are shown in light gray.

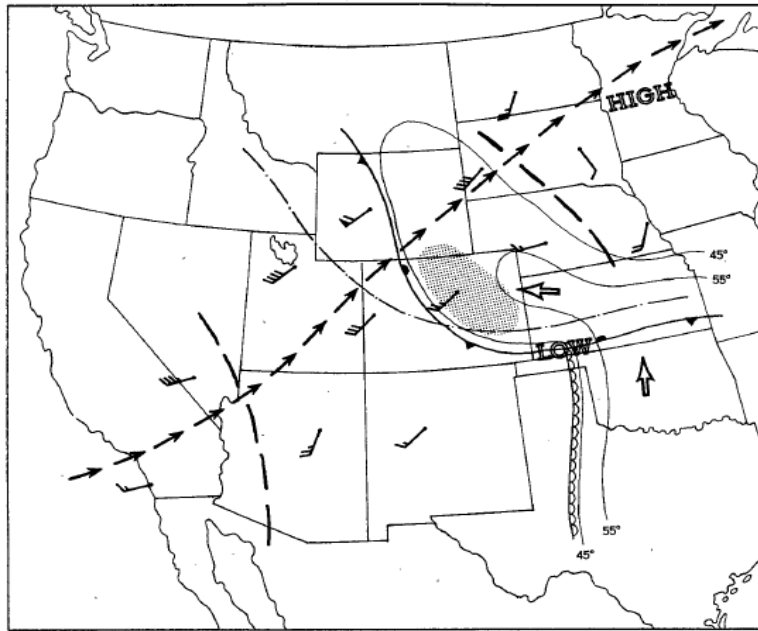


FIG. 2. Composite High Plains severe thunderstorm parameter chart. Frontal symbols are conventional, surface isodrosotherms ( $^{\circ}\text{F}$ ) denoted by fine lines, scalloped line indicates surface dry-line, large arrows depict surface flow, and "High" and "Low" refer to surface pressure centers. Dash-dot line locates the 700 mb thermal ridge. Wind bars show 500 mb winds (full barb signifies  $5 \text{ m s}^{-1}$ , flag signifies  $25 \text{ m s}^{-1}$ ), and heavy dashed lines locate short-wave trough axes. Chain of arrows is aligned along core of strong high-level winds, above 500 mb. Stippling denotes region of expected severe thunderstorms.

Figure 2.18: Figure 2 from Doswell (1980). This figure is reproduced under blanket permission provided by the American Meteorological Society.

1997; Petersen et al. 1999).

The meteorological patterns discussed above for 00 UTC on April 29 (5 pm LST on April 28; see Figures 2.10a and b) conform to those described by Doswell (1980) for severe thunderstorms over the western High Plains. The archetype schematic for these storm events (Doswell 1980, Figure 2) is shown in Figure 2.18. Maddox et al. (1978) found that similar patterns preceded flash flood events in the Big Thompson Canyon, Colorado (July 31, 1976), and in Rapid City, South Dakota (June 9, 1972).

The meteorological patterns described for 12 UTC (5 am LST) on May 1 (see Figures 2.13a and b) generally conform to those characterized by Maddox et al. (1980) for "Type I" western flash flood events. Characteristically, a surface cyclone forms on the east side of

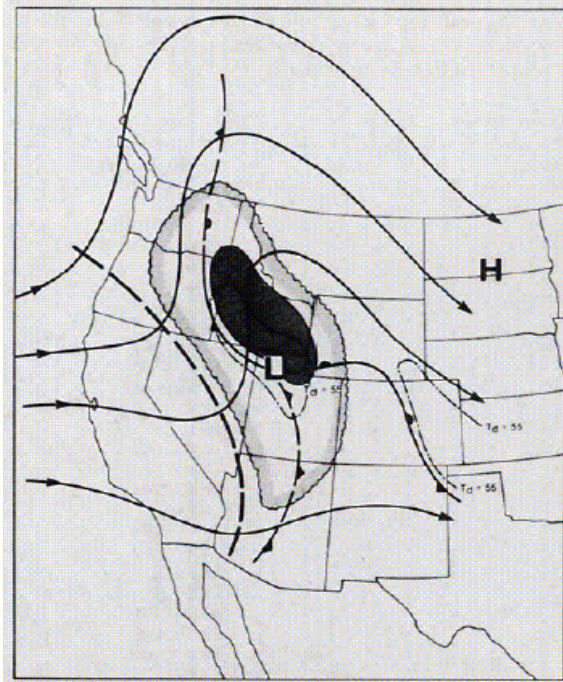


FIG. 1. Generalized 500 mb and surface patterns for Type I western flash floods. Streamlines for 500 mb flow are shown and 500 mb trough position is depicted as a heavy dashed line. Region at 500 mb with  $T - T_d \leq 6^\circ\text{C}$  is outlined. Surface fronts and pressure centers are indicated, as well as isopleths for regions with high surface dewpoint temperatures. Time of analysis is just prior (0–3 h) to onset of storm activity. Region with potential for heavy precipitation is shaded.

Figure 2.19: Figure 1 from Maddox et al. (1980). This figure is reproduced under blanket permission provided by the American Meteorological Society.

an upper-level trough and produces conditions favorable for flash flooding to the east and north of the surface low pressure center. The archetype schematic for these storm events (Maddox et al. 1980, Figure 1) is shown in Figure 2.19, where the map of western North America is provided primarily for reference of scale.

Maddox et al. (1980) associated similar Type I patterns with flash flood events along the Rocky Mountain Front Range in Cheyenne, Wyoming (July 19 and September 8, 1973), in the Big Thompson Canyon, Colorado (July 31, 1976), and across Larimer and Weld Counties, Colorado (July 24, 1977). Other publicized historical events that resulted from similar weather patterns included flash floods in Rapid City, South Dakota (June 9, 1972;

Maddox et al. 1980) and Fort Collins, Colorado (July 28–29, 1997; Petersen et al. 1999). According to available rainfall records, the Colorado Springs NWS station recorded 3.90 inches of rainfall during July 27–30, 1997, the period over which the same storm system affected the Fort Collins area even more significantly. It is interesting to note that flash flooding and river flooding were also observed in Fort Collins, Colorado, on April 30, 1999, following more than 3.5 inches of liquid-equivalent precipitation in the previous week and nearly 4.0 inches of rainfall during April 29–30, 1999 (Weaver et al. 2000).

## 2.4 Discussion

It has been demonstrated that the succession of meteorological patterns favorable for western High Plains and Rocky Mountain Front Range flash floods events is not unique. Conditions similar to the severe event archetypes for this region have produced extensive flash flooding in the Big Thompson Canyon, Colorado (July 31, 1976), in Fort Collins, Colorado (July 28–29, 1997), and for the event discussed here in Colorado Springs, Colorado (April 28–May 2, 1999). As some flood events may occur from localized heavy rainstorms, and others under conditions of widespread and sustained precipitation, these floods resulted from combining both of these storm types in a single event. The precipitation amounts recorded at the Colorado Springs NWS station over the period described here support this conclusion of a long-lasting hybrid event archetype, during which a storm of one type was followed closely by another storm with a slightly different supporting pattern.

However, the original purposes of this work were not simply to diagnose the morphology of a flood-producing storm event in the vicinity of Colorado Springs, Colorado, but to determine (1) the extent of extreme rainfall during that storm event, and (2) the possible contribution of development and urbanization in the City of Colorado Springs to

the observed stream discharges in various locations along Monument and Fountain Creeks. By the methods employed in solving this latter aspect, and on the basis of the observed discharge records themselves, it was determined that the extent of extreme rainfall must have been greater than observed. The methods by which that conclusion could be drawn are discussed in Chapter 3.

## Chapter 3

### EVENT MODELING

The methodology applied to simulation of the storm and flood event discussed in Chapter 2 is described in detail here. This methodology may be described as the determination of those spatial and temporal distributions of rainfall, by application of a distributed physical hydrology model, that are required for the accurate simulation of observed stream discharge records in the Monument and Fountain Creek watershed. The construction and operation of this model is discussed, and the method by which existing rainfall data were applied is described. The formulation of supplemental rainfall data is also given here; this technique, sometimes employed by the National Weather Service River Forecast System (NWSRFS), is shown to provide greater simulation accuracy than data from the existing sparse network of rainfall gauges. The methods by which this accuracy is measured are also described here.

#### **3.1 Modeling Methodology**

From the sources listed in Section 1.4, the two data sets of primary interest for this work were spatially distributed observations of rainfall and stream discharge. During this storm event, however, stream discharges at various locations on Monument and Fountain Creeks (and several tributaries of those) were of such a magnitude that measurements at USGS gauges became unreliable. For the diagnosis of storm-related response at locations of

particular interest, existing data sets were therefore inadequate. Several methods exist for the reconstruction of these data at effectively ungauged locations and are discussed here.

### 3.1.1 *Aggregated Models*

One of the simplest methods for the diagnosis of stream flows at ungauged sites might rely on the available stream flow observations at the nearest upstream gauge and calculations of rainfall and resulting runoff that occurred in the region between the two stream flow gauges. These calculations may be based on the rational method, which depends on the rainfall intensity and the total watershed area. The applied runoff coefficient is derived by various methods for the specific impervious areas, soil types, antecedent moisture conditions, roughness elements, ground slope, etc. within the watershed. The calculations may also be based on the construction of a partial-watershed model that considers only the region between the locations of observed and desired stream flows, for which many of the same watershed parameters would be required. In either case, the runoff hydrograph for the intervening area would simply be added to the observed hydrograph for the upstream watershed area in order to find the stream discharge hydrograph at the desired location.

Alternatively, an aggregated watershed model might rely on the formulation of a unit hydrograph (e.g. Chow et al. 1988) from known events and data records. However, even the more sophisticated of these methods such as the Geomorphological Instantaneous Unit Hydrograph (GIUH) become insensitive to the spatial distribution of rainfall provided the overall mean areal precipitation (MAP) is preserved.

These methods, while simply formulated and easily parameterized, can also be described as event-specific. The partial-watershed method would provide little opportunity for the exploration of alternative configurations of the upstream area that contributed to

the known hydrograph. Such configurations may include alternative spatial and temporal rainfall distributions, as for the simulation of hydrographs resulting from an entirely different storm event, as well as alternative scenarios of land use and development within the watershed. Unit hydrograph methods, unless formulated in a distributed fashion for a divided watershed, remove the opportunity for use of meteorological analyses (such as that presented in Chapter 2) and any understanding of event morphology in the determination of runoff hydrographs.

### 3.1.2 *Statistical Methods*

Another method available for the diagnosis of stream discharge at ungauged sites is the development of a statistical model that would rely on spatial and temporal correlations between observations at gauged locations in the surrounding region. It is certainly possible to find non-zero correlations between time series of rainfall and stream discharge measured at respective gauges within close proximity, and for measurements at gauges several miles apart along the same stream. However, it is also possible to find non-zero correlations between measurements of rainfall and stream discharge at gauges that are located two counties, two countries or two continents apart. The presence of simple correlation between two series of observations, or even a complex correlation between many combinations of rainfall and stream discharge observations in many locations, does not necessarily bring to light the underlying *causality* that provides a physical or conceptual connection between these measurements. A purely statistical model cannot describe details of the process by which rainfall is converted to runoff upon meeting the ground—it can only describe some integral aspect of the relation between the input to the system, the rainfall, and the output from the system, the stream discharge.

A statistical method can be formulated and parameterized in a manner as simple or complex as the researcher desires, but in an overall sense the resulting model can be described as condition-specific and purely empirical. The statistical model considers only the strict spatial and temporal relationships between actual measurements under the specific surrounding conditions. This model can therefore account neither for conditions and measurements in the intervening areas and times, nor for the alternative scenarios that imply changes in those conditions and measurements. Specifically for this work, changes in the spatial and temporal distributions of rainfall (i.e., for alternative storm events) and the level and density of development in a watershed area cannot be adequately addressed in a purely statistical model.

### *3.1.3 Distributed Physical Hydrology*

It is these alternatives, which are not treated sufficiently by either the partial-watershed event-specific method or the purely empirical condition-specific method, that have been of great interest in the work discussed here. Considering this, the most viable method is one that remains general in both event and condition, that is, a system for which both the input and internal parameters can be changed as needed in the investigation of alternative scenarios. A distributed hydrologic watershed model, within the limitations of our knowledge regarding the physical characteristics of the watershed, can thus be considered the most accurate representation of the processes by which rainfall is converted to runoff throughout the watershed, regardless of event morphology or surface conditions, and is thus most useful for the investigation of alternatives in those parameters.

Using such a flexible hydrologic model, the methodology adopted here can then best be described as an effort to fit the simulated hydrographs to known USGS hydrographs at

all corresponding locations where such observations are available in the modeled watershed. For this storm event, stream discharge records were available at only four USGS gauge locations in the Monument and Fountain Creek watersheds where corresponding locations were appropriately represented in the SWMM RUNOFF model described below. These USGS gauges are listed in Table 3.1, and their locations are shown on a schematic map in Figure 3.1.

Several gauges for which stream discharge records were available were not represented in this model. These are listed in the middle portion of Table 3.1. In one location along a tributary of Cottonwood Creek (USGS gauge 07103985) in the northeastern portion of the City of Colorado Springs, stream discharge data was available but, because of the applied method of sub-basin aggregation, this tributary was not represented in the RUNOFF model for this portion of the Monument Creek watershed. In another location along Bear Creek (USGS gauge 07105000) in the southwestern portion of Colorado Springs, the close proximity of this gauge to another at which greater discharges were observed (USGS gauge 07105490) led to the exclusion of this gauge on the basis of redundancy.

In other locations, USGS gauge data were considered unreliable due to the high flow conditions that occurred during the major storm event addressed here and were not released to the author for the purposes of this work. These gauges are listed in the bottom portion of Table 3.1. As another benefit of the distributed hydrologic modeling approach, the work presented here led to the reconstruction of discharge records at those locations for this storm event.

This work focused primarily on refining the interpretation of spatial variations in rainfall over the affected watersheds until the hydrographs at the four USGS stream gauges listed in the top portion of Table 3.1 were simulated as closely as possible. Two of these gauges

Table 3.1: Names and locations of USGS stream gauges along Monument and Fountain Creeks and various tributaries. Map locations, as shown in Figure 3.1, are given in feet north and east of the confluence of Monument and Fountain Creeks in Colorado Springs, Colorado.

USGS Designator	Gauge Name	Map Location	
		X (ft)	Y (ft)
<b>Available and employed gauges</b>			
07104000	Monument Creek at Pikeview, Colorado	5000	33200
07105490	Cheyenne Creek at Evans Ave. at Colorado Springs, Colorado	-14000	-13000
07105500	Fountain Creek at Colorado Springs, Colorado	3600	-3800
07105530	Fountain Creek below Janitell Rd. below Colorado Springs, Colorado	10000	-8000
<b>Available but not employed gauges</b>			
07103797	West Monument Creek below Rampart Reservoir, Colorado	-36000	53000
07103980	Cottonwood Creek at Woodmen Rd. near Colorado Springs, Colorado	27000	41000
07103985	Cottonwood Creek Tributary above Rangewood Dr. at Colorado Springs, Colorado	25000	36000
07105000	Bear Creek near Colorado Springs, Colorado	-16000	-4000
<b>Unavailable (reconstructed) gauges</b>			
07103700	Fountain Creek near Colorado Springs, Colorado	-10800	8400
07103703	Camp Creek at Garden of the Gods, Colorado	-11600	21200
07103780	Monument Creek above North Gate Blvd. at USAF Academy, Colorado	-2500	70500
07103800	West Monument Creek at Air Force Academy, Colorado	-20500	52500
07103970	Monument Creek above Woodmen Rd. at Colorado Springs, Colorado	5000	36500
07103977	Cottonwood Creek at Cowpoke Rd. at Colorado Springs, Colorado	36000	46000
07103990	Cottonwood Creek at mouth, at Pikeview, Colorado	5600	35200
07105800	Fountain Creek at Security, Colorado	28200	-33300

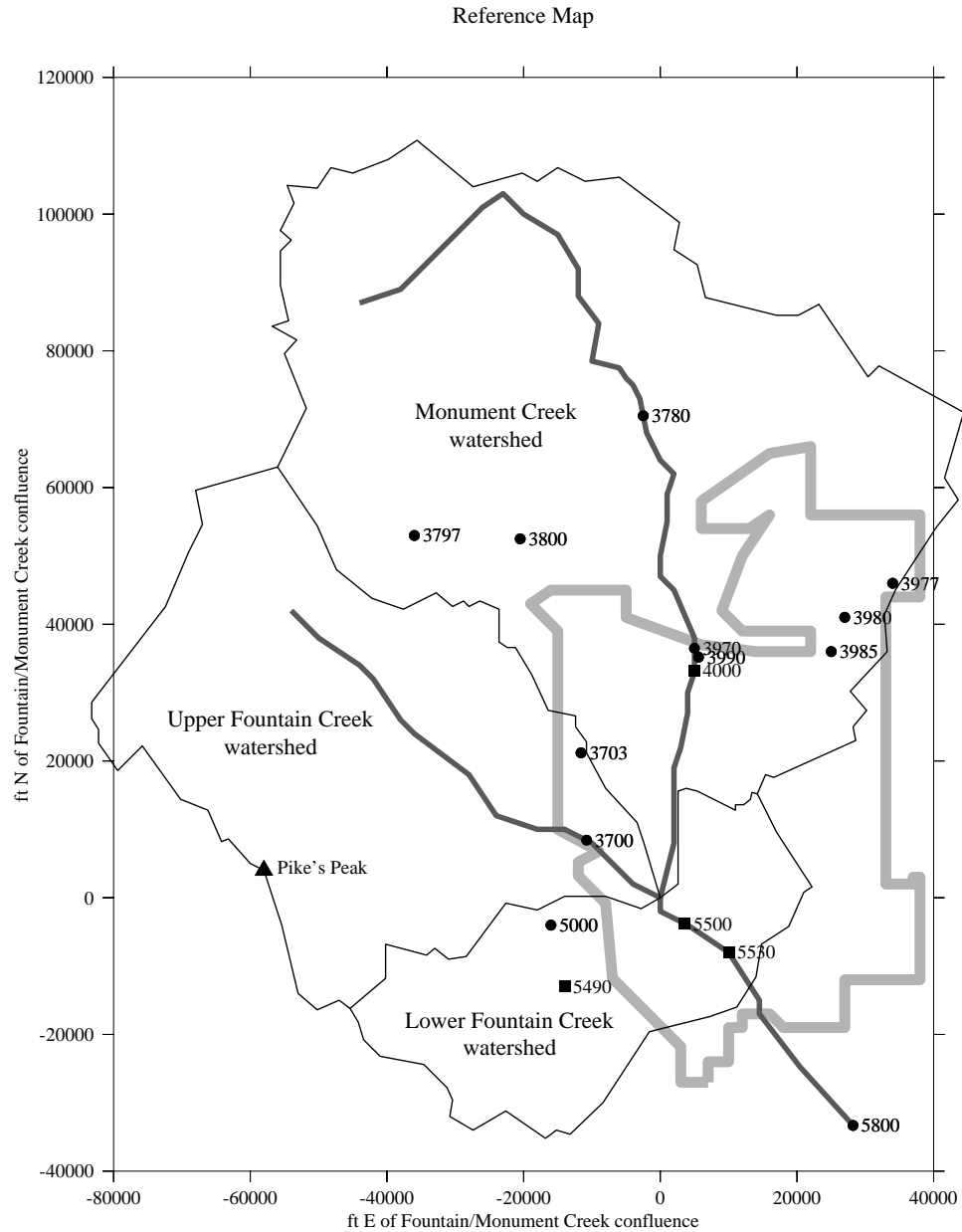


Figure 3.1: Locations of USGS stream gauges in the modeled watersheds. The approximate boundaries of the City of Colorado Springs are shown in light gray. Gauges are labeled by the last four digits of their USGS designator (0710xxxx). Names and locations of employed (filled boxes) and other (filled circles) gauges are listed in Table 3.1.

are located outside of regions of dense development and urbanization (USGS 07104000 and 07105490) and are expected to experience primarily low-intensity, long-response-time runoff processes. The two gauges located along Fountain Creek (USGS 07105500 and 07105530) are expected to be the most affected by high-intensity, short-response-time surface runoff from urbanized and developed surrounding areas.

### 3.2 Watershed Model

Sub-basin surface and routing parameters extracted from the data sources listed above were compiled for use in the U.S. Environmental Protection Agency (EPA) Storm Water Management Model (SWMM). Hydrologic production and routing of surface runoff during an applied rainfall event is handled by the RUNOFF block of SWMM. The general formulation of RUNOFF is described here, followed by a discussion of required parameters for input to the model.

#### 3.2.1 *RUNOFF Formulation and Procedure*

Generally, SWMM RUNOFF treats sub-basin areas as planar surfaces that are divided between pervious areas and impervious areas according to the specified impervious percentage. A schematic diagram of this division is shown in Figure 3.2

This schematic representation of a sub-basin area shows the pervious portion ( $A_2$ ), the impervious portion with depression storage ( $A_1$ ), and the impervious portion without depression storage ( $A_3$ ). All of these are derived from the specified total sub-basin area  $A$ , the specified impervious area  $I$  (as a percentage of  $A$ ), and a specified percentage  $I_{nds}$  of the impervious area that allows no depression storage. Respectively,

$$A_1 = \frac{I}{100} \left( 1 - \frac{I_{nds}}{100} \right) A, \quad (3.1)$$

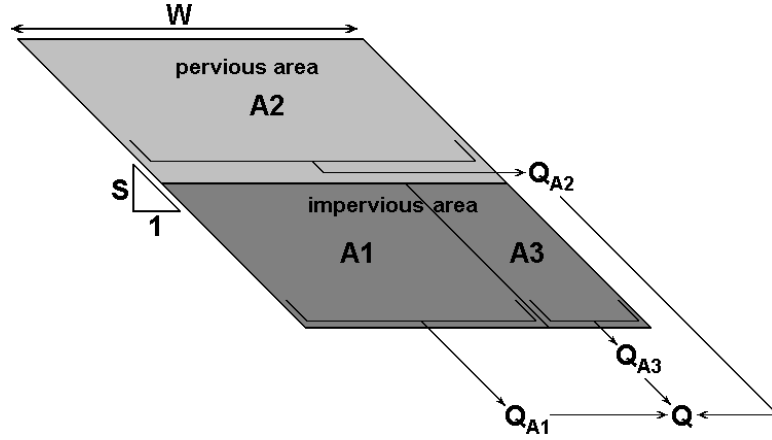


Figure 3.2: Schematic diagram of SWMM RUNOFF sub-basin representation. Indicated variables are described in the text.

$$A2 = \left(1 - \frac{I}{100}\right) A, \quad (3.2)$$

and

$$A3 = \frac{I}{100} \frac{I_{nds}}{100} A, \quad (3.3)$$

such that

$$A = A1 + A2 + A3. \quad (3.4)$$

Infiltration of rainfall occurs only on the pervious areas and is calculated here using the Horton model. In a recent study of infiltration models using widely varied soil types, Mishra et al. (2003) found that the semi-empirical Horton model performed better than the physical Green–Ampt model, which is also available for use in SWMM RUNOFF. The fundamental equation of the Horton model is given as

$$f_p(t) = f_\infty + (f_0 - f_\infty) \exp(-\alpha t), \quad (3.5)$$

where  $f_p(t)$  is the potential infiltration rate,  $f_0$  and  $f_\infty$  are the maximum (initial) and minimum (ultimate) infiltration rates, respectively, and  $\alpha$  is a decay parameter for the time-dependent relaxation of the infiltration rate from the initial value to the ultimate

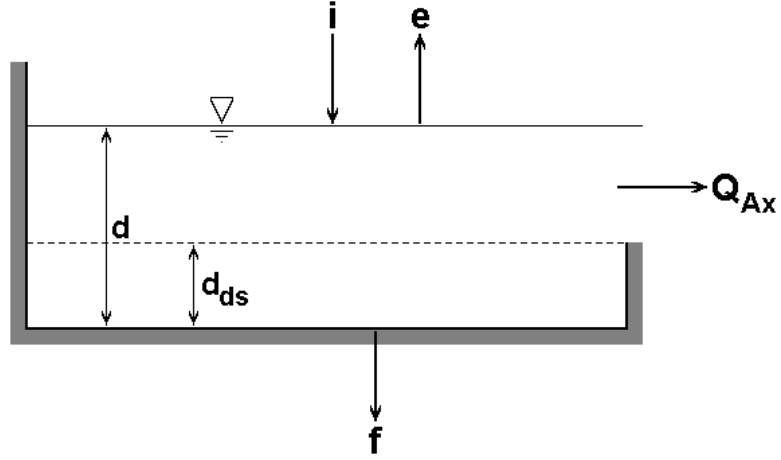


Figure 3.3: Schematic diagram of non-linear reservoir model for sub-basin areas. Indicated variables are described in the text.

value. The actual infiltration on a pervious surface is the lesser of the potential infiltration rate  $f_p(t)$  and the rate of incident rainfall  $i(t)$ , or

$$f(t) = \min [f_p(t), i(t)]. \quad (3.6)$$

Infiltration-excess runoff from a pervious surface, also known as Horton overland flow, occurs when  $i(t) > f_p(t)$ . For the impervious portion of the sub-basin area,  $f(t) = f_p(t) = 0$ , thus runoff occurs at all times for which  $i(t) \neq 0$ .

Runoff from each of the sub-basin areas is not directed over another area but is placed directly into the designated channel or “hydraulic load point.” A schematic diagram of the non-linear reservoir model that is applied to each portion of the sub-basin area is shown in Figure 3.3.

The runoff rate for each portion of the sub-basin area is then determined by a modified form of the Manning equation,

$$Q_{Ax}(t) = \frac{\Phi}{n_{Ax}} W_{Ax} [d(t) - d_{ds}]^{5/3} S^{1/2}, \quad (3.7)$$

where  $\Phi$  is a unit-based constant ( $\Phi = 1.49$  when using U.S. customary units;  $\Phi = 1$  when

using S.I. units),  $n_{Ax}$  is an area-specific surface roughness parameter,  $W_{Ax}$  is the width of the portion,  $d(t)$  is the depth of overland flow,  $d_{ds}$  is the portion-specific depth of surface depression storage, and  $S$  is the specified sub-basin surface slope. It should be noted that

$$n_{A1} = n_{A3} \quad (3.8)$$

for the impervious areas,

$$W_{A1} = \left(1 - \frac{I_{nds}}{100}\right) W_{A2} \quad (3.9)$$

and

$$W_{A3} = \frac{I_{nds}}{100} W_{A2} \quad (3.10)$$

such that

$$W_{A1} + W_{A3} = W_{A2}, \quad (3.11)$$

where  $W_{A2}$  is the specified sub-basin width, and

$$S_{A1} = S_{A2} = S_{A3}. \quad (3.12)$$

The overland flow depth  $d(t)$  for each area is determined using a continuity equation,

$$\frac{dd(t)}{dt} = i(t) - f(t) - e(t) - \frac{Q_{Ax}(t)}{Ax}, \quad (3.13)$$

where  $i(t)$  and  $f(t)$  are the rainfall and infiltration rates, respectively and as described above,  $e(t)$  is a specified evaporation rate, and  $Ax$  represents  $A1$ ,  $A2$ , or  $A3$  as appropriate.

The combined runoff from pervious and impervious portions of a sub-basin area is found by

$$Q(t) = Q_{A1}(t) + Q_{A2}(t) + Q_{A3}(t). \quad (3.14)$$

The total sub-basin discharge  $Q(t)$  is then routed through the specified drainage network from channel to channel by integration of the continuity equation,

$$\frac{dS(t)}{dt} = Q_{inflow} - Q_{outflow}, \quad (3.15)$$

where  $S(t)$  is the stored volume of water in a particular channel segment, along with the use of the Manning equation,

$$Q = \frac{\Phi}{n_{chan}} A^{5/3} P^{-2/3} S_{chan}^{1/2}, \quad (3.16)$$

where  $\Phi$  is a unit-based constant (as above),  $n_{chan}$  is a specified channel surface roughness parameter,  $A$  is the channel-geometry-dependent cross-sectional area of the flow,  $P$  is the wetted (channel) perimeter of the flow, and  $S_{chan}$  is the specified channel slope. Where no further channels are specified in the drainage network, the time series of inflow to the designated end junction is saved by the SWMM RUNOFF program in a specified file for input to other portions of the program, such as a hydraulic model (SWMM TRANSPORT or SWMM EXTRAN).

Further discussion of the information required for adequate representation of the watershed sub-basins and drainage channels in the SWMM RUNOFF model is included here.

### 3.2.2 *RUNOFF Data Requirements*

In addition to time step and general calculation parameters provided to the model, data requirements for the RUNOFF block include those rainfall, sub-basin surface and channel routing parameters discussed above. These parameters are listed in Table 3.2. Additional data such as sub-basin and channel coordinates (in feet or meters north and east of a reference point) may be provided in a separate file and are useful in spatial representations of the constructed model. It should be noted, however, that these coordinates are not employed in the calculation of sub-basin sizes, drainage channel lengths, or other physical parameters relevant to the processes of runoff production and routing in this model.

Table 3.2: Listing of SWMM RUNOFF input parameters.

<b>Rainfall records (“hyetographs”) at hourly time intervals</b>
<p><b>Sub-basin surface parameters</b></p> <ul style="list-style-type: none"> <li>• Sub-basin name or other unique identifier</li> <li>• Index/identifier of applied rainfall hyetograph</li> <li>• Hydraulic load point (name of receiving channel for routing)</li> <li>• Sub-basin width (typ. in ft)</li> <li>• Sub-basin total area (typ. in acres)</li> <li>• Sub-basin imperviousness, as a percentage of total sub-basin area</li> <li>• Average sub-basin surface slope (typ. in ft/ft)</li> <li>• Manning roughness coefficients (“<i>n</i>”) for pervious and impervious areas</li> <li>• Surface depression depth for pervious and impervious areas (typ. in inches)</li> <li>• Maximum and minimum infiltration rates for Horton equation (typ. in inches/hr)</li> <li>• Infiltration rate decay coefficient for Horton equation (typ. in sec<sup>-1</sup>)</li> </ul>
<p><b>Runoff routing parameters</b></p> <ul style="list-style-type: none"> <li>• Channel name or other unique identifier</li> <li>• Hydraulic load point (name/identifier of next channel in routing sequence)</li> <li>• Indexed shape of channel (trapezoidal, circular pipe, etc.)</li> <li>• Channel bottom width or pipe diameter (typ. in ft)</li> <li>• Channel length (typ. in ft)</li> <li>• Average channel slope (typ. in ft/ft)</li> <li>• Left- and right-side lateral slopes for trapezoidal channels (typ. in ft/ft)</li> <li>• Manning roughness coefficient (“<i>n</i>”) for channel material</li> <li>• Total channel depth (typ. in ft)</li> <li>• Initial depth of water in channel (typ. in ft)</li> </ul>

### 3.2.3 Sub-basin Parameters

For the model constructed here, sub-basins specified for the areas covered by the Fountain Creek and Monument Creek Drainage Basin Planning Studies (FCDBPS and MCDBPS, respectively) were aggregated where surface parameters such as land use and land cover, ground slope, applied hyetograph, sub-basin width and hydraulic load point would remain consistent. This procedure allowed a reduction in the total number of sub-basins for which input parameters would be compiled. Together, the FCDBPS and MCDBPS specified a total of 365 sub-basins covering a total area of 415.5 mi<sup>2</sup>. Using this sub-basin aggregation procedure, this model represents a total area of more than 495 mi<sup>2</sup> (including areas outside of those previous studies) with 233 sub-basins.

For each specified sub-basin, area-weighted-mean values for imperviousness and infiltration rates were calculated using tabular data listed in the available planning studies.

Complete listings of the sub-basin surface parameters employed for the simulations described here are included in the SWMM RUNOFF input files listed in Appendix C. Of some importance here is the naming convention for sub-basins in the RUNOFF model: the names of sub-basins in this model were derived from basin names and numerical designators listed in the FCDBPS and MCDBPS tables. These names are linked directly to those of the receiving channel segments, as described below.

### *Imperviousness*

In the case of imperviousness, it should be recognized that SWMM RUNOFF relies on the *directly connected impervious area* (DCIA) for its calculations of surface runoff production. The DCIA is typically some fraction of the total impervious area (TIA) in a developed basin, though *a priori* calculation of this fraction for large areas is often difficult or ambiguous. As a brief example, we may consider the effects of two components of imperviousness after the work of Schueler (1994): rooftops (e.g. homes, commercial buildings, etc.), and transport systems (e.g. driveways, sidewalks, streets and highways).

Though rooftops may present an impervious surface to rainfall, the resulting rooftop runoff is often collected in gutters that direct the runoff onto a pervious surface, such as a lawn or other undeveloped surface. However, in densely urbanized areas, the rooftop runoff may be conveyed by gutter systems directly into the street or storm sewer system. For transport systems, which typically lie on or above ground, gutter systems most often direct surface runoff into the storm sewer system, whether that is a surface channel or subsurface conduit. The DCIA considers only that portion of impervious surfaces from which runoff is conveyed directly to the storm sewer system, and not across some intervening pervious surface where infiltration may occur. In this sense, the conceptualization of DCIA

is consistent with the sub-basin schematic employed in the formulation of SWMM RUNOFF as shown in Figure 3.2.

The DCIA can be a much larger fraction of the total impervious area in a sub-basin that is densely developed with a high density of transport systems (e.g.  $\sim 90\%$  total impervious area), such as a downtown commercial or municipal district, than in a sub-basin with more distributed development (e.g.  $\sim 40\%$  total impervious area) such as a residential subdivision. The procedure discussed here employs the lower end of each range of imperviousness listed in the tables of sub-basin surface data presented in the Drainage Basin Planning Studies. Specifically, portions of sub-basins with imperviousness fractions in the ranges of 0-5%, 5-15%, 15-40%, 40-70%, and 70-100% were listed there. Thus, the portion of a sub-basin (as a percentage of sub-basin area, typically) that was listed with 5-15% impervious area is here considered the same portion of the sub-basin area with 5% imperviousness. Similarly, the portion of a sub-basin that has been listed with 70-100% impervious area is considered the same portion of the sub-basin area with 70% imperviousness. Aggregate imperviousness values as a single percentage are then calculated for each sub-basin, based on these area-weighted values, according to

$$DCIA = \frac{\sum_i A_i I_{L,i}}{\sum_i A_i}, \quad (3.17)$$

where  $A_i$  is the fraction of the total sub-basin area occupied by the imperviousness classification for which the low-end value is given by  $I_{L,i}$ .

Additional methods for the calculation of DCIA may be formulated, including simple modifications of the above such as replacement of the range-minimum imperviousness  $I_L$  with the range-average or range-maximum. However, it would be difficult to justify a formulation based on the range-average imperviousness without detailed knowledge of the

statistical distribution of land use within the sub-basin, and employment of the range-maximum imperviousness may actually result in a net increase between the given TIA and the desired DCIA. Alternative methods for the reduction of TIA to DCIA have been suggested by Alley and Veenhuis (1983) and Lee and Heaney (2003). The former study presented a functional reduction according to

$$DCIA = 0.15 (TIA)^{1.41}, \quad (3.18)$$

such that ranges of imperviousness, which are generally consistent with specific land uses, are discarded in favor of detailed calculations over the studied area. In this case, detailed knowledge of the actual (as compared with the statistical) distribution of land use within the sub-basin is required for confidence in the accuracy of DCIA calculation. Similarly, the method employed by Lee and Heaney (2003) requires knowledge of the spatial distribution of land use and transport systems that may be obtained only with detailed investigation of aerial photographs and available survey data.

Though such analyses remain beyond the scope of this work, some example calculations of DCIA using equations (3.17) and (3.18) are listed in Table 3.3, where aggregate values of TIA employed for equation (3.18) are found by

$$TIA = \frac{\sum_i A_i I_{A,i}}{\sum_i A_i}, \quad (3.19)$$

using the range-average imperviousness  $I_A$ . It is demonstrated there that the DCIA calculated using equation (3.17) is greater than that found using equations (3.18) and (3.19) in lightly and moderately developed areas, but is generally less than that found by the latter method in heavily developed areas. The implications and results of these differences in DCIA when applied to the model described here are left to future work.

Table 3.3: Example calculations of sub-basin directly connected impervious area (DCIA). Values of total impervious area (TIA) are given as the portion (%) of total sub-basin area with the listed range of total imperviousness. Calculations using eq. (3.17) employ the range-minimum imperviousness in the direct calculation of DCIA, while those using eq. (3.18) after Alley and Veenhuis (1983) employ the range-average imperviousness in the calculation of aggregate TIA by eq. (3.19) before the given functional reduction to DCIA.

Total Impervious Area (%)						DCIA (%)	
0-5%	5-15%	15-40%	40-70%	70-100%	Total	eq. (3.17)	eq. (3.18)
100	0	0	0	0	100	0.00	0.55
50	50	0	0	0	100	2.50	1.99
25	50	25	0	0	100	6.25	5.28
0	50	50	0	0	100	10.00	9.35
0	50	25	25	0	100	16.25	14.53
20	20	20	20	20	100	26.00	23.47
10	15	20	25	30	100	34.75	33.67
0	0	25	25	50	100	48.75	51.81
0	0	0	25	75	100	62.50	69.18
0	0	0	0	100	100	70.00	78.81

Table 3.4: Horton infiltration parameters, after UDFCD USDCM Table RO-7.

SCS/NRCS Hydrologic Soil Group	General Soil Character	Infiltration Rates (in/hr)		Decay Coeff. $\alpha$ ( $s^{-1}$ )
		$f_0$	$f_\infty$	
A	sand/gravel	5.0	1.0	0.0007
B	silt-loam	4.5	0.6	0.0018
C	clay-loam	3.0	0.5	0.0018
D	clay	3.0	0.5	0.0018

### *Infiltration Rates*

The calculation of average parameters for hydrologic soil groups present in a given sub-basin proceeded as follows. First, the maximum and minimum infiltration rates and decay coefficients for each soil group present in the sub-basin were calculated using recommended Horton equation parameters from Table RO-7 in Volume I of the Denver Urban Drainage and Flood Control District (UDFCD) Urban Storm Drainage Criteria Manual (USDCM). These parameters rely on hydrologic soil classifications established by the U.S. Soil Conservation Service (SCS) and the U.S. Natural Resources Conservation Service (NRCS). Some of that information regarding soil types and infiltration parameters is reproduced here in Table 3.4.

The infiltration parameters resulting from these calculations were then aggregated for each sub-basin based on the percentage of the sub-basin area to which each soil group was assigned in the tables of source data. This calculation is similar to that employed above for the determination of aggregate DCIA for each sub-basin:

$$f_0 = \frac{\sum_i A_i f_{0,i}}{\sum_i A_i}, \quad (3.20)$$

$$f_\infty = \frac{\sum_i A_i f_{\infty,i}}{\sum_i A_i}, \quad (3.21)$$

and

$$\alpha = \frac{\sum_i A_i \alpha_i}{\sum_i A_i} \quad (3.22)$$

for the parameters employed in equation (3.5) above.

A similar method was applied to the additional modeled areas south of Colorado Springs that are included in this model but for which completed Drainage Basin Planning Studies were not available. It was found upon consultation with SCS/NRCS maps (listed in section 1.4) that the major portions of those sub-basins fell within single hydrologic soil groups.

It should be noted that the subsurface flow of infiltrated water is excluded from the model and simulations presented here. This subsurface flow typically occurs in two layers during a rainfall event: a near-surface, near-saturated layer of “through-flow” or “interflow” that moves slowly toward the stream, and a deeper layer of groundwater flow that typically occurs below the stream bottom. The interflow has a relatively slow time of response to the infiltrated fraction of incident rainfall and its magnitude is typically small. The contribution of interflow to changes in the surface stream discharge is generally neglected

in flood studies, due to the significantly greater contribution of surface runoff to the stream discharge hydrograph.

### *Hydrograph Separation*

The much slower process of groundwater flow is a mechanism by which the discharge in a stream or river may change in periods during which no contributing rainfall or snowmelt is recorded. The stream discharge during these dry periods is often termed “base flow” and remains important to the accurate simulation of observed hydrographs for isolated storm events. In the simulations discussed here, the model hydrographs are added to a derived base flow function that is based on the gauged discharges immediately prior to the beginning of the storm event and at least twelve hours following the end of the storm event. The combined (simulated discharge + base flow) hydrograph is then compared with that observed at the gauged locations for accuracy. The four available stream discharge records at USGS gauge locations listed in the upper portion of Table 3.1, along with their corresponding derived base flow functions, are shown in Figure 3.4. Specifically, the discharge record and base flow function for USGS gauge 07104000 is shown in Figure 3.4a, for USGS gauge 07105490 in Figure 3.4b, for USGS gauge 07105500 in Figure 3.4c, and for USGS gauge 07105530 in Figure 3.4d. Calculated statistics for these discharge records are listed in Table 3.5, where the mean discharge is designated by  $\mu_Q$ , the standard deviation by  $\sigma_Q$ , the total (5-day) discharge volume by  $V_Q$ , and the lag-1 serial correlation coefficient by  $\rho_{1,Q}$ . the formulations of these statistics will be given in Section 3.3 below. These statistics will be important for the determination of simulation accuracy in Chapter 4.

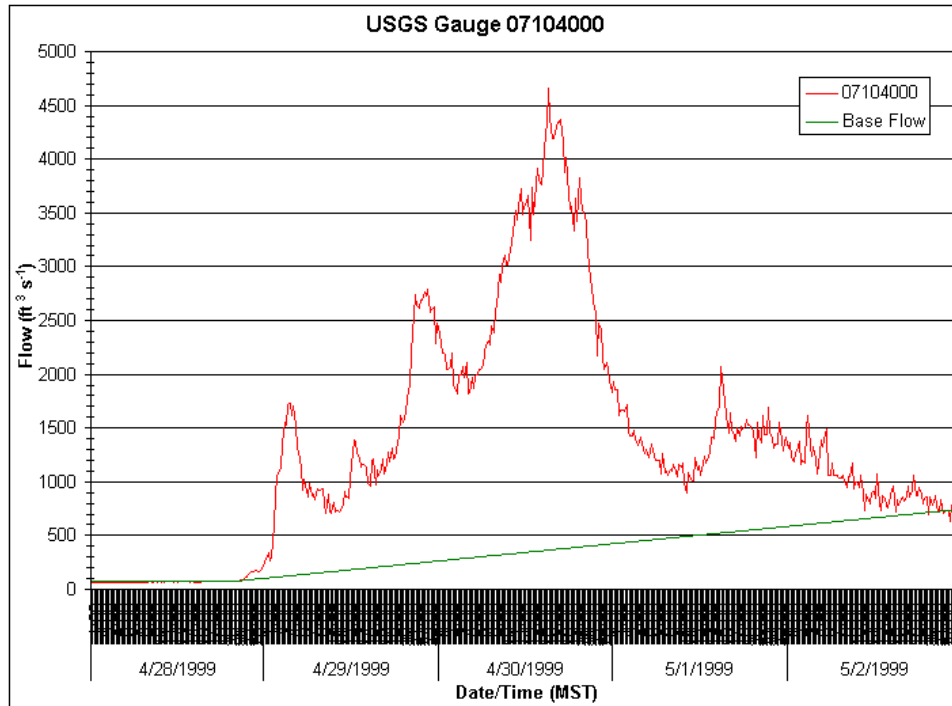


Figure 3.4a: Stream discharge (red) and base flow (green) at USGS gauge 07104000.

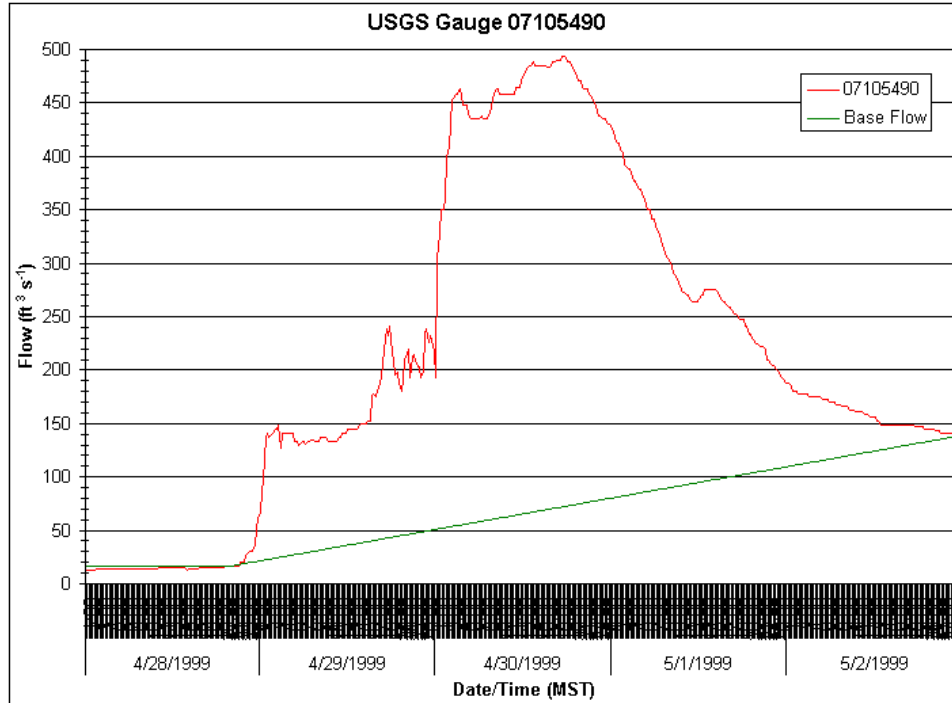


Figure 3.4b: Stream discharge (red) and base flow (green) at USGS gauge 07105490.

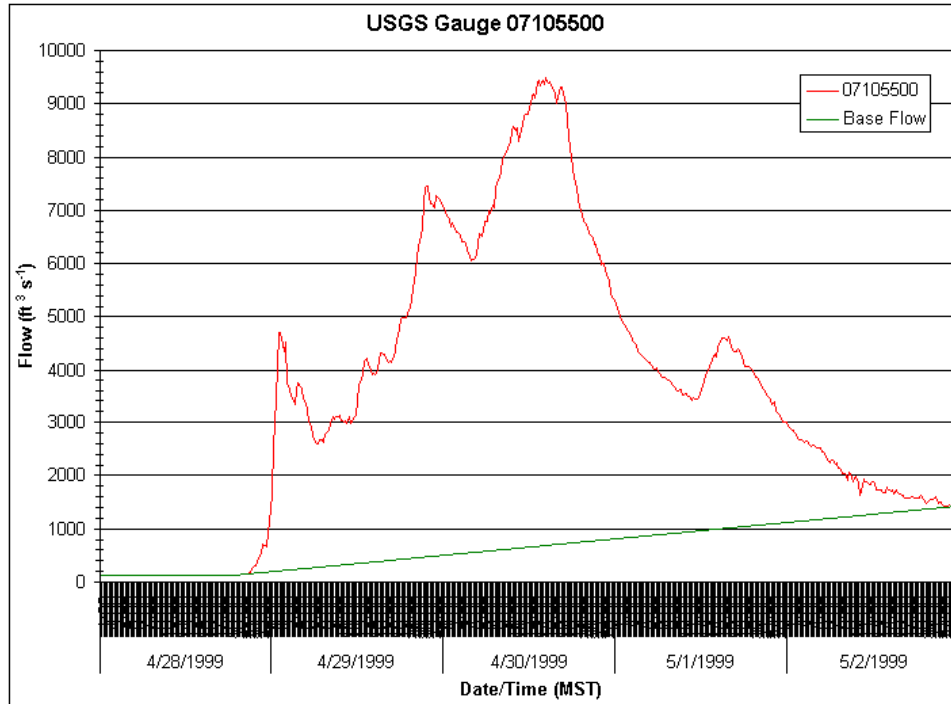


Figure 3.4c: Stream discharge (red) and base flow (green) at USGS gauge 07105500.

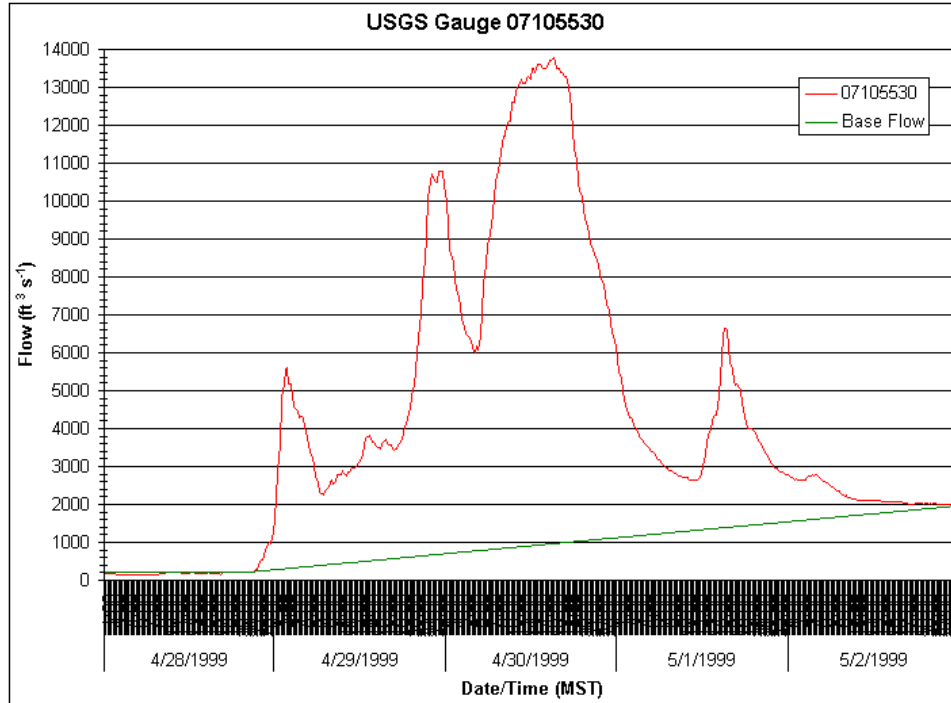


Figure 3.4d: Stream discharge (red) and base flow (green) at USGS gauge 07105530.

Table 3.5: Summary of observed hydrograph statistics at selected USGS gauge locations.

Hydrograph Statistic	USGS Gauge			
	07104000	07105490	07105500	07105530
Contributing Area (mi <sup>2</sup> )	204	21.7	392	413
Base Flow (ft <sup>3</sup> s <sup>-1</sup> )	73.0	16.0	137.0	200.0
$\mu_Q$ (ft <sup>3</sup> s <sup>-1</sup> )	1507.4	253.0	4172.6	4748.0
$\max[Q]$ (ft <sup>3</sup> s <sup>-1</sup> )	4660.0	494.0	9490.0	13800.0
$\sigma_Q$ (ft <sup>3</sup> s <sup>-1</sup> )	1004.5	134.9	2376.9	3701.4
$V_Q$ (ac-ft)	13236.1	2117.1	35260.5	41692.3
$\rho_{1,Q}$	0.9914	0.9981	0.9982	0.9982

### 3.2.4 Routing Network Formulation

The delineation of runoff channels proceeded generally with the extraction of channel lengths and slopes from either HEC-1 input files (for the area covered by the Fountain Creek Drainage Basin Planning Study) or USGS topographic maps (for the remaining watershed area). An overall plan of the constructed watershed network is shown in Figure 3.5. Labeled portions of the network plan are shown in Figures 3.6a (Northwest area), 3.6b (North area), 3.6c (East area), 3.6d (Central area), 3.6e (West area), 3.6f (Southwest area), and 3.6g (Southeast area). Sub-basin positions shown in these figures should be considered generally representative of geographical location, but were not employed in the calculation of basin sizes, channel length, or other surface parameters important to the proper simulation of runoff production and routing processes.

In addition to the watershed network plan, other views of the network are sometimes useful in the determination of physical consistency. Using the slopes and lengths of only the RUNOFF channels, the distance from and elevation above the network outlet (point 07105800 in Figure 3.6g) can be calculated and are plotted in Figure 3.7a. That figure demonstrates the generally concave-upward shape of channel longitudinal profiles, consistent with common observations of drainage network and natural river evolution over long times (Knighton 1998). The total (upstream) area drained by each RUNOFF channel is plotted

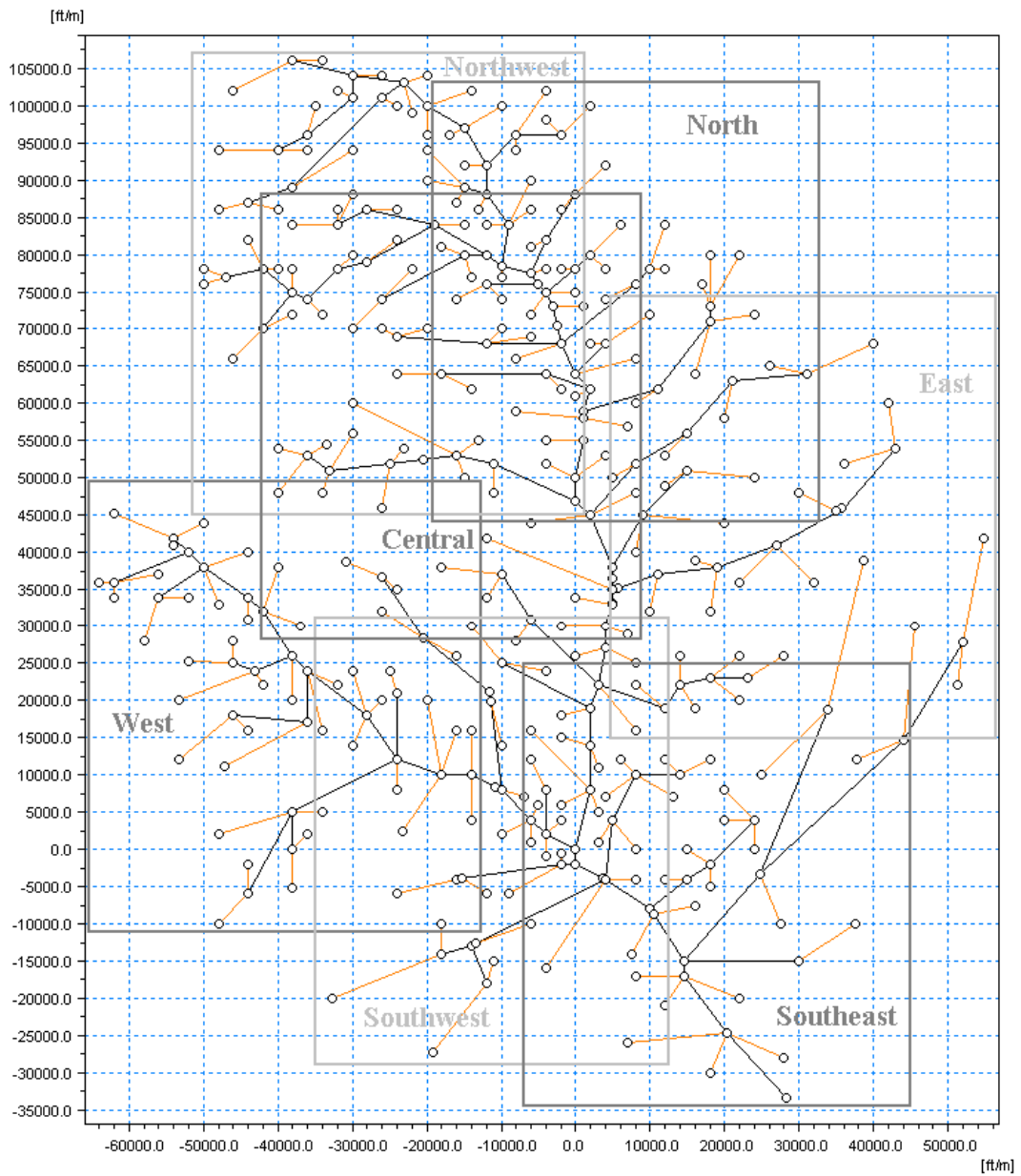


Figure 3.5: Overall plan of constructed watershed network. Coordinates are given in feet north and east of the confluence of Monument and Fountain Creeks in Colorado Springs, Colorado.

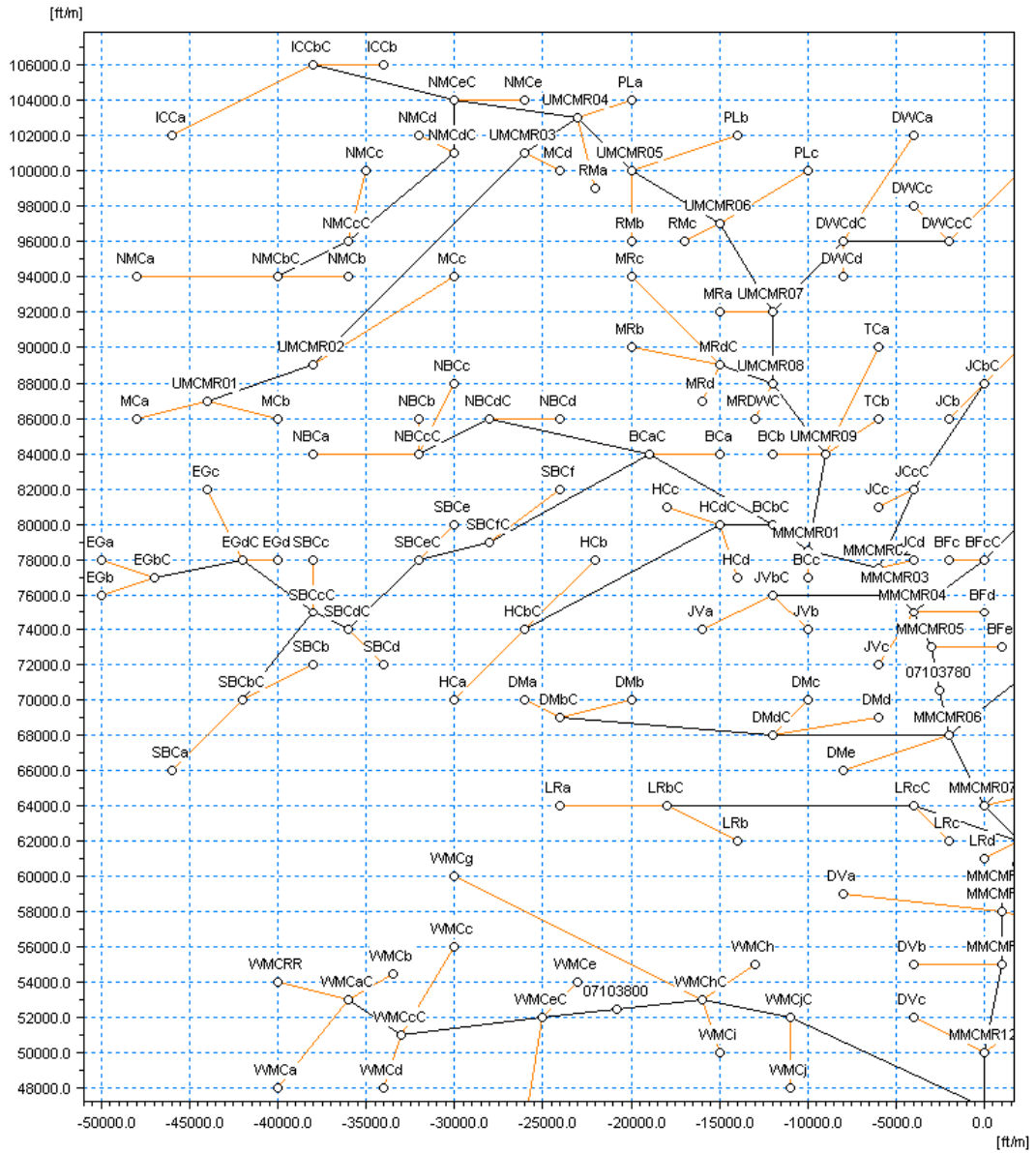


Figure 3.6a: Northwest area of constructed watershed network. Coordinates are given in feet north and east of the confluence of Monument and Fountain Creeks in Colorado Springs, Colorado.

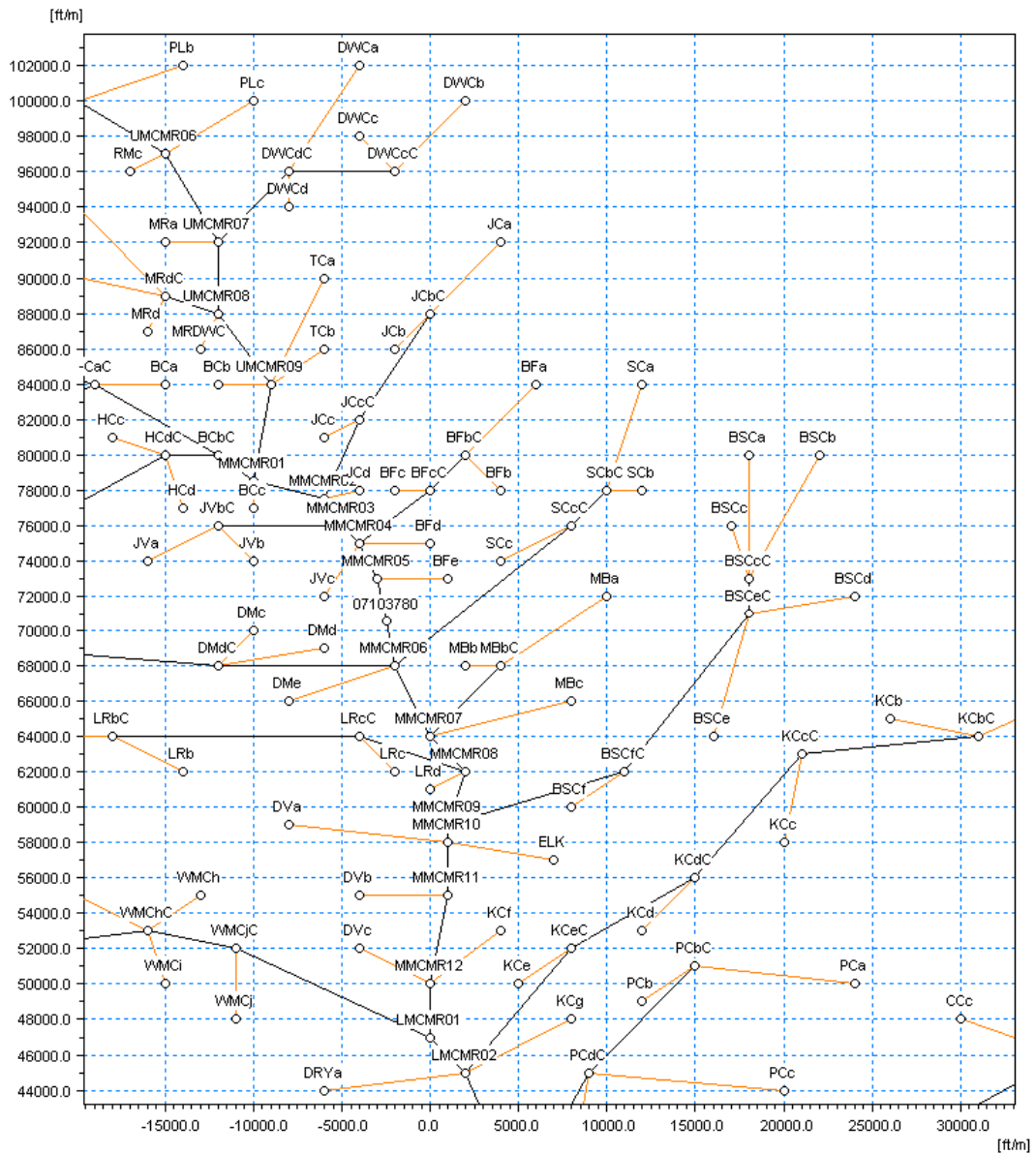


Figure 3.6b: Northeast area of constructed watershed network. Coordinates are given in feet north and east of the confluence of Monument and Fountain Creeks in Colorado Springs, Colorado.



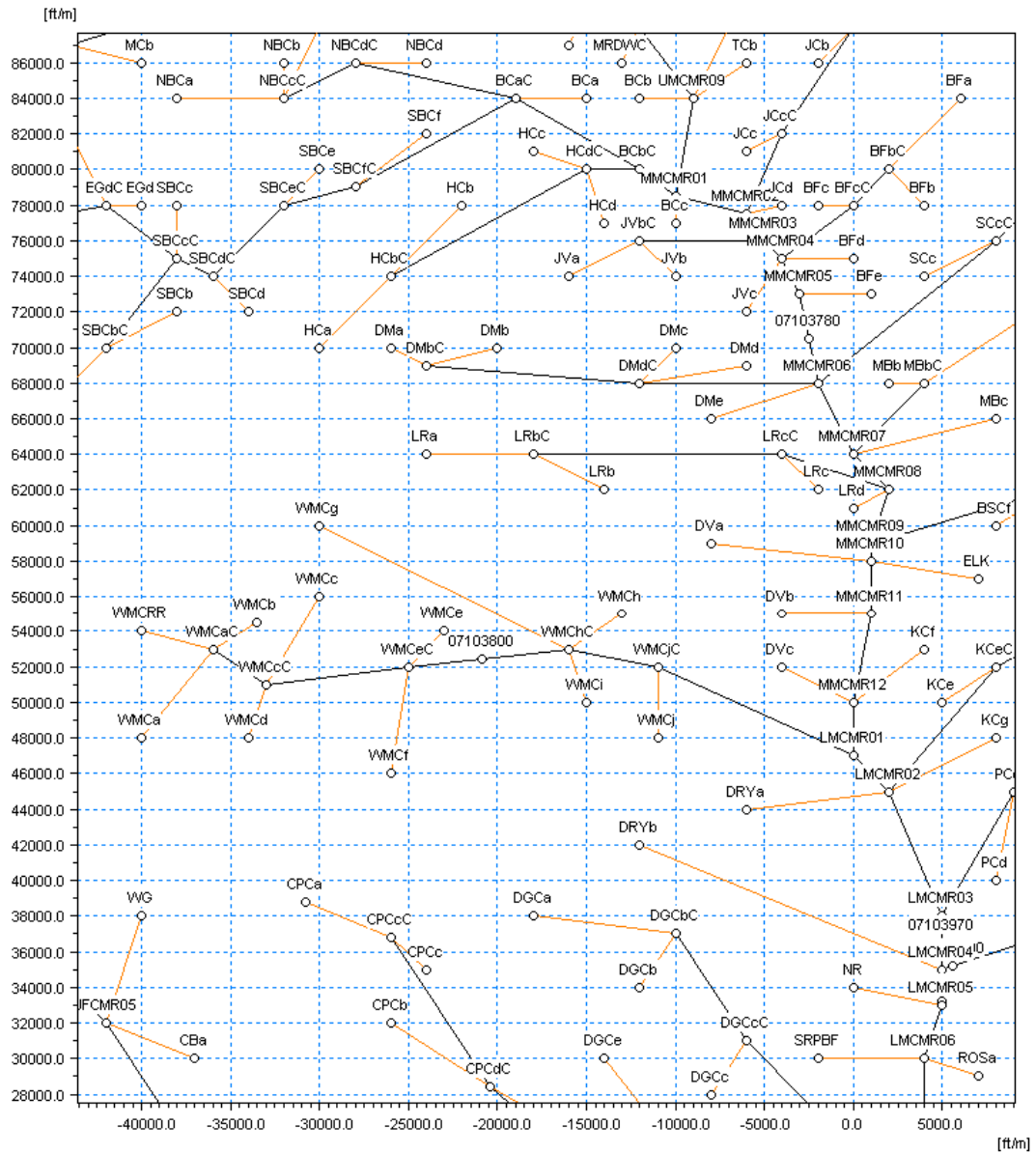


Figure 3.6d: Central area of constructed watershed network. Coordinates are given in feet north and east of the confluence of Monument and Fountain Creeks in Colorado Springs, Colorado.

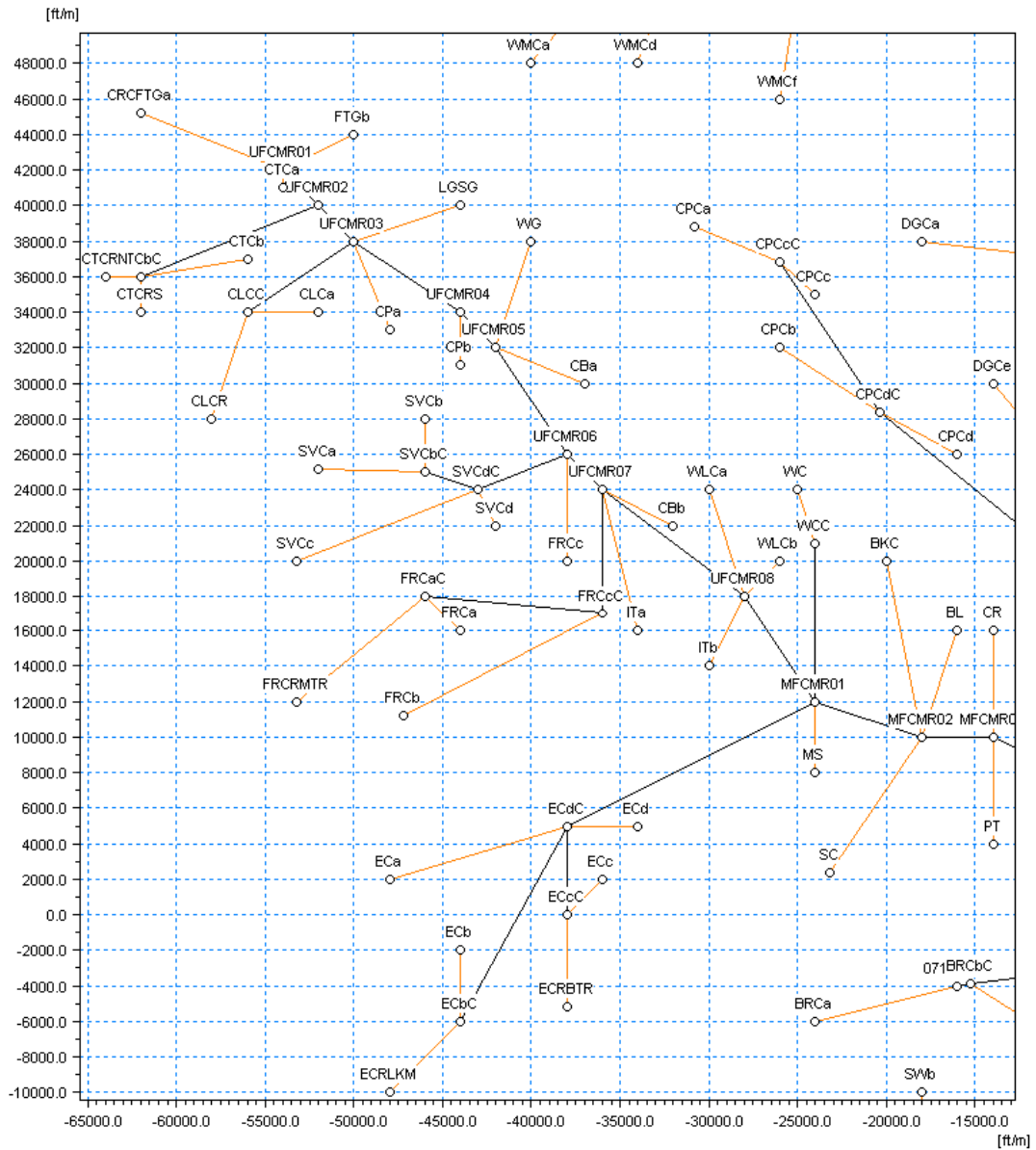


Figure 3.6e: West area of constructed watershed network. Coordinates are given in feet north and east of the confluence of Monument and Fountain Creeks in Colorado Springs, Colorado.

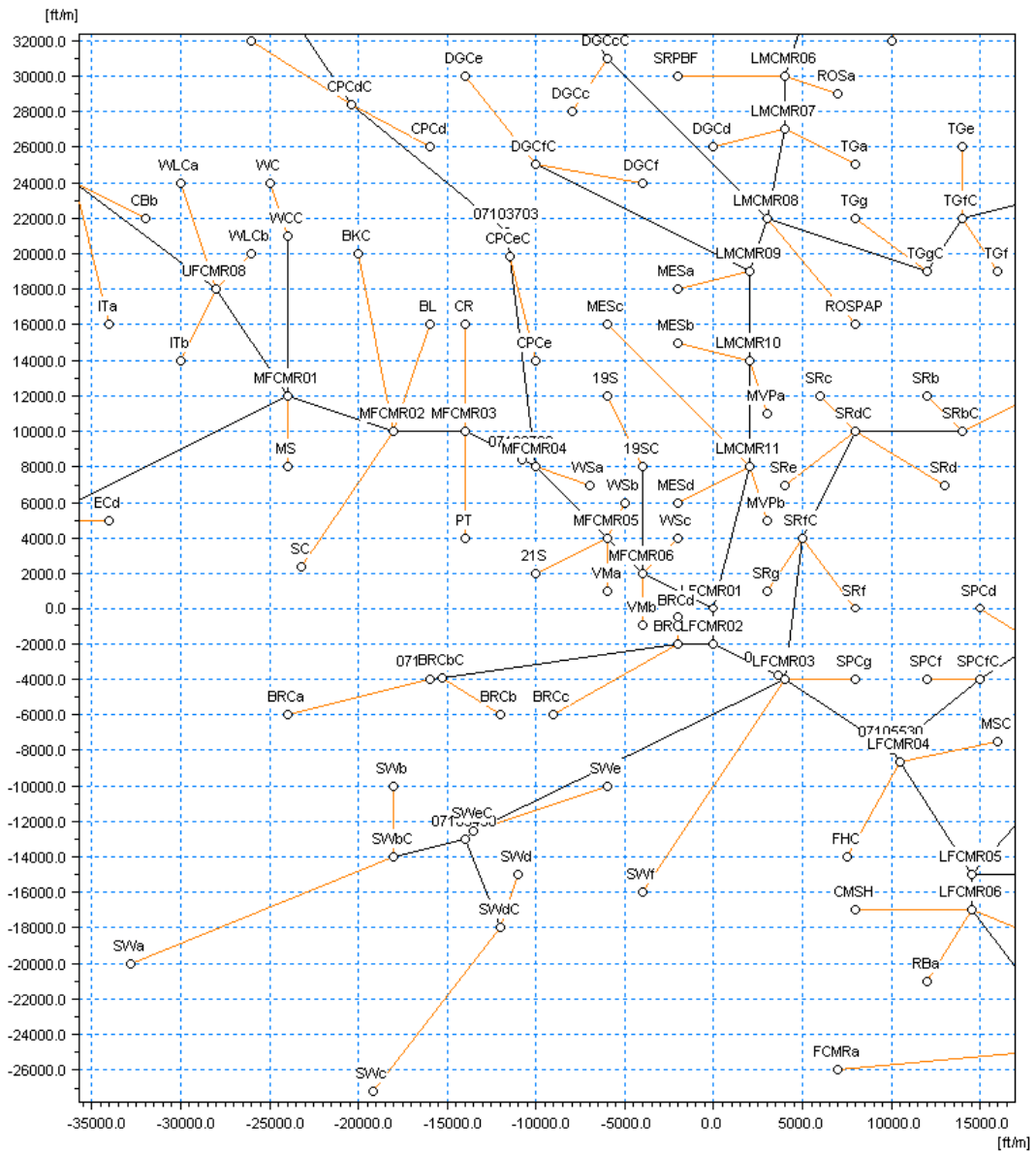


Figure 3.6f: Southwest area of constructed watershed network. Coordinates are given in feet north and east of the confluence of Monument and Fountain Creeks in Colorado Springs, Colorado.

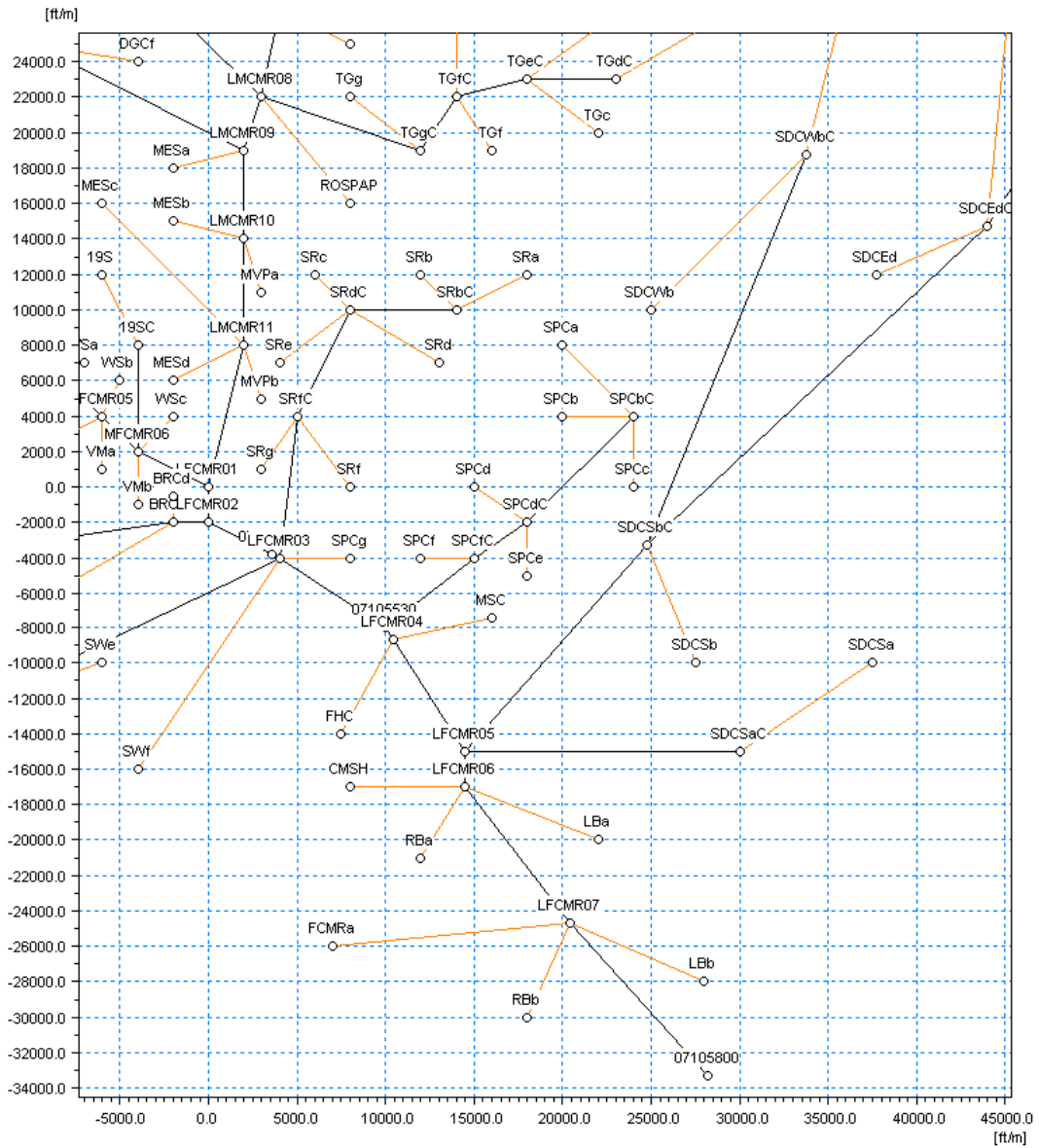


Figure 3.6g: Southeast area of constructed watershed network. Coordinates are given in feet north and east of the confluence of Monument and Fountain Creeks in Colorado Springs, Colorado.

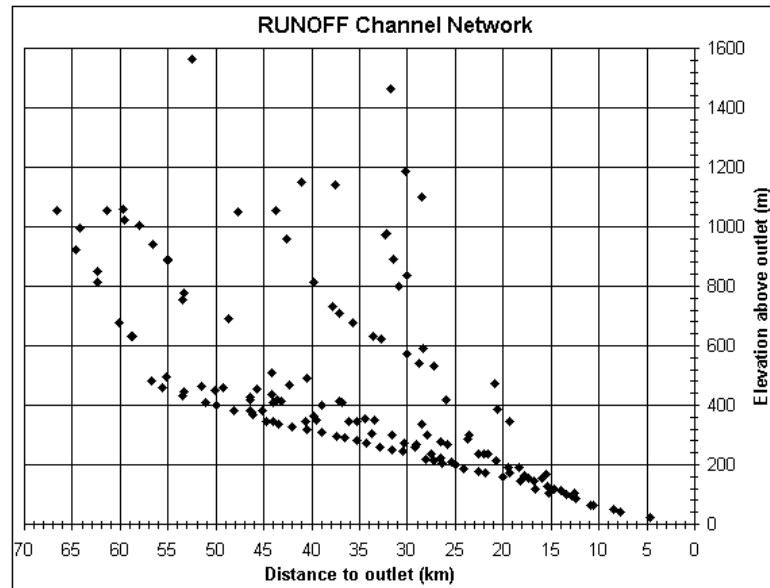


Figure 3.7a: Plot of network channel distance from and elevation above outlet.

with respect to along-channel distance from the network outlet in Figure 3.7b. This plot demonstrates noticeable trends toward greater total drainage area at locations closer to the network outlet, even along the tributary reaches. A similar plot of relative elevation with respect to total drainage area is shown in Figure 3.7c, demonstrating a general trend toward greater drainage areas at lower elevations as well as the overall relief of the modeled watershed areas.

Using the constructed basin plan, an order (index) was assigned to each stream segment (runoff channel) according to a modified Strahler (1964) ordering scheme. The rules of the applied scheme are given here:

- (1) The smallest channels are implicit in the delineated sub-basins, may generally flow only during wet weather, and are designated order 1.
- (2) Where two (or more) channels of the same order join, the downstream channel is of the next higher order.

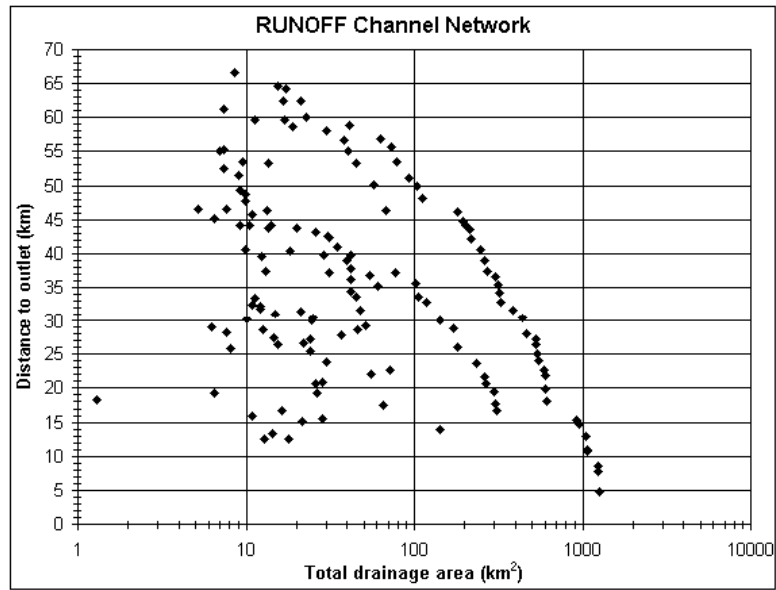


Figure 3.7b: Plot of network channel distance from outlet vs. total drainage area.

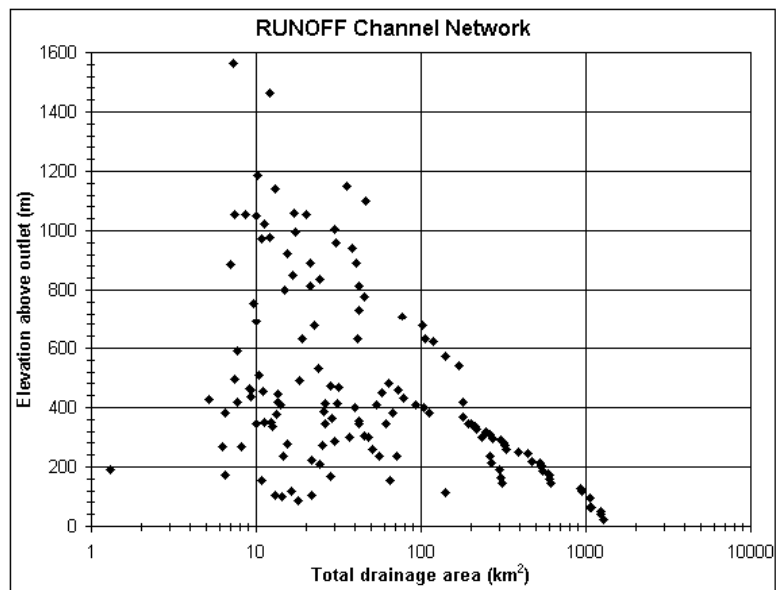


Figure 3.7c: Plot of network channel elevation above outlet vs. total drainage area.

- (3) Where a channel of lower order joins a channel of any higher order, the downstream channel is of the higher order.

An example schematic of this ordering scheme as applied to stream segments in the upper Fountain Creek watershed is shown in Figure 3.8.

The assigned order of each stream channel was then employed in the specification of channel bottom widths and total channel depths for the conveyance of expected surface runoff flows from the entire contributing (upstream) area. In the course of simulation, however, it was found that several channels were expected to convey much greater discharges and volumes than this system would permit. In order to prevent errors that could be attributed to the delayed or attenuated routing of channel overflows, the width and depth dimensions of these channels were alternately increased until it was found that they conveyed all required discharges. So as to simulate the effective widening of a given channel by bank erosion and overflow onto its floodplain before increasing its depth by processes of scour and bed erosion, channel widths were increased before their depths during this alternation. This sometimes resulted in the apparent shift of a channels order to the next higher order. The likelihood of realizing *a priori* the need for such a shift of some stream orders may be related to the imperviousness of the contributing area, but a systematic relationship remains unclear without further analysis that is beyond the scope of this work.

The shapes of channels that may be simulated using the RUNOFF model include regular (e.g. rectangular, trapezoidal, parabolic) geometries. For simplicity, and to approximate the natural configurations of stream channels as accurately as possible with the available methods, streams in the Fountain and Monument Creek watershed were represented using trapezoidal channels with 45° lateral side slopes. Manning roughness (“*n*”) coefficients indicate the channel’s frictional resistance to flow and were extracted from HEC-

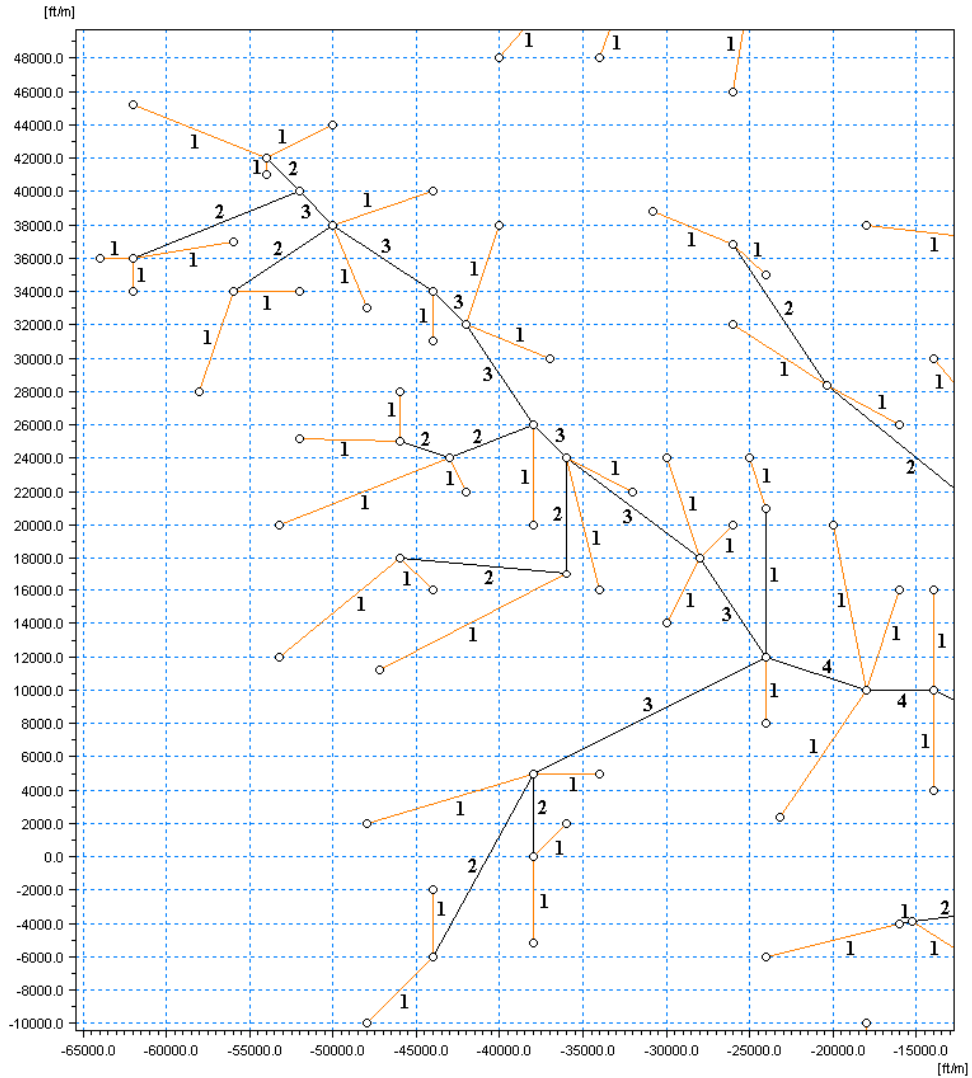


Figure 3.8: Example application of modified Strahler scheme to network channels. The rules of this ordering scheme are given in the text. Sub-basin and channel labels for this region (the upper Fountain Creek watershed) are shown in Figure 3.6e. Coordinates are given in feet north and east of the confluence of Monument and Fountain Creeks in Colorado Springs, Colorado.

1 input files for the FCDBPS area. For the remainder of the watershed areas modeled here, the FCDBPS roughness coefficients were employed where an adequate analogy between likely channel morphology could be found.

The naming convention for channels in the RUNOFF model presented here was derived from stream orders and natural geographic divisions of watershed areas. For tributary streams, as examples, the designator TGgC labels the stream that runs adjacent to or through sub-basin TGg and is also known as the Templeton Gap Floodway. The designator SPCbC labels the portion of Spring Creek that runs adjacent to or through sub-basin SPCb, which is different from SBCbC (a portion of South Beaver Creek adjacent to sub-basin SBCb) and SCbC (a portion of Severy Creek adjacent to sub-basin SCb). For main streams, as examples, the designator UFCMR01 labels Upper Fountain Creek Mainstem Reach number 01; the designator MMCMR12 labels Middle Monument Creek Mainstem Reach number 12; the designator LFCMR04 labels Lower Fountain Creek Mainstem Reach number 04. As such, any channel designator is intended to help the modeler (and reader) identify the general geographic area and watershed basin or sub-basin in which that stream channel occurs.

### 3.2.5 *Routing Network Diagnostics*

For the stream network ordered by the method described above, certain diagnostic parameters may be obtained and evaluated against accepted values for other studied systems. The formulation of these parameters is attributed to Horton (1945) and are found as ratios of stream numbers, lengths and drainage areas between streams of successive order. The bifurcation ratio  $R_B$  is found from

$$N_i = R_B^{\Omega-i}, \quad (3.23)$$

where  $N_i$  is the number of streams of order  $i$  in the network, and  $\Omega$  is the highest order of all streams in the network, that is, the order of the stream segment that reaches the network outlet. Taking the  $\log_{10}$  of both sides and rearranging,

$$\begin{aligned}\log_{10}N_i &= (\Omega - i) \log_{10}R_B, \\ &= (-\log_{10}R_B) i + \Omega \log_{10}R_B.\end{aligned}$$

Assuming a linear function fitted to the set of values  $(i, \log_{10}N_i)$  as  $(x, y)$  with the form  $y = mx + b$ , where  $m$  is the slope of the function and  $b$  is its  $y$ -intercept, the value of the bifurcation ratio is found as  $R_B = 10^{-m/B}$ . The calculated value of  $R_B$  for this channel network is given below.

The length ratio  $R_L$  is found from

$$\overline{L}_i = \overline{L}_1 R_L^{i-1} \quad (3.24)$$

by an equivalent method, where  $\overline{L}_i$  is the average length of stream segments of order  $i$ . The area ratio  $R_A$  is similarly found from

$$\overline{A}_i = \overline{A}_1 R_A^{i-1}, \quad (3.25)$$

where  $\overline{A}_i$  is the average drainage area of stream segments of order  $i$ .

The compiled stream number, length and drainage area statistics are listed in Tables 3.6, 3.7 and 3.8, respectively. Corresponding figures demonstrating the fitted linear functions are shown in Figures 3.9, 3.10 and 3.11, respectively.

Horton ratios for this drainage network were found as  $R_B = 2.23$ ,  $R_L = 2.28$ , and  $R_A = 3.93$ . Commonly observed and widely accepted values for these Horton ratios are often given as  $3 \leq R_B \leq 5$  with a theoretical minimum value of  $R_B = 2$ ,  $1.5 \leq R_L \leq 3.5$ , and  $3 \leq R_A \leq 6$ . The values of the length ratio  $R_L$  and the area ratio  $R_A$  for the drainage

Table 3.6: Calculation of Horton bifurcation ratio for constructed channel network. The title “DS Channel Order” refers to the number of channels with the indicated order located immediately downstream of channels of order  $i$ .

Order $i$	DS Channel Order					$N_i$	$\log N_i$
	1	2	3	4	5		
1	4	147	32	42	11	236	2.3729
2	0	40	20	16	3	79	1.8976
3	0	0	17	4	2	23	1.3617
4	0	0	0	27	2	29	1.4624
5	0	0	0	0	7	7	0.8451
Total	4	187	69	89	25	374	—

Table 3.7: Calculation of Horton length ratio for constructed channel network.

Order $i$	$N_i$	$\Sigma L_i$ (km)	$\bar{L}_i$ (km)	$\bar{L}_i/\bar{L}_1$	$\log(\bar{L}_i/\bar{L}_1)$
1	236	245.03	1.04	1.00	0.0000
2	79	393.37	4.98	4.80	0.6809
3	23	202.88	8.82	8.50	0.9292
4	29	521.30	17.98	17.31	1.2384
5	7	233.17	33.31	32.08	1.5063

Table 3.8: Calculation of Horton area ratio for constructed channel network.

Order $i$	$N_i$	$\Sigma A_i$ (km <sup>2</sup> )	$\bar{A}_i$ (km <sup>2</sup> )	$\bar{A}_i/A_1$	$\log(\bar{A}_i/A_1)$
1	236	1296.96	5.50	1.00	0.0000
2	79	1705.09	21.58	3.93	0.5941
3	23	1992.55	86.63	15.76	1.1977
4	29	10583.31	364.94	66.41	1.8222
5	7	8805.58	1257.94	228.90	2.3596

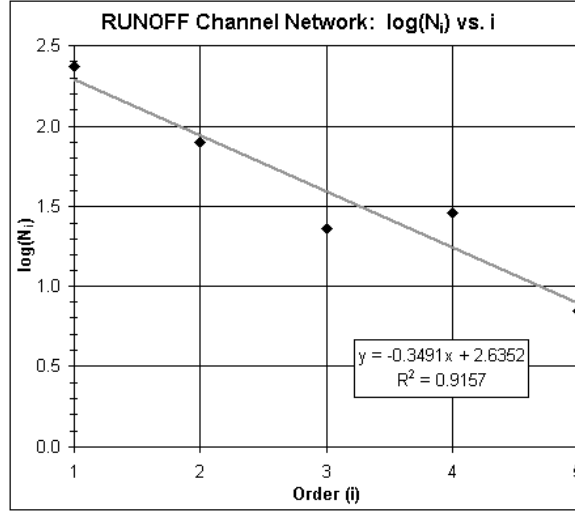


Figure 3.9: Determination of Horton bifurcation ratio by fitted linear function. The data employed here are listed in Table 3.6 according to the method described in the text.

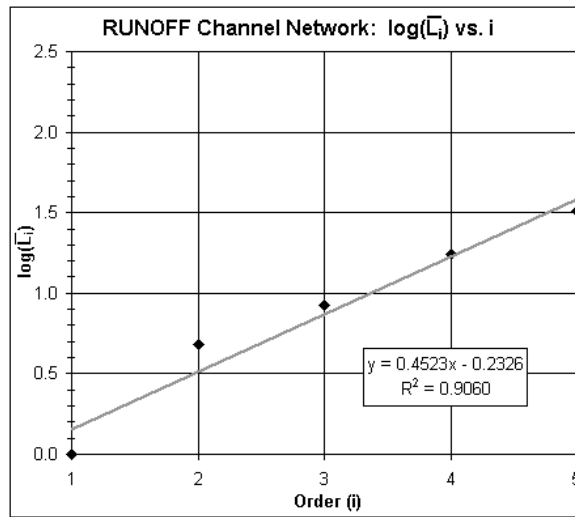


Figure 3.10: Determination of Horton length ratio by fitted linear function. The data employed here are listed in Table 3.7 according to the method described in the text.

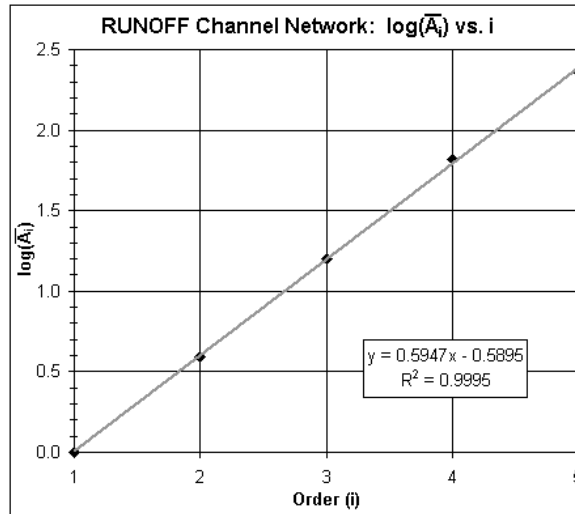


Figure 3.11: Determination of Horton area ratio by fitted linear function. The data employed here are listed in Table 3.8 according to the method described in the text.

network constructed here occur within these accepted ranges, but the value of the bifurcation ratio  $R_B$  falls below the range of commonly observed stream networks (though still above the minimum theoretical value for  $R_B$ ). This may be due to an over-simplification of the drainage network for this model, and could likely be corrected with a detailed review of sub-basin areas and re-assignment of stream orders on a case-by-case basis throughout the study watershed. As the obtained value for  $R_B$  is still acceptable, such a review is currently beyond the scope of this work. It may be concluded that, while oversimplified to some degree, the specified channel network adequately represents the real channel network in the Monument and upper Fountain Creek watersheds. With regard to the accuracy of discharge simulations, the occurrence of  $R_A$  and  $R_L$  within observed ranges is encouraging with respect to the proper representation of runoff generation and flow timing processes, respectively.

### 3.2.6 *Application of Recorded Rainfall Data*

A method is described here by which recorded rainfall data at hourly and daily gauges in and near the Monument and Fountain Creek watersheds are applied to the SWMM RUNOFF model. Spatially, rainfall records were assigned to RUNOFF sub-basins according to the nearest neighbor or “Thiessen” (1911) polygon method. Temporally, rainfall records at gauges for which only daily totals were available were disaggregated to hourly intervals by a quadrant-based nearest neighbor method using inverse-distance-squared weighting. The formulation of this method is given below.

#### *Thiessen Polygons*

For the assignment of rainfall records to specified sub-basins in SWMM RUNOFF, this work relied on the delineation of Thiessen polygons using a representative map of the model network. Thiessen polygons result from the simple “nearest-neighbor” method of spatial disaggregation (Thiessen 1911), such that the rainfall gauge and corresponding hourly record assigned to a modeled sub-basin is that which is located closest to the sub-basin in the RUNOFF network. Thus, for a system of  $M$  rainfall gauges and their corresponding records applied to a watershed of  $S$  sub-basins, where  $S > M$ , there will be  $M$  distinct rainfall records represented in the watershed model. For this work, no further spatial interpolation of rainfall gauge records to subdivided areas was performed.

The applied spatial distributions of rainfall records for the gauge network shown in Figure 2.4, with gauge locations listed in Table 2.2, are given here. For the network of only hourly rainfall gauges (nos. 1–6), the applied Thiessen polygons are shown in Figure 3.12a. For the complete existing network of rainfall gauges (nos. 1–14), the applied Thiessen polygons are shown in Figure 3.12b.

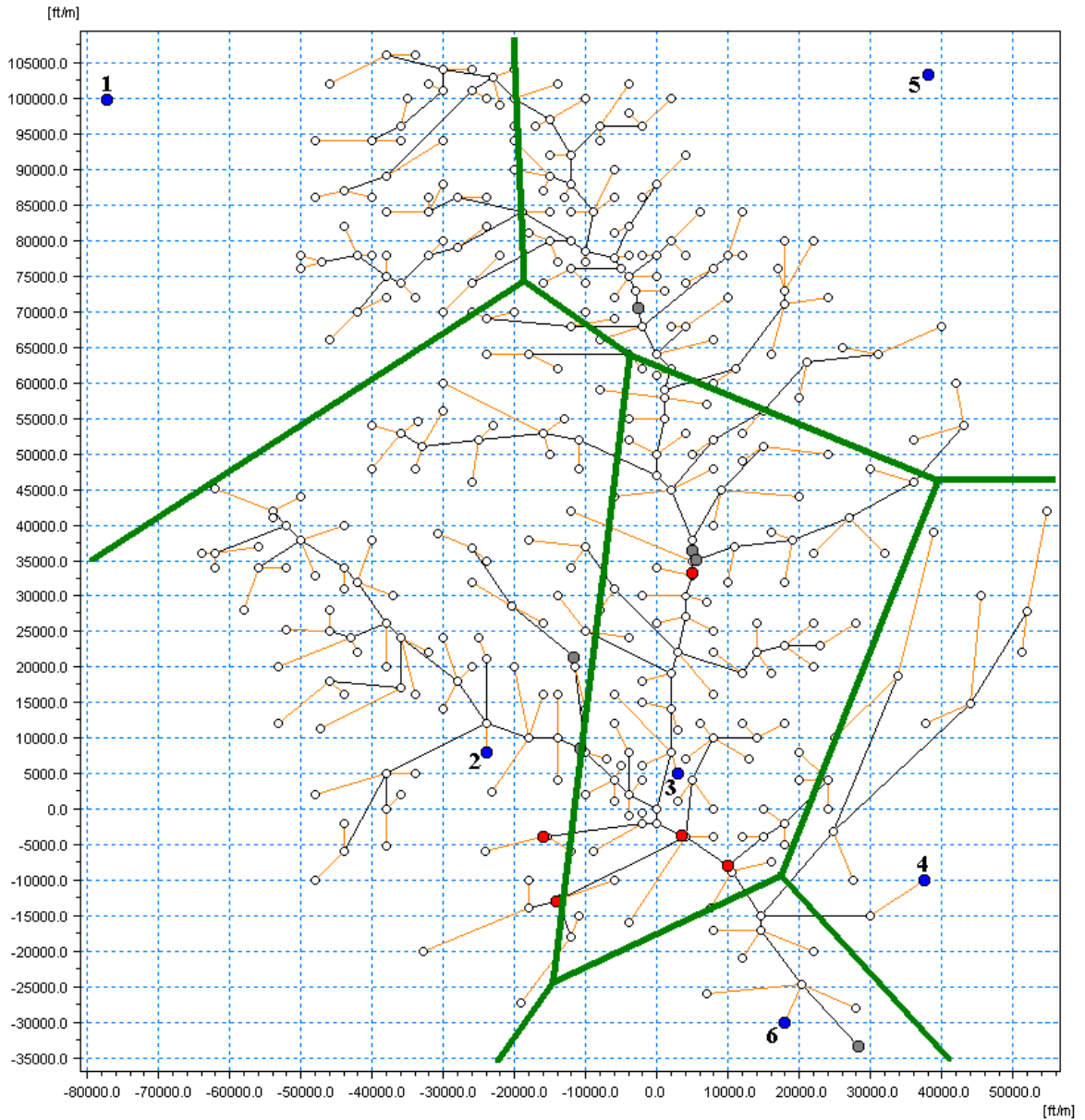


Figure 3.12a: Thiessen polygons for existing hourly rainfall gauges (nos. 1–6). Gauge locations are listed in Table 2.2.

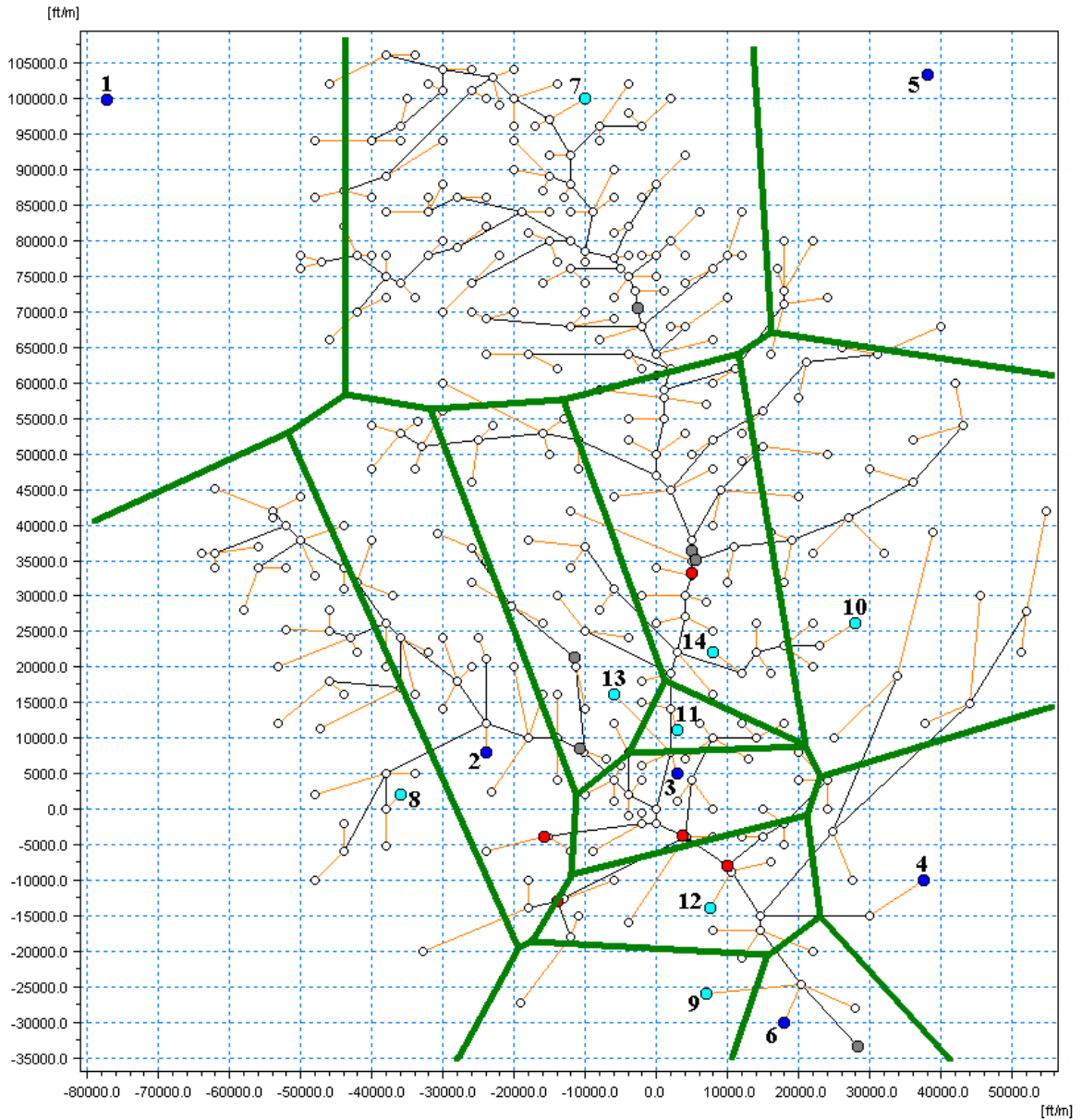


Figure 3.12b: Thiessen polygons for all existing rainfall gauges (nos. 1–14). Gauge locations are listed in Table 2.2.

*Disaggregation of Daily Rainfall Data*

An inverse-distance-squared calculation was applied to quadrant-based nearest neighbors for (1) the determination of missing daily total rainfall values at two stations, and (2) the disaggregation of daily rainfall data to hourly intervals for input to the SWMM RUNOFF model. This method was derived from available documentation for the NWS River Forecast System (NWSRFS; <http://hydrology.nws.noaa.gov/oh/hrl/nwsrfs.htm>).

The daily total rainfall data during April 28–May 2, 1999, for the hourly and daily gauges employed in this work are listed in Table 3.9. For the values listed there in *italicized* type, daily total rainfall data were originally missing. These values were determined by a quadrant-based nearest-neighbor method using all available surrounding gauges.

Specifically, for each missing datum, the area surrounding the affected gauge was divided into quadrants bounded by the North–South and West–East axes. In each quadrant, the nearest gauge with available rainfall data was then selected, and the weight assigned to that gauge was determined by

$$w_{ij} = \frac{1}{d_{ij}^2}, \quad (3.26)$$

where  $i$  is the index or representative label for the gauge with a missing datum,  $j$  is that for the nearest available gauge in the quadrant, and  $d_{ij}$  is the distance between the two gauges as calculated using the map locations listed in Table 2.2:

$$d_{ij} = \left[ (X_j - X_i)^2 + (Y_j - Y_i)^2 \right]^{1/2}. \quad (3.27)$$

By this method, the weights for a total of  $J$  nearby gauges were determined for each gauge with a missing datum, where  $J = 1 \dots 4$ . The missing datum was then calculated by

$$P_{i,d} = \sum_{j=1}^J \frac{w_{ij} P_{j,d}}{W_i}, \quad (3.28)$$

Table 3.9: Daily (April 28–May 2, 1999) and event total rainfall at precipitation gauges in and near the Monument and Fountain Creek watersheds. Values listed in *italics* are explained in the text.

Gauge Number	Gauge Name	Daily total rainfall (in)					Event Total (in)
		Apr 28	Apr 29	Apr 30	May 1	May 2	
1	Woodland Park 8 NNW	0.60	0.60	0.90	0.20	0.10	2.40
2	Manitou Springs	0.50	4.70	1.60	0.60	0.40	7.80
3	Colorado College	1.19	3.57	3.58	0.96	0.06	9.36
4	Colorado Springs	0.35	1.78	2.64	0.82	0.16	5.75
5	Greenland 9 SE	0.70	1.80	2.50	0.60	0.10	5.70
6	Pinello Ranch	0.22	0.42	0.11	0.20	0.00	0.95
7	(Town of) Monument	0.08	3.99	1.57	0.68	0.10	6.42
8	Ruxton Park	0.51	2.30	0.61	0.03	0.00	3.45
9	Fort Carson	0.00	1.21	2.37	<i>0.34</i>	<i>0.02</i>	3.94
10	Old Farm	0.30	2.43	2.93	0.62	0.46	6.74
11	Monument Valley Park	0.92	3.40	3.43	0.86	0.07	8.68
12	Quail Lake	0.43	2.31	2.44	0.80	0.09	6.07
13	Water Operations	1.57	4.05	2.98	0.75	0.08	9.43
14	4-Diamond Sports Complex	<i>1.05</i>	<i>3.21</i>	3.31	0.75	0.06	8.38

where  $P_{j,d}$  is the total rainfall for day  $d$  at gauge  $j$ , and  $W_i$  is the sum of hourly station weights assigned to gauge  $i$  found by

$$W_i = \sum_{j=1}^J w_{ij}. \quad (3.29)$$

For the disaggregation of daily total rainfall data at gauges where no hourly data were available (see Tables 2.2 and 3.9), the procedure was similar to that begun with equations (3.26) and (3.27) except that  $j$  represents the index of the nearest hourly gauge in each quadrant. The rainfall at daily gauge  $i$  for hour  $h$  of the event was then found by

$$p_{i,h} = P_{i,d} \sum_{j=1}^J \frac{w_{ij} p_{j,h}}{W_i P_{j,d}}, \quad (3.30)$$

where  $P_{i,d}$  ( $P_{j,d}$ ) is the total daily rainfall at gauge  $i$  ( $j$ ),  $p_{j,h}$  is the rainfall for hour  $h$  at hourly gauge  $j$ , and  $W_i$  is the sum of hourly station weights assigned to daily gauge  $i$  found by equation (3.29).

This method was applied to the rainfall gauges for which only daily total rainfall data is available. The hourly stations and distances assigned to each daily gauge are listed in Table 3.10, and the corresponding station weights are listed in Table 3.11. The resulting hourly rainfall records at each daily gauge are shown in Figure 3.13.

### 3.2.7 *Formulation of Supplemental Rainfall Records*

The reader will recall that large portions of the Monument and Fountain Creek watersheds, especially in locations upstream of Colorado Springs and in the nearby foothills, remain ungauged with respect to rainfall and stream discharge measurements. The reference maps provided in Figures 2.4 and 3.1 indicate that large areas north and west of the confluence of Monument and Fountain Creeks remain ungauged with respect to rainfall, and that the numerous tributaries of Monument Creek in that region are only sparsely gauged with respect to stream discharge.

Table 3.10: Precipitation gauge distances for disaggregation of daily total rainfall to hourly intervals. The corresponding station weights are given in Table 3.11.

Daily Gauge $i$	Distance to selected hourly gauge $j$ (ft)					
	1	2	3	4	5	6
7	67254	93059	95885	—	48107	—
8	105660	13416	—	—	—	62769
9	—	—	31257	34442	—	11705
10	128245	—	32650	37232	77845	—
11	119300	—	6000	40389	98620	—
12	—	—	19526	30265	—	19138
13	109596	19698	14213	—	97672	—
14	115061	—	17720	43523	86565	—

Table 3.11: Precipitation gauge weights for disaggregation of daily total rainfall to hourly intervals. The corresponding station distances are given in Table 3.10

Daily Gauge $i$	Weight for selected hourly gauge $j$ ( $10^{-10}$ ft $^{-2}$ )						$W_i$ (ft $^{-2}$ )
	1	2	3	4	5	6	
7	2.21	1.15	1.09	—	4.32	—	$8.77 * 10^{-10}$
8	0.896	55.6	—	—	—	2.54	$5.90 * 10^{-9}$
9	—	—	10.2	8.43	—	73.0	$9.17 * 10^{-9}$
10	0.608	—	9.38	7.21	1.65	—	$1.89 * 10^{-9}$
11	0.703	—	278	6.13	1.03	—	$2.86 * 10^{-8}$
12	—	—	26.2	10.9	—	27.3	$6.45 * 10^{-9}$
13	0.833	25.8	49.5	—	1.05	—	$7.72 * 10^{-9}$
14	0.755	—	31.8	5.28	1.33	—	$3.92 * 10^{-9}$

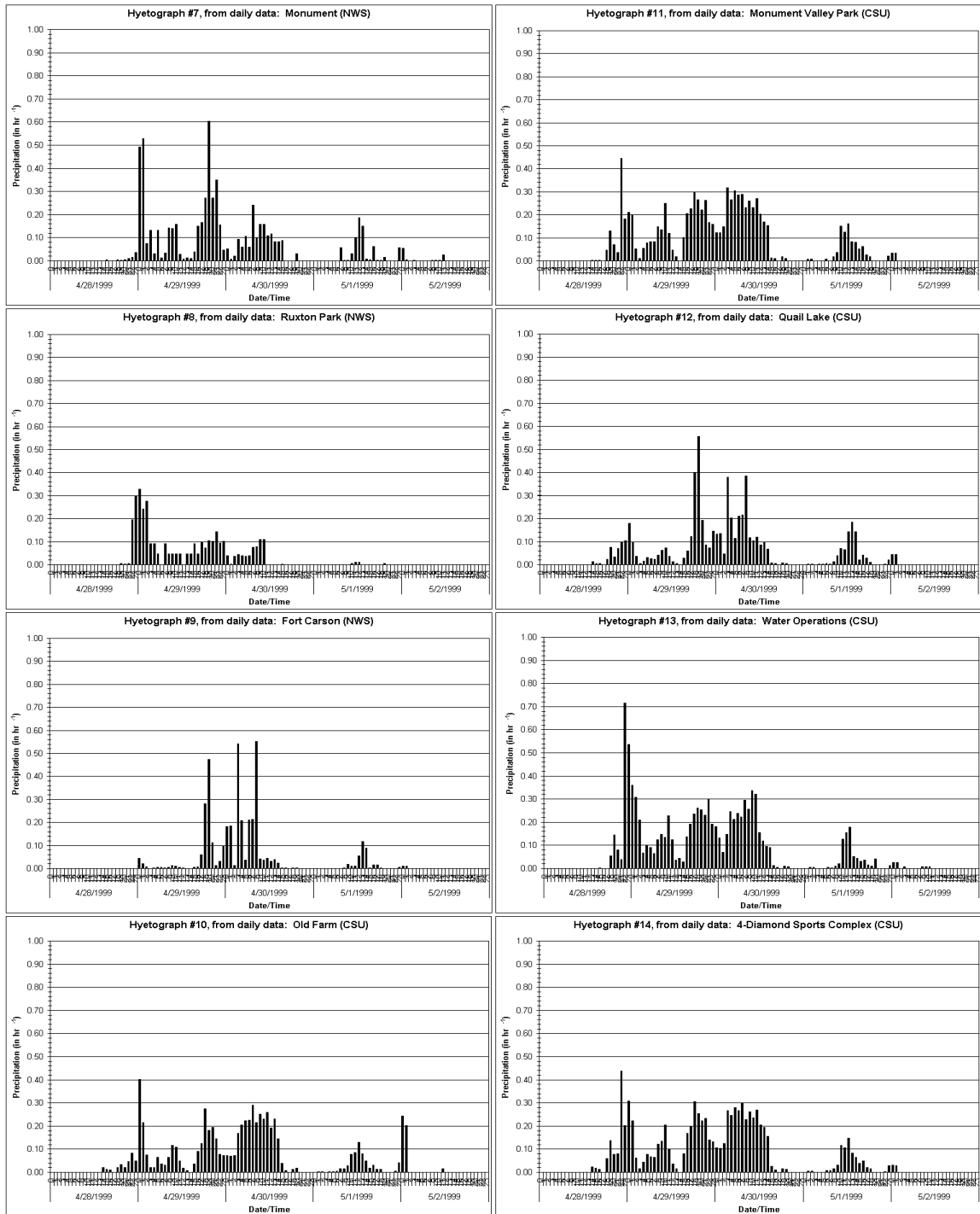


Figure 3.13: Disaggregated hourly rainfall at daily gauges for April 28-May 2, 1999. Gauge names and locations are listed in Table 2.2, daily total rainfall data are listed in Table 3.9, and calculated hourly station weights for the procedure described in the text are listed in Table 3.11.

For the purposes of event simulation, supplemental hyetographs were formulated to improve the spatial representation of rainfall totals, especially in those areas that are distant from existing rainfall gauges. Several factors influenced the placement of these “virtual” rainfall gauges:

- (1) Number and locations of available high-resolution USGS stream gauge records.
- (2) Locations of existing rainfall gauges, especially the available hourly gauges.
- (3) Locations of major topographical features, especially the Rampart Range, with respect to the observed storm and overall event morphology.
- (4) Resulting spatial coverage of a supplemental gauge, as determined by the Thiessen polygon method.

High-resolution (15-minute) records were available for the four USGS gauge locations listed in the upper portion of Table 3.1. Supplemental rainfall gauges were placed at four locations in the Monument and Fountain Creek watersheds that were otherwise ungauged, and each rainfall gauge is designated for the goal of hydrograph fitting at a particular USGS stream gauge location. These locations fall generally in the foothills west and northwest of the confluence of Monument and Fountain Creeks. In order to prevent interference between supplemental gauges in the simulation procedure described below, the supplemental gauges were placed in locations for which the corresponding Thiessen polygons would not require the simultaneous determination of two or more supplemental rainfall records in the fitting of an observed hydrograph at any particular USGS stream gauge location.

The resulting locations of these supplemental rainfall gauges (nos. 15–18) were listed in Table 2.2 and shown in Figure 2.4. The resulting Thiessen polygons delineating spatial distribution of the applied rainfall records are shown in Figure 3.14.

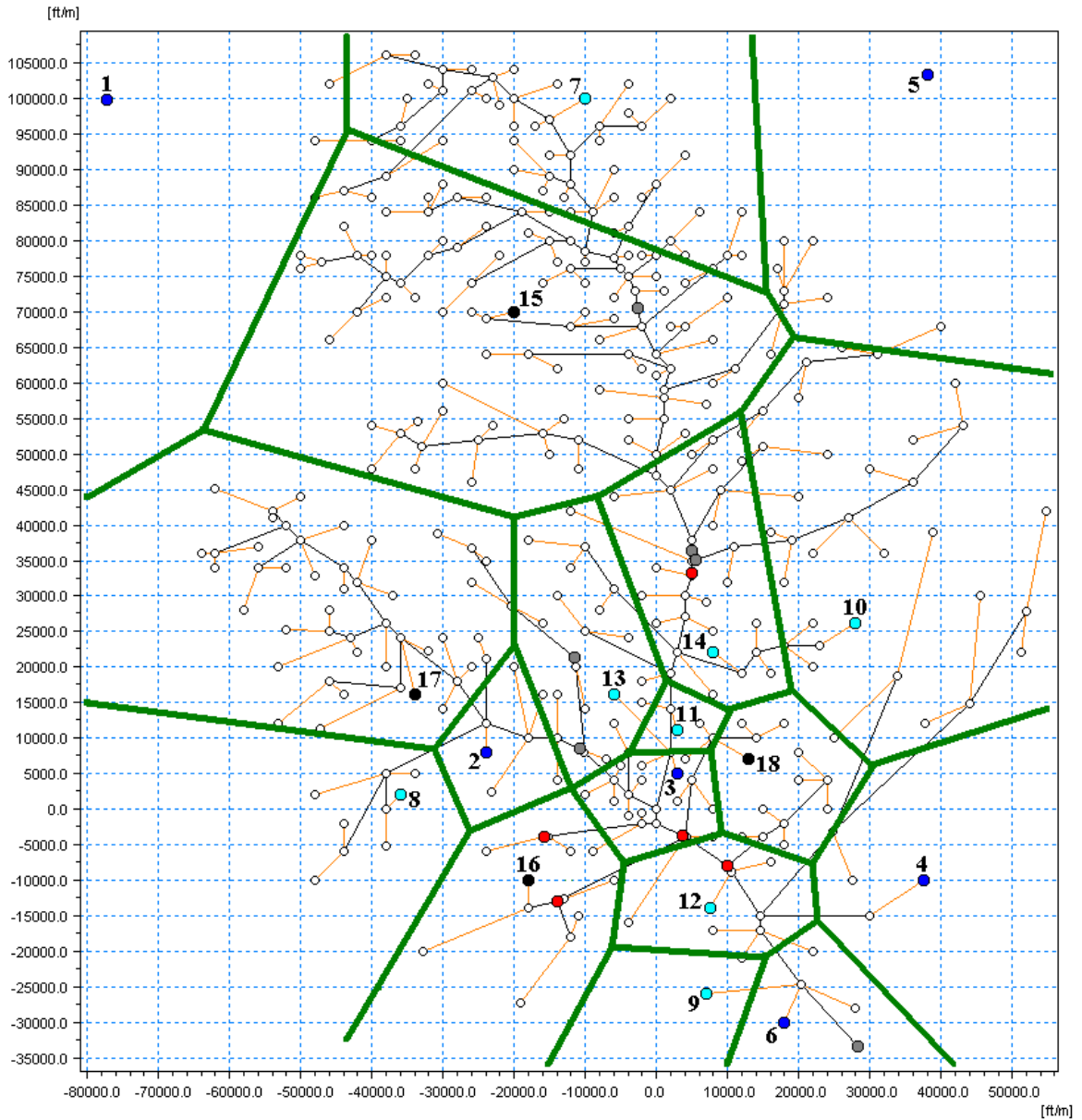


Figure 3.14: Thiessen polygons for all existing and supplemental rainfall gauges. Gauge locations are listed in Table 2.2.

*Inverse-distance-squared Method*

The simplest method applied for the determination of hourly supplemental data employed quadrant-based nearest neighbors. This method follows that described above in equations (3.26) through (3.29), treating the supplemental gauges as locations for which missing data is to be found. Two alternatives are explored for this application: the first method employed only hourly gauges for the determination of rainfall at the supplemental gauges, and the second method employed all (hourly and disaggregated daily) gauges for that determination.

The resulting weights assigned to each supplemental gauge under the first alternative method (using only hourly gauges) are listed in Table 3.12. The resulting hyetographs at the supplemental gauges are shown in Figure 3.15. The reader should note that the maximum hourly total rainfall at any of the supplemental gauges is inherently limited to some value less than or equal to the largest hourly rainfall, recorded at the pre-existing gauges, that is applied to each supplemental gauge. This limitation will be shown to produce inadequate results in the simulation of stream discharge records at available locations in the Monument and Fountain Creek watersheds.

The calculated weights assigned to each supplemental gauge under the second alternative method (using all available gauges) are listed in Table 3.13. The resulting hyetographs at the supplemental gauges are shown in Figure 3.16. For these records, several differences from those given in Figure 3.15 are evident. Specifically for hyetograph 15, these differences can be attributed to changes in the selected surrounding gauges assigned for the formulation of hourly rainfall data. (Hyetograph 7 demonstrated significantly more “peaked” hourly rainfall totals during the first half of the storm event than the record that it replaced, that for hyetograph 5.) Overall, though, the reader should note again that maximum hourly

Table 3.12: Gauge weights for derivation of rainfall at supplemental locations using only hourly gauges. The data given here apply to the use of only hourly gauges (nos. 1–6) in a quadrant-based method, as described in the text.

Daily Gauge $i$	Weight for selected hourly gauge $j$ ( $10^{-10} \text{ ft}^{-2}$ )						$W_i$ ( $\text{ft}^{-2}$ )
	1	2	3	4	5	6	
15	2.42	2.59	2.10	—	2.24	—	$9.35 * 10^{-10}$
16	—	27.8	15.0	—	—	5.90	$4.87 * 10^{-9}$
17	1.14	61.0	6.71	—	0.782	—	$6.96 * 10^{-9}$
18	—	7.30	96.2	11.2	1.01	—	$1.09 * 10^{-8}$

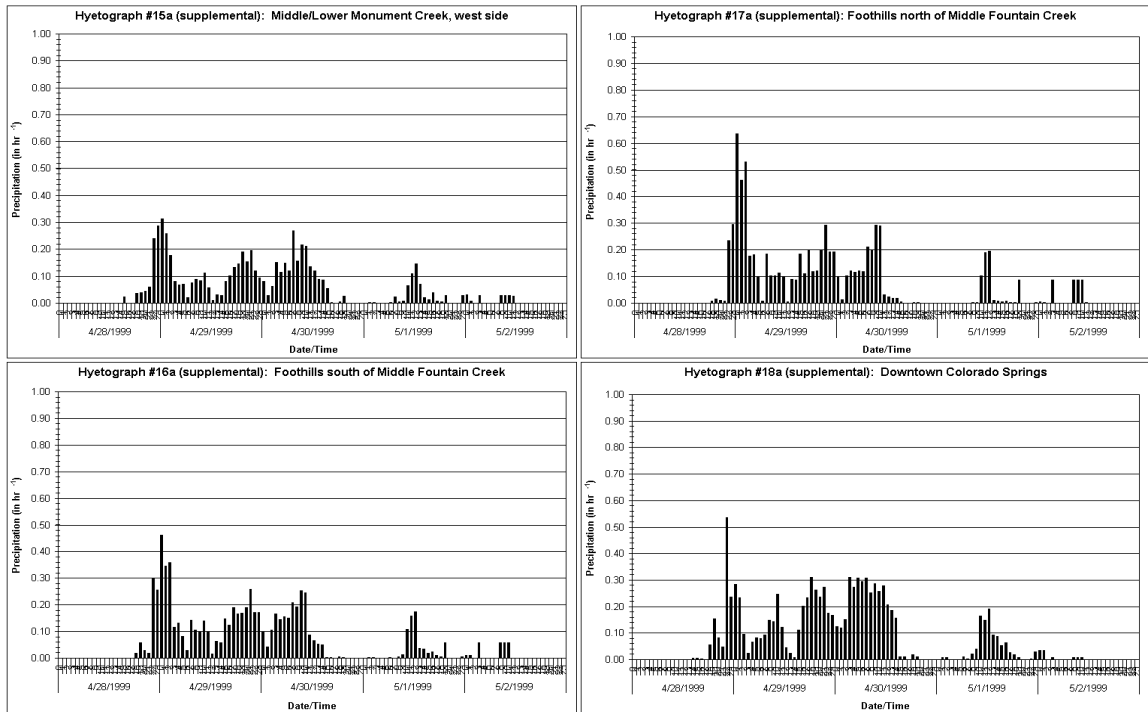


Figure 3.15: Rainfall at supplemental gauges derived from existing hourly gauges. Gauge names and locations are listed in Table 2.2, and calculated hourly station weights for the procedure described in the text are listed in Table 3.12.

Table 3.13: Gauge weights for derivation of rainfall at supplemental locations using all existing gauges. The data given here apply to the use of all existing gauges (nos. 1–14) in a quadrant-based method, as described in the text.

Gauge $i$	Weight for selected gauge $j$ ( $10^{-10}$ ft $^{-2}$ )														$W_i$ (ft $^{-2}$ )
	1	2	3	4	5	6	7	8	9	10	11	12	13	14	
15	2.42	2.59	—	—	—	—	10.0	—	—	—	—	—	3.21	—	1.82 * 10 $^{-9}$
16	—	27.8	15.0	—	—	—	—	—	—	—	—	15.0	—	—	5.78 * 10 $^{-9}$
17	1.14	61.0	—	—	0.782	—	—	—	—	—	—	—	12.8	—	7.56 * 10 $^{-9}$
18	—	—	96.2	11.2	—	—	—	—	—	17.1	86.2	—	—	—	2.11 * 10 $^{-8}$

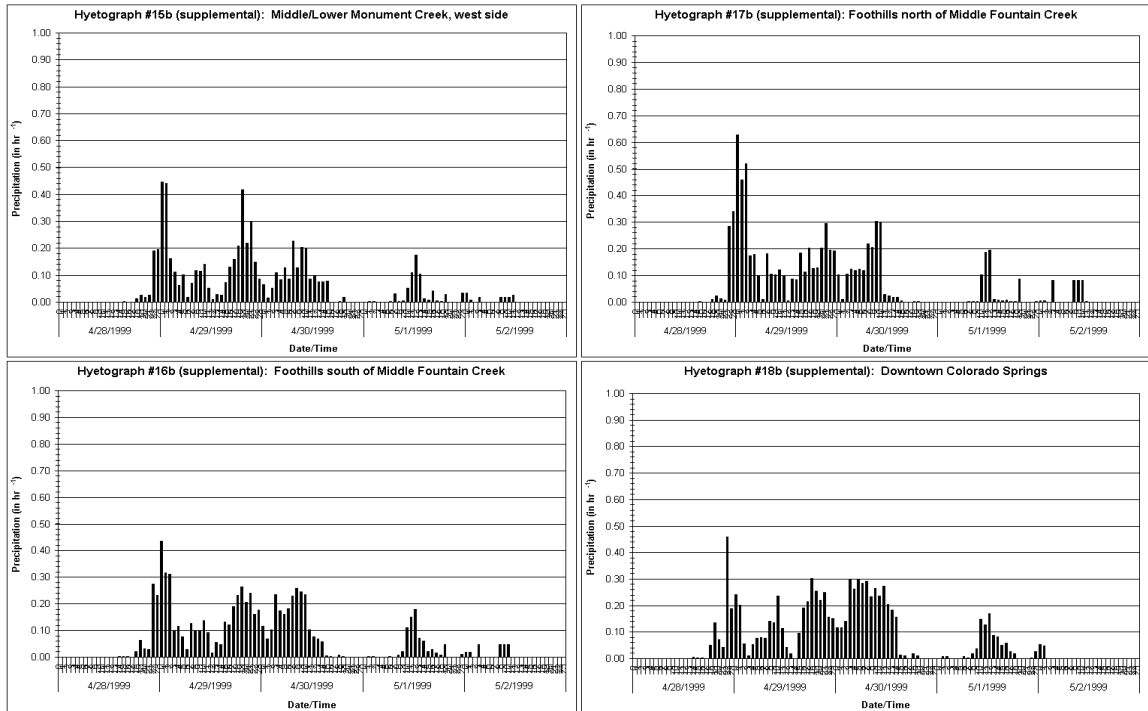


Figure 3.16: Rainfall at supplemental gauges derived from all existing gauges. Gauge names and locations are listed in Table 2.2, and calculated station weights for the procedure described in the text are listed in Table 3.13.

total rainfall at any of the supplemental gauges is inherently limited to some value less than or equal to the largest hourly rainfall, recorded (or determined by disaggregation of daily totals) at the pre-existing gauges, that is applied to each supplemental gauge. As well, this limitation will be shown to produce inadequate results in the simulation of stream discharge records at available locations in the Monument and Fountain Creek watersheds.

### *Characteristics Method*

Considering the limitation imposed on the rainfall totals at supplemental gauge locations by using only the inverse-distance-squared method for spatial interpolation, an alternative formulation for the NWSRFS involves a method of “characteristics” for which climatological rainfall totals are employed. In this case, the long-term mean rainfall at all gauge locations listed in Table 2.2 for the months of April and May, corresponding to the

Table 3.14: PRISM-derived mean April + May precipitation at all gauge locations for the period 1961–1990. These data were provided by the Spatial Climate Analysis Service (see text for website address).

Gauge $i$	April + May $P_{total}$
1	4.2421
2	4.8551
3	3.8378
4	3.2752
5	4.6110
6	3.6138
7	4.9693
8	5.6004
9	4.0291
10	3.8059
11	3.9260
12	3.7862
13	4.1870
14	4.0618
15	5.3102
16	5.6433
17	4.7094
18	3.8354

specific period during which this event occurred, are required. Since no such observational data exists at the locations of the supplemental gauges, an alternative source of data is preferred.

Gridded data sets of mean monthly and annual rainfall for the period 1961–1990 at a spatial resolution of  $\sim 3.6$  km have been produced for the entire United States by the PRISM methodology (Daly et al. 1994) and are available on-line from the Spatial Climate Analysis Service (SCAS; <http://www.ocs.orst.edu/prism/>). The use of such isohyetal data for the derivation of mean areal precipitation (MAP) in Thiessen polygon determinations of watershed rainfall has been explored by Fiedler (2003). In this case, however, the PRISM-derived total rainfall for April and May in each representative grid square is assigned without interpolation or averaging to the modeled rainfall station located there. It was found that each modeled rainfall station occupied only one PRISM grid square, and that no grid square contained more than one rainfall station, such that unique values for climatological rainfall at the stations were obtained. These values are listed in Table 3.14.

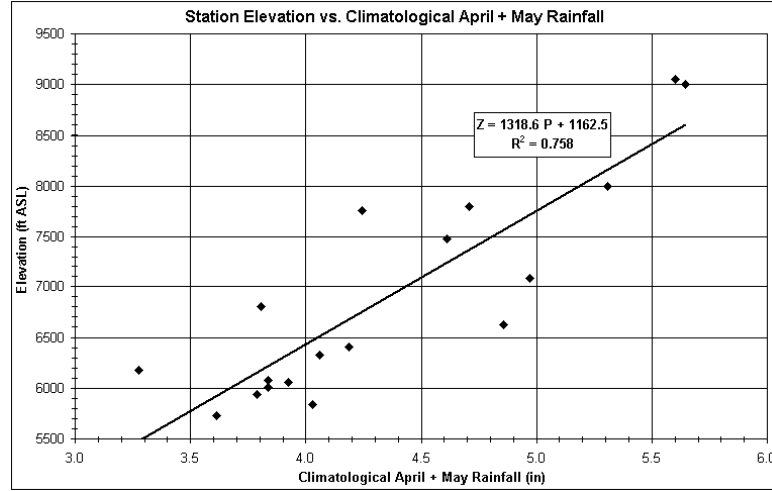


Figure 3.17: Rainfall gauge elevation and normal April + May total precipitation. Rainfall gauge elevations are listed in Table 2.2, and climatological precipitation values are listed in Table 3.14.

It is interesting to note that a positive correlation between gauge elevation, as listed in Table 2.2, and climatological rainfall can be found. This correlation is shown by the trend line in Figure 3.17, which demonstrates the long-term effects of topography spring synoptic and mesoscale storm events. It was expected that this correlation would result in a bias of the event-based rainfall totals at supplemental gauges toward those expected at higher elevations in the modeled watershed for this event.

The characteristics of climatological rainfall for each station were found by

$$c_{ij} = \frac{P_{c,i}}{P_{c,j}}, \quad (3.31)$$

where  $P_{c,i}$  is the climatological (April + May, 1961–1990) precipitation at the location of station  $i$ . The resulting characteristics for the quadrant-based hourly and daily stations assigned to each supplemental station by this method are listed in Table 3.15. The hourly rainfall records for the supplemental stations were then found by a method similar to that

Table 3.15: Climate-based gauge characteristics for derivation of rainfall at supplemental locations using all existing gauges. The data given here employ the climate data listed in Table 3.14 and apply to the use of all existing gauges (nos. 1–14) in a quadrant-based method, as described in the text.

Gauge $i$	Characteristic with respect to gauge													
	1	2	3	4	5	6	7	8	9	10	11	12	13	14
15	1.2518	1.0937	—	—	—	—	1.0686	—	—	—	—	—	1.2683	—
16	—	1.1623	1.4705	—	—	—	—	—	—	—	—	1.4905	—	—
17	1.1102	0.9700	—	—	1.0213	—	—	—	—	—	—	—	1.1248	—
18	—	—	0.9994	1.1710	—	—	—	—	—	1.0078	0.9769	—	—	—

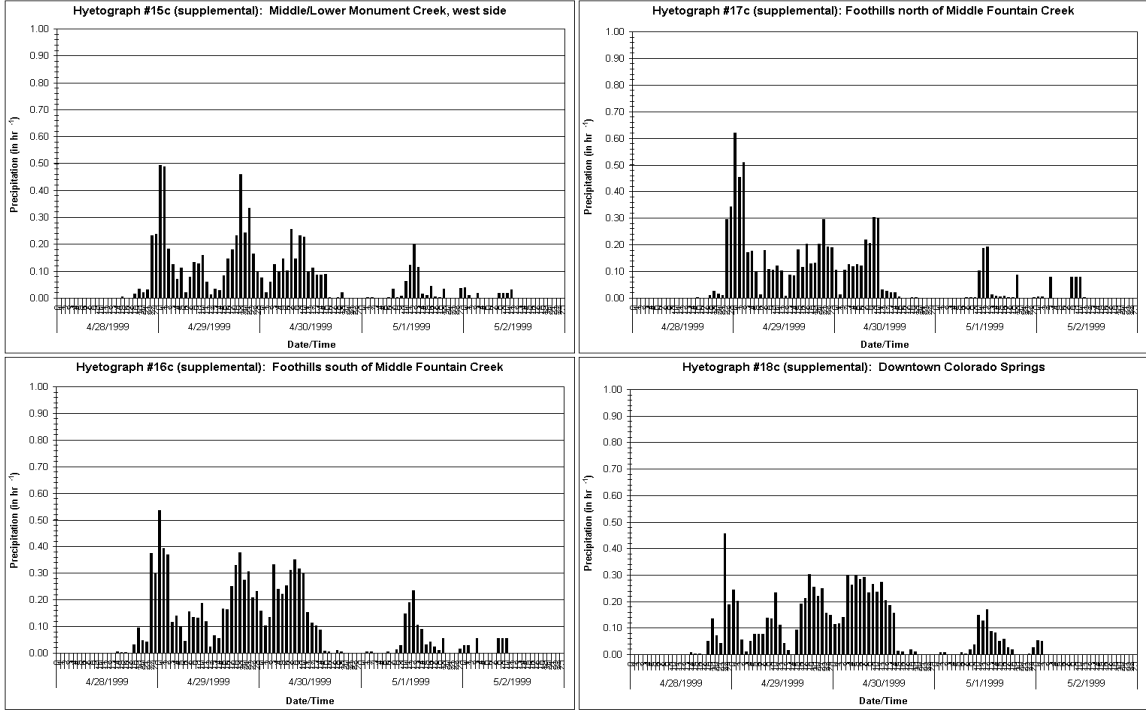


Figure 3.18: Rainfall at supplemental gauges derived by characteristics method. Gauge names and locations are listed in Table 2.2, calculated station weights for the procedure described in the text are listed in Table 3.13, and calculated station characteristics are listed in Table 3.15.

described above:

$$p_{i,h} = \sum_{j=1}^J \frac{c_{ij} w_{ij} p_{j,h}}{W_i}, \quad (3.32)$$

where  $c_{ij}$  is the characteristic corresponding to gauge  $j$  with respect to gauge  $i$ ,  $w_{ij}$  is the inverse-distance-squared weight corresponding to gauge  $j$  that is assigned to gauge  $i$ ,  $p_{j,h}$  is the rainfall for hour  $h$  at gauge  $j$ , and  $W_i$  is the sum of station weights assigned to daily gauge  $i$  as found by equation (3.29). The resulting hourly rainfall hyetographs for the supplemental gauges found by this characteristics method are shown in Figure 3.17.

For the three methods of record interpolation described here, the resulting daily and event total rainfall data are summarized in Table 3.16.

Table 3.16: Daily (April 28–May 2, 1999) and event total rainfall at supplemental gauges as determined by various interpolation methods. The applied methods listed here are explained in the text.

Gauge Number	Daily total rainfall (in)					Event Total (in)
	Apr 28	Apr 29	Apr 30	May 1	May 2	
<b>By <math>1/d^2</math> weighting using only hourly gauges</b>						
15	0.73	2.69	2.08	0.58	0.17	6.25
16	0.68	3.83	2.03	0.66	0.25	7.45
17	0.57	4.49	1.79	0.63	0.36	7.84
18	1.13	3.66	3.56	0.98	0.10	9.42
<b>By <math>1/d^2</math> weighting using all gauges</b>						
15	0.47	3.65	1.73	0.62	0.14	6.61
16	0.66	3.79	2.33	0.75	0.23	7.76
17	0.68	4.50	1.83	0.62	0.34	7.97
18	0.96	3.31	3.42	0.88	0.10	8.68
<b>By method of characteristics</b>						
15	0.58	4.08	1.99	0.69	0.16	7.49
16	0.90	4.88	3.21	1.01	0.28	10.28
17	0.71	4.47	1.86	0.62	0.33	7.99
18	0.96	3.30	3.41	0.88	0.10	8.65

#### *Hydrograph-fitting Method*

Finally, as an alternative to the methods for *a priori* determination of rainfall at the supplemental gauge locations that are described above, the hourly supplemental rainfall records may be found as those required for an acceptable fit of simulation results to the observed discharge records at available stream gauge locations. The objective criteria by which that accuracy may be determined will be discussed in the next section. The adoption of such a solution method depends on the lack of such an acceptable solution produced by any of the other methods employed here. At this point in the discussion of such methods, the reader will deduce just such a lack of acceptable results from *a priori* methods.

This method relied on (1) specification of input hyetographs at the supplemental gauge locations on an hour-by-hour basis for simulation with the RUNOFF model described above, and (2) comparison of the simulated hydrographs with those recorded by the USGS at corresponding locations in the watershed. This was, essentially, a trial-and-error solution to the problem of unknown rainfall records using known watershed discharge

records. Each hour of the hyetograph was specified and adjusted until an acceptable fit to the observed discharge hydrograph was obtained, and then the next hour was specified in a similar manner. For watershed areas with short response times and relatively simple drainage networks, this process was relatively simple and straightforward. However, for those portions of the watershed with slow response times and relatively complex channel networks, the determination of relationships between rainfall and stream discharge was often difficult and required greater effort at the accurate determination of the hyetographs required for simulation of the observed hydrographs.

An alternative method for the solution of such a hydrologic inverse problem exists in the specification (or derivation) of a unit hydrograph (UH) function as described by various authors, e.g. Chow et al. (1988). Such efforts by the present author at the determination of rainfall hyetographs for this event at the supplemental gauge locations, using partial hydrographs determined through model simulations, resulted in oscillatory UHs for all attempts. As the character of such derived UHs are highly sensitive to the choice of UH (and thus storm) duration, and as various storm durations were observed during the event under study here, a highly complicated system of UH functions is likely required for the advancement of such a solution method. The specification of such a system remains beyond the scope of the present work.

Some of the simulations described in the next chapter thus demonstrate the determination of supplemental rainfall records by this trial-and-error method. The resulting hydrographs are shown to be an acceptable fit to the observed stream discharge records at available locations in the watershed. However, these hyetographs would not be fully determined until the simulations themselves are complete, and as such are not shown here. These records will be presented with the simulation results discussed in Chapter 4.

### 3.2.8 Derivation of Mean Areal Precipitation (MAP)

The overall mean areal precipitation (MAP) for each simulation was found by

$$\text{MAP} = \frac{\sum_{s=1}^S A_s P_{m,s}}{\sum_{s=1}^S A_s}, \quad (3.33)$$

where  $A_s$  is the area of sub-basin  $s$  and  $P_{m,s}$  is the event-total rainfall for hyetograph  $m$  that is applied to sub-basin  $s$ , as found by

$$P_{m,s} = \sum_{h=1}^H P_{m,s,h}, \quad (3.34)$$

for an event of duration  $H$  hours. The MAP found in this manner is a diagnostic measure of simulation total rainfall over the entire modeled watershed area, and is not intended to include any indication of the spatial variability of event total rainfall at smaller scales within that modeled area. Such variability would arise primarily from orographic effects on storm formation, evolution and movement, as discussed in Chapter 2. The problem of MAP estimation in regions of orographic influence is a complex issue that is often addressed with geostatistical (i.e., “kriging”) methods as by Chua and Bras (1980, 1982) and Kyriakidis et al. (2001). Using these methods, additional factors such as surface elevation, slope, aspect (orientation) and resulting exposure to moist flows can be incorporated into the determination of MAP in mountainous regions. Though the results presented below may indicate these influences on the morphology of the storm event addressed here, no consideration has been given to such advanced attempts at the objective determination of the spatial variability of total event rainfall for this work.

### 3.3 Hydrograph Evaluation Methods

The methods described above apply to the determination of rainfall records at four supplemental gauge locations in the Monument and Fountain Creek watersheds. The goal of those methods is the preservation of statistical characteristics demonstrated by the observed hydrographs for the period of the rainfall and flood event (approximately 8 p.m. LST on April 28 to 12 a.m. LST on May 3, 1999). Along with these statistical parameters, several relative and absolute measures of error are discussed here.

#### 3.3.1 Preserved Hydrograph Statistics

Five statistical measures or characteristics of the observed and simulated hydrographs are discussed here. Each relies on the evaluation of a time-series record that, in this case, consists of more than four days of instantaneous stream discharge measurements at a temporal resolution of 15 minutes. The observed (USGS) stream discharge records will be denoted here as  $Q_i$ , where  $i$  is a specific time-series observation, and the simulated stream discharge records will be denoted here as  $S_i$ .

#### *Mean Discharge*

The arithmetic mean discharge for a time-series record of observations is found by

$$\mu_Q = \frac{1}{N} \sum_{i=1}^N Q_i, \quad (3.35)$$

where  $Q_i$  is an individual discharge observation and  $N$  is the total number of discharge observations in the time series. The absolute simulation error for the mean discharge is thus

$$\epsilon_\mu = \mu_S - \mu_Q, \quad (3.36)$$

and is often expressed here as found by  $\epsilon_\mu/\mu_Q$ .

*Maximum Discharge*

The maximum discharge for a time-series record of observations is found by

$$Q_{max} = \max[Q_i], \quad (3.37)$$

and the absolute simulation error for the maximum discharge is thus

$$\epsilon_{max} = S_{max} - Q_{max}. \quad (3.38)$$

This error is often expressed here as found by  $\epsilon_{max}/Q_{max}$ .

*Discharge Variance and Standard Deviation*

The unbiased discharge variance for a time-series record of observations is found by

$$\sigma_Q^2 = \frac{1}{N-1} \sum_{i=1}^N (Q_i - \mu_Q)^2, \quad (3.39)$$

such that the discharge standard deviation is given as

$$\sigma_Q = \sqrt{\frac{1}{N-1} \sum_{i=1}^N (Q_i - \mu_Q)^2}. \quad (3.40)$$

The absolute simulation error for the discharge standard deviation is thus

$$\epsilon_\sigma = \sigma_S - \sigma_Q, \quad (3.41)$$

and is often expressed here as found by  $\epsilon_\sigma/\sigma_Q$ .

*Total Discharge Volume*

The total discharge volume is found by

$$V_Q = \sum_{i=1}^N Q_i \Delta t, \quad (3.42)$$

where  $\Delta t$  is the time between observations, in this case a constant interval of 15 minutes (900 s). In most results presented here, the sum of discharges in  $\text{ft}^3 \text{ s}^{-1}$  produces a total

discharge volume in  $\text{ft}^3$  that is then converted to ac-ft (1 ac = 43,560  $\text{ft}^2$ ). The absolute simulation error for the total discharge volume is

$$\epsilon_V = V_S - V_Q, \quad (3.43)$$

and is often expressed here as found by  $\epsilon_V/V_Q$ .

### *Serial Correlation of Discharge Series*

The lag- $k$  serial correlation coefficient for a single discharge time-series record is found by

$$\rho_k = \frac{c_k}{c_0}, \quad (3.44)$$

for which

$$c_k = \frac{1}{N} \sum_{i=1}^{N-k} (Q_{i+k} - \mu_Q)(Q_i - \mu_Q). \quad (3.45)$$

The reader will note that  $c_0 = \sigma_Q^2$ . For the results presented here, only the lag-1 serial correlation coefficient is employed in the evaluation of results. The resulting value satisfies  $-1 \leq \rho_1 \leq 1$  and indicates the degree of linear dependence of each observation on the previous observation. The absolute simulation error for the serial correlation is

$$\epsilon_{\rho_1} = \rho_{1,S} - \rho_{1,Q}, \quad (3.46)$$

and is often expressed here as found by  $\epsilon_{\rho_1}/\rho_{1,Q}$ .

### *3.3.2 Relative Error Measures*

The primary measure of relative error between the simulated and observed time-series records is the Pearson's product moment correlation coefficient, found by

$$\rho_{Q,S} = \frac{1}{N} \sum_{i=1}^N \frac{(Q_i - \mu_Q)(S_i - \mu_S)}{\sigma_Q \sigma_S}. \quad (3.47)$$

The resulting value satisfies  $-1 \leq \rho_{Q,S} \leq 1$  and indicates the degree of linear dependence of concurrent measurements for each time series  $Q, S$ . The coefficient of determination is derived from the correlation coefficient as

$$R^2 = \rho_{Q,S}^2, \quad (3.48)$$

for which the resulting value satisfies  $0 \leq R^2 \leq 1$  and indicates the degree of “agreement” between the two time series. However, the use of  $R^2$  alone in order to determine “goodness of fit” between the simulated and observed discharge time series is limited by its insensitivity to additive and proportional differences between the two series (Legates and McCabe 1999). In other words, though the two time series may exhibit similar shapes and variations about their respective mean values, the concurrent measurements may differ in actual value by orders of magnitude without affecting the value of  $R^2$ . As such, the coefficient of determination will be most useful in the determination of “goodness of fit” in conjunction with some absolute measure of simulation error.

### 3.3.3 *Absolute Error Measures*

In a statistical sense, the error measures described above such as  $\epsilon_\mu$  and  $\epsilon_V$  would be sufficient for evaluation, along with the coefficient of determination, of correspondence between observed and simulated discharge time series. Qualitative evaluations of simulation results presented in Chapter 4 will depend primarily on the combination of  $\epsilon_\mu$  and  $R^2$ . One other absolute measure of simulation error is included here for the reader’s benefit.

The mean absolute error (MAE) is a measure of the simulation error for concurrent measurements, and is found by

$$\text{MAE} = \frac{1}{N} \sum_{i=1}^N |S_i - Q_i|. \quad (3.49)$$

The MAE thus retains the units of the evaluated records ( $\text{ft}^3 \text{s}^{-1}$  for the discharge records shown here) and represents the absolute deviation of the simulated measurements from those observed.

## Chapter 4

### SIMULATION OF THE APRIL 28–MAY 2, 1999, EVENT

The results of simulations introduced in Chapter 3 are described here. Each simulation is designated with an abbreviation that indicates the extent of the rainfall gauge network employed as well as a unique alphanumeric identifier. The first and second sets of simulations ( $Hx$  and  $HDx$ , respectively) demonstrate the adjustment of infiltration parameters as a “calibration” of the rainfall–runoff model described in Chapter 3. These simulations also demonstrate the inadequacy of existing rainfall records for the accurate simulation of available USGS stream discharge records. The third set of simulations ( $HDSa$ ,  $b$ , and  $c$ ) demonstrates the application of interpolated rainfall records at supplemental gauge locations according to the hyetographs derived in Section 3.2.7.

The fourth set of simulations demonstrates the hydrograph-fitting method discussed near the end of Chapter 3. The zone of modeled sub-basins affected by each supplemental rainfall gauge is addressed individually in an effort to simulate as accurately as possible the contribution of event runoff from that zone to the observed discharge record at the corresponding USGS gauge location. The resulting necessary hyetographs are then incorporated into the complete watershed model and a simulation is performed to determine the overall correspondence between simulated and observed hydrographs at the USGS gauges. Based on the accuracy of these results, hydrographs at eight additional locations in the watershed

where USGS discharge records were unavailable during the storm event are reconstructed from the model simulation.

Finally, the results of simulations that address alternative scenarios of development in the area of downtown Colorado Springs are discussed. Specifically, the discharge records for a virtual stream gauge placed at the mouth of Shooks Run, just upstream of its confluence with Fountain Creek in downtown Colorado Springs, are determined for current and historical conditions of development. The role of the Templeton Gap Floodway in the reduction of peak discharge along Shooks Run during flood events is explored with these scenarios.

#### 4.1 **H $x$ Simulations**

RUNOFF simulations that employed only the hourly rainfall gauges in and near the Monument and Fountain Creek watersheds for which storm event records were available are designated H $x$  here, where  $x$  denotes various experiments with the minimum infiltration parameter assigned to each modeled sub-basin in the watersheds. These simulations employed the rainfall hyetographs shown in Figure 2.17 and were applied to the modeled sub-basins according to the schematic map of Thiessen polygon areas shown in Figure 3.12a.

##### 4.1.1 *H1 Experiment*

Simulation H1 employed the minimum infiltration parameters for SCS/NRCS soil types that are listed in Table 3.4 according to the sub-basin aggregation/averaging procedure described in Section 3.2.3 above. The resulting SWMM RUNOFF hydrographs at the locations of USGS gauges for which event records were available are shown in Figure 4.1. Statistical parameters for the observed and simulated discharge records shown there are listed in Table 4.1. The reader is referred to Section 3.3 above for explanations of the

hydrograph evaluation parameters listed there.

It is shown in Figure 4.1 that the minimum infiltration rates for each sub-basin as listed in Table 3.4 were too large to allow the runoff to occur at the volumes and discharges observed during this storm event. Physically, this result suggested that watershed soils were saturated by antecedent moisture conditions beyond the degree generally assumed for the design of urban drainage systems. For the applied minimum infiltration rates, available rainfall data produced far too little runoff and stream discharge when compared with stream gauge measurements observed during the event.

#### *4.1.2 H2 Experiment*

The saturating effects of winter storms in the Monument and Fountain Creek watersheds prior to this flood event, as discussed in Section 2.3.1 and shown in Figure 2.5, suggested that the minimum infiltration rates applied to watershed sub-basins should be much lower than first assumed. Simulation H2 employed a reduction of the initial minimum infiltration rate for each sub-basin in the modeled watershed by a factor of 4. The results of this simulation are shown in Figure 4.2, and statistical measures of these results are listed in Table 4.1.

It is shown in Figure 4.2 and Table 4.1 that most statistical comparisons between observed and simulated hydrographs are vastly improved by the 75% reduction in minimum infiltration rates applied to sub-basins in simulation H2. However, the correspondence between hydrograph shapes (as indicated by the  $R^2$  parameter) was actually reduced at most locations for this simulation.

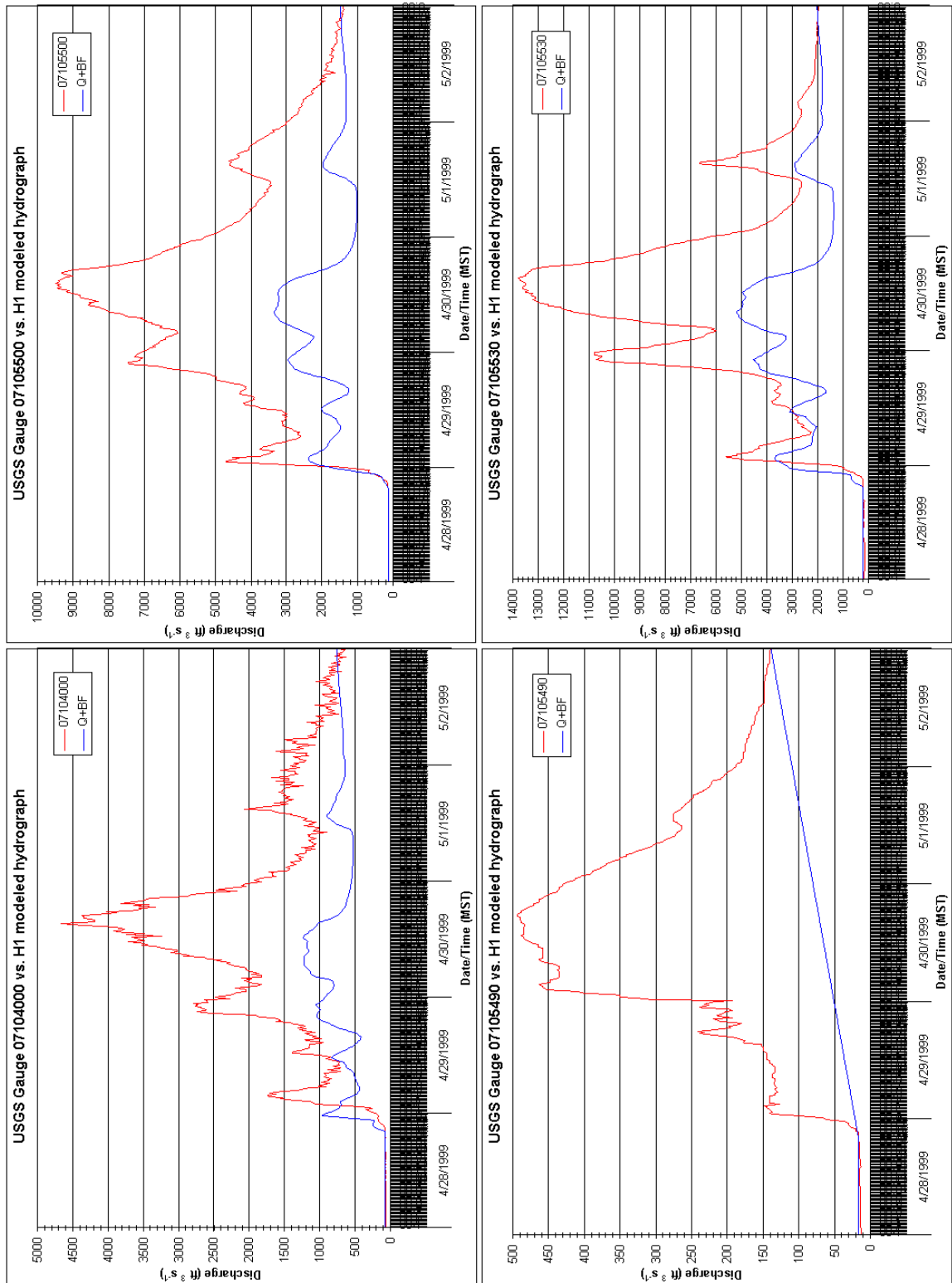


Figure 4.1: Results for simulation H1 at USGS stream gauge locations. Observed and simulated hydrographs are shown in red and blue, respectively. Gauges are labeled by their USGS designator as listed in Table 3.1. Summarized results are listed in Table 4.1.

Table 4.1: Summary of hydrologic model calibration results.

	Simulation Designator					
	H1	H2	H3	HD1	HD2	
Rain Gauges	1-6	1-6	1-6	1-14	1-14	
Overall MAP	6.75	6.75	6.75	6.21	6.21	
$f_0/\beta$ , with $\beta =$	1	4	5	1	5	
<b>Results at USGS gauge 07104000</b>						
$\epsilon_\mu$ (ft <sup>3</sup> s <sup>-1</sup> )	-815.2 (-54.1%)	-512.4 (-34.0%)	-191.6 (-12.7%)	-856.4 (-56.8%)	-171.4 (-11.4%)	
$\epsilon_{max}$ (ft <sup>3</sup> s <sup>-1</sup> )	-3422.4 (-73.4%)	-2189.6 (-47.0%)	-431.5 (-9.3%)	-3413.1 (-73.2%)	+486.3 (+10.4%)	
$\epsilon_\sigma$ (ft <sup>3</sup> s <sup>-1</sup> )	-743.2 (-74.0%)	-417.8 (-41.6%)	+25.4 (+2.5%)	-740.7 (-73.7%)	+252.6 (+25.1%)	
$\epsilon_V$ (ac-ft)	-7158.2 (-54.1%)	-4499.8 (-34.0%)	-1682.3 (-12.7%)	-7520.4 (-56.8%)	-1504.7 (-11.4%)	
$\epsilon_{\rho_1}^2$	+0.0036 (+0.4%)	+0.0044 (+0.4%)	+0.0064 (+0.6%)	+0.0059 (+0.6%)	+0.0072 (+0.7%)	
$R^2$	0.3954	0.3793	0.5618	0.4605	0.4925	
MAE (ft <sup>3</sup> s <sup>-1</sup> )	851.7	712.1	569.3	869.1	653.5	
<b>Results at USGS gauge 07105490</b>						
$\epsilon_\mu$ (ft <sup>3</sup> s <sup>-1</sup> )	-175.8 (-69.5%)	-39.8 (-15.7%)	+64.0 (+25.3%)	-175.8 (-69.5%)	-123.4 (-48.8%)	
$\epsilon_{max}$ (ft <sup>3</sup> s <sup>-1</sup> )	-355.0 (-71.9%)	+1272.4 (+257.6%)	+1501.4 (+303.9%)	-355.0 (-71.9%)	+216.4 (+43.8%)	
$\epsilon_\sigma$ (ft <sup>3</sup> s <sup>-1</sup> )	-99.1 (-73.5%)	+160.1 (+118.7%)	+252.3 (+187.0%)	-99.1 (-73.5%)	-28.7 (-21.3%)	
$\epsilon_V$ (ac-ft)	-1471.2 (-69.5%)	-332.7 (-15.7%)	+535.8 (+25.3%)	-1471.2 (-69.5%)	-1032.6 (-48.8%)	
$\epsilon_{\rho_1}^2$	+0.0019 (+0.2%)	-0.0063 (-0.6%)	-0.0046 (-0.5%)	+0.0019 (+0.2%)	-0.0077 (-0.8%)	
$R^2$	0.0000	0.0162	0.0000	0.0000	0.1195	
MAE (ft <sup>3</sup> s <sup>-1</sup> )	175.8	210.8	248.8	175.8	143.4	
<b>Results at USGS gauge 07105500</b>						
$\epsilon_\mu$ (ft <sup>3</sup> s <sup>-1</sup> )	-2474.6 (-59.3%)	-1278.7 (-30.6%)	-270.9 (-6.5%)	-2600.7 (-62.3%)	-986.4 (-23.6%)	
$\epsilon_{max}$ (ft <sup>3</sup> s <sup>-1</sup> )	-6163.9 (-65.0%)	-530.9 (-5.6%)	+2798.6 (+29.5%)	-6316.4 (-66.6%)	+1060.0 (+11.2%)	
$\epsilon_\sigma$ (ft <sup>3</sup> s <sup>-1</sup> )	-1652.5 (-69.5%)	-153.9 (-6.5%)	+1003.7 (+42.2%)	-1741.8 (-73.3%)	+309.6 (+13.0%)	
$\epsilon_V$ (ac-ft)	-20911.8 (-59.3%)	-10805.7 (-30.6%)	-2289.6 (-6.5%)	-21976.6 (-62.3%)	-8335.4 (-23.6%)	
$\epsilon_{\rho_1}^2$	-0.0005 (0.0%)	-0.0001 (0.0%)	+0.0004 (0.0%)	-0.0003 (0.0%)	+0.0008 (+0.1%)	
$R^2$	0.5760	0.2960	0.4694	0.5790	0.5902	
MAE (ft <sup>3</sup> s <sup>-1</sup> )	2489.9	2027.8	1863.7	2609.8	1628.5	
<b>Results at USGS gauge 07105530</b>						
$\epsilon_\mu$ (ft <sup>3</sup> s <sup>-1</sup> )	-2357.4 (-49.6%)	-950.8 (-20.0%)	+183.7 (+3.9%)	-2538.0 (-53.5%)	-820.8 (-17.3%)	
$\epsilon_{max}$ (ft <sup>3</sup> s <sup>-1</sup> )	-8603.8 (-62.3%)	-3009.4 (-21.8%)	+2170.3 (+15.7%)	-8895.8 (-64.5%)	-766.4 (-5.6%)	
$\epsilon_\sigma$ (ft <sup>3</sup> s <sup>-1</sup> )	-2498.0 (-67.5%)	-767.1 (-20.7%)	+615.2 (+16.6%)	-2637.9 (-71.3%)	-375.3 (-10.1%)	
$\epsilon_V$ (ac-ft)	-20699.9 (-49.6%)	-8349.0 (-20.0%)	+1613.3 (+3.9%)	-22286.6 (-53.5%)	-7207.3 (-17.3%)	
$\epsilon_{\rho_1}^2$	-0.0010 (-0.1%)	-0.0001 (0.0%)	+0.0004 (0.0%)	-0.0010 (-0.1%)	+0.0005 (+0.1%)	
$R^2$	0.5634	0.3776	0.5114	0.6009	0.6469	
MAE (ft <sup>3</sup> s <sup>-1</sup> )	2445.7	2106.8	2073.1	2591.0	1627.5	

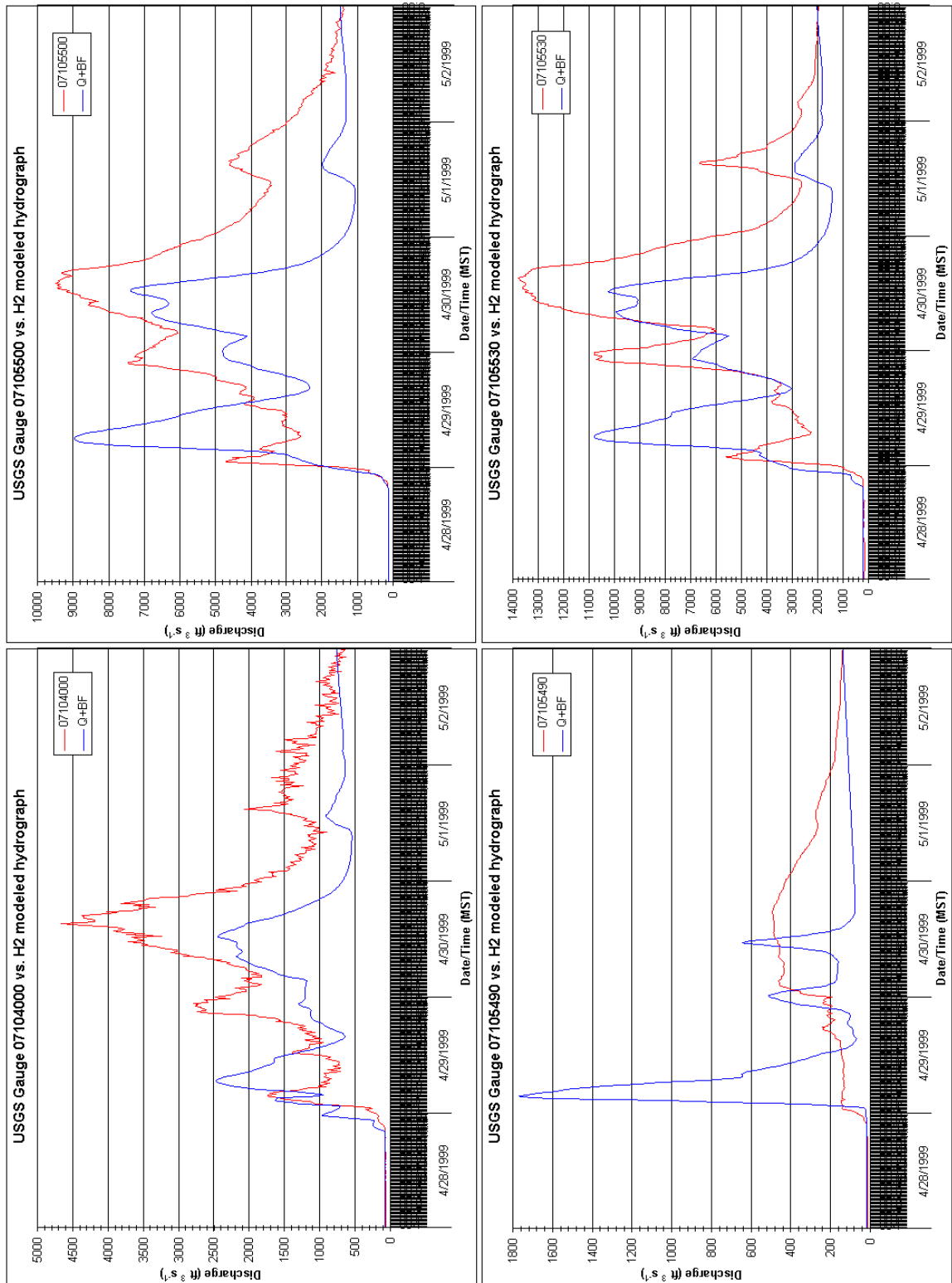


Figure 4.2: Results for simulation H2 at USGS stream gauge locations. Observed and simulated hydrographs are shown in red and blue, respectively. Gauges are labeled by their USGS designator as listed in Table 3.1. Summarized results are listed in Table 4.1.

### 4.1.3 H3 Experiment

Finally, simulation H3 employed a reduction of the initial minimum infiltration rate for each sub-basin in the modeled watershed by a factor of 5. The results of this simulation are shown in Figure 4.3, and statistical measures of these results are listed in Table 4.1.

It is shown in Figure 4.3 and Table 4.1 that most statistical comparisons between observed and simulated hydrographs are even more improved by the 80% reduction in minimum infiltration rates applied to sub-basins in simulation H3. The correspondence between hydrograph shapes (as indicated by the  $R^2$  parameter) was improved at most locations when compared with the results of simulation H2, though in some locations was still not as great as for simulation H1. It was anticipated that these statistics would all improve with the further consideration of rainfall records at additional locations in and near the Monument and Fountain Creek watersheds, as described below.

## 4.2 HD $x$ Simulations

RUNOFF simulations that employed all available rainfall gauges in and near the Monument and Fountain Creek watersheds for which storm event records were available are designated HD $x$  here, where  $x$  denotes experiments with the minimum infiltration parameter assigned to each modeled sub-basin in the watersheds as described above. These simulations employed the rainfall hyetographs for hourly gauges that were shown in Figure 2.17 and the disaggregated hourly hyetographs for daily gauges that were shown in Figure 3.13. All of these hyetographs were applied to the modeled sub-basins according to the schematic map of Thiessen polygon areas shown in Figure 3.12b.

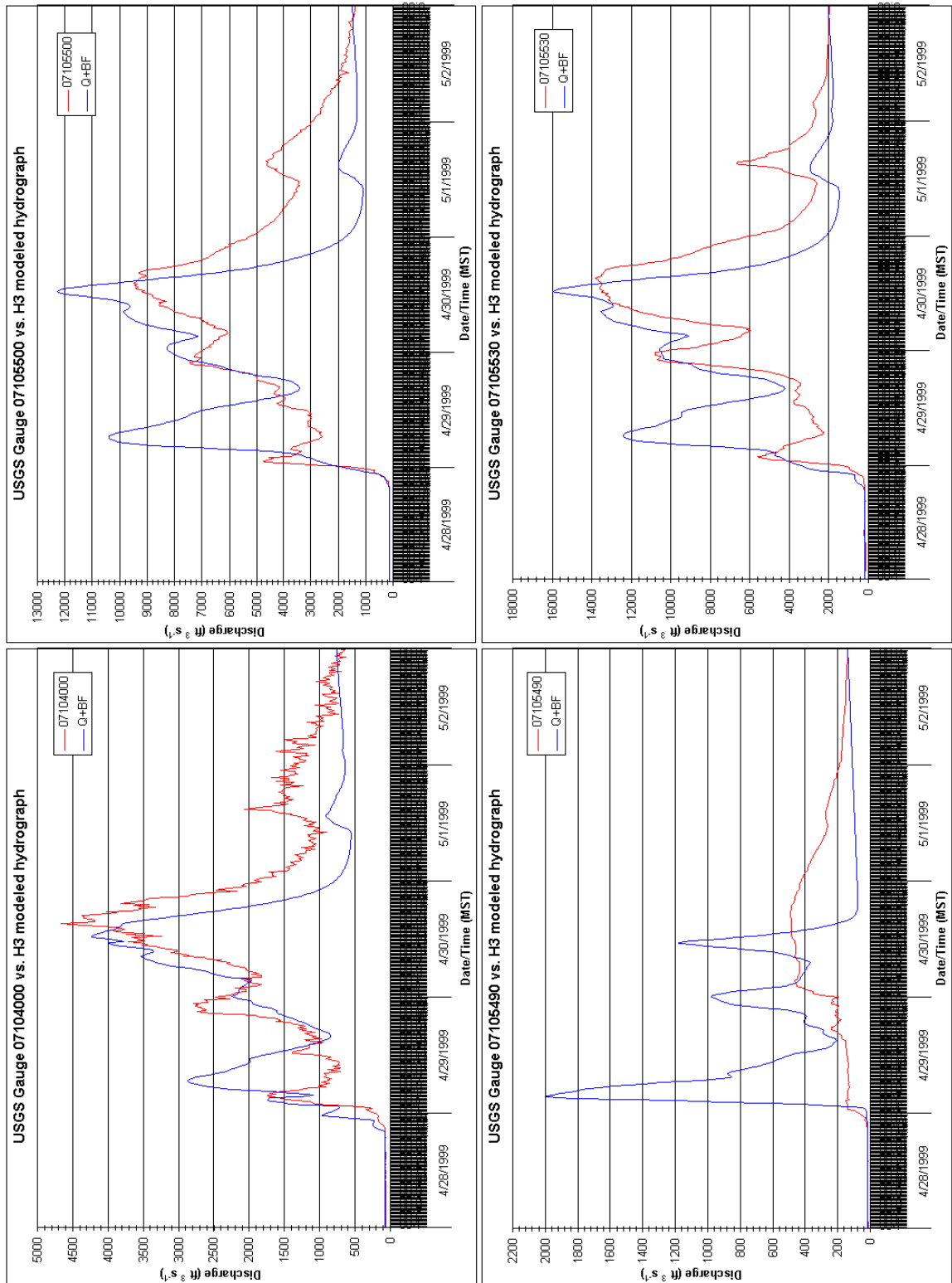


Figure 4.3: Results for simulation H3 at USGS stream gauge locations. Observed and simulated hydrographs are shown in red and blue, respectively. Gauges are labeled by their USGS designator as listed in Table 3.1. Summarized results are listed in Table 4.1.

#### 4.2.1 *HD1 Experiment*

As for simulation H1 described above, simulation HD1 employed the minimum infiltration parameters for SCS/NRCS soil types that are listed in Table 3.4 according to the sub-basin aggregation/averaging procedure described in Section 3.2.3. The resulting SWMM RUNOFF hydrographs at the locations of USGS gauges for which event records were available are shown in Figure 4.4. Statistical parameters for the observed and simulated discharge records shown there are listed in Table 4.1.

It is shown in Figure 4.4 that the minimum infiltration rates for each sub-basin as listed in Table 3.4 were too large to allow the runoff to occur at the volumes and discharges observed during this storm event. Again, for the applied minimum infiltration rates, the employment of all available rainfall data produced far too little runoff and stream discharge when compared with stream gauge measurements observed during the event.

#### 4.2.2 *HD2 Experiment*

Following on the improvement in results between simulations H2 and H3 described above, simulation HD2 employed a reduction of the initial minimum infiltration rate for each sub-basin in the modeled watershed by a factor of 5. The results of this simulation are shown in Figure 4.5, and statistical measures of these results are listed in Table 4.1.

It is shown in Figure 4.5 and Table 4.1 that statistical comparisons between observed and simulated hydrographs were most improved by the 80% reduction in minimum infiltration rates applied to all watershed sub-basins in simulations H3 and HD2. Most comparisons were further improved by the inclusion of all available rainfall records in and near the Monument and Fountain Creek watersheds. The correspondence between hydrograph shapes (as indicated by the  $R^2$  parameter) at most locations and mean discharges at all locations

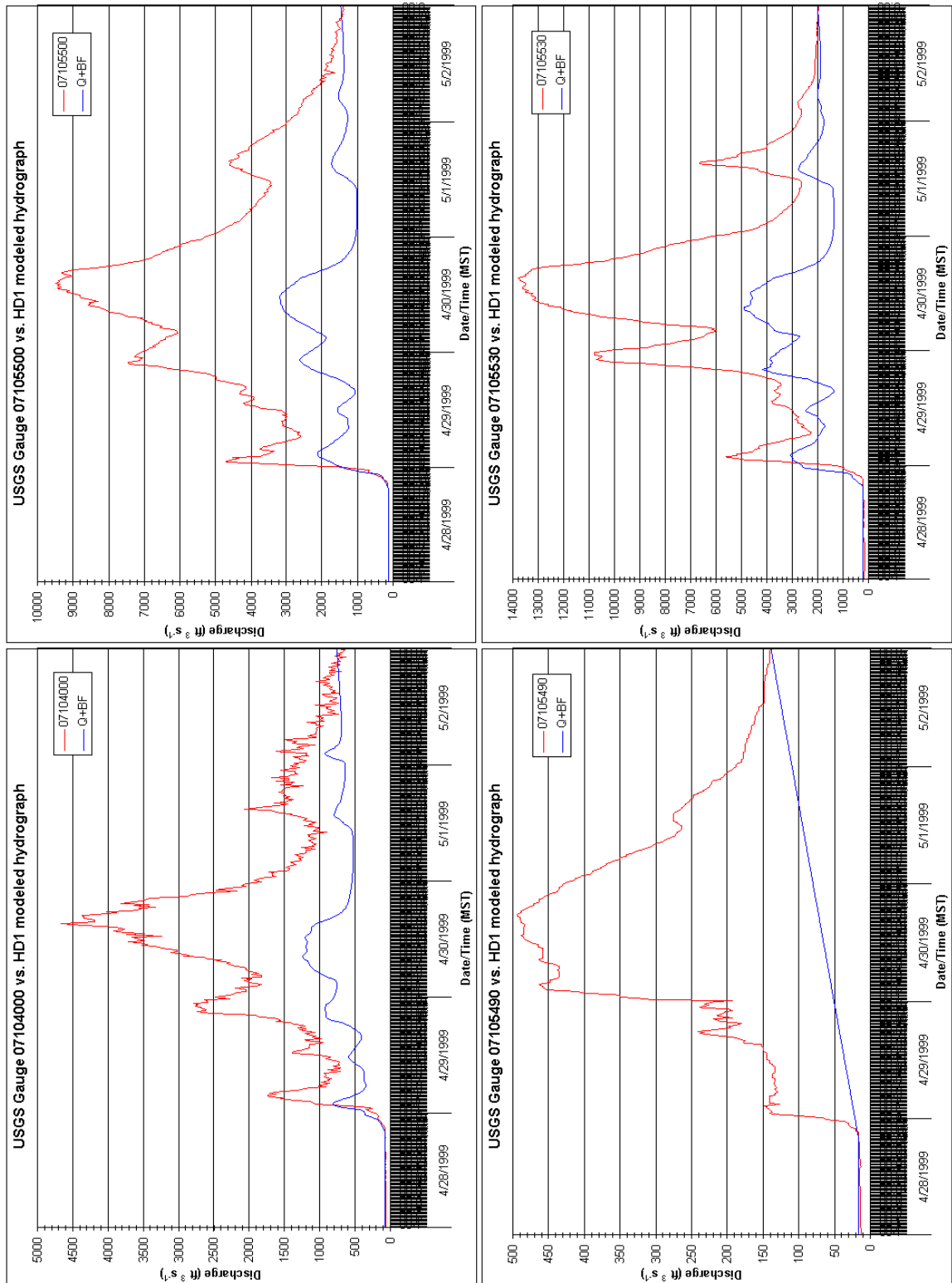


Figure 4.4: Results for simulation HD1 at USGS stream gauge locations. Observed and simulated hydrographs are shown in red and blue, respectively. Gauges are labeled by their USGS designator as listed in Table 3.1. Summarized results are listed in Table 4.1.

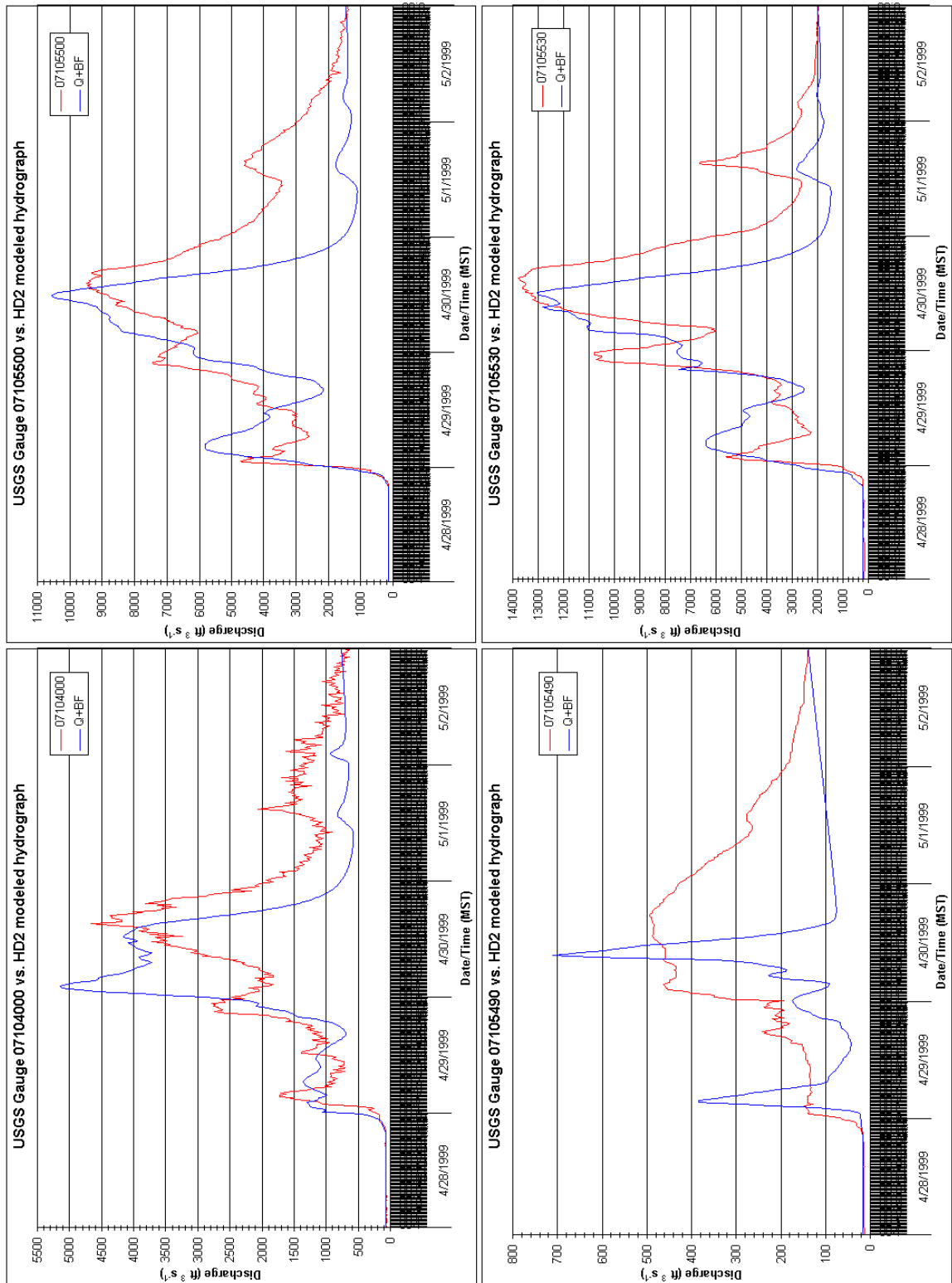


Figure 4.5: Results for simulation HD2 at USGS stream gauge locations. Observed and simulated hydrographs are shown in red and blue, respectively. Gauges are labeled by their USGS designator as listed in Table 3.1. Summarized results are listed in Table 4.1.

was improved in comparison with the results of simulations H1, H2 and HD1.

It was decided that further experimentation with the applied minimum infiltration rates for modeled sub-basins in the watershed was unnecessary, as the present results could be expected to provide an adequate basis for the evaluation of supplemental hyetograph methods described below. In addition, the further reduction of minimum infiltration rates could be expected to result in greater deviations between simulated and observed hydrographs than those shown around the minor peak discharges in Figure 4.3. This effort is intended to remain consistent with the methodology of using supplemental rainfall records for the representation of greater rainfall totals at higher elevations. Therefore, it must be considered that the supplemental hyetograph records will be employed as a means of adding rainfall and resultant runoff volume to the modeled watershed, instead of the removal of runoff volume from that watershed for the simulated event by the specification of smaller rainfall totals than observed in the surrounding region. Therefore, it was more desirable to find a slight underestimation of discharge peaks and total runoff volumes in the present experiments than to adjust the minimum infiltration parameters until an overestimation of those discharge quantities resulted.

### **4.3 Application of Derived Supplemental Rainfall Records**

RUNOFF simulations that employed all available rainfall gauges in and near the Monument and Fountain Creek watersheds as well as the supplemental gauges discussed in Section 3.2.7 are designated HDS here. As a result of the above experiments, these simulations employed the infiltration parameters established in simulations H3 and HD2 above. These simulations employed the rainfall hyetographs for hourly gauges that were shown in Figure 2.17, the disaggregated hourly hyetographs for daily gauges that were shown

in Figure 3.13, and the various sets of derived supplemental hyetographs as established in Chapter 3 (Figures 3.15, 3.16 and 3.18). All of these hyetographs were applied to the modeled sub-basins according to the schematic map of Thiessen polygon areas shown in Figure 3.14.

#### 4.3.1 *HDSa Simulation*

The simulation that employed the supplemental hyetographs established by an inverse-distance-squared method using only the existing hourly gauges, as shown in Figure 3.15, is designated HDSa. The resulting SWMM RUNOFF hydrographs at the locations of USGS gauges for which event records were available are shown in Figure 4.6. Statistical parameters for the observed and simulated discharge records shown there are listed in Table 4.2. For ease of comparison, discharge statistics resulting from the most accurate simulation described above (HD2) are also included in Table 4.2.

It is shown in Table 4.2 that the results of this simulation, when compared with those of simulation HD2, were mixed with respect to improvements in the accuracy of discharge estimation. Specifically, at the location of gauge 07104000 the correlation between simulated and observed hydrographs ( $R^2$ ) was improved but the error in the discharge mean ( $\epsilon_\mu$ ) was greatly increased, and the mean absolute error (MAE) was slightly increased. A slight decrease in the overall accuracy of simulation was found at the location of gauge 07105500, as indicated by a greater overestimation of the maximum discharge ( $\epsilon_{max}$ ) and a slight decrease in the value of  $R^2$ . At the location of gauge 07105530, however, improvements in the accuracy of simulation were found for all measures indicated in Table 4.2.

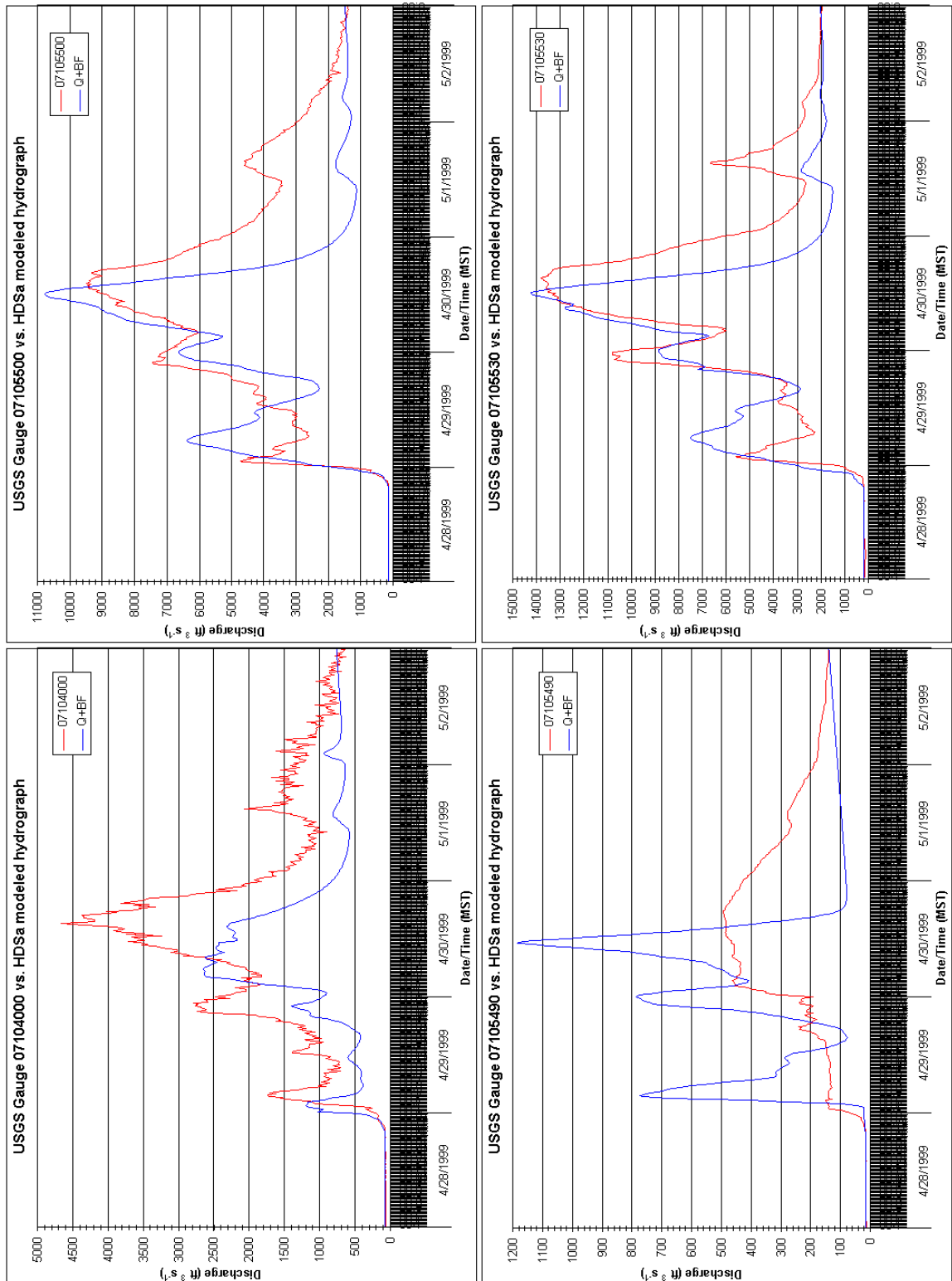


Figure 4.6: Results for simulation HDSa at USGS stream gauge locations. Observed and simulated hydrographs are shown in red and blue, respectively. Gauges are labeled by their USGS designator as listed in Table 3.1. Summarized results are listed in Table 4.2.

Table 4.2: Summary of flood event hydrologic simulation results.

	HD2		HDSa		Simulation Designator		HDSd	
	1-14	6.21	1-18	6.85	HDSb	1-18	HDSc	1-18
Rain Gauges								
Overall MAP						1-18	7.28	8.76
<b>Results at USGS gauge 07104000</b>								
$\epsilon_\mu$ (ft <sup>3</sup> s <sup>-1</sup> )	-171.4 (-11.4%)		-590.4 (-39.2%)		-434.8 (-28.8%)		-165.7 (-11.0%)	+105.1 (+7.0%)
$\epsilon_{max}$ (ft <sup>3</sup> s <sup>-1</sup> )	+486.3 (+10.4%)		-2013.8 (-43.2%)		-867.4 (-18.6%)		+575.6 (+12.4%)	-110.4 (-2.4%)
$\epsilon_\sigma$ (ft <sup>3</sup> s <sup>-1</sup> )	+252.6 (+25.1%)		-358.8 (-35.7%)		-129.6 (-12.9%)		+227.7 (+22.7%)	+28.6 (+2.8%)
$\epsilon_V$ (ac-ft)	-1504.7 (-11.4%)		-5184.6 (-39.2%)		-3817.7 (-28.8%)		-1455.0 (-11.0%)	+923.0 (+7.0%)
$\epsilon_{\rho^2}$	+0.0072 (+0.7%)		+0.0061 (+0.6%)		+0.0069 (+0.7%)		+0.0071 (+0.7%)	+0.0068 (+0.7%)
$R^2$	0.4925		0.6144		0.5346		0.5498	0.9122
MAE (ft <sup>3</sup> s <sup>-1</sup> )	653.5		660.1		631.4		585.9	193.4
<b>Results at USGS gauge 07105490</b>								
$\epsilon_\mu$ (ft <sup>3</sup> s <sup>-1</sup> )	-123.4 (-48.8%)		-9.2 (-3.6%)		+8.7 (+3.4%)		+278.7 (+110.1%)	+1.4 (+0.6%)
$\epsilon_{max}$ (ft <sup>3</sup> s <sup>-1</sup> )	+216.4 (+43.8%)		+689.3 (+139.5%)		+934.5 (+189.2%)		+2065.1 (+418.0%)	+3.3 (+0.7%)
$\epsilon_\sigma$ (ft <sup>3</sup> s <sup>-1</sup> )	-28.7 (-21.3%)		+116.1 (+86.1%)		+178.8 (+132.5%)		+537.3 (+398.2%)	+1.2 (+0.9%)
$\epsilon_V$ (ac-ft)	-1032.6 (-48.8%)		-77.1 (-3.6%)		+72.9 (+3.4%)		+2331.7 (+110.1%)	+11.8 (+0.6%)
$\epsilon_{\rho^2}$	-0.0077 (-0.8%)		-0.0024 (-0.2%)		-0.0006 (-0.1%)		-0.0002 (0.0%)	+0.0012 (+0.1%)
$R^2$	0.1195		0.1328		0.2486		0.1824	0.9957
MAE (ft <sup>3</sup> s <sup>-1</sup> )	143.4		172.7		190.4		430.0	5.3
<b>Results at USGS gauge 07105500</b>								
$\epsilon_\mu$ (ft <sup>3</sup> s <sup>-1</sup> )	-986.4 (-23.6%)		-986.1 (-23.6%)		-757.6 (-18.2%)		-334.2 (-8.0%)	+188.5 (+4.5%)
$\epsilon_{max}$ (ft <sup>3</sup> s <sup>-1</sup> )	+1060.0 (+11.2%)		+1287.5 (+13.6%)		+1972.3 (+20.8%)		+3122.1 (+32.9%)	+230.8 (+2.4%)
$\epsilon_\sigma$ (ft <sup>3</sup> s <sup>-1</sup> )	+309.6 (+13.0%)		+233.0 (+9.8%)		+530.0 (+22.3%)		+1007.9 (+42.4%)	+72.0 (+3.0%)
$\epsilon_V$ (ac-ft)	-8335.4 (-23.6%)		-8332.9 (-23.6%)		-6401.6 (-18.2%)		-2823.9 (-8.0%)	+1592.9 (+4.5%)
$\epsilon_{\rho^2}$	+0.0008 (+0.1%)		+0.0006 (+0.1%)		+0.0008 (+0.1%)		+0.0010 (+0.1%)	+0.0008 (+0.1%)
$R^2$	0.5902		0.5855		0.6020		0.6267	0.9785
MAE (ft <sup>3</sup> s <sup>-1</sup> )	1628.5		1578.6		1611.7		1727.4	228.5
<b>Results at USGS gauge 07105530</b>								
$\epsilon_\mu$ (ft <sup>3</sup> s <sup>-1</sup> )	-820.8 (-17.3%)		-652.8 (-13.7%)		-441.9 (-9.3%)		+271.9 (+5.7%)	+653.8 (+13.8%)
$\epsilon_{max}$ (ft <sup>3</sup> s <sup>-1</sup> )	-766.4 (-5.6%)		+431.1 (+3.1%)		+1229.3 (+8.9%)		+3557.7 (+25.9%)	+49.8 (+0.4%)
$\epsilon_\sigma$ (ft <sup>3</sup> s <sup>-1</sup> )	-375.3 (-10.1%)		-251.7 (-6.8%)		+85.8 (+2.3%)		+953.9 (+25.8%)	-120.9 (-3.3%)
$\epsilon_V$ (ac-ft)	-7207.3 (-17.3%)		-5732.2 (-13.7%)		-3880.1 (-9.3%)		+2387.6 (+5.7%)	+5740.8 (+13.8%)
$\epsilon_{\rho^2}$	+0.0005 (+0.1%)		+0.0005 (0.0%)		+0.0007 (+0.1%)		+0.0009 (+0.1%)	+0.0005 (0.0%)
$R^2$	0.6469		0.6482		0.6608		0.6639	0.9728
MAE (ft <sup>3</sup> s <sup>-1</sup> )	1627.5		1560.1		1625.9		1949.0	675.6

#### 4.3.2 *HDSb Simulation*

It was considered in Chapter 3 that the limited dependence of supplemental rainfall gauge records on only those existing hourly gauges in the surrounding area may lead to inadequacy in the simulation of observed stream discharge records. As an alternative, the derivation of supplemental rainfall gauge records by the inverse-distance-squared method may rely on all available (existing) rainfall gauges in the surrounding area. The derived supplemental rainfall records were shown in Figure 3.16, and the simulation that employed these records is designated HDSb. The resulting SWMM RUNOFF hydrographs at the locations of USGS gauges for which event records were available are shown in Figure 4.7, and statistical parameters for the observed and simulated discharge records shown there are listed in Table 4.2.

It is shown in Table 4.2 that general improvements in the accuracy of simulation were found at the location of gauge 07104000, though the correlation decreased slightly from that of the HDSa simulation there. Similar results were found at the locations of gauges 07105500 and 07105530, though the MAE increased slightly from that of the HDSa simulation for both of these.

#### 4.3.3 *HDSc Simulation*

Supplemental hyetographs derived by the characteristics method discussed in Chapter 3 are basically an extension of those employed in simulation HDSb but provide a greater total depth of rainfall to the modeled watersheds. The supplemental hyetographs for the characteristics method were shown in Figure 3.17, and the simulation that employed these records is designated HDSc. The resulting SWMM RUNOFF hydrographs at the locations of USGS gauges for which event records were available are shown in Figure 4.8, and statis-

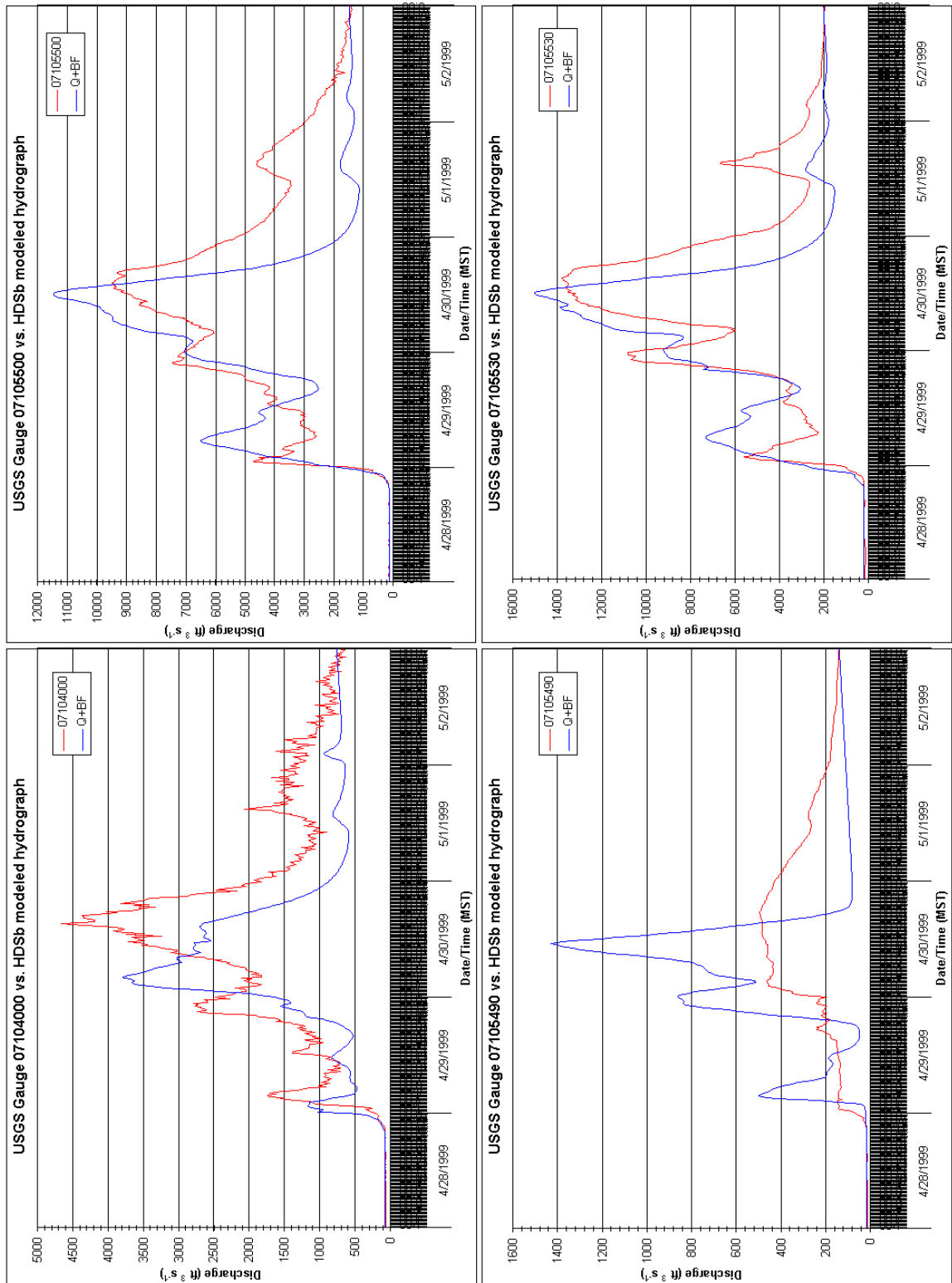


Figure 4.7: Results for simulation HDSb at USGS stream gauge locations. Observed and simulated hydrographs are shown in red and blue, respectively. Gauges are labeled by their USGS designator as listed in Table 3.1. Summarized results are listed in Table 4.2.

tical parameters for the observed and simulated discharge records shown there are listed in Table 4.2.

Again, it is shown in Table 4.2 that general improvements in the accuracy of simulation, as indicated by the combination of statistics  $R^2$  and  $(\epsilon_\mu)$ , were found at most locations. However, the overestimation of discharge maxima was found at all locations, and the MAE was found to increase significantly from that of the HDSa and HDSb simulations at the locations of gauges 07105500 and 07105530. At the location of gauge 07105490, the largest errors in most statistics thus far were found for this simulation.

Overall, though the results of this simulation provided the most accurate simulation of observed discharges at most of the available stream gauge locations, this accuracy was still considered inadequate for the determination of missing rainfall and stream discharge records at other locations in the modeled watersheds. Specifically, the total discharge volume remained underestimated in areas upstream of the confluence of Monument and Fountain Creeks, even though the peak discharges were overestimated at all locations. In addition, the reliance of this simulation on climatological rainfall records did not necessarily indicate the true spatial variation of rainfall totals, especially the effects of topography, during this particular storm event.

#### 4.4 HDSd Simulations

The simulations described above were performed under a concept of fixed or known input, the known and supplemental rainfall records, such that the resulting discharge records were expected to deviate from the observed records to some degree. The alternative to this method is a hydrologic inverse problem involving the determination of input rainfall records using known discharge records. Given the obvious complexity of a distributed, nonlinear

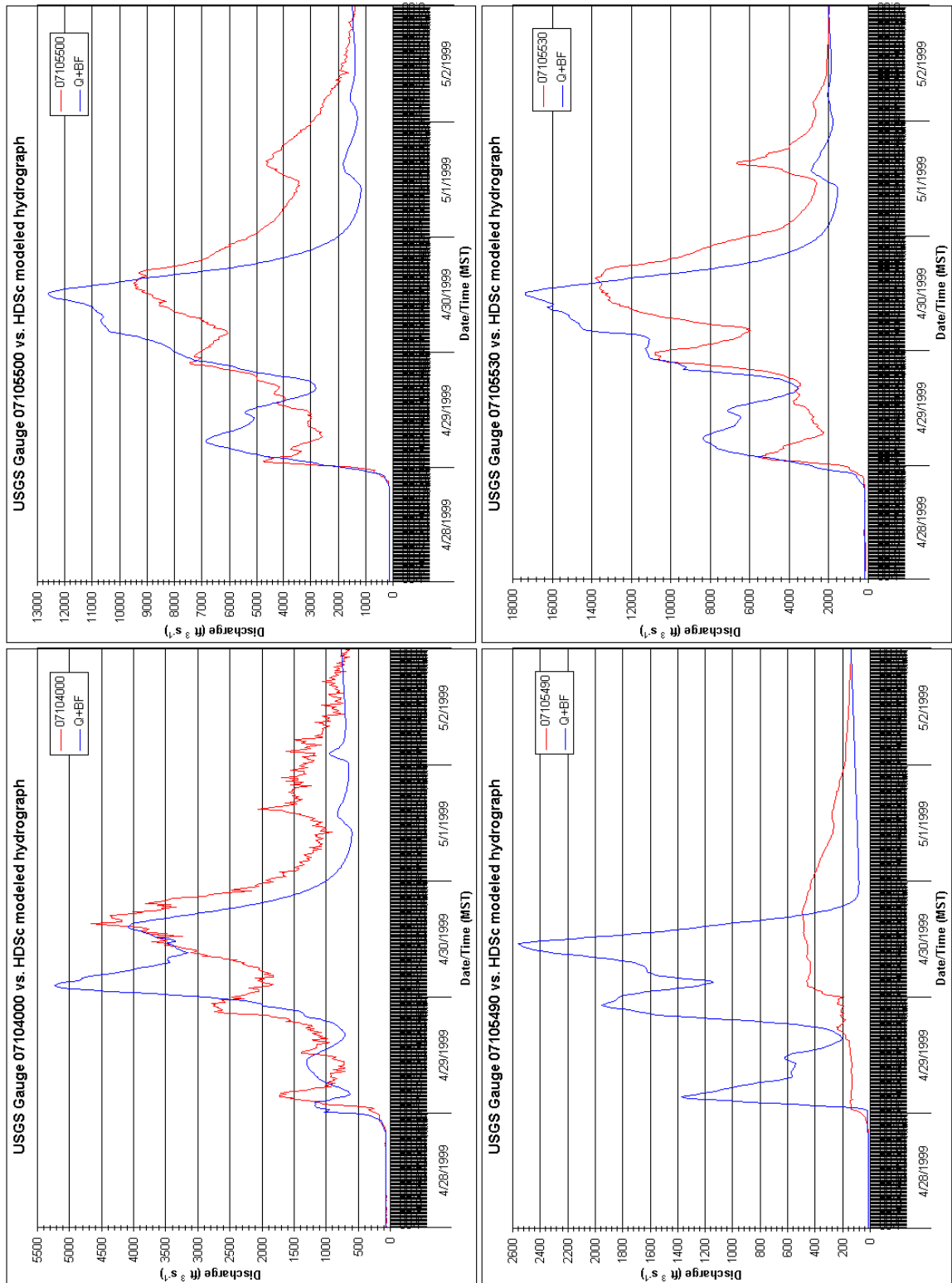


Figure 4.8: Results for simulation HDSc at USGS stream gauge locations. Observed and simulated hydrographs are shown in red and blue, respectively. Gauges are labeled by their USGS designator as listed in Table 3.1. Summarized results are listed in Table 4.2.

rainfall–runoff model on this spatial and temporal scale, the solution to such a problem cannot be expected to develop easily.

The following sections describe a process by which this particular inverse problem may be solved in a quasi-objective fashion. It was considered, before this process was undertaken, that subjective influences on the number or placement of supplemental rainfall gauges and the area represented by each, especially under the influences of topographical variation in the modeled watersheds, would only add complexity to the processes of problem definition and solution. As such, the following process relies on the model parameters and spatial distribution of rainfall gauges described above. These simulations employed the minimum infiltration parameters established in simulations H3 and HD2 and employed in simulations HDSa, b and c above. The rainfall hyetographs for hourly gauges were shown in Figure 2.17, and the disaggregated hourly hyetographs for daily gauges were shown in Figure 3.13. All of the hyetographs were applied to the modeled sub-basins according to the schematic map of Thiessen polygon areas shown in Figure 3.14.

For ease of both problem definition and problem solution, the modeled watersheds were grouped in representative zones corresponding to each of the supplemental rainfall gauges (nos. 15–18) indicated in Figure 3.14. Though the general process of problem solution is consistent in the progression through these zones, the determination of hyetograph records for each zone will be described individually.

#### *4.4.1 Hyetograph 15 (USGS gauge 07104000)*

The zone assigned to supplemental rainfall gauge 15 included portions of the upper and middle Monument Creek watershed, as shown in Figure 3.14. The hyetograph for rainfall gauge 15 was assigned to 59 forested and grassland sub-basins covering a total area

of nearly 90 mi<sup>2</sup> within the contributing area for USGS gauge 07104000.

For the determination of rainfall records in this zone, the existing watershed model was truncated at the location of USGS gauge 07104000 and a simulation was performed with the remaining watershed for which  $P_{15} = 0.00$  inches ( $P_{15} = P$  at rainfall gauge 15). It should be noted explicitly that other rainfall records (at gauges 1, 5, 7, 10, 13 and 14) were applied to the remaining portions of the contributing area for USGS gauge 07104000 as in previous simulations. The resulting hydrograph at gauge 07104000 was then subtracted from the observed discharge record for the storm event at that location to produce a “partial hydrograph” for which runoff from zone 15 would be responsible. The goal of this method was to determine the rainfall record at supplemental gauge 15 that would lead, by a simulation of rainfall–runoff process on a portion of the modeled watershed area, to this partial hydrograph at the location of USGS gauge 07104000.

The watershed model was then further reduced to only those sub-basins to which hyetograph 15 was assigned, and the routing network was configured such that all of the runoff from these sub-basins was conveyed to the location of USGS gauge 07104000. A schematic of the resulting watershed model is shown in Figure 4.9, and may be compared with the complete watershed sub-basin and routing network schematics shown in Figure 3.6. The reader will note that, within the contributing area for USGS gauge 07104000, all of those sub-basins to which a hyetograph other than no. 15 was assigned have been eliminated in order to produce the schematic shown in Figure 4.9.

Simulations were performed on an hour-by-hour basis using this model for zone 15. At each iteration of this simulation procedure, individual hours of the rainfall hyetograph were specified or adjusted until the partial hydrograph discharges and shapes were reproduced to the author’s satisfaction (objectively,  $R^2 \geq 0.9$ ). The resulting simulated hydrograph is

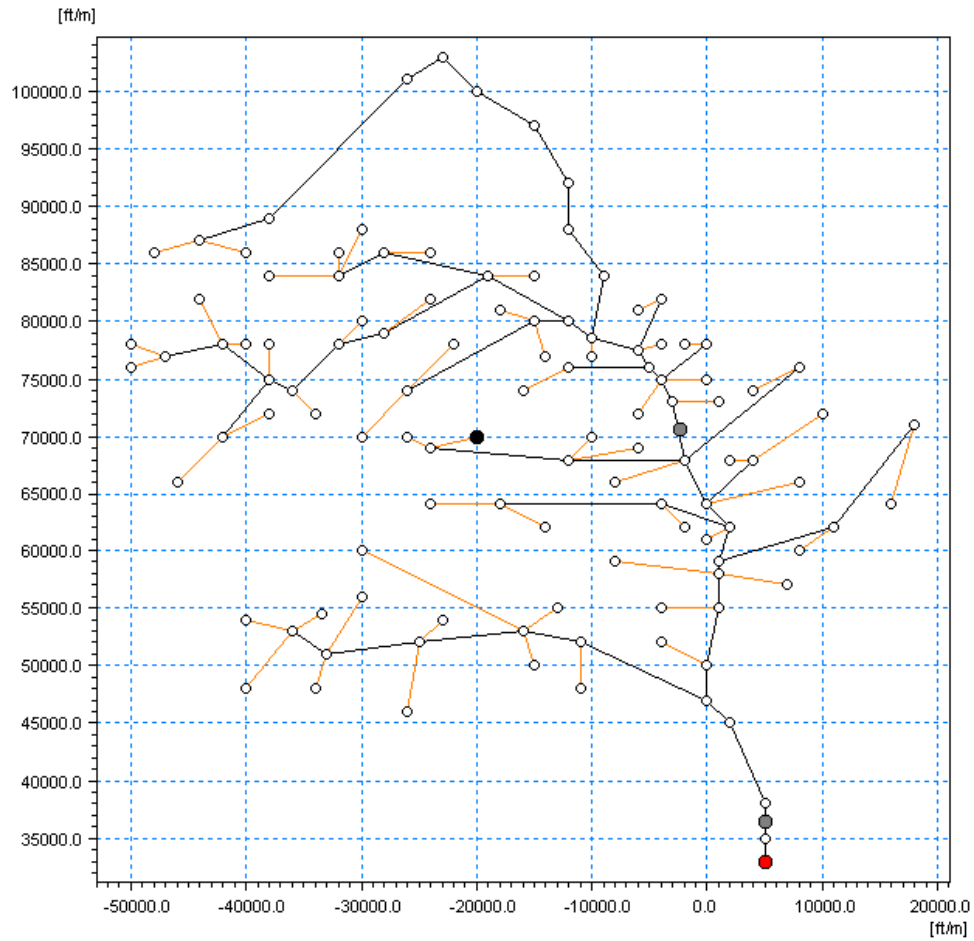


Figure 4.9: Modeled sub-basins affected by hyetograph 15. The location of (supplemental) rainfall gauge no. 15 is shown in black; the location of USGS gauge 07104000 is shown in red; inoperable or unavailable gauges are shown in gray. Coordinates are given in feet north and east of the confluence of Monument and Fountain Creeks in Colorado Springs, Colorado.

compared to the required partial hydrograph in Figure 4.10a. The hyetograph at supplemental gauge 15 required for this accuracy will be shown below. Various statistical measures of this simulation accuracy are summarized in Table 4.3. When the resulting partial hydrograph was recombined with the results of the  $P_{15} = 0.00$  simulation at USGS gauge 07104000, as well as the derived base flow function for that location as shown in Figure 3.4a, the resulting simulated discharge record is shown in Figure 4.10b.

#### 4.4.2 *Hyetograph 16 (USGS gauge 07105490)*

The zone assigned to supplemental rainfall gauge 16 included the headwaters for Bear and Cheyenne Creeks in southwestern Colorado Springs, as shown in Figure 3.14. Each of these creeks is a tributary to Fountain Creek below its confluence with Monument Creek. However, for reasons described in Chapter 3, the USGS gauge on Bear Creek is not employed in this analysis. Therefore, under the modeling methodology employed here, the hyetograph for rainfall gauge 16 is assigned to only 4 mostly forested sub-basins covering a total area of just more than 21 mi<sup>2</sup>, representing almost the entire contributing area for USGS gauge 07105490.

For the determination of rainfall records in this zone, the existing watershed model was truncated at the location of USGS gauge 07105490. A simulation for which  $P_{16} = 0.00$  inches would have produced only the observed discharge record, reduced by the derived base flow function at that location as described in Section 3.2.3 and shown in Figure 3.4b. It is this direct-runoff (“partial”) hydrograph for which zone 16 was entirely responsible. The goal of this method was to determine the rainfall record at supplemental gauge 16 that would lead, by a simulation of rainfall–runoff process on the modeled watershed area, to this partial hydrograph at the location of USGS gauge 07105490. A schematic of the

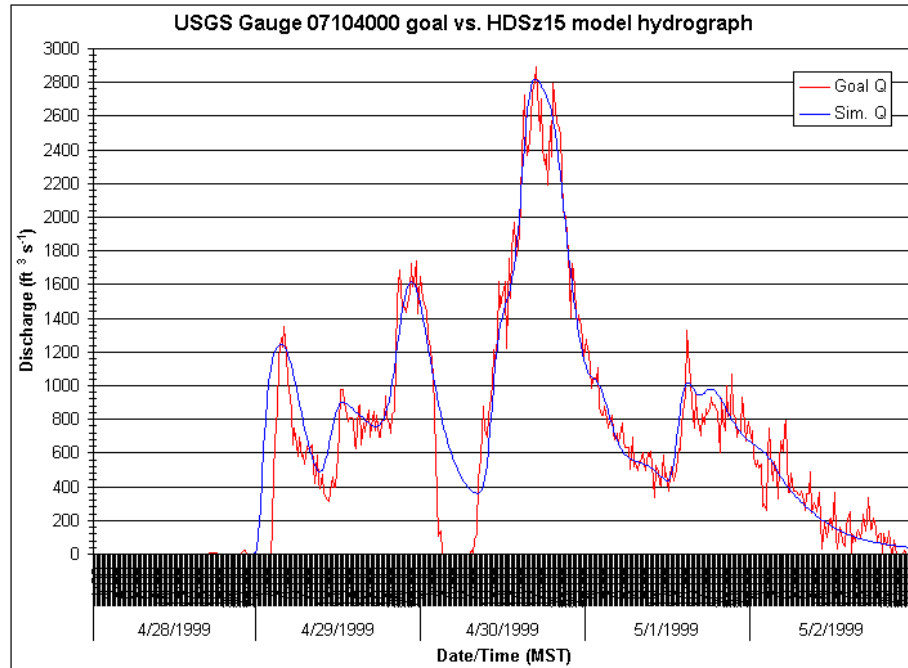


Figure 4.10a: Results of partial hydrograph simulation at USGS gauge 07104000. Observed and simulated hydrographs are shown in red and blue, respectively.

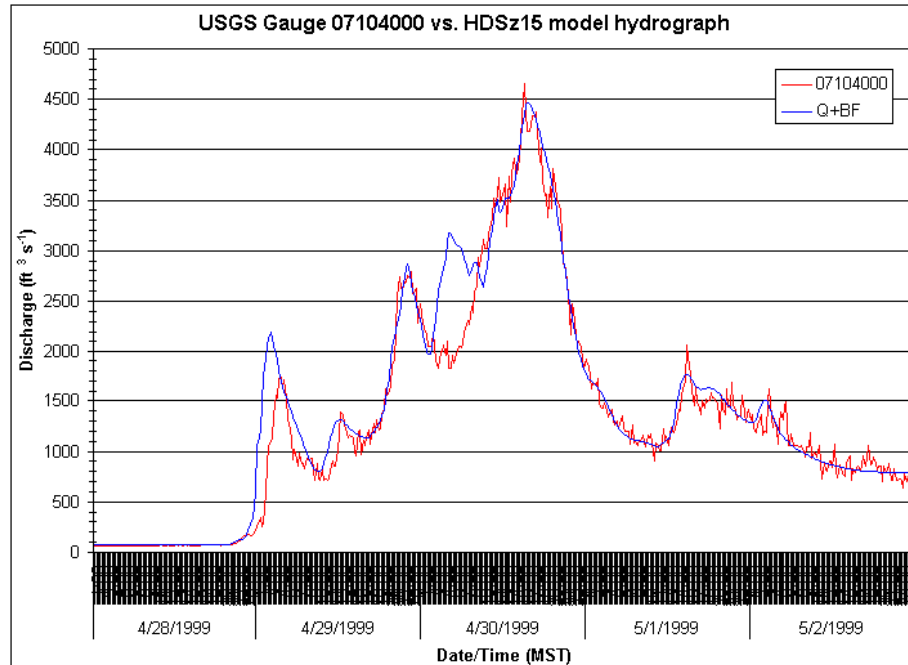


Figure 4.10b: Results of partial model simulation at USGS gauge 07104000. Observed and simulated hydrographs are shown in red and blue, respectively.



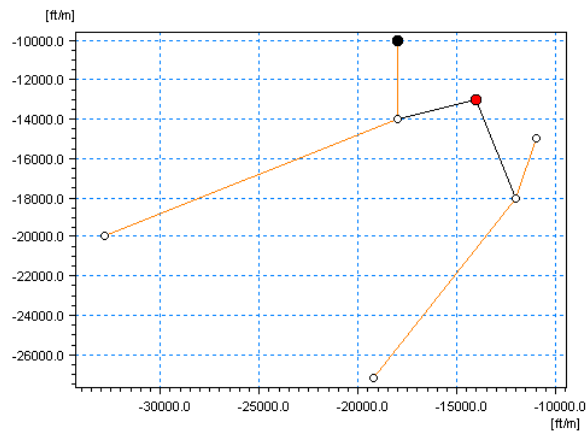


Figure 4.11: Modeled sub-basins affected by hyetograph 16. The location of (supplemental) rainfall gauge no. 16 is shown in black, and the location of USGS gauge 07105490 is shown in red. Coordinates are given in feet north and east of the confluence of Monument and Fountain Creeks in Colorado Springs, Colorado.

resulting watershed model is shown in Figure 4.11, and may be compared with the complete watershed sub-basin and routing network schematics shown in Figure 3.6.

Simulations were performed on an hour-by-hour basis using this model for zone 16. At each iteration of this simulation procedure, individual hours of the rainfall hyetograph were specified or adjusted until the partial hydrograph discharges and shapes were reproduced to the author's satisfaction ( $R^2 \geq 0.9$ ). The resulting simulated hydrograph is compared to the required partial hydrograph in Figure 4.12a. The hyetograph at supplemental gauge 16 required for this accuracy will be shown below. Various statistical measures of this simulation accuracy are summarized in Table 4.3. When these results were combined with the derived base flow function shown in Figure 3.4b, the resulting simulated discharge record at USGS gauge 07105490 is shown in Figure 4.12b.

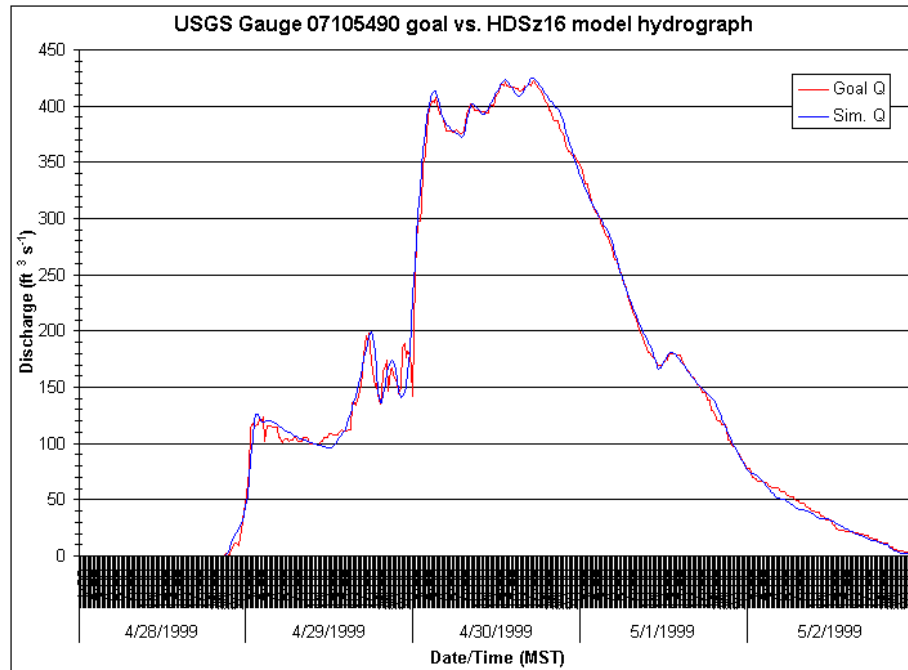


Figure 4.12a: Results of partial hydrograph simulation at USGS gauge 07105490. Observed and simulated hydrographs are shown in red and blue, respectively.

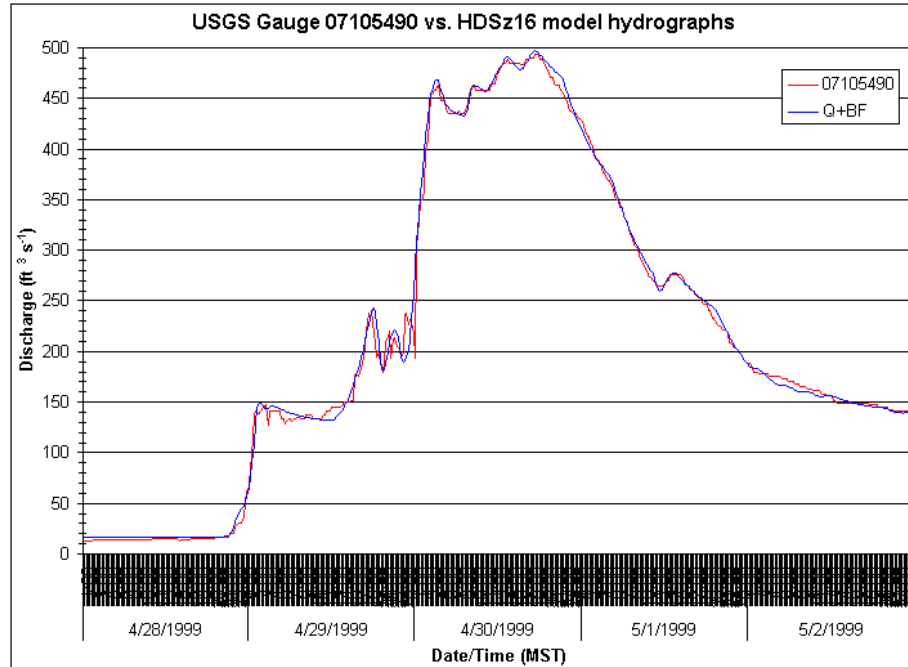


Figure 4.12b: Results of partial model simulation at USGS gauge 07105490. Observed and simulated hydrographs are shown in red and blue, respectively.

#### 4.4.3 *Hyetograph 17 (USGS gauge 07105500)*

The zone assigned to supplemental rainfall gauge 17 included the headwaters for Fountain Creek and various small tributaries on the northern slopes of Pike's Peak west of Colorado Springs, as shown in Figure 3.14. The hyetograph for rainfall gauge 17 was assigned to 30 mostly forested sub-basins covering a total area of nearly 80 mi<sup>2</sup>. However, because of the confluence of Fountain Creek with Monument Creek just upstream of USGS gauge 07105500, zone 17 represented only 20% of the contributing area for that gauge.

For the determination of rainfall records in this zone, the existing watershed model was truncated at the location of USGS gauge 07105500 and a simulation was performed with the remaining watershed for which  $P_{17} = 0.00$  inches. It should be noted explicitly that other rainfall records (at gauges 1–3, 5, 7, 8, 10, 11, 13, 14, and 15 and 16 as found above) were applied to the remaining portions of the area that contributed to discharge records at USGS gauge 07105500 as in previous simulations. The resulting hydrograph at the location of gauge 07105500 was then subtracted from the observed discharge record for the storm event at that location to produce a partial hydrograph for which runoff from zone 17 would be responsible. The goal of this method was to determine the rainfall record at supplemental gauge 17 that would lead, by a simulation of rainfall–runoff process on a portion of the modeled watershed area, to this partial hydrograph at the location of USGS gauge 07105500.

The watershed model was then further reduced to only those sub-basins to which hyetograph 17 was assigned, and the routing network was configured such that all of the runoff from these sub-basins was conveyed to the location of USGS gauge 07105500. A schematic of the resulting watershed model is shown in Figure 4.13, and may be compared with the complete watershed sub-basin and routing network schematics shown in Figure

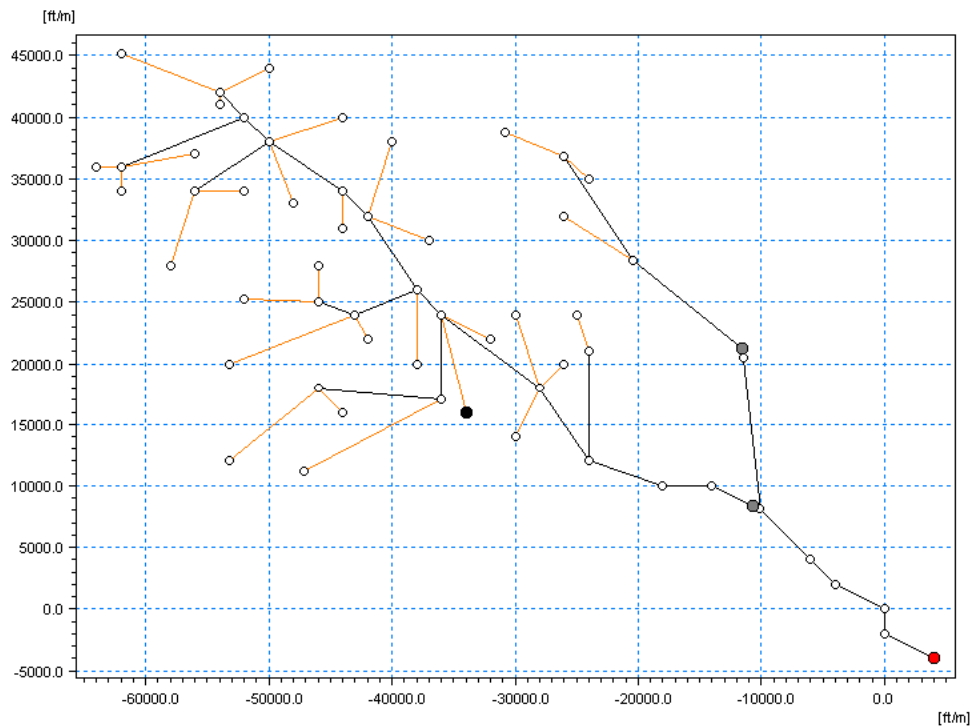


Figure 4.13: Modeled sub-basins affected by hyetograph 17. The location of (supplemental) rainfall gauge no. 17 is shown in black; the location of USGS gauge 07105500 is shown in red; inoperable or unavailable gauges are shown in gray. Coordinates are given in feet north and east of the confluence of Monument and Fountain Creeks in Colorado Springs, Colorado.

3.6. The reader will note that, within the contributing area for USGS gauge 07105500, all of those sub-basins to which a hyetograph other than no. 17 was assigned have been eliminated in order to produce the schematic shown in Figure 4.13.

Simulations were performed on an hour-by-hour basis using this model for zone 17. At each iteration of this simulation procedure, individual hours of the rainfall hyetograph were specified or adjusted until the partial hydrograph discharges and shapes were reproduced to the author's satisfaction ( $R^2 \geq 0.9$ ). The resulting simulated hydrograph is compared to the required partial hydrograph in Figure 4.14a. The hyetograph at supplemental gauge 17 required for this accuracy will be shown below. Various statistical measures of this simulation accuracy are summarized in Table 4.3. When the resulting partial hydrograph

was recombined with the results of the  $P_{17} = 0.00$  simulation at USGS gauge 07105500, as well as the derived base flow function for that location as shown in Figure 3.4c, the resulting simulated discharge record is shown in Figure 4.14b.

#### 4.4.4 *Hyetograph 18 (USGS gauge 07105530)*

The zone assigned to supplemental rainfall gauge 18 included portions of Shooks Run and Spring Creek in Colorado Springs, as shown in Figure 3.14. The hyetograph for rainfall gauge 18 was assigned to 9 urbanized sub-basins covering a total area of more than 11 mi<sup>2</sup>. Because of its size and location within the Monument and Fountain Creek watersheds, zone 18 represents only a small portion of the contributing area for USGS gauge 07105530.

For the determination of rainfall records in this zone, the existing watershed model was truncated at the location of USGS gauge 07105530 and a simulation was performed with the remaining watershed for which  $P_{18} = 0.00$  inches. It should be noted explicitly that other rainfall records (at gauges 1–3, 5, 7, 8, 10–14, and 15–17 as found above) were applied to the remaining portions of the contributing area for USGS gauge 07105530, as in previous simulations. The resulting hydrograph at the location of gauge 07105530 was then subtracted from the observed discharge record for the storm event at that location to produce a partial hydrograph for which runoff from zone 18 would be responsible. The goal of this method was to determine the rainfall record at supplemental gauge 18 that would lead, by a simulation of rainfall–runoff process on a portion of the modeled watershed area, to this partial hydrograph at USGS gauge 07105530.

The watershed model was then further reduced to only those sub-basins to which hyetograph 18 was assigned, and the routing network was configured such that all of the runoff from these sub-basins was conveyed to the location of USGS gauge 07105530. A

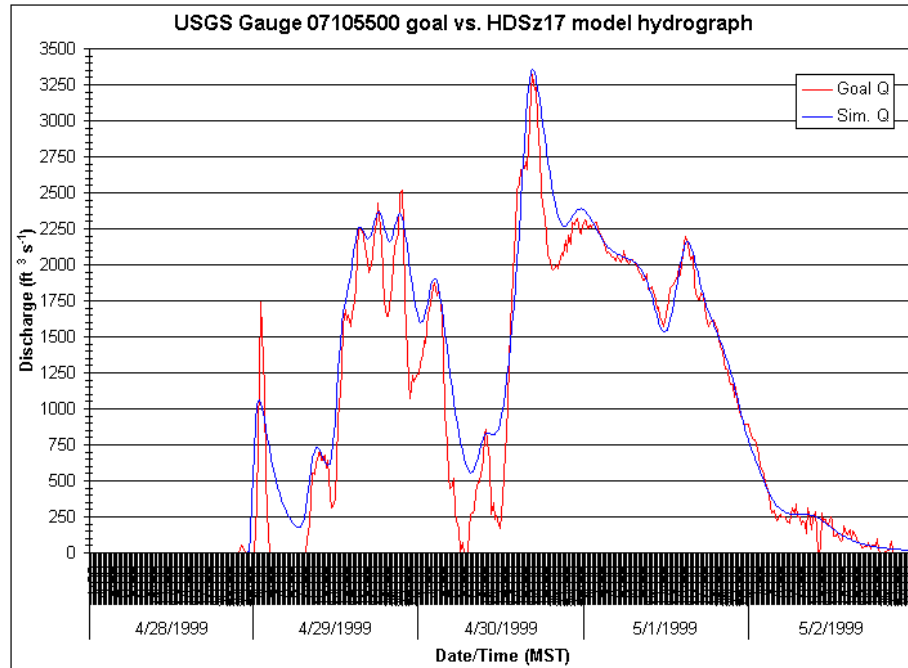


Figure 4.14a: Results of partial hydrograph simulation at USGS gauge 07105500. Observed and simulated hydrographs are shown in red and blue, respectively.

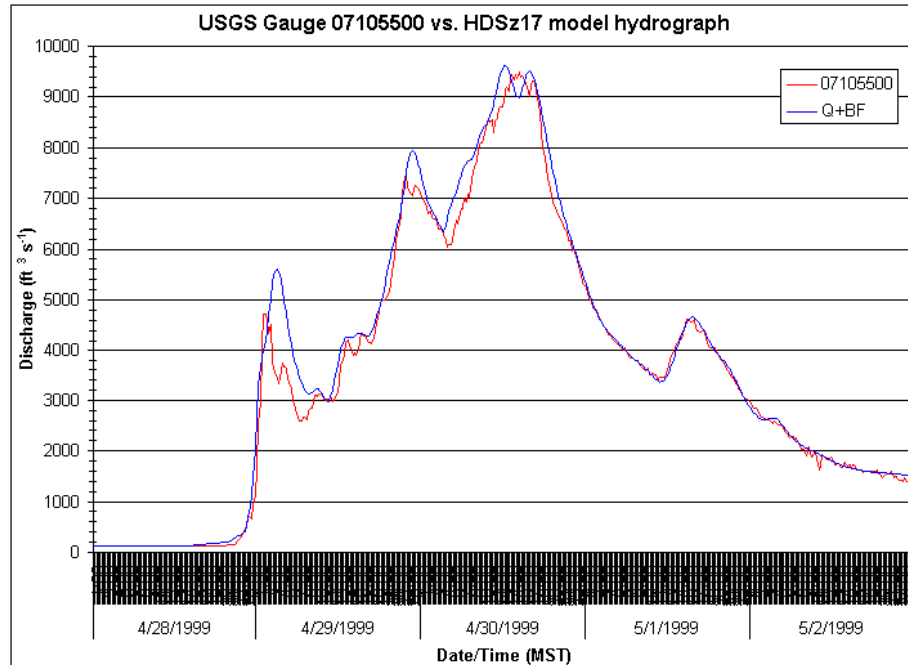


Figure 4.14b: Results of partial model simulation at USGS gauge 07105500. Observed and simulated hydrographs are shown in red and blue, respectively.

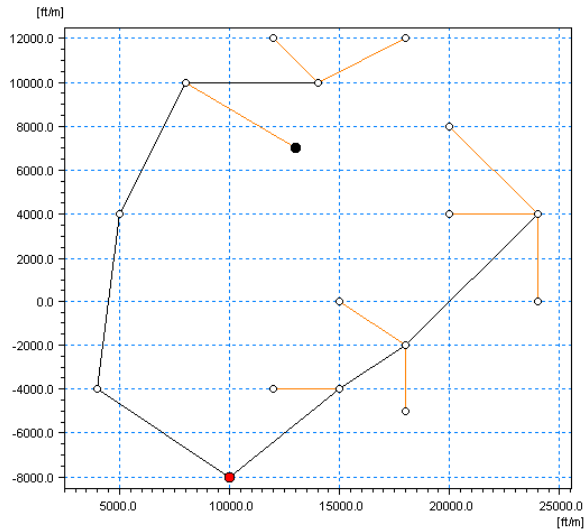


Figure 4.15: Modeled sub-basins affected by hyetograph 18. The location of (supplemental) rainfall gauge no. 18 is shown in black, and the location of USGS gauge 07105530 is shown in red. Coordinates are given in feet north and east of the confluence of Monument and Fountain Creeks in Colorado Springs, Colorado.

schematic of the resulting watershed model is shown in Figure 4.15, and may be compared with the complete watershed sub-basin and routing network schematics shown in Figure 3.6. The reader will note that, within the contributing area for USGS gauge 07105530, all of those sub-basins to which a hyetograph other than no. 18 was assigned have been eliminated in order to produce the schematic shown in Figure 4.15.

Simulations were performed on an hour-by-hour basis using this model for zone 18. At each iteration of this simulation procedure, individual hours of the rainfall hyetograph were specified or adjusted until the partial hydrograph discharges and shapes were reproduced to the author's satisfaction ( $R^2 \geq 0.9$ ). The resulting simulated hydrograph is compared to the required partial hydrograph in Figure 4.16a. The hyetograph at supplemental gauge 18 required for this accuracy will be shown below. Various statistical measures of this simulation accuracy are summarized in Table 4.3. When the resulting partial hydrograph was recombined with the results of the  $P_{18} = 0.00$  simulation at USGS gauge 07105530, as

well as the derived base flow function for that location as shown in Figure 3.4d, the resulting simulated discharge record is shown in Figure 4.16b.

#### 4.4.5 *Overall Results*

The supplemental hyetographs required for accuracy demonstrated in the above zone-based simulations are shown in Figure 4.17. These supplemental records indicated greater storm event rainfall totals than occurred at all of the existing rainfall gauges in the region (cf. Table 3.9). The resulting regional distribution of event rainfall is shown in Figure 4.18, and should be compared with the spatial distribution of observed rainfall totals shown in Figure 2.18.

The reader will note that greater rainfall totals were found for these simulation results on the eastern slopes of the Rampart Range, in the vicinity of Cheyenne Mountain in southwestern Colorado Springs, and in the central portion of the City of Colorado Springs. However, rain shadows persist in the northwestern part of the region (rainfall gauge 1), as for the climatological observations presented above, and in the vicinity of Pike's Peak and Cheyenne Mountain (rainfall gauges 2 and 8) in the southwestern part of the modeled watershed area. The latter result will be discussed below with regard to the possibility of small-scale near-surface wind patterns that may have been present during this event.

Consistent correlations between rainfall totals and gauge elevations were also found for these results. In Figure 4.19, it is shown that a positive correlation exists between simulated rainfall totals and gauge elevation for each storm during the event, according to the divisions listed in Section 2.3.3, as well as for the total event rainfall. However, these positive correlations were found only after those stations for which rain shadow effects were evident (rainfall gauges 1, 2 and 8) were excluded from the determination of the trend lines

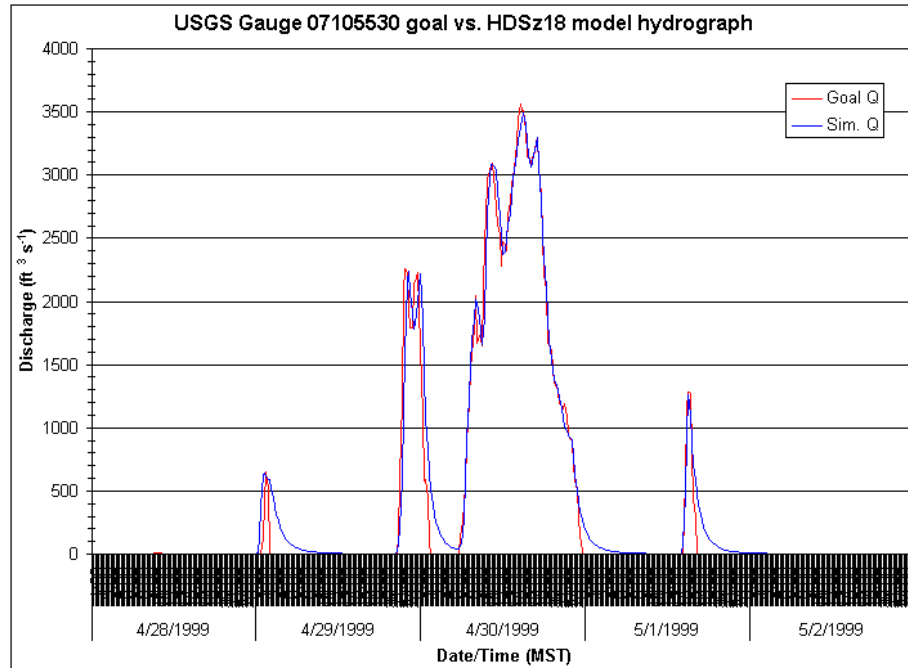


Figure 4.16a: Results of partial hydrograph simulation at USGS gauge 07105530. Observed and simulated hydrographs are shown in red and blue, respectively.

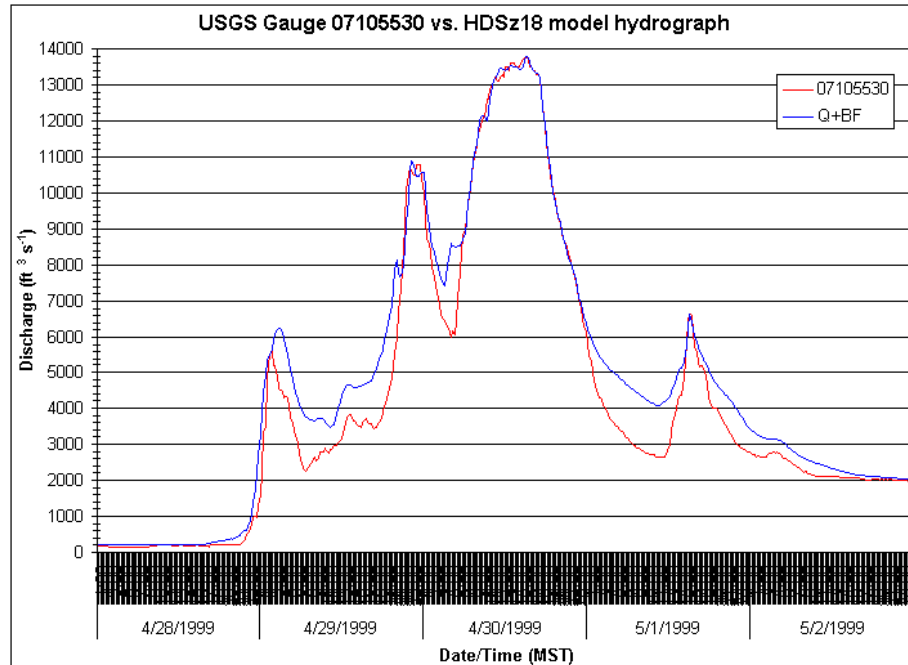


Figure 4.16b: Results of partial model simulation at USGS gauge 07105530. Observed and simulated hydrographs are shown in red and blue, respectively.

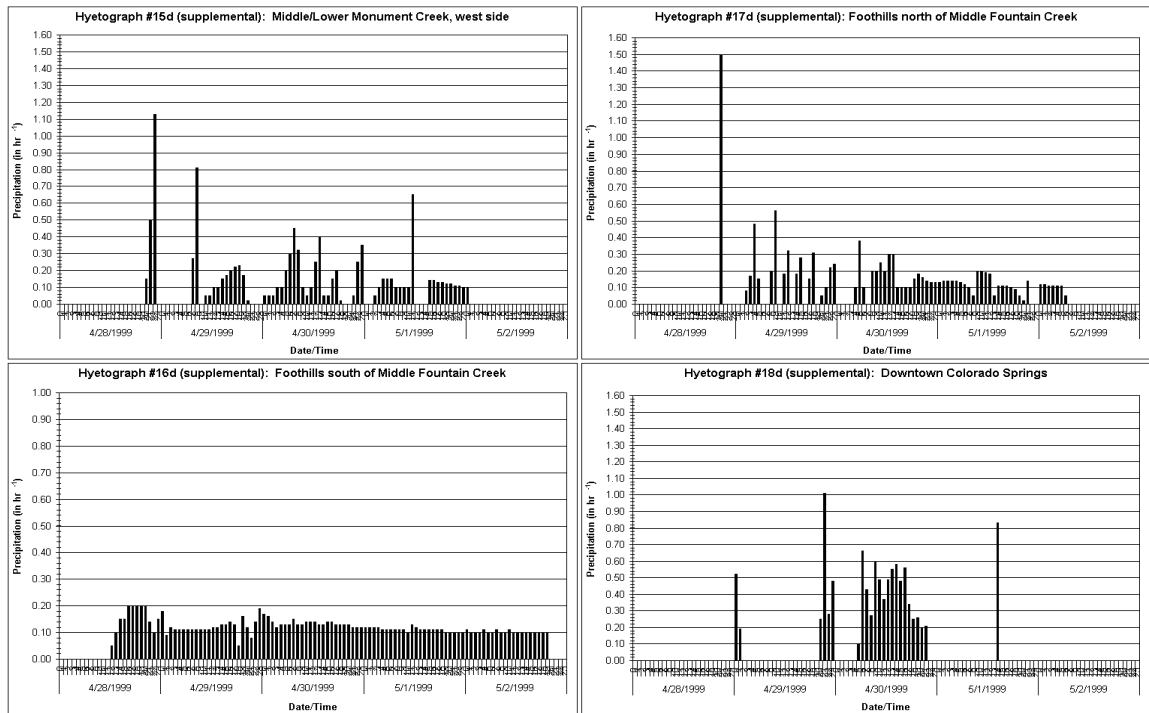


Figure 4.17: Rainfall at supplemental gauges derived by hydrograph-fitting method. Gauge names and locations are listed in Table 2.2.

shown on the graphs in Figure 4.19.

When the supplemental hyetographs shown in Figure 4.17 were combined with those shown previously for the existing hourly and daily gauges in the region (Figures 2.17 and 3.13, respectively), according to the schematic map of Thiessen polygon areas shown in Figure 3.14, the overall simulation results at the locations of the four USGS stream gauges of interest are shown in Figure 4.20. Statistical measures of these results have been summarized in Table 4.2 above. It is shown there that improvements in the accuracy of discharge simulations at the USGS gauge locations are significant for the HDSd hydrograph-fitting method.

Interpolated total rainfall during April 28-May 2, 1999

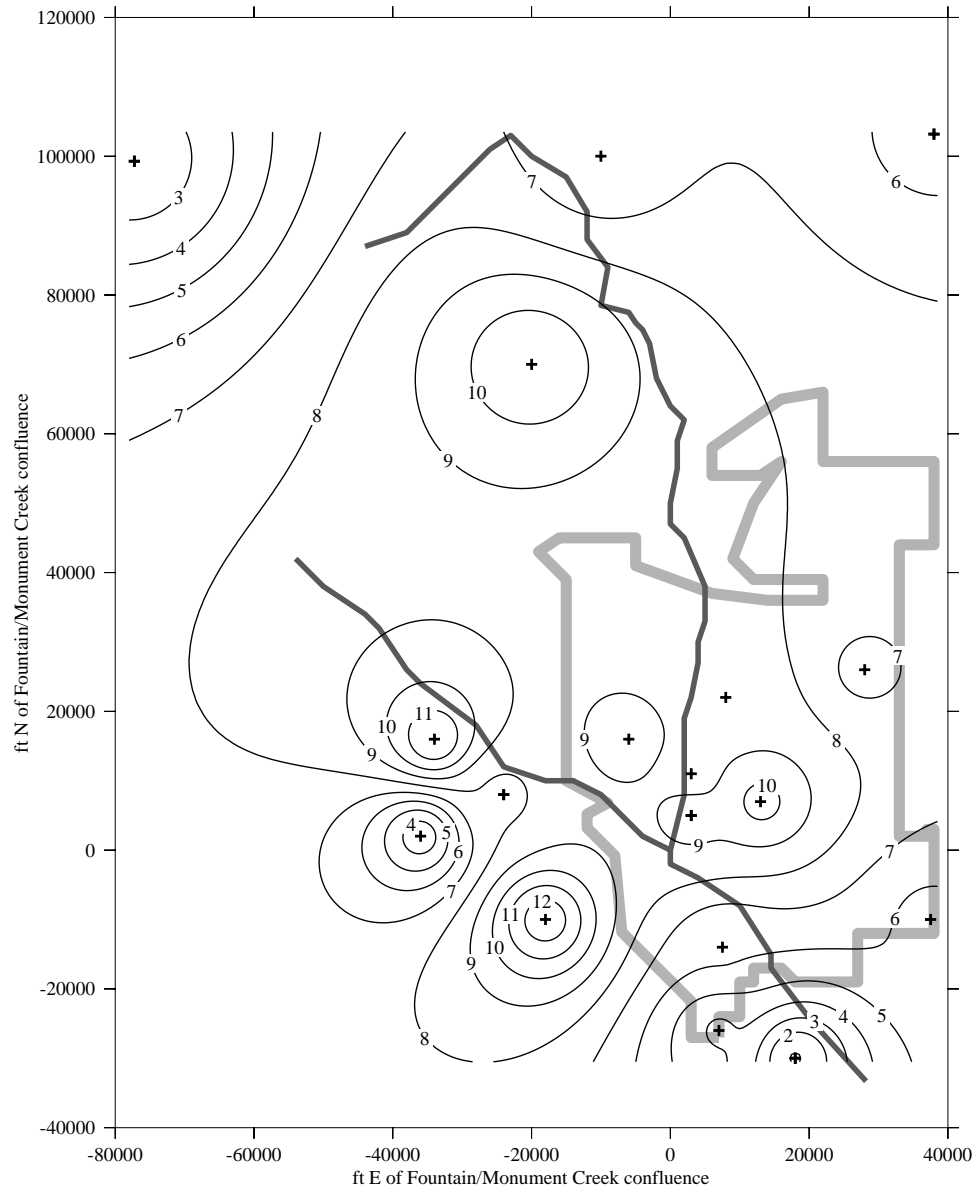


Figure 4.18: Interpolated total rainfall during April 28–May 2, 1999.

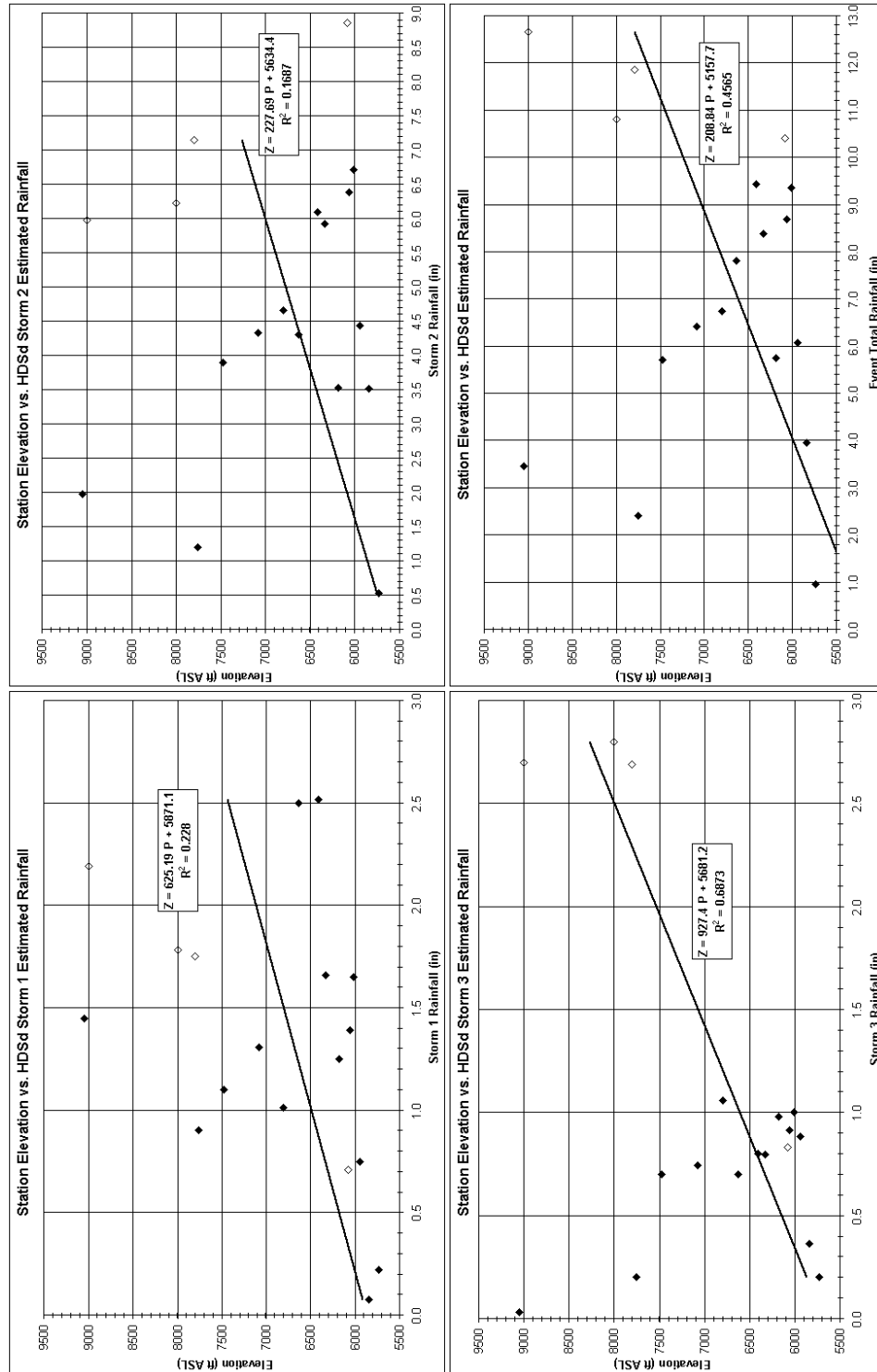


Figure 4.19: Correlations between storm and event total rainfall and gauge elevation.

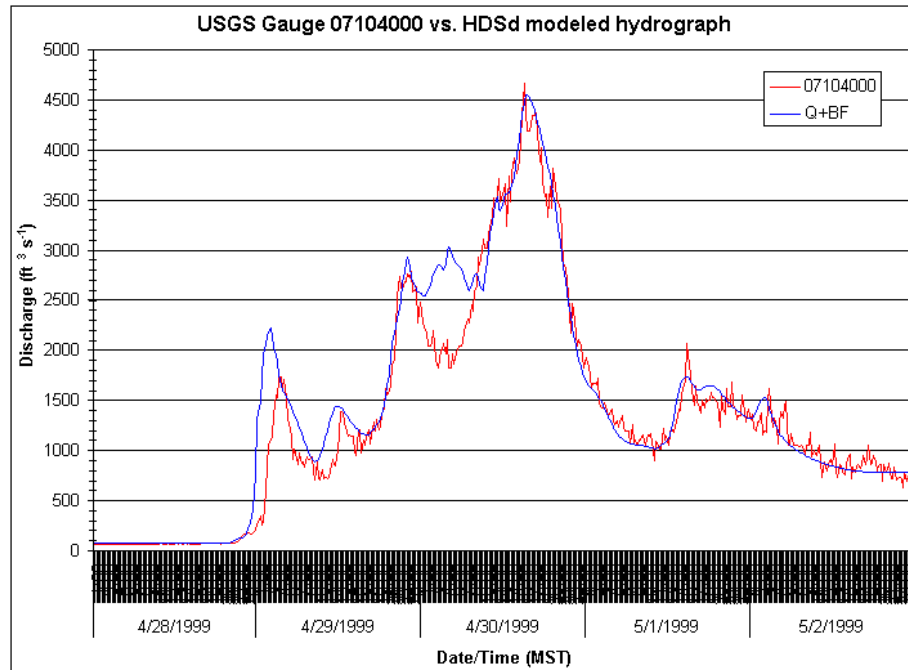


Figure 4.20a: Results of full model simulation at USGS gauge 07104000. Observed and simulated hydrographs are shown in red and blue, respectively.

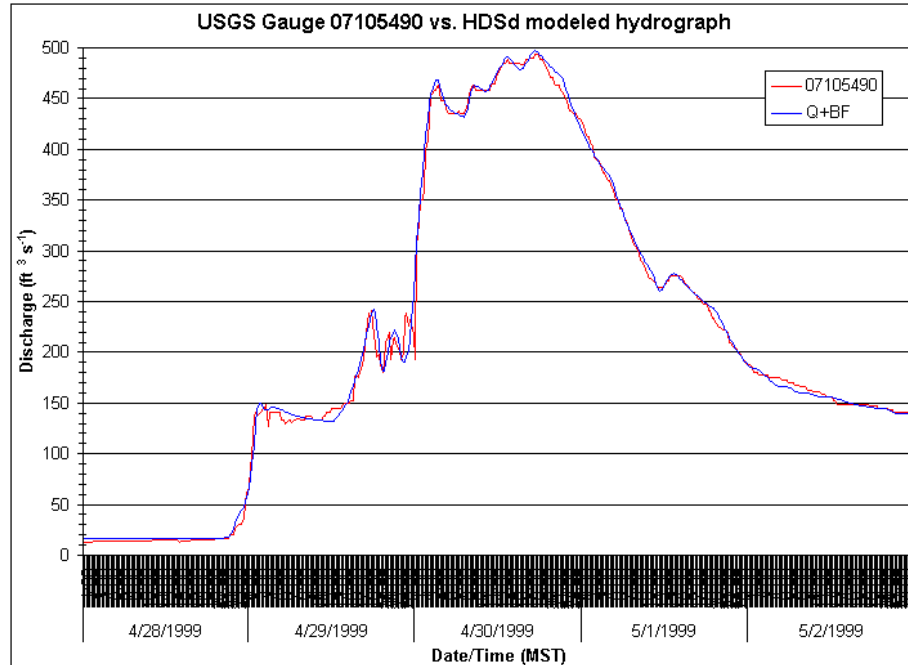


Figure 4.20b: Results of full model simulation at USGS gauge 07105490. Observed and simulated hydrographs are shown in red and blue, respectively.

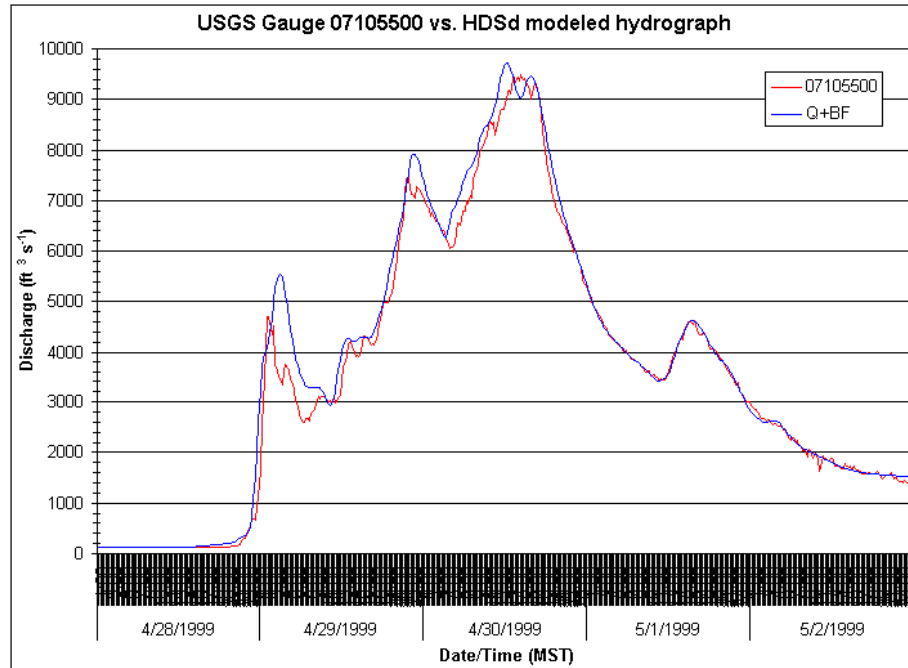


Figure 4.20c: Results of full model simulation at USGS gauge 07105500. Observed and simulated hydrographs are shown in red and blue, respectively.

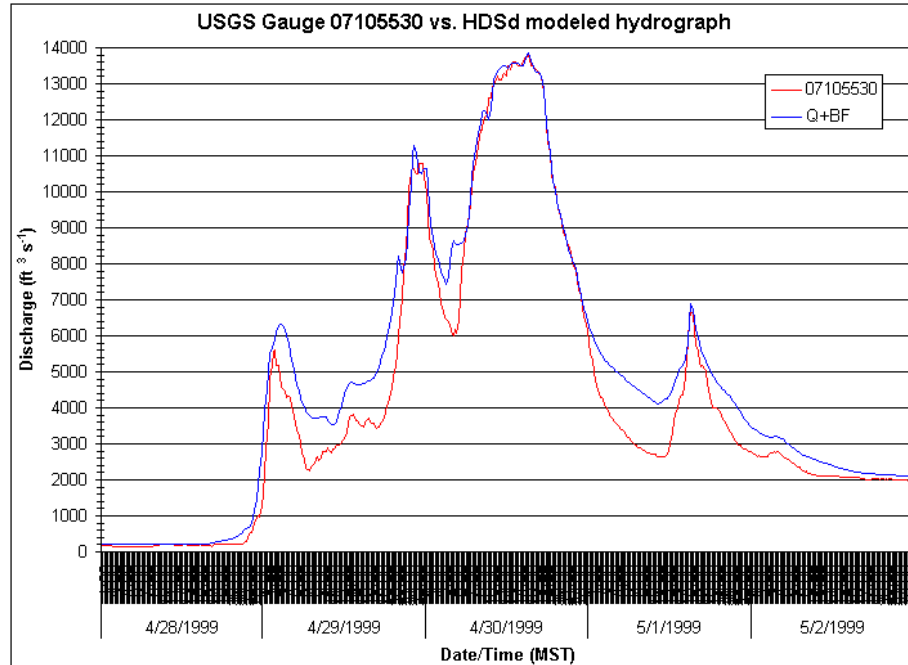


Figure 4.20d: Results of full model simulation at USGS gauge 07105530. Observed and simulated hydrographs are shown in red and blue, respectively.

#### 4.4.6 *Reconstructed Stream Gauge Records*

The results of simulation HDSd above led to some confidence in the reconstruction of discharge records at otherwise unavailable USGS stream gauge locations in the Monument and Fountain Creek watersheds. Eight locations with missing or unavailable data were shown in Figure 3.1 and listed in the bottom portion of Table 3.1. Stream discharge results for corresponding locations in the modeled watershed are shown here: reconstructed discharge records for USGS gauges 07103700, 07103703, 07103780 and 07103800 are shown in Figure 4.21a; reconstructed discharge records for USGS gauges 07103970, 07103977, 07103990 and 07105800 are shown in Figure 4.21b. The determination of this last discharge record was of primary importance to the original work that led to this thesis.

#### 4.4.7 *Results for the Templeton Gap/Shooks Run Region*

An examination of discharges and total flow volumes in portions of Shooks Run in Colorado Springs provided an interesting measure by which the accuracy of this SWMM RUNOFF model may be evaluated. As stated previously, alternative scenarios of pre-development conditions in the area of the City of Colorado Springs were considered as a major focus of the the work that led to this thesis. For such a scenario, the only change to much of the modeled watershed was a reduction of the surface imperviousness parameter to 0% for all sub-basins within the City limits. In the Templeton Gap and Shooks Run portions of Colorado Springs, this alternative scenario also required removal of a constructed floodway (bypass channel) and restoration of the affected drainage channels to their historical configurations.

The pre-development configuration of Shooks Run sub-basins and drainage channels in Colorado Springs is shown in Figure 4.22a. This configuration should be compared with

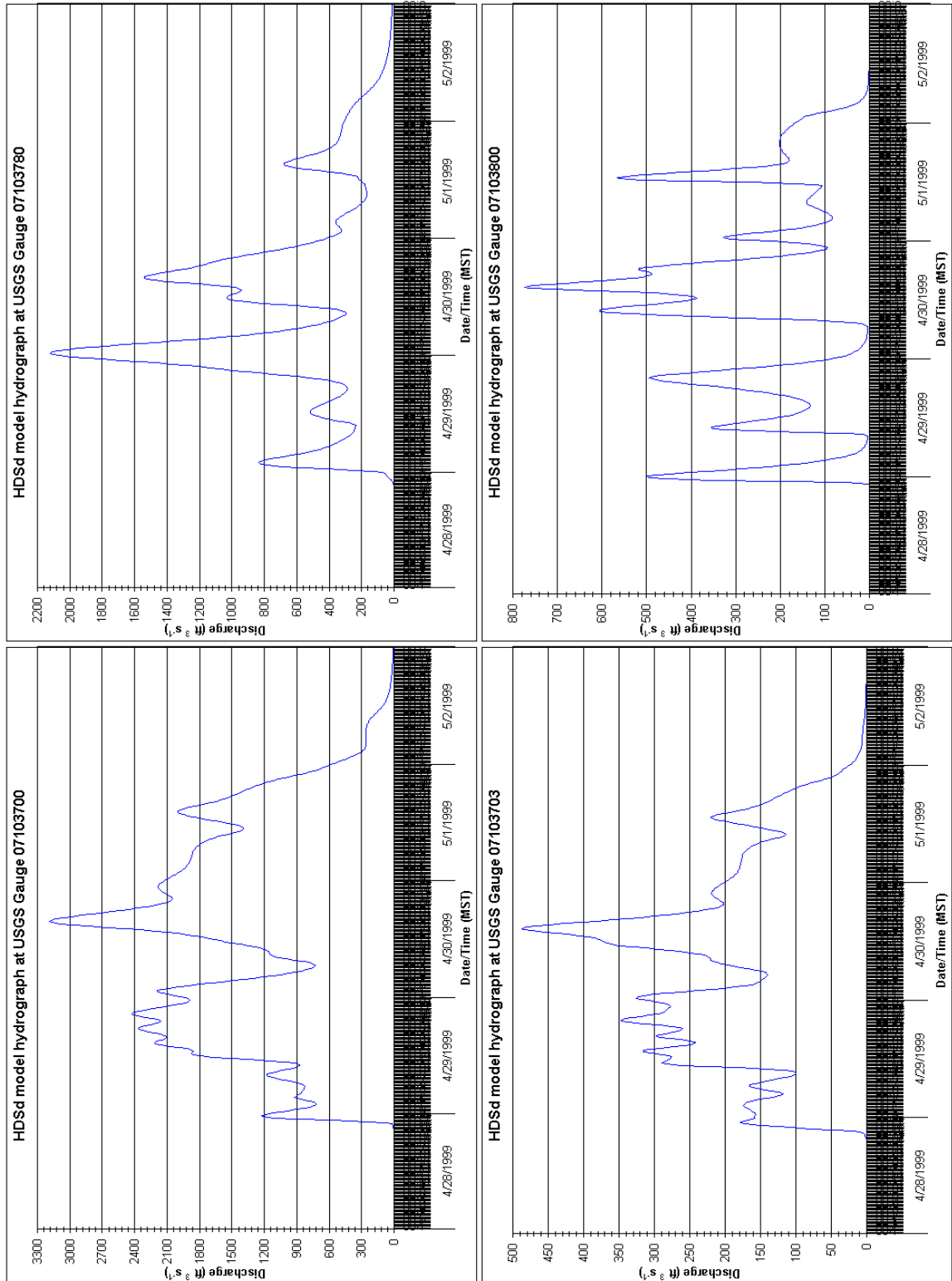


Figure 4.21a: Reconstructed stream gauge records for the modeled watershed. Gauges are labeled by their USGS designators, and gauge names and locations are listed in Table 3.1.

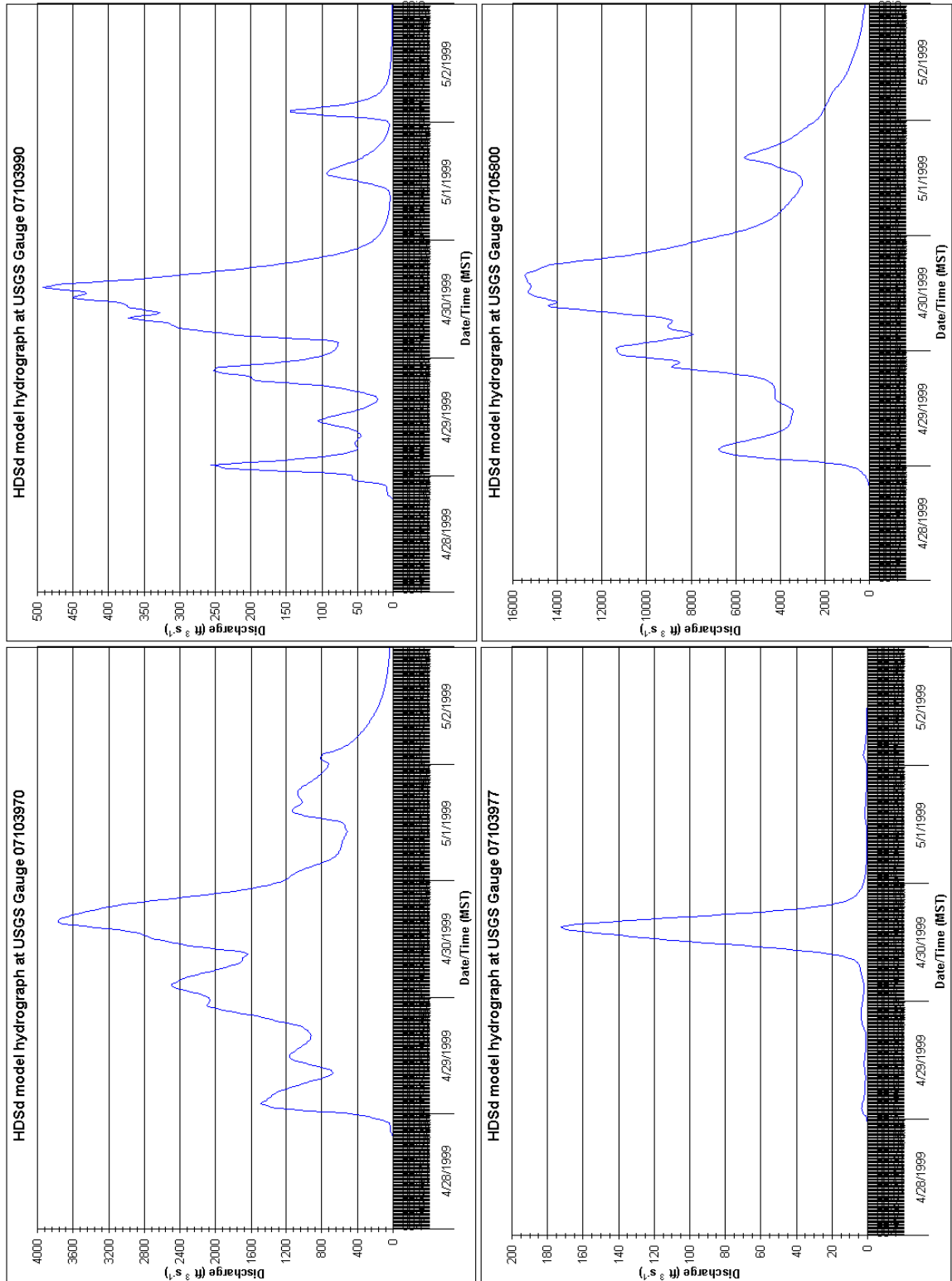


Figure 4.21b: Reconstructed stream gauge records for the modeled watershed. Gauges are labeled by their USGS designators, and gauge names and locations are listed in Table 3.1.

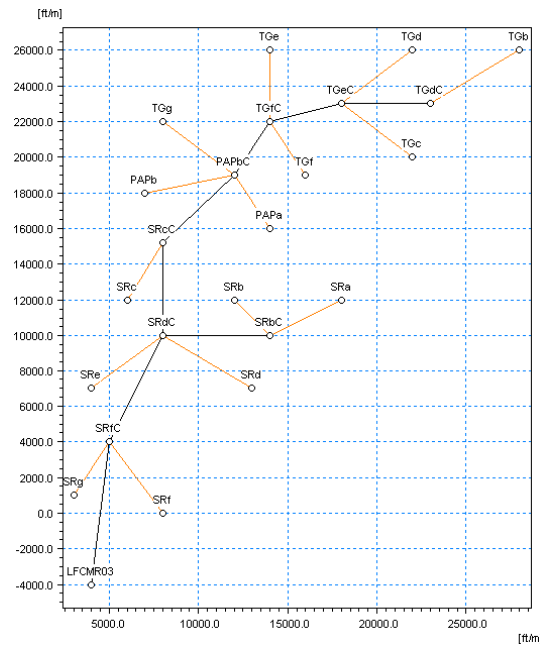


Figure 4.22a: Pre-development drainage network in the Shooks Run area. Coordinates are given in feet north and east of the confluence of Monument and Fountain Creeks in Colorado Springs, Colorado.

that of the Templeton Gap and Shooks Run sub-basins shown previously in Figure 3.6. With the construction of the Templeton Gap Floodway, shown as the channel designated ‘TGgC’ in Figure 3.6g, the course of Shooks Run was hydraulically interrupted. Following this development, runoff from the upstream portions of Shooks Run was directed to the lower reaches of Monument Creek in an effort to alleviate flooding conditions along downstream portions of Shooks Run in downtown Colorado Springs. The resulting hydraulically-intact portion of Shooks Run is shown in its current configuration in Figure 4.22b.

For this work, three scenarios were examined. The two primary alternatives include both current conditions, as modeled extensively above, and pre-development conditions as described here. An intermediate scenario was explored for which (1) current conditions of development (imperviousness) were maintained in the region, but (2) the RUNOFF channel representing the Templeton Gap Floodway was removed from the model and the

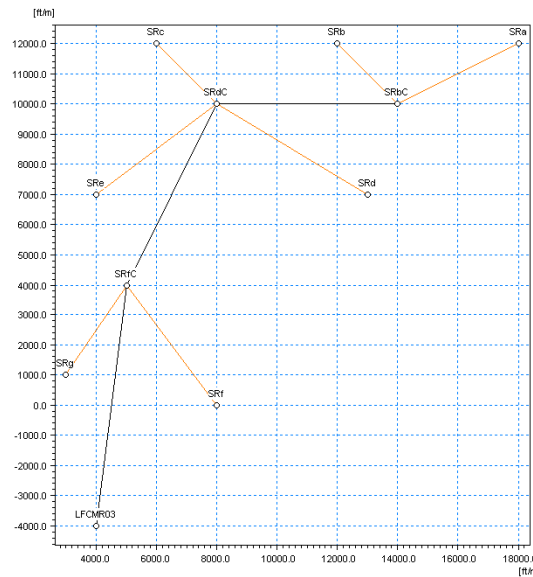


Figure 4.22b: Post-development drainage network in the Shooks Run area. Coordinates are given in feet north and east of the confluence of Monument and Fountain Creeks in Colorado Springs, Colorado.

surrounding sub-basins and channels were reconfigured in the historical route of Shooks Run through downtown Colorado Springs to its confluence with Fountain Creek. For the hyetographs employed in simulation HDSd above, the results of these simulations are shown in Figure 4.23. Statistical measures of these simulations and results are summarized in Table 4.4.

It is shown in Figure 4.23 and Table 4.4 that, under conditions of current development, the peak discharge near the mouth of Shooks Run would have been more than 60% greater during this major storm event if the Templeton Gap Floodway had not been constructed. It should also be noted that total flow volume at that location would have been nearly 70% greater under this scenario. Examination of the discharges and total flow volumes in Shooks Run for pre-development conditions yielded an interesting result: the peak discharges and total flow volumes near the mouth of Shooks Run under conditions of current development and with the Templeton Gap Floodway are approximately the same

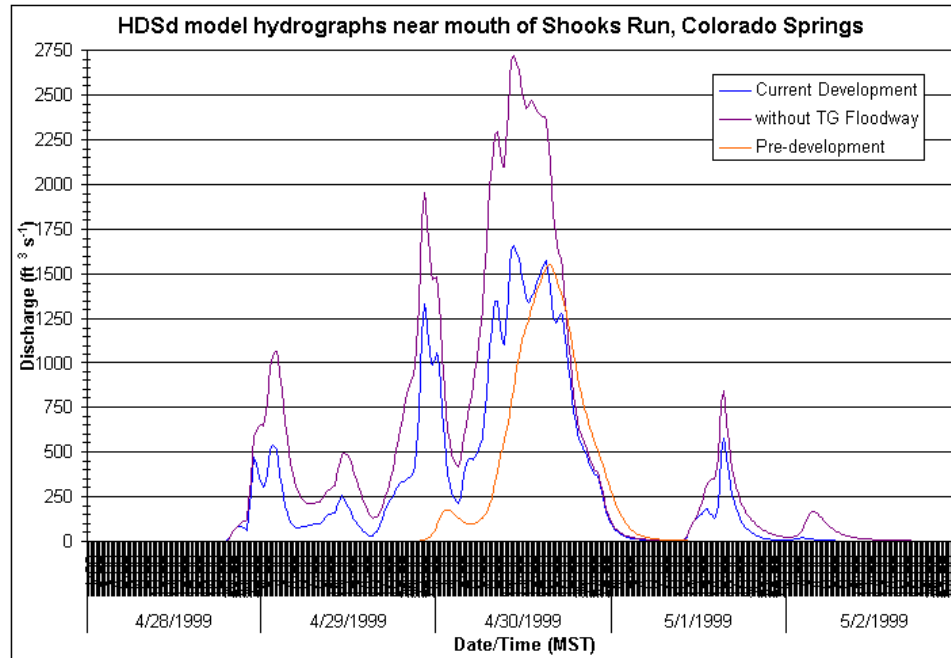


Figure 4.23: Results of simulations at the mouth of Shooks Run.

Table 4.4: Summary of Shooks Run development-based hydrologic simulation results.

Discharge Statistic at mouth of Shooks Run	Pre-development Configuration	Post-development without Floodway	Configuration with Floodway
No. of Sub-basins	15	15	7
Total Area (mi <sup>2</sup> )	20.14	20.14	8.36
Regional % Imperviousness	0.00	35.81	42.01
Regional MAP (in)	8.52	8.52	9.82
$\mu_Q$ (ft <sup>3</sup> s <sup>-1</sup> )	143.8	438.6	259.7
$\max[Q]$ (ft <sup>3</sup> s <sup>-1</sup> )	1551.4	2720.9	1662.2
$\sigma_Q$ (ft <sup>3</sup> s <sup>-1</sup> )	358.0	680.1	422.9
$V_Q$ (ac-ft)	1425.7	4349.4	2575.1
$\rho_{1,Q}$	0.9990	0.9971	0.9952

as those for pre-development conditions. This result is consistent with the common method of engineering design for flood control projects involving the reduction of peak stream discharges in a developed basin to those for the same basin under pre-development conditions. Regarding the accuracy of the methods applied in the construction of this RUNOFF model, it is encouraging that such a simulation of changes in peak discharges, under physically consistent scenarios of sub-basin development and stream channel routing in a densely urbanized portion of the watershed, should agree almost exactly with established engineering design principles.

## Chapter 5

### SUMMARY AND CONCLUSIONS

A summary and discussion of this hydrometeorological analysis and modeling effort is presented here. From this work, several conclusions regarding the event itself and the utility of the employed modeling methods may be drawn. Various means by which this work may be extended are also discussed.

#### 5.1 Summary Discussion

A brief introduction to the problem of flash flood prediction and analysis in mountainous areas, such as the Colorado Front Range, has been presented. The importance of increasing our understanding of flood-producing storm events in this region is stressed by recent growth in the population of the Front Range urban corridor. The Monument and Fountain Creek watersheds in the vicinity of Colorado Springs, Colorado, have been described, and various sources of the data employed for this analysis and modeling effort have been listed.

Rainfall totals observed during the April 28–May 2, 1999, storm event in the vicinity of Colorado Springs, Colorado, exceeded those previously measured for daily and monthly periods in that region. A detailed meteorological analysis demonstrated that this flood-producing storm event was actually composed of three distinct episodes occurring over a period of approximately four days. It was determined that the supporting meteorological

features conformed substantially with previously-observed and -documented flood-related patterns for the surrounding region. The influences of nearby topographical features, especially the Rampart Range, are considered significant for the production of excessive rainfall totals in storms of this type.

The simulation of this storm event, for the original purpose of investigating alternative scenarios of development in the City of Colorado Springs, commenced with a methodology based on a distributed, physically-based hydrologic model. The employment of the SWMM RUNOFF program provided an ideal environment in which the effects of changes to watershed surface parameters, such as imperviousness and infiltration coefficients, could be explored in a modular fashion. An extensive watershed model was constructed to include the entire Monument and Fountain Creek watershed areas to a point immediately downstream of the City of Colorado Springs. It was shown that Horton ratios for the drainage network in this model conformed reasonably well with those observed in natural stream networks.

Recorded rainfall data was applied to the hydrologic model by various methods. Available hourly rainfall records were employed for the temporal disaggregation of daily rainfall totals at several gauges in and near the modeled watersheds, and all of these were employed for the formulation of supplemental rainfall gauge records in data-sparse regions of the model. Additional criteria for the placement of supplemental gauges in the modeled watershed included the number of available USGS hydrograph records, non-interference of the resulting spatial coverages of each rainfall gauge by the Thiessen polygon method, and the locations of major topographical features in the watershed with respect to the analyzed morphology of the storms during this event. The purpose of these supplemental gauges was, primarily, the accurate simulation of stream discharge records at the USGS gauge locations

in the watersheds.

Following the calibration of the model simulations in order to account for antecedent moisture conditions, the application of several variations in the extent of the rainfall gauge network for the simulation of these stream discharge records was described. It was shown that the existing hourly and daily rainfall records were inadequate for the accurate simulation of observed discharge hydrographs in the watersheds. The introduction of supplemental rainfall gauges at four locations, with records derived by various traditional methods including reliance on climatological rainfall totals, was also found to be inadequate for simulation accuracy.

The hydrologic inverse problem of rainfall record determination from observed stream discharge hydrographs was addressed here with a novel approach involving the calculation of partial hydrographs for zone-based watershed areas. Required supplemental rainfall records were determined individually by an iterative procedure of hydrograph simulation and hyetograph adjustment until satisfactory correspondence between simulated and observed discharge records was obtained. It was found by this process that the total event rainfall at these supplemental gauges exceeded all recorded rainfall totals in the region for this event.

On the basis of overall simulation accuracy using these resulting supplemental rainfall gauge records, stream discharge records were determined for locations of USGS gauges that were rendered inoperable or otherwise unavailable by the flood event. This simulation accuracy was reinforced with an examination of alternative scenarios of development and runoff routing in one of the most heavily urbanized portions of the City of Colorado Springs. As a byproduct, the rainfall required at these gauges for accurate simulations of stream discharge led to greater resolution of the orographic effects of the Rampart Range on the upslope dynamics of this storm event. The reader will recall from Figure 2.18 that little

evidence of orographic influence is demonstrated by the existing rainfall data from NWS and City of Colorado Springs sources. The results presented in Figure 4.18 represent an advancement in the overall description of event morphology.

For this event, large rainfall totals would be expected on the eastern slopes of the Rampart Range based on the dynamics of orographic rainfall and convective events in this region. A subjective analysis of the event, working from the basis provided by Figure 4.18, would likely resemble that shown in Figure 5.1. This hand-drawn analysis, performed by the author, takes into account the primary topographical features of the Monument and Fountain Creek watershed as well as the general near-surface wind directions (southeast and east-southeast) at the Colorado Springs NWS gauge during the three storm episodes that comprised this event. This analysis also takes into account the low values of total rainfall recorded at three of the gauge stations in and near the modeled watershed. One of these is located in the northwestern part of the region and is found in a rain shadow for upslope events such as this one. That gauge is protected to some degree by the Rampart Range, and exhibits rainfall totals consistent with rain shadow effects found for locations such as the Sierra Nevada in California (Lee 1911) and portions of the Great Basin (Houghton 1979).

The two other gauges that demonstrated rainfall totals inconsistent with their elevations are located in the southwestern part of the region. Although the proximity of these gauges to Pike's Peak and its eastern ridgeline might suggest some rain shadow effect from those topographic features, the observation of primarily southeasterly winds throughout this event would discount that proposal. Given the large rainfall total required at the supplemental gauge located on Cheyenne Mountain, in the southwestern portion of Colorado Springs, for the accurate simulation of stream discharges there, these results suggest a pattern of local upslope convection at Cheyenne Mountain and nearby rain shadow effects

Subjective analysis: total rainfall during April 28-May 2, 1999

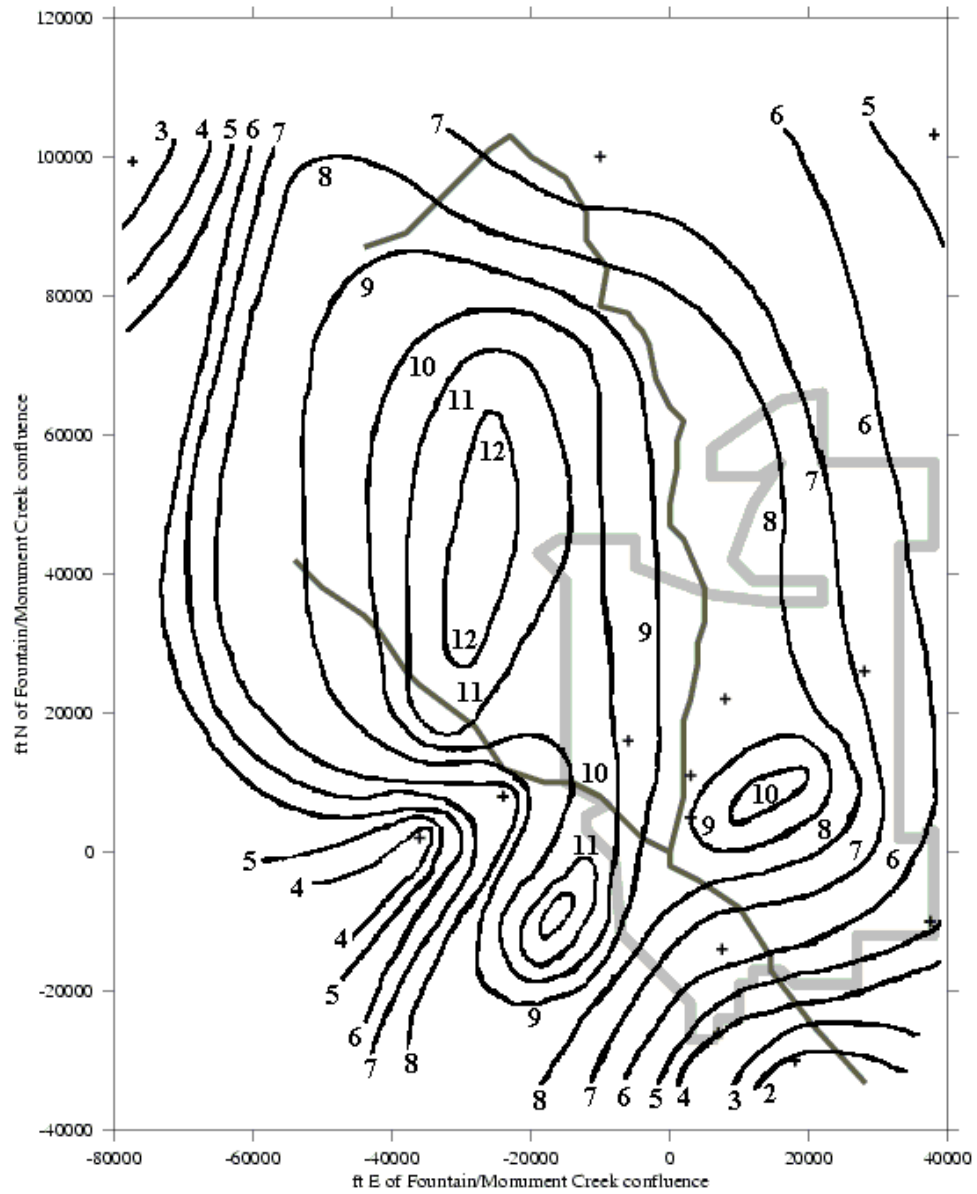


Figure 5.1: Subjective analysis of rainfall totals during April 28–May 2, 1999.

to the northwest of that feature. These local effects are consistent with those found in the vicinity of the Olympic Mountains in northwestern Washington by Parsons and Hobbs (1983) and Colle and Mass (1996), and for this event could not have been diagnosed with the existing rainfall data discussed in Chapter 2. Additional, similar topographic influences may be evident in the observation of large rainfall totals in the center of Colorado Springs, possibly related to local upslope effects on the event morphology, and relatively low rainfall totals in the Monument Creek valley just northwest of the local rainfall maximum.

On a slightly larger scale, it is possible that local near-surface wind patterns were influenced significantly by the presence of topographic features in and near the City of Colorado Springs. In general, these patterns might resemble a smaller version of the “Denver cyclone” that occurs in the vicinity of the Palmer Divide when surface winds in the region are generally from the south-southeast (Wilczak and Glendening, 1998). This cyclonic circulation results primarily from surface slope and baroclinic (temperature-gradient) effects, processes that may have been evident in the vicinity of Colorado Springs during this storm event. Similar alterations of the near-surface flow patterns were found by Akaeda et al. (1995) to have contributed to extreme rainfall and flash-flood conditions in mountainous areas of the island of Taiwan in 1987.

## **5.2 Conclusions**

Several conclusions may be drawn regarding the occurrence, evolution, and effects of the April 28–May 2, 1999, storm event in the vicinity of Colorado Springs, Colorado.

Climatologically, the period April–August of 1999 was characterized as a wet season with regard to rainfall in the vicinity of Colorado Springs, despite pre-season indications of a dry spring and summer due to La Niña conditions in the eastern equatorial Pacific

Ocean. The April 28–May 2, 1999, event was preceded by heavy snowstorms in upstream portions of the Monument and Fountain Creek watersheds that likely led to near-saturated soil conditions in that region. This combination of antecedent soil moisture conditions and heavy initial rainfall during the major storm event led to greater runoff than might have occurred for dry conditions.

The weather patterns supporting the storm event discussed here were easily identified, and the contribution of these patterns to heavy, sometimes flood-producing rainfall along the Colorado Front Range is well known. Though the meteorological conditions found to have supported the April 28–May 2, 1999, event have been documented previously, a succession of these specific weather patterns is rare and, in previous known cases, has produced excessive rainfall and devastating flood and flash flood conditions. Specifically, similar conditions and events have been observed for the Big Thompson Canyon flood on July 31, 1976, and for the Fort Collins flood on July 27–29, 1997.

Existing rainfall records for this event at various gauge locations were shown to be inadequate for the identification of likely rainfall patterns in the vicinity of Colorado Springs and the Rampart Range as well as for the accurate simulation of observed stream discharge records at available USGS gauge locations in the modeled watersheds. The introduction of supplemental rainfall gauges to the model was a useful technique by which this simulation accuracy could be improved, but not necessarily by traditional methods of spatial record interpolation as employed by the NWS River Forecast System (NWSRFS). The determination of supplemental rainfall records by a hydrograph-fitting method described here was required for high levels of simulation accuracy. It was shown that event rainfall totals at most locations were consistent with the expected positive correlation of rainfall with elevation. However, the resulting total rainfall distribution was only a first step toward

the accurate depiction of likely rainfall patterns in the region as found by a subjective meteorological analysis of the storm event.

The distributed, physically-based hydrologic modeling environment provided by the use of SWMM RUNOFF was ideal for the investigation of alternative development scenarios and their effects on hydrologic/hydraulic events in the modeled watersheds. These investigations led to certain modeling results for the area of downtown Colorado Springs that lend validity to the methodology employed here. At the same time, the employment of a distributed watershed model assisted in the determination of event hydrographs at locations in the watershed for which USGS stream discharge records were unavailable.

The methods and results presented in this thesis contribute in several ways toward our understanding of similar storm and flood events along the Colorado Front Range. Primarily, the technique employed here for the determination of area-average rainfall in ungauged regions from observed stream discharge records can assist in the diagnosis of spatial and temporal distributions of rainfall in regions of varied topography and during orographically-influenced storm events. The use of a distributed hydrological modeling approach assists in the reconstruction of stream discharge hydrographs at inoperable or otherwise ungauged locations in the modeled watersheds.

By better understanding the behavior and spatial variability of historical events such as these, efforts may be made at establishment or improvement of rainfall and stream gauge networks for the purposes of watershed monitoring and, in the event of a flood-producing storm, emergency management. The examination and simulation of historical rainfall records for such events can also contribute to the planning of stormwater management systems in urban areas where development exacerbates the problems of runoff volume and rapid changes in stream discharge during storm events.

### 5.3 Future Work

Further work toward the validation of the techniques and results presented here is required. Primarily, techniques exist for the more accurate determination of rainfall data in ungauged areas than those found by the simple quadratic and characteristic methods presented here. Specifically, geostatistical methods such as that presented by Chua and Bras (1980, 1982) present an opportunity for the incorporation of multiple bases for the interpolation of rainfall data. For this event, it is likely that the modeling of rainfall–runoff processes and resulting stream discharge records can benefit greatly from the inclusion of such bases as sub-basin elevation, slope and orientation with respect to the prevailing near-surface winds, and barrier effects as in previous studies.

The opportunity exists for the reproduction of the simulations presented here “from scratch” as well as for an attempt at the independent determination of observed rainfall records at existing gauge locations by the hydrograph-fitting method employed in Chapter 4. The opportunity for alternative configurations of the supplemental gauge network, including more subjective methods for the delineation of representative zones, and the subsequent determination of supplemental rainfall records also exists. Using the existing network of gauges, it may be possible to subdivide further the modeled watershed zones in an effort at greater simulation accuracy.

The opportunity exists for the extension of this work, of course, through the examination of other similar storm and flood events in the Monument and Fountain Creek watersheds. Such investigations would not only lend validity to (or help to improve) the methodology and techniques employed here, but would also further enhance our understanding of the spatial variability and temporal behavior of these orographically-forced storms. The examination of storm events with a wide variety of observed intensities and spatial

patterns of rainfall can only lead to the improvement of the techniques presented here.

Toward the simplification of these techniques, the opportunity exists for the automation of the hydrograph-fitting method employed in Chapter 4 of this thesis. This step in the determination of supplemental rainfall records was, by far, the most time-consuming step of the analysis and solution procedure presented here. However, it is considered that the nonlinearities of this solution procedure may require advanced programming techniques and extensive validation of results. Both of these aspects of procedural automation exceeded the scope and schedule of the present work.

## REFERENCES

- Akaeda, K., J. Reisner, and D. Parsons, 1995: The role of mesoscale and topographically induced circulations in initiating a flash-flood observed during the TAMEX project. *Monthly Weather Review*, **123**, pp. 1720–1739.
- Alley, W.M., and J.E. Veenhuis, 1983: Effective impervious area in urban runoff modeling. *J. Hydraulic Engineering*, **109**, 313–319.
- Alpert, P., and H. Shafir, 1991: Role of detailed wind-topography interaction in orographic rainfall. *Quarterly J. Royal Meteorological Society*, **117**, 421–426.
- Banta, R.M., and C.B. Schaaf, 1987: Thunderstorm genesis zones in the Colorado Rocky Mountains as determined by traceback of geosynchronous satellite images. *Monthly Weather Review*, **115**, 463–476.
- Bluestein, H.B., 1993: *Synoptic-Dynamic Meteorology in Midlatitudes, Volume II: Observations and Theory of Weather Systems*. Oxford University Press, New York. 594 pp.
- Bradley, A.A., and J.A. Smith, 1994: The hydrometeorological environment of extreme rainstorms in the southern plains of the United States. *J. Applied Meteorology*, **33**, 1418–1431.
- Chow, V.T., D.R. Maidment, and L.W. Mays, 1988: *Applied Hydrology*. McGraw-Hill, Inc., New York. 572 pp.

- Chua, S.-H., and R.L. Bras, 1980: *Estimation of stationary and non-stationary random fields: Kriging in the analysis of orographic precipitation*. Massachusetts Institute of Technology, Department of Civil Engineering, Ralph M. Parsons Laboratory for Water Resources and Hydrodynamics, Report No. 255. 171 pp.
- Chua, S.-H., and R.L. Bras, 1982: Optimal estimators of mean areal precipitation in regions of orographic influence. *J. Hydrology*, **57**, 23–48.
- Colle, B.A., and C.F. Mass, 1996: An observational and modelling study of the interaction of low-level southwesterly flow with the Olympic Mountains during COAST IOP 4. *Monthly Weather Review*, **124**, 2152–2175.
- Daly, C., R.P. Neilson, and D.L. Phillips, 1994: A statistical–topographic model for mapping climatological precipitation over mountainous terrain. *J. Applied Meteorology*, **33**, 140–158.
- Doswell, C.A. III, H.E. Brooks, and R.A. Maddox, 1996: Flash flood forecasting: An ingredients-based methodology. *Weather and Forecasting*, **11**, 560–581.
- Doswell, C.A. III, 1980: Synoptic-scale environments associated with High Plains severe thunderstorms. *Bulletin of the American Meteorological Society*, **61**, 1388–1400.
- Fiedler, F.R., 2003: Simple, practical method for determining station weights using Thiessen polygons and isohyetal maps. *J. Hydrologic Engineering*, **8**, 219–221.
- Garcia, M., 1999: *Simulated Tropical Convection*. Colorado State University, Department of Atmospheric Science, Report No. 690. 273 pp.
- Higgins, R.W., Y. Yao, and X.L. Wang, 1997: Influence of the North American monsoon system on the U.S. summer precipitation regime. *J. Climate*, **10**, 2600–2622.
- Higgins, R.W., Y. Yao, E.S. Yarosh, J.E. Janiwoak, and K.C. Mo, 1997: Influence of the

- Great Plains low-level jet on summertime precipitation and moisture transport over the Central United States. *J. Climate*, **10**, 481–507.
- Horton, R.E., 1945: Erosional development of streams and their drainage basins; hydrophysical approach to quantitative morphology. *Bulletin of the Geological Society of America*, **56**, 275–370.
- Houghton, J.G., 1979: A model for orographic precipitation in the North-central Great Basin. *Monthly Weather Review*, **107**, pp. 1462–1475.
- Houze, R.A., Jr., 1993: *Cloud Dynamics*. Academic Press, Inc., San Diego. 573 pp.
- Karr, T.W., and R.L. Wooten, 1976: Summer radar echo distribution around Limon, Colorado. *Monthly Weather Review*, **104**, 728–734.
- Knighton, D., 1998: *Fluvial Forms and Processes: A New Perspective*. Arnold (Hodder Headline Group), London. 383 pp.
- Kyriakidis, P.C., J. Kim, and N.L. Miller, 2001: Geostatistical mapping of precipitation from rain gauge data using atmospheric and terrain characteristics. *J. Applied Meteorology*, **40**, 1855–1877.
- Lee, C.H., 1911: Precipitation and altitude in the Sierra. *Monthly Weather Review*, **39**, pp. 1092–1099.
- Lee, J.G., and J.P. Heaney, 2003: Estimation of urban imperviousness and its impacts on storm water systems. *J. Water Resources Planning and Management*, **129**, 419–426.
- Legates, D.R., and G.J. McCabe, Jr., 1999: Evaluating the use of “goodness-of-fit” measures in hydrologic and hydroclimatic model validation. *Water Resources Research*, **35**, 233–241.
- Lin, Y.-L., S. Chiao, T.-A. Wang, M.L. Kaplan, and R.P. Weglarz, 2001: Some common

- ingredients for heavy orographic rainfall. *Weather and Forecasting*, **16**, 633–660.
- Maddox, R.A., 1980: Mesoscale convective complexes. *Bulletin of the American Meteorological Society*, **61**, 1374–1387.
- Maddox, R.A., F. Canova, and L.R. Hoxit, 1980: Meteorological characteristics of flash flood events over the western United States. *Monthly Weather Review*, **108**, 1866–1877.
- Maddox, R.A., D.F. Chappell, and L.R. Hoxit, 1979: Synoptic and meso- $\alpha$  scale aspects of flash flood events. *Bulletin of the American Meteorological Society*, **60**, 115–123.
- Maddox, R.A., L.R. Hoxit, C.F. Chappell, and F. Caracena, 1978: Comparison of meteorological aspects of the Big Thompson and Rapid City flash floods. *Monthly Weather Review*, **106**, 375–389.
- Mahoney, J.L., J.M. Brown, and E.I. Tollerud, 1995: Contrasting meteorological conditions associated with winter storms at Denver and Colorado Springs. *Weather and Forecasting*, **10**, 245–260.
- Mass, C.F., and G.K. Ferber, 1990: Surface pressure perturbations produced by an isolated mesoscale topographic barrier. Part I: General characteristics and dynamics. *Monthly Weather Review*, **118**, pp. 2579–2592.
- McCuen, R.H., and W.M. Snyder, 1975: A proposed index for comparing hydrographs. *Water Resources Research*, **11**, 1021–1024.
- Mishra, S., J.V. Tyagi, and V.P. Singh, 2003: Comparison of infiltration models. *Hydrological Processes*, **17**, 2629–2652.
- Ogden, F.L., H.O. Sharif, S.U.S. Senarath, J.A. Smith, M.L. Baeck, and J.R. Richardson, 2000: Hydrologic analysis of the Fort Collins, Colorado, flash flood of 1997. *J. Hydrology*, **228**, 82–100.

- Oki, T., K. Musiake, and T. Koike, 1991: Spatial rainfall distribution at a storm event in mountain regions, estimated by orography and wind direction. *Water Resources Research*, **27**, 359–369.
- Parsons, D.B., and P.V. Hobbs, 1983: The mesoscale and microscale structure and organization of clouds and precipitation in midlatitude cyclones. IX: Some effects of orography on rainbands. *J. Atmospheric Sciences*, **40**, pp. 1930–1949.
- Petersen, W.A., L.D. Carey, S.A. Rutledge, J.C. Knievel, N.J. Doesken, R.H. Johnson, T.B. McKee, T. Vonder Haar, and J.F. Weaver, 1999: Mesoscale and radar observations of the Fort Collins flash flood of 28 July 1997. *Bulletin of the American Meteorological Society*, **80**, 191–216.
- Schumm, S.A., 1956: Evolution of drainage systems and slopes in badlands at Perth Amboy, New Jersey. *Bulletin of the Geological Society of America*, **67**, 597–646.
- Shreve, R.L., 1966: Statistical law of stream numbers. *J. Geology*, **74**, 17–37.
- Strahler, A.N., 1964: Quantitative geomorphology of drainage basins and channel networks. Section 4-II in *Handbook of Applied Hydrology*, V.T. Chow (ed.). McGraw-Hill, New York. Various pagination.
- Thiessen, A.H., 1911: Precipitation averages for large areas. *Monthly Weather Review*, **39**, pp. 1082–1084.
- Toth, J.J., and R.H. Johnson, 1985: Summer surface flow characteristics over Northeast Colorado. *Monthly Weather Review*, **113**, 1458–1469.
- USGS Water-Resources Investigations Report No. 88-4136, 1989: Suspended sediment and sediment source areas in the Fountain Creek drainage basin upstream from Widefield, southeastern Colorado. 36 pp.

- Weaver, J.F., E. Grunfest, and G.M. Levy, 2000: Two floods in Fort Collins, Colorado: Learning from a natural disaster. *Bulletin of the American Meteorological Society*, **81**, 2359–2366.
- Weston, K.J., and M.G. Roy, 1994: The directional-dependence of the enhancement of rainfall over complex orography. *Meteorological Applications*, **1**, 267–275.
- Wilczak, J.M., and J.W. Glendening, 1988: Observations and mixed-layer modeling of a terrain-induced mesoscale gyre—the Denver Cyclone. *Monthly Weather Review*, **116**, pp. 1599–1622.
- Willmott, C.J., S.G. Ackleson, R.E. Davis, J.J. Feddema, K.M. Klink, D.R. Legates, J. O'Donnell, and C.M. Rowe, 1985: Statistics for the evaluation and comparison of models. *J. Geophysical Research*, **90** (C5), 8995–9005.

## Appendix A

### RAINFALL RECORDS

Table A.1: Observed hourly rainfall records at existing gauges (nos. 1–6). Records were provided by the National Weather Service (NWS) and the City of Colorado Springs Utilities Department (CSU), as listed in Table 2.2.

Date	Hour	Rainfall at hourly gauges					
		1	2	3	4	5	6
4/28/1999	0	0.00	0.00	0.00	0.00	0.00	0.00
	1	0.00	0.00	0.00	0.00	0.00	0.00
	2	0.00	0.00	0.00	0.00	0.00	0.00
	3	0.00	0.00	0.00	0.00	0.00	0.00
	4	0.00	0.00	0.00	0.00	0.00	0.00
	5	0.00	0.00	0.00	0.00	0.00	0.00
	6	0.00	0.00	0.00	0.00	0.00	0.00
	7	0.00	0.00	0.00	0.00	0.00	0.00
	8	0.00	0.00	0.00	0.00	0.00	0.00
	9	0.00	0.00	0.00	0.00	0.00	0.00
	10	0.00	0.00	0.00	0.00	0.00	0.00
	11	0.00	0.00	0.00	0.00	0.00	0.00
	12	0.00	0.00	0.00	0.00	0.00	0.00
	13	0.00	0.00	0.00	0.00	0.00	0.00
	14	0.00	0.00	0.00	0.06	0.00	0.00
	15	0.00	0.00	0.00	0.03	0.10	0.00
	16	0.00	0.00	0.00	0.03	0.00	0.00
	17	0.00	0.00	0.00	0.00	0.00	0.00
	18	0.00	0.00	0.06	0.03	0.10	0.01
	19	0.00	0.00	0.17	0.04	0.00	0.05
	20	0.00	0.00	0.09	0.02	0.10	0.02
	21	0.10	0.00	0.04	0.11	0.10	0.05
	22	0.20	0.20	0.59	0.02	0.00	0.01
	23	0.30	0.30	0.24	0.01	0.30	0.08

*continued on next page*

Table A.1, continued from previous page

Date	Hour	1	2	3	4	5	6
4/29/1999	0	0.10	0.70	0.20	0.57	0.20	0.00
	1	0.20	0.50	0.20	0.21	0.10	0.00
	2	0.00	0.60	0.05	0.11	0.00	0.00
	3	0.00	0.20	0.01	0.01	0.10	0.00
	4	0.00	0.20	0.06	0.00	0.00	0.00
	5	0.00	0.10	0.08	0.05	0.10	0.00
	6	0.00	0.00	0.09	0.01	0.00	0.00
	7	0.00	0.20	0.09	0.00	0.00	0.00
	8	0.00	0.10	0.16	0.00	0.10	0.00
	9	0.00	0.10	0.14	0.11	0.10	0.00
	10	0.00	0.10	0.27	0.01	0.10	0.00
	11	0.00	0.10	0.13	0.01	0.00	0.00
	12	0.00	0.00	0.05	0.00	0.00	0.00
	13	0.00	0.10	0.02	0.00	0.00	0.00
	14	0.00	0.10	0.00	0.00	0.00	0.00
	15	0.00	0.20	0.11	0.00	0.00	0.00
	16	0.00	0.10	0.22	0.01	0.10	0.00
	17	0.00	0.20	0.24	0.06	0.10	0.02
	18	0.00	0.10	0.31	0.28	0.20	0.11
	19	0.20	0.10	0.28	0.07	0.20	0.20
	20	0.00	0.20	0.23	0.18	0.20	0.04
	21	0.10	0.30	0.28	0.05	0.10	0.00
	22	0.00	0.20	0.18	0.01	0.10	0.01
	23	0.00	0.20	0.17	0.03	0.00	0.04
4/30/1999	0	0.00	0.10	0.13	0.02	0.10	0.01
	1	0.00	0.00	0.13	0.04	0.00	0.01
	2	0.00	0.10	0.16	0.02	0.00	0.00
	3	0.00	0.10	0.34	0.02	0.20	0.03
	4	0.00	0.10	0.28	0.19	0.10	0.01
	5	0.10	0.10	0.32	0.17	0.10	0.00
	6	0.00	0.10	0.30	0.22	0.10	0.01
	7	0.10	0.20	0.30	0.25	0.50	0.01
	8	0.00	0.20	0.24	0.23	0.20	0.03
	9	0.10	0.30	0.27	0.26	0.20	0.00
	10	0.10	0.30	0.24	0.24	0.20	0.00
	11	0.00	0.00	0.28	0.27	0.30	0.00
	12	0.10	0.00	0.21	0.18	0.20	0.00
	13	0.10	0.00	0.17	0.33	0.10	0.00
	14	0.10	0.00	0.16	0.14	0.10	0.00
	15	0.20	0.00	0.01	0.03	0.00	0.00
	16	0.00	0.00	0.01	0.01	0.00	0.00
	17	0.00	0.00	0.00	0.00	0.00	0.00

continued on next page

Table A.1, continued from previous page

Date	Hour	1	2	3	4	5	6
4/30/1999	18	0.00	0.00	0.02	0.01	0.00	0.00
	19	0.00	0.00	0.01	0.01	0.10	0.00
	20	0.00	0.00	0.00	0.00	0.00	0.00
	21	0.00	0.00	0.00	0.00	0.00	0.00
	22	0.00	0.00	0.00	0.00	0.00	0.00
	23	0.00	0.00	0.00	0.00	0.00	0.00
	5/1/1999	0	0.00	0.00	0.00	0.00	0.00
1		0.00	0.00	0.01	0.00	0.00	0.00
2		0.00	0.00	0.01	0.00	0.00	0.00
3		0.00	0.00	0.00	0.00	0.00	0.00
4		0.00	0.00	0.00	0.01	0.00	0.00
5		0.00	0.00	0.00	0.01	0.00	0.00
6		0.00	0.00	0.01	0.01	0.00	0.00
7		0.00	0.00	0.00	0.02	0.10	0.00
8		0.00	0.00	0.02	0.03	0.00	0.00
9		0.00	0.00	0.04	0.05	0.00	0.01
10		0.00	0.10	0.17	0.08	0.00	0.00
11		0.00	0.20	0.14	0.11	0.10	0.00
12		0.10	0.20	0.18	0.18	0.10	0.03
13		0.10	0.00	0.09	0.11	0.10	0.08
14		0.00	0.00	0.09	0.07	0.00	0.06
15		0.00	0.00	0.06	0.00	0.00	0.00
16		0.00	0.00	0.07	0.00	0.10	0.01
17		0.00	0.00	0.03	0.01	0.00	0.01
18		0.00	0.00	0.02	0.02	0.00	0.00
19		0.00	0.10	0.00	0.00	0.00	0.00
20		0.00	0.00	0.00	0.00	0.00	0.00
21		0.00	0.00	0.00	0.00	0.00	0.00
22		0.00	0.00	0.00	0.02	0.00	0.00
23	0.00	0.00	0.02	0.09	0.10	0.00	
5/2/1999	0	0.00	0.00	0.03	0.08	0.10	0.00
	1	0.00	0.00	0.03	0.08	0.00	0.00
	2	0.00	0.00	0.00	0.00	0.00	0.00
	3	0.00	0.10	0.00	0.00	0.00	0.00
	4	0.00	0.00	0.00	0.00	0.00	0.00
	5	0.00	0.00	0.00	0.00	0.00	0.00
	6	0.00	0.00	0.00	0.00	0.00	0.00
	7	0.00	0.00	0.00	0.00	0.00	0.00
	8	0.00	0.10	0.00	0.00	0.00	0.00
	9	0.00	0.10	0.00	0.00	0.00	0.00
	10	0.00	0.10	0.00	0.00	0.00	0.00
11	0.10	0.00	0.00	0.00	0.00	0.00	

continued on next page

Table A.1, continued from previous page

Date	Hour	1	2	3	4	5	6
5/2/1999	12	0.00	0.00	0.00	0.00	0.00	0.00
	13	0.00	0.00	0.00	0.00	0.00	0.00
	14	0.00	0.00	0.00	0.00	0.00	0.00
	15	0.00	0.00	0.00	0.00	0.00	0.00
	16	0.00	0.00	0.00	0.00	0.00	0.00
	17	0.00	0.00	0.00	0.00	0.00	0.00
	18	0.00	0.00	0.00	0.00	0.00	0.00
	19	0.00	0.00	0.00	0.00	0.00	0.00
	20	0.00	0.00	0.00	0.00	0.00	0.00
	21	0.00	0.00	0.00	0.00	0.00	0.00
	22	0.00	0.00	0.00	0.00	0.00	0.00
	23	0.00	0.00	0.00	0.00	0.00	0.00
Event Total		2.40	7.80	9.36	5.75	5.70	0.95

Table A.2: Disaggregated hourly rainfall records at existing daily gauges (nos. 7–14). Records were provided by the National Weather Service (NWS) and the City of Colorado Springs Utilities Department (CSU), as listed in Table 2.2.

Date	Hour	Disaggregated rainfall at daily gauges							
		7	8	9	10	11	12	13	14
4/28/1999	0	0.00	0.00	0.00	0.00	0.00	0.00	0.00	0.00
	1	0.00	0.00	0.00	0.00	0.00	0.00	0.00	0.00
	2	0.00	0.00	0.00	0.00	0.00	0.00	0.00	0.00
	3	0.00	0.00	0.00	0.00	0.00	0.00	0.00	0.00
	4	0.00	0.00	0.00	0.00	0.00	0.00	0.00	0.00
	5	0.00	0.00	0.00	0.00	0.00	0.00	0.00	0.00
	6	0.00	0.00	0.00	0.00	0.00	0.00	0.00	0.00
	7	0.00	0.00	0.00	0.00	0.00	0.00	0.00	0.00
	8	0.00	0.00	0.00	0.00	0.00	0.00	0.00	0.00
	9	0.00	0.00	0.00	0.00	0.00	0.00	0.00	0.00
	10	0.00	0.00	0.00	0.00	0.00	0.00	0.00	0.00
	11	0.00	0.00	0.00	0.00	0.00	0.00	0.00	0.00
	12	0.00	0.00	0.00	0.00	0.00	0.00	0.00	0.00
	13	0.00	0.00	0.00	0.00	0.00	0.00	0.00	0.00
	14	0.00	0.00	0.00	0.02	0.00	0.01	0.00	0.02
	15	0.01	0.00	0.00	0.01	0.00	0.01	0.00	0.02
	16	0.00	0.00	0.00	0.01	0.00	0.01	0.00	0.01
	17	0.00	0.00	0.00	0.00	0.00	0.00	0.00	0.00
	18	0.01	0.00	0.00	0.02	0.05	0.02	0.05	0.06
	19	0.00	0.00	0.00	0.03	0.13	0.07	0.14	0.14
	20	0.01	0.00	0.00	0.02	0.07	0.03	0.08	0.08
	21	0.01	0.01	0.00	0.05	0.04	0.07	0.04	0.08
	22	0.02	0.20	0.00	0.08	0.45	0.10	0.71	0.44
	23	0.04	0.30	0.00	0.05	0.18	0.10	0.54	0.20
4/29/1999	0	0.49	0.33	0.04	0.40	0.21	0.18	0.36	0.31
	1	0.53	0.24	0.02	0.22	0.20	0.10	0.31	0.22
	2	0.07	0.28	0.01	0.07	0.05	0.04	0.21	0.06
	3	0.13	0.09	0.00	0.02	0.01	0.00	0.07	0.02
	4	0.03	0.09	0.00	0.02	0.06	0.02	0.10	0.04
	5	0.13	0.05	0.01	0.07	0.08	0.03	0.09	0.08
	6	0.01	0.00	0.00	0.04	0.08	0.03	0.07	0.07
	7	0.03	0.09	0.00	0.03	0.08	0.02	0.12	0.07
	8	0.14	0.05	0.01	0.07	0.15	0.04	0.15	0.12
	9	0.14	0.05	0.01	0.12	0.13	0.06	0.13	0.14
	10	0.16	0.05	0.01	0.11	0.25	0.07	0.23	0.21
	11	0.03	0.05	0.01	0.05	0.12	0.04	0.12	0.10

*continued on next page*

Table A.2, continued from previous page

Date	Hour	7	8	9	10	11	12	13	14
4/29/1999	12	0.01	0.00	0.00	0.02	0.05	0.01	0.04	0.04
	13	0.01	0.05	0.00	0.01	0.02	0.01	0.04	0.01
	14	0.01	0.05	0.00	0.00	0.00	0.00	0.03	0.00
	15	0.04	0.09	0.00	0.04	0.10	0.03	0.14	0.08
	16	0.15	0.05	0.01	0.09	0.20	0.06	0.19	0.17
	17	0.16	0.10	0.06	0.12	0.23	0.12	0.24	0.20
	18	0.27	0.07	0.28	0.27	0.30	0.40	0.26	0.31
19	0.60	0.10	0.47	0.18	0.27	0.56	0.25	0.25	
20	0.27	0.10	0.11	0.20	0.22	0.19	0.23	0.22	
21	0.35	0.14	0.01	0.15	0.26	0.08	0.30	0.23	
22	0.16	0.09	0.03	0.08	0.17	0.07	0.19	0.14	
23	0.05	0.10	0.10	0.07	0.16	0.14	0.18	0.13	
4/30/1999	0	0.05	0.04	0.18	0.07	0.12	0.13	0.13	0.11
	1	0.01	0.00	0.18	0.07	0.12	0.14	0.07	0.10
	2	0.02	0.04	0.01	0.07	0.15	0.05	0.15	0.12
	3	0.09	0.04	0.54	0.17	0.32	0.38	0.25	0.27
	4	0.06	0.04	0.21	0.20	0.27	0.20	0.21	0.25
	5	0.11	0.04	0.04	0.22	0.30	0.12	0.24	0.28
6	0.06	0.04	0.21	0.23	0.29	0.21	0.22	0.27	
7	0.24	0.08	0.21	0.29	0.29	0.22	0.30	0.30	
8	0.10	0.08	0.55	0.22	0.23	0.38	0.26	0.23	
9	0.16	0.11	0.04	0.25	0.26	0.12	0.34	0.26	
10	0.16	0.11	0.04	0.23	0.23	0.10	0.32	0.24	
11	0.11	0.00	0.04	0.26	0.27	0.12	0.15	0.27	
12	0.12	0.00	0.03	0.19	0.20	0.09	0.12	0.20	
13	0.08	0.00	0.04	0.23	0.17	0.10	0.10	0.19	
14	0.08	0.00	0.02	0.15	0.15	0.07	0.09	0.16	
15	0.09	0.00	0.00	0.04	0.01	0.01	0.01	0.03	
16	0.00	0.00	0.00	0.01	0.01	0.00	0.01	0.01	
17	0.00	0.00	0.00	0.00	0.00	0.00	0.00	0.00	
18	0.00	0.00	0.00	0.01	0.02	0.01	0.01	0.02	
19	0.03	0.00	0.00	0.02	0.01	0.00	0.01	0.01	
20	0.00	0.00	0.00	0.00	0.00	0.00	0.00	0.00	
21	0.00	0.00	0.00	0.00	0.00	0.00	0.00	0.00	
22	0.00	0.00	0.00	0.00	0.00	0.00	0.00	0.00	
23	0.00	0.00	0.00	0.00	0.00	0.00	0.00	0.00	
5/1/1999	0	0.00	0.00	0.00	0.00	0.00	0.00	0.00	0.00
	1	0.00	0.00	0.00	0.00	0.01	0.00	0.01	0.01
	2	0.00	0.00	0.00	0.00	0.01	0.00	0.01	0.01
	3	0.00	0.00	0.00	0.00	0.00	0.00	0.00	0.00
	4	0.00	0.00	0.00	0.00	0.00	0.00	0.00	0.00
	5	0.00	0.00	0.00	0.00	0.00	0.00	0.00	0.00

continued on next page

Table A.2, continued from previous page

Date	Hour	7	8	9	10	11	12	13	14
5/1/1999	6	0.00	0.00	0.00	0.01	0.01	0.01	0.01	0.01
	7	0.06	0.00	0.00	0.01	0.00	0.00	0.00	0.01
	8	0.00	0.00	0.00	0.02	0.02	0.01	0.01	0.02
	9	0.00	0.00	0.02	0.03	0.04	0.04	0.02	0.03
	10	0.03	0.00	0.01	0.08	0.15	0.07	0.13	0.12
	11	0.10	0.01	0.01	0.09	0.12	0.07	0.16	0.11
	12	0.19	0.01	0.05	0.13	0.16	0.14	0.18	0.15
	13	0.15	0.00	0.12	0.08	0.08	0.18	0.05	0.08
	14	0.01	0.00	0.09	0.05	0.08	0.14	0.05	0.07
	15	0.01	0.00	0.00	0.02	0.05	0.02	0.03	0.04
	16	0.06	0.00	0.02	0.03	0.06	0.04	0.04	0.05
	17	0.00	0.00	0.02	0.01	0.03	0.03	0.02	0.02
	18	0.00	0.00	0.00	0.01	0.02	0.01	0.01	0.02
	19	0.01	0.00	0.00	0.00	0.00	0.00	0.04	0.00
	20	0.00	0.00	0.00	0.00	0.00	0.00	0.00	0.00
	21	0.00	0.00	0.00	0.00	0.00	0.00	0.00	0.00
	22	0.00	0.00	0.00	0.01	0.00	0.00	0.00	0.00
	23	0.06	0.00	0.00	0.04	0.02	0.02	0.01	0.03
5/2/1999	0	0.06	0.00	0.01	0.24	0.04	0.05	0.03	0.03
	1	0.01	0.00	0.01	0.20	0.03	0.05	0.03	0.03
	2	0.00	0.00	0.00	0.00	0.00	0.00	0.00	0.00
	3	0.00	0.00	0.00	0.00	0.00	0.00	0.01	0.00
	4	0.00	0.00	0.00	0.00	0.00	0.00	0.00	0.00
	5	0.00	0.00	0.00	0.00	0.00	0.00	0.00	0.00
	6	0.00	0.00	0.00	0.00	0.00	0.00	0.00	0.00
	7	0.00	0.00	0.00	0.00	0.00	0.00	0.00	0.00
	8	0.00	0.00	0.00	0.00	0.00	0.00	0.01	0.00
	9	0.00	0.00	0.00	0.00	0.00	0.00	0.01	0.00
	10	0.00	0.00	0.00	0.00	0.00	0.00	0.01	0.00
	11	0.03	0.00	0.00	0.01	0.00	0.00	0.00	0.00
	12	0.00	0.00	0.00	0.00	0.00	0.00	0.00	0.00
	13	0.00	0.00	0.00	0.00	0.00	0.00	0.00	0.00
	14	0.00	0.00	0.00	0.00	0.00	0.00	0.00	0.00
	15	0.00	0.00	0.00	0.00	0.00	0.00	0.00	0.00
	16	0.00	0.00	0.00	0.00	0.00	0.00	0.00	0.00
	17	0.00	0.00	0.00	0.00	0.00	0.00	0.00	0.00
	18	0.00	0.00	0.00	0.00	0.00	0.00	0.00	0.00
	19	0.00	0.00	0.00	0.00	0.00	0.00	0.00	0.00
	20	0.00	0.00	0.00	0.00	0.00	0.00	0.00	0.00
	21	0.00	0.00	0.00	0.00	0.00	0.00	0.00	0.00
	22	0.00	0.00	0.00	0.00	0.00	0.00	0.00	0.00
	23	0.00	0.00	0.00	0.00	0.00	0.00	0.00	0.00
Event Total		6.42	3.45	3.94	6.74	8.68	6.07	9.43	8.38

Table A.3: Derived hourly rainfall records for simulations HDSa and HDSb at supplemental gauges (nos. 15–18).

Date	Hour	HDSa rainfall at gauges				HDSb rainfall at gauges			
		15	16	17	18	15	16	17	18
4/28/1999	0	0.00	0.00	0.00	0.00	0.00	0.00	0.00	0.00
	1	0.00	0.00	0.00	0.00	0.00	0.00	0.00	0.00
	2	0.00	0.00	0.00	0.00	0.00	0.00	0.00	0.00
	3	0.00	0.00	0.00	0.00	0.00	0.00	0.00	0.00
	4	0.00	0.00	0.00	0.00	0.00	0.00	0.00	0.00
	5	0.00	0.00	0.00	0.00	0.00	0.00	0.00	0.00
	6	0.00	0.00	0.00	0.00	0.00	0.00	0.00	0.00
	7	0.00	0.00	0.00	0.00	0.00	0.00	0.00	0.00
	8	0.00	0.00	0.00	0.00	0.00	0.00	0.00	0.00
	9	0.00	0.00	0.00	0.00	0.00	0.00	0.00	0.00
	10	0.00	0.00	0.00	0.00	0.00	0.00	0.00	0.00
	11	0.00	0.00	0.00	0.00	0.00	0.00	0.00	0.00
	12	0.00	0.00	0.00	0.00	0.00	0.00	0.00	0.00
	13	0.00	0.00	0.00	0.00	0.00	0.00	0.00	0.00
	14	0.00	0.00	0.00	0.01	0.00	0.00	0.00	0.01
	15	0.02	0.00	0.00	0.00	0.00	0.00	0.00	0.00
	16	0.00	0.00	0.00	0.00	0.00	0.00	0.00	0.00
	17	0.00	0.00	0.00	0.00	0.00	0.00	0.00	0.00
	18	0.04	0.02	0.01	0.06	0.01	0.02	0.01	0.05
	19	0.04	0.06	0.02	0.15	0.03	0.06	0.02	0.14
	20	0.04	0.03	0.01	0.08	0.02	0.03	0.01	0.07
	21	0.06	0.02	0.01	0.05	0.03	0.03	0.01	0.04
	22	0.24	0.30	0.24	0.54	0.19	0.28	0.28	0.46
	23	0.29	0.25	0.29	0.24	0.20	0.23	0.34	0.19
4/29/1999	0	0.31	0.46	0.64	0.28	0.45	0.43	0.63	0.24
	1	0.26	0.35	0.46	0.23	0.44	0.32	0.46	0.20
	2	0.18	0.36	0.53	0.10	0.16	0.31	0.52	0.06
	3	0.08	0.12	0.18	0.02	0.11	0.10	0.17	0.01
	4	0.07	0.13	0.18	0.07	0.06	0.12	0.18	0.05
	5	0.07	0.08	0.10	0.08	0.10	0.08	0.10	0.08
	6	0.02	0.03	0.01	0.08	0.02	0.03	0.01	0.08
	7	0.08	0.14	0.18	0.09	0.07	0.13	0.18	0.08
	8	0.09	0.11	0.10	0.15	0.12	0.10	0.11	0.14
	9	0.08	0.10	0.10	0.14	0.11	0.10	0.10	0.13
	10	0.11	0.14	0.11	0.25	0.14	0.14	0.12	0.24
	11	0.06	0.10	0.10	0.12	0.05	0.09	0.10	0.11

*continued on next page*

Table A.3, continued from previous page

Date	Hour	15	16	17	18	15	16	17	18	
4/29/1999	12	0.01	0.02	0.00	0.04	0.01	0.02	0.01	0.04	
	13	0.03	0.06	0.09	0.02	0.03	0.05	0.09	0.02	
	14	0.03	0.06	0.09	0.01	0.03	0.05	0.09	0.00	
	15	0.08	0.15	0.19	0.11	0.07	0.13	0.18	0.09	
	16	0.10	0.12	0.11	0.20	0.13	0.12	0.11	0.19	
	17	0.13	0.19	0.20	0.23	0.16	0.19	0.20	0.22	
	18	0.15	0.17	0.12	0.31	0.21	0.23	0.13	0.30	
	19	0.19	0.17	0.12	0.26	0.42	0.26	0.13	0.26	
	20	0.16	0.19	0.20	0.24	0.22	0.21	0.20	0.22	
	21	0.20	0.26	0.29	0.27	0.30	0.24	0.30	0.25	
	22	0.12	0.17	0.19	0.17	0.15	0.16	0.19	0.16	
	23	0.09	0.17	0.19	0.17	0.09	0.18	0.19	0.15	
	4/30/1999	0	0.08	0.10	0.10	0.12	0.07	0.12	0.10	0.12
		1	0.03	0.04	0.01	0.12	0.02	0.07	0.01	0.12
2		0.06	0.11	0.10	0.15	0.05	0.10	0.11	0.14	
3		0.15	0.17	0.12	0.31	0.11	0.23	0.12	0.30	
4		0.11	0.14	0.12	0.27	0.08	0.17	0.12	0.26	
5		0.15	0.16	0.12	0.31	0.13	0.16	0.12	0.30	
	6	0.12	0.15	0.12	0.29	0.09	0.18	0.12	0.28	
	7	0.27	0.21	0.21	0.31	0.23	0.23	0.22	0.29	
	8	0.16	0.19	0.20	0.25	0.13	0.26	0.21	0.23	
	9	0.22	0.25	0.29	0.29	0.20	0.24	0.30	0.26	
	10	0.21	0.25	0.29	0.26	0.20	0.23	0.30	0.24	
	11	0.13	0.09	0.03	0.28	0.09	0.10	0.03	0.27	
	12	0.12	0.06	0.02	0.21	0.10	0.08	0.02	0.20	
	13	0.09	0.05	0.02	0.18	0.08	0.07	0.02	0.18	
	14	0.09	0.05	0.02	0.16	0.08	0.06	0.02	0.16	
	15	0.05	0.00	0.00	0.01	0.08	0.00	0.01	0.01	
	16	0.00	0.00	0.00	0.01	0.00	0.00	0.00	0.01	
	17	0.00	0.00	0.00	0.00	0.00	0.00	0.00	0.00	
	18	0.00	0.01	0.00	0.02	0.00	0.01	0.00	0.02	
	19	0.03	0.00	0.00	0.01	0.02	0.00	0.00	0.01	
	20	0.00	0.00	0.00	0.00	0.00	0.00	0.00	0.00	
	21	0.00	0.00	0.00	0.00	0.00	0.00	0.00	0.00	
	22	0.00	0.00	0.00	0.00	0.00	0.00	0.00	0.00	
	23	0.00	0.00	0.00	0.00	0.00	0.00	0.00	0.00	
	5/1/1999	0	0.00	0.00	0.00	0.00	0.00	0.00	0.00	0.00
		1	0.00	0.00	0.00	0.01	0.00	0.00	0.00	0.01
2		0.00	0.00	0.00	0.01	0.00	0.00	0.00	0.01	
3		0.00	0.00	0.00	0.00	0.00	0.00	0.00	0.00	
4		0.00	0.00	0.00	0.00	0.00	0.00	0.00	0.00	
5		0.00	0.00	0.00	0.00	0.00	0.00	0.00	0.00	

continued on next page

Table A.3, continued from previous page

Date	Hour	15	16	17	18	15	16	17	18
5/1/1999	6	0.00	0.00	0.00	0.01	0.00	0.00	0.00	0.01
	7	0.02	0.00	0.00	0.00	0.03	0.00	0.00	0.00
	8	0.00	0.01	0.00	0.02	0.00	0.01	0.00	0.02
	9	0.01	0.01	0.00	0.04	0.01	0.02	0.00	0.04
	10	0.07	0.11	0.10	0.16	0.05	0.11	0.10	0.15
	11	0.11	0.16	0.19	0.15	0.11	0.15	0.19	0.13
	12	0.15	0.17	0.20	0.19	0.18	0.18	0.19	0.17
13	0.07	0.04	0.01	0.09	0.10	0.07	0.01	0.09	
14	0.02	0.04	0.01	0.09	0.01	0.06	0.01	0.08	
15	0.01	0.02	0.01	0.05	0.01	0.02	0.01	0.05	
16	0.04	0.02	0.01	0.06	0.04	0.03	0.01	0.06	
17	0.01	0.01	0.00	0.03	0.00	0.02	0.00	0.03	
18	0.00	0.01	0.00	0.02	0.00	0.01	0.00	0.02	
19	0.03	0.06	0.09	0.01	0.03	0.05	0.09	0.00	
20	0.00	0.00	0.00	0.00	0.00	0.00	0.00	0.00	
21	0.00	0.00	0.00	0.00	0.00	0.00	0.00	0.00	
22	0.00	0.00	0.00	0.00	0.00	0.00	0.00	0.00	
23	0.03	0.01	0.00	0.03	0.03	0.01	0.00	0.03	
5/2/1999	0	0.03	0.01	0.00	0.04	0.04	0.02	0.01	0.05
	1	0.01	0.01	0.00	0.03	0.01	0.02	0.00	0.05
	2	0.00	0.00	0.00	0.00	0.00	0.00	0.00	0.00
	3	0.03	0.06	0.09	0.01	0.02	0.05	0.08	0.00
	4	0.00	0.00	0.00	0.00	0.00	0.00	0.00	0.00
	5	0.00	0.00	0.00	0.00	0.00	0.00	0.00	0.00
6	0.00	0.00	0.00	0.00	0.00	0.00	0.00	0.00	
7	0.00	0.00	0.00	0.00	0.00	0.00	0.00	0.00	
8	0.03	0.06	0.09	0.01	0.02	0.05	0.08	0.00	
9	0.03	0.06	0.09	0.01	0.02	0.05	0.08	0.00	
10	0.03	0.06	0.09	0.01	0.02	0.05	0.08	0.00	
11	0.03	0.00	0.00	0.00	0.03	0.00	0.00	0.00	
12	0.00	0.00	0.00	0.00	0.00	0.00	0.00	0.00	
13	0.00	0.00	0.00	0.00	0.00	0.00	0.00	0.00	
14	0.00	0.00	0.00	0.00	0.00	0.00	0.00	0.00	
15	0.00	0.00	0.00	0.00	0.00	0.00	0.00	0.00	
16	0.00	0.00	0.00	0.00	0.00	0.00	0.00	0.00	
17	0.00	0.00	0.00	0.00	0.00	0.00	0.00	0.00	
18	0.00	0.00	0.00	0.00	0.00	0.00	0.00	0.00	
19	0.00	0.00	0.00	0.00	0.00	0.00	0.00	0.00	
20	0.00	0.00	0.00	0.00	0.00	0.00	0.00	0.00	
21	0.00	0.00	0.00	0.00	0.00	0.00	0.00	0.00	
22	0.00	0.00	0.00	0.00	0.00	0.00	0.00	0.00	
23	0.00	0.00	0.00	0.00	0.00	0.00	0.00	0.00	
Event Total		6.25	7.45	7.84	9.42	6.61	7.76	7.97	8.68

Table A.4: Derived hourly rainfall records for simulations HDS<sub>c</sub> and HDS<sub>d</sub> at supplemental gauges (nos. 15–18).

Date	Hour	HDS <sub>c</sub> rainfall at gauges				HDS <sub>d</sub> rainfall at gauges			
		15	16	17	18	15	16	17	18
4/28/1999	0	0.00	0.00	0.00	0.00	0.00	0.00	0.00	0.00
	1	0.00	0.00	0.00	0.00	0.00	0.00	0.00	0.00
	2	0.00	0.00	0.00	0.00	0.00	0.00	0.00	0.00
	3	0.00	0.00	0.00	0.00	0.00	0.00	0.00	0.00
	4	0.00	0.00	0.00	0.00	0.00	0.00	0.00	0.00
	5	0.00	0.00	0.00	0.00	0.00	0.00	0.00	0.00
	6	0.00	0.00	0.00	0.00	0.00	0.00	0.00	0.00
	7	0.00	0.00	0.00	0.00	0.00	0.00	0.00	0.00
	8	0.00	0.00	0.00	0.00	0.00	0.00	0.00	0.00
	9	0.00	0.00	0.00	0.00	0.00	0.00	0.00	0.00
	10	0.00	0.00	0.00	0.00	0.00	0.00	0.00	0.00
	11	0.00	0.00	0.00	0.00	0.00	0.00	0.00	0.00
	12	0.00	0.00	0.00	0.00	0.00	0.05	0.00	0.00
	13	0.00	0.00	0.00	0.00	0.00	0.10	0.00	0.00
	14	0.00	0.00	0.00	0.01	0.00	0.15	0.00	0.00
	15	0.00	0.00	0.00	0.00	0.00	0.15	0.00	0.00
	16	0.00	0.00	0.00	0.00	0.00	0.20	0.00	0.00
	17	0.00	0.00	0.00	0.00	0.00	0.20	0.00	0.00
	18	0.02	0.03	0.01	0.05	0.00	0.20	0.00	0.00
	19	0.03	0.09	0.03	0.13	0.00	0.20	0.00	0.00
	20	0.02	0.05	0.02	0.07	0.15	0.20	1.50	0.00
	21	0.03	0.04	0.01	0.04	0.50	0.14	0.00	0.00
	22	0.23	0.38	0.30	0.46	1.13	0.10	0.00	0.00
	23	0.24	0.30	0.34	0.19	0.00	0.15	0.00	0.00
4/29/1999	0	0.49	0.54	0.62	0.24	0.00	0.18	0.00	0.52
	1	0.49	0.39	0.45	0.20	0.00	0.09	0.00	0.19
	2	0.18	0.37	0.51	0.06	0.00	0.12	0.08	0.00
	3	0.12	0.12	0.17	0.01	0.00	0.11	0.17	0.00
	4	0.07	0.14	0.18	0.05	0.00	0.11	0.48	0.00
	5	0.11	0.10	0.10	0.08	0.00	0.11	0.15	0.00
	6	0.02	0.04	0.01	0.08	0.00	0.11	0.00	0.00
	7	0.08	0.16	0.18	0.08	0.27	0.11	0.00	0.00
	8	0.13	0.13	0.11	0.14	0.81	0.11	0.20	0.00
	9	0.13	0.13	0.10	0.13	0.00	0.11	0.56	0.00
	10	0.16	0.19	0.12	0.23	0.05	0.11	0.00	0.00
	11	0.06	0.12	0.10	0.11	0.05	0.11	0.18	0.00

*continued on next page*

Table A.4, continued from previous page

Date	Hour	15	16	17	18	15	16	17	18
4/29/1999	12	0.01	0.02	0.01	0.04	0.10	0.12	0.32	0.00
	13	0.03	0.07	0.09	0.02	0.10	0.12	0.00	0.00
	14	0.03	0.06	0.08	0.00	0.15	0.13	0.18	0.00
	15	0.08	0.16	0.18	0.09	0.17	0.13	0.28	0.00
	16	0.15	0.16	0.12	0.19	0.20	0.14	0.00	0.00
	17	0.18	0.25	0.20	0.21	0.22	0.13	0.15	0.00
	18	0.23	0.33	0.13	0.30	0.23	0.05	0.31	0.00
	19	0.46	0.38	0.13	0.25	0.17	0.16	0.00	0.00
	20	0.24	0.27	0.20	0.22	0.02	0.12	0.05	0.25
	21	0.34	0.31	0.29	0.25	0.00	0.08	0.10	1.01
	22	0.17	0.21	0.19	0.16	0.00	0.14	0.22	0.28
	23	0.10	0.23	0.19	0.15	0.00	0.19	0.24	0.48
4/30/1999	0	0.08	0.16	0.10	0.12	0.05	0.17	0.00	0.00
	1	0.02	0.10	0.01	0.12	0.05	0.16	0.00	0.00
	2	0.06	0.14	0.11	0.14	0.05	0.14	0.00	0.00
	3	0.13	0.33	0.13	0.30	0.10	0.12	0.00	0.00
	4	0.10	0.24	0.12	0.26	0.10	0.13	0.10	0.00
	5	0.15	0.22	0.13	0.30	0.20	0.13	0.38	0.10
	6	0.10	0.25	0.12	0.28	0.30	0.13	0.10	0.66
	7	0.26	0.31	0.22	0.29	0.45	0.15	0.00	0.43
	8	0.15	0.35	0.21	0.23	0.32	0.13	0.20	0.27
	9	0.23	0.32	0.30	0.26	0.10	0.13	0.20	0.60
	10	0.23	0.30	0.30	0.24	0.05	0.14	0.25	0.49
	11	0.10	0.15	0.03	0.27	0.10	0.14	0.20	0.37
	12	0.11	0.11	0.03	0.20	0.25	0.14	0.30	0.49
	13	0.09	0.10	0.02	0.18	0.40	0.13	0.30	0.55
	14	0.09	0.09	0.02	0.16	0.05	0.13	0.10	0.58
	15	0.09	0.01	0.01	0.01	0.05	0.14	0.10	0.48
	16	0.00	0.01	0.00	0.01	0.15	0.14	0.10	0.56
	17	0.00	0.00	0.00	0.00	0.20	0.13	0.10	0.34
	18	0.00	0.01	0.00	0.02	0.02	0.13	0.15	0.25
	19	0.02	0.01	0.00	0.01	0.00	0.13	0.18	0.26
	20	0.00	0.00	0.00	0.00	0.00	0.13	0.16	0.20
	21	0.00	0.00	0.00	0.00	0.05	0.12	0.14	0.21
	22	0.00	0.00	0.00	0.00	0.25	0.12	0.13	0.00
5/1/1999	23	0.00	0.00	0.00	0.00	0.35	0.12	0.13	0.00
	0	0.00	0.00	0.00	0.00	0.00	0.12	0.13	0.00
	1	0.00	0.01	0.00	0.01	0.00	0.12	0.14	0.00
	2	0.00	0.01	0.00	0.01	0.05	0.12	0.14	0.00
	3	0.00	0.00	0.00	0.00	0.10	0.12	0.14	0.00
	4	0.00	0.00	0.00	0.00	0.15	0.11	0.14	0.00
	5	0.00	0.00	0.00	0.00	0.15	0.11	0.13	0.00

continued on next page

Table A.4, continued from previous page

Date	Hour	15	16	17	18	15	16	17	18
5/1/1999	6	0.00	0.01	0.00	0.01	0.15	0.11	0.12	0.00
	7	0.03	0.00	0.00	0.00	0.10	0.11	0.10	0.00
	8	0.00	0.01	0.00	0.02	0.10	0.11	0.05	0.00
	9	0.01	0.03	0.00	0.04	0.10	0.11	0.20	0.00
	10	0.06	0.15	0.10	0.15	0.10	0.10	0.20	0.00
	11	0.12	0.19	0.19	0.13	0.65	0.13	0.19	0.00
	12	0.20	0.24	0.19	0.17	0.00	0.12	0.18	0.00
	13	0.12	0.11	0.01	0.09	0.00	0.11	0.05	0.00
	14	0.01	0.09	0.01	0.08	0.00	0.11	0.11	0.83
	15	0.01	0.03	0.01	0.05	0.14	0.11	0.11	0.00
	16	0.04	0.04	0.01	0.06	0.14	0.11	0.11	0.00
	17	0.00	0.02	0.00	0.03	0.13	0.11	0.10	0.00
	18	0.00	0.01	0.00	0.02	0.13	0.11	0.09	0.00
	19	0.03	0.06	0.09	0.00	0.12	0.10	0.05	0.00
	20	0.00	0.00	0.00	0.00	0.12	0.10	0.02	0.00
	21	0.00	0.00	0.00	0.00	0.11	0.10	0.14	0.00
	22	0.00	0.00	0.00	0.00	0.11	0.10	0.00	0.00
	23	0.04	0.02	0.00	0.03	0.10	0.10	0.00	0.00
5/2/1999	0	0.04	0.03	0.01	0.05	0.10	0.11	0.12	0.00
	1	0.01	0.03	0.00	0.05	0.00	0.10	0.12	0.00
	2	0.00	0.00	0.00	0.00	0.00	0.10	0.11	0.00
	3	0.02	0.06	0.08	0.00	0.00	0.10	0.11	0.00
	4	0.00	0.00	0.00	0.00	0.00	0.11	0.11	0.00
	5	0.00	0.00	0.00	0.00	0.00	0.10	0.11	0.00
	6	0.00	0.00	0.00	0.00	0.00	0.10	0.05	0.00
	7	0.00	0.00	0.00	0.00	0.00	0.11	0.00	0.00
	8	0.02	0.06	0.08	0.00	0.00	0.10	0.00	0.00
	9	0.02	0.06	0.08	0.00	0.00	0.10	0.00	0.00
	10	0.02	0.06	0.08	0.00	0.00	0.11	0.00	0.00
	11	0.03	0.00	0.00	0.00	0.00	0.10	0.00	0.00
	12	0.00	0.00	0.00	0.00	0.00	0.10	0.00	0.00
	13	0.00	0.00	0.00	0.00	0.00	0.10	0.00	0.00
	14	0.00	0.00	0.00	0.00	0.00	0.10	0.00	0.00
	15	0.00	0.00	0.00	0.00	0.00	0.10	0.00	0.00
	16	0.00	0.00	0.00	0.00	0.00	0.10	0.00	0.00
	17	0.00	0.00	0.00	0.00	0.00	0.10	0.00	0.00
	18	0.00	0.00	0.00	0.00	0.00	0.10	0.00	0.00
	19	0.00	0.00	0.00	0.00	0.00	0.10	0.00	0.00
	20	0.00	0.00	0.00	0.00	0.00	0.00	0.00	0.00
	21	0.00	0.00	0.00	0.00	0.00	0.00	0.00	0.00
	22	0.00	0.00	0.00	0.00	0.00	0.00	0.00	0.00
23	0.00	0.00	0.00	0.00	0.00	0.00	0.00	0.00	
Event Total		7.49	10.28	7.99	8.65	10.81	12.65	11.86	10.40

## Appendix B

### USGS DISCHARGE RECORDS

Table B.1: Discharge records for April 28–May 2, 1999, at USGS gauge 07104000.

UNITED STATES DEPARTMENT OF THE INTERIOR GEOLOGICAL SURVEY - COLORADO DISTRICT											
STATION NUMBER 07104000 MONUMENT CREEK AT PIKEVIEW, CO.											
STREAM SOURCE AGENCY USGS											
LATITUDE 385504 LONGITUDE 1044905 DRAINAGE AREA 204.00											
DATUM 6203.26 STATE 08 COUNTY 041											
DISCHARGE FROM DCP, IN CFS											
COMPUTED UNIT VALUES (INSTANTANEOUS)											
APRIL 28, 1999 Mountain Daylight Time											
0:15:00	59	5:15:00	64	10:15:00	68	15:15:00	66	20:15:00	77		
0:30:00	64	5:30:00	64	10:30:00	70	15:30:00	70	20:30:00	75		
0:45:00	64	5:45:00	63	10:45:00	70	15:45:00	70	20:45:00	83		
1:00:00	61	6:00:00	64	11:00:00	71	16:00:00	73	21:00:00	85		
1:15:00	63	6:15:00	61	11:15:00	70	16:15:00	71	21:15:00	96		
1:30:00	63	6:30:00	61	11:30:00	68	16:30:00	71	21:30:00	115		
1:45:00	63	6:45:00	63	11:45:00	70	16:45:00	73	21:45:00	138		
2:00:00	63	7:00:00	66	12:00:00	64	17:00:00	79	22:00:00	152		
2:15:00	64	7:15:00	64	12:15:00	71	17:15:00	77	22:15:00	168		
2:30:00	63	7:30:00	66	12:30:00	70	17:30:00	79	22:30:00	165		
2:45:00	61	7:45:00	66	12:45:00	73	17:45:00	77	22:45:00	174		
3:00:00	66	8:00:00	68	13:00:00	70	18:00:00	77	23:00:00	165		
3:15:00	61	8:15:00	70	13:15:00	70	18:15:00	71	23:15:00	165		
3:30:00	64	8:30:00	66	13:30:00	73	18:30:00	77	23:30:00	174		
3:45:00	63	8:45:00	68	13:45:00	68	18:45:00	70	23:45:00	211		
4:00:00	63	9:00:00	70	14:00:00	71	19:00:00	75	24:00:00	253		
4:15:00	63	9:15:00	68	14:15:00	68	19:15:00	71				
4:30:00	64	9:30:00	70	14:30:00	64	19:30:00	73				
4:45:00	68	9:45:00	68	14:45:00	68	19:45:00	73				
5:00:00	64	10:00:00	71	15:00:00	66	20:00:00	75				

*continued on next page*

Table B.1, continued from previous page

APRIL 29, 1999 Mountain Daylight Time									
0:15:00	278	5:15:00	919	10:15:00	717	15:15:00	972	20:15:00	2200
0:30:00	346	5:30:00	1020	10:30:00	727	15:30:00	1110	20:30:00	2550
0:45:00	261	5:45:00	927	10:45:00	799	15:45:00	1060	20:45:00	2740
1:00:00	299	6:00:00	859	11:00:00	910	16:00:00	1130	21:00:00	2640
1:15:00	589	6:15:00	981	11:15:00	859	16:15:00	1210	21:15:00	2610
1:30:00	867	6:30:00	876	11:30:00	850	16:30:00	1070	21:30:00	2690
1:45:00	1060	6:45:00	884	11:45:00	1020	16:45:00	1160	21:45:00	2690
2:00:00	1100	7:00:00	831	12:00:00	1160	17:00:00	1280	22:00:00	2760
2:15:00	1140	7:15:00	936	12:15:00	1390	17:15:00	1190	22:15:00	2730
2:30:00	1350	7:30:00	919	12:30:00	1370	17:30:00	1310	22:30:00	2790
2:45:00	1550	7:45:00	919	12:45:00	1280	17:45:00	1210	22:45:00	2580
3:00:00	1530	8:00:00	936	13:00:00	1230	18:00:00	1230	23:00:00	2600
3:15:00	1720	8:15:00	810	13:15:00	1140	18:15:00	1360	23:15:00	2630
3:30:00	1730	8:30:00	708	13:30:00	1160	18:30:00	1410	23:30:00	2280
3:45:00	1620	8:45:00	884	13:45:00	1150	18:45:00	1620	23:45:00	2480
4:00:00	1710	9:00:00	737	14:00:00	1140	19:00:00	1550	24:00:00	2390
4:15:00	1530	9:15:00	708	14:15:00	990	19:15:00	1590		
4:30:00	1330	9:30:00	810	14:30:00	954	19:30:00	1660		
4:45:00	1270	9:45:00	717	14:45:00	1200	19:45:00	1850		
5:00:00	1140	10:00:00	727	15:00:00	1210	20:00:00	1900		
APRIL 30, 1999 Mountain Daylight Time									
0:15:00	2280	5:15:00	2000	10:15:00	3330	15:05:00	4890	20:00:00	3480
0:30:00	2200	5:30:00	2050	10:30:00	3520	15:15:00	4390	20:15:00	3400
0:45:00	2180	5:45:00	2040	10:45:00	3440	15:30:00	4190	20:30:00	3140
1:00:00	2050	6:00:00	2080	11:00:00	3560	15:45:00	4190	20:45:00	2880
1:15:00	2050	6:15:00	2200	11:15:00	3720	16:00:00	4240	21:00:00	2830
1:30:00	2070	6:30:00	2270	11:30:00	3480	16:15:00	4340	21:15:00	2680
1:45:00	2200	6:45:00	2310	11:45:00	3560	16:30:00	4340	21:30:00	2580
2:00:00	1910	7:00:00	2270	12:00:00	3600	16:45:00	4370	21:45:00	2170
2:15:00	1860	7:15:00	2450	12:15:00	3660	17:00:00	4170	22:00:00	2470
2:30:00	1820	7:30:00	2390	12:30:00	3240	17:15:00	3880	22:15:00	2410
2:45:00	2000	7:45:00	2600	12:45:00	3740	17:30:00	4020	22:30:00	2170
3:00:00	2000	8:00:00	2640	13:00:00	3480	17:45:00	3680	22:45:00	2050
3:15:00	2070	8:15:00	2930	13:15:00	3760	18:00:00	3540	23:00:00	2110
3:30:00	1970	8:30:00	2850	13:30:00	3920	18:15:00	3560	23:15:00	2040
3:45:00	2110	8:45:00	3000	13:45:00	3800	18:30:00	3330	23:30:00	1940
4:00:00	1820	9:00:00	3110	14:00:00	3760	18:45:00	3640	23:45:00	1830
4:15:00	1830	9:15:00	3020	14:15:00	3900	19:00:00	3420	24:00:00	1930
4:30:00	1970	9:30:00	3020	14:30:00	4090	19:15:00	3820		
4:45:00	1870	9:45:00	3160	14:45:00	4340	19:30:00	3640		
5:00:00	1980	10:00:00	3220	15:00:00	4660	19:45:00	3520		

continued on next page

Table B.1, continued from previous page

MAY 01, 1999 Mountain Daylight Time									
0:15:00	1860	5:15:00	1350	10:15:00	1090	15:15:00	1760	20:15:00	1360
0:30:00	1850	5:30:00	1240	10:30:00	1060	15:30:00	1610	20:30:00	1620
0:45:00	1620	5:45:00	1200	10:45:00	1010	15:45:00	1450	20:45:00	1440
1:00:00	1670	6:00:00	1200	11:00:00	1010	16:00:00	1640	21:00:00	1440
1:15:00	1670	6:15:00	1200	11:15:00	1220	16:15:00	1490	21:15:00	1690
1:30:00	1660	6:30:00	1070	11:30:00	1110	16:30:00	1430	21:30:00	1460
1:45:00	1720	6:45:00	1260	11:45:00	1150	16:45:00	1370	21:45:00	1420
2:00:00	1480	7:00:00	1080	12:00:00	1060	17:00:00	1500	22:00:00	1310
2:15:00	1430	7:15:00	1100	12:15:00	1170	17:15:00	1430	22:15:00	1350
2:30:00	1430	7:30:00	1060	12:30:00	1240	17:30:00	1520	22:30:00	1350
2:45:00	1480	7:45:00	1110	12:45:00	1180	17:45:00	1490	22:45:00	1550
3:00:00	1400	8:00:00	1100	13:00:00	1230	18:00:00	1510	23:00:00	1480
3:15:00	1340	8:15:00	1160	13:15:00	1280	18:15:00	1580	23:15:00	1290
3:30:00	1370	8:30:00	1100	13:30:00	1410	18:30:00	1530	23:30:00	1370
3:45:00	1410	8:45:00	1050	13:45:00	1400	18:45:00	1520	23:45:00	1410
4:00:00	1310	9:00:00	1160	14:00:00	1550	19:00:00	1490	24:00:00	1310
4:15:00	1260	9:15:00	1140	14:15:00	1660	19:15:00	1480		
4:30:00	1300	9:30:00	1170	14:30:00	1690	19:30:00	1230		
4:45:00	1230	9:45:00	999	14:45:00	2070	19:45:00	1550		
5:00:00	1280	10:00:00	901	15:00:00	1850	20:00:00	1430		
MAY 02, 1999 Mountain Daylight Time									
0:15:00	1360	5:15:00	1490	10:15:00	901	15:15:00	788	20:15:00	876
0:30:00	1220	5:30:00	1060	10:30:00	727	15:30:00	831	20:30:00	717
0:45:00	1190	5:45:00	1060	10:45:00	884	15:45:00	859	20:45:00	717
1:00:00	1280	6:00:00	1170	11:00:00	831	16:00:00	820	21:00:00	831
1:15:00	1290	6:15:00	1060	11:15:00	799	16:15:00	859	21:15:00	708
1:30:00	1370	6:30:00	1060	11:30:00	901	16:30:00	954	21:30:00	717
1:45:00	1160	6:45:00	1060	11:45:00	910	16:45:00	859	21:45:00	727
2:00:00	1200	7:00:00	1040	12:00:00	842	17:00:00	927	22:00:00	717
2:15:00	1180	7:15:00	1040	12:15:00	1070	17:15:00	1060	22:15:00	633
2:30:00	1490	7:30:00	1060	12:30:00	799	17:30:00	867	22:30:00	778
2:45:00	1620	7:45:00	1010	12:45:00	737	17:45:00	876	22:45:00	698
3:00:00	1340	8:00:00	945	13:00:00	867	18:00:00	945	23:00:00	747
3:15:00	1240	8:15:00	1050	13:15:00	842	18:15:00	893	23:15:00	679
3:30:00	1330	8:30:00	1050	13:30:00	778	18:30:00	799	23:30:00	660
3:45:00	1230	8:45:00	1180	13:45:00	757	18:45:00	850	23:45:00	642
4:00:00	1070	9:00:00	936	14:00:00	876	19:00:00	859	24:00:00	747
4:15:00	1260	9:15:00	999	14:15:00	919	19:15:00	698		
4:30:00	1390	9:30:00	981	14:30:00	963	19:30:00	859		
4:45:00	1320	9:45:00	945	14:45:00	717	19:45:00	788		
5:00:00	1450	10:00:00	1060	15:00:00	831	20:00:00	810		

Table B.2: Discharge records for April 28–May 2, 1999, at USGS gauge 07105490.

UNITED STATES DEPARTMENT OF THE INTERIOR GEOLOGICAL SURVEY - COLORADO DISTRICT									
STATION NUMBER 07105490									
CHEYENNE CREEK AT EVANS AVE AT COLORADO SPRINGS, CO.									
STREAM SOURCE AGENCY USGS									
LATITUDE 384726 LONGITUDE 1045149 DRAINAGE AREA 21.7									
DATUM 6280 STATE 08 COUNTY 041									
DISCHARGE FROM DCP, IN CFS									
COMPUTED UNIT VALUES (INSTANTANEOUS)									
APRIL 28, 1999 Mountain Daylight Time									
0:15:00	13	5:15:00	14	10:15:00	15	15:15:00	14	20:15:00	16
0:30:00	13	5:30:00	14	10:30:00	15	15:30:00	14	20:30:00	16
0:45:00	13	5:45:00	14	10:45:00	15	15:45:00	15	20:45:00	17
1:00:00	13	6:00:00	14	11:00:00	15	16:00:00	15	21:00:00	17
1:15:00	13	6:15:00	14	11:15:00	15	16:15:00	15	21:15:00	20
1:30:00	13	6:30:00	14	11:30:00	15	16:30:00	15	21:30:00	20
1:45:00	14	6:45:00	14	11:45:00	15	16:45:00	15	21:45:00	20
2:00:00	14	7:00:00	14	12:00:00	15	17:00:00	15	22:00:00	25
2:15:00	14	7:15:00	14	12:15:00	15	17:15:00	15	22:15:00	28
2:30:00	14	7:30:00	14	12:30:00	15	17:30:00	15	22:30:00	31
2:45:00	14	7:45:00	14	12:45:00	15	17:45:00	15	22:45:00	30
3:00:00	14	8:00:00	14	13:00:00	15	18:00:00	15	23:00:00	30
3:15:00	14	8:15:00	14	13:15:00	15	18:15:00	15	23:15:00	37
3:30:00	14	8:30:00	14	13:30:00	15	18:30:00	15	23:30:00	51
3:45:00	14	8:45:00	14	13:45:00	15	18:45:00	15	23:45:00	62
4:00:00	14	9:00:00	14	14:00:00	13	19:00:00	15	24:00:00	66
4:15:00	14	9:15:00	14	14:15:00	14	19:15:00	16		
4:30:00	14	9:30:00	14	14:30:00	14	19:30:00	16		
4:45:00	14	9:45:00	14	14:45:00	14	19:45:00	16		
5:00:00	14	10:00:00	14	15:00:00	14	20:00:00	16		

*continued on next page*

Table B.2, continued from previous page

APRIL 29, 1999 Mountain Daylight Time									
0:15:00	87	5:15:00	129	10:15:00	133	15:15:00	175	20:15:00	220
0:30:00	96	5:30:00	131	10:30:00	133	15:30:00	178	20:30:00	193
0:45:00	137	5:45:00	133	10:45:00	137	15:45:00	175	20:45:00	212
1:00:00	141	6:00:00	133	11:00:00	137	16:00:00	180	21:00:00	214
1:15:00	137	6:15:00	131	11:15:00	141	16:15:00	183	21:15:00	209
1:30:00	139	6:30:00	133	11:30:00	141	16:30:00	193	21:30:00	203
1:45:00	141	6:45:00	133	11:45:00	141	16:45:00	206	21:45:00	203
2:00:00	145	7:00:00	135	12:00:00	145	17:00:00	220	22:00:00	193
2:15:00	145	7:15:00	135	12:15:00	145	17:15:00	238	22:15:00	198
2:30:00	148	7:30:00	133	12:30:00	145	17:30:00	232	22:30:00	235
2:45:00	127	7:45:00	133	12:45:00	145	17:45:00	241	22:45:00	238
3:00:00	141	8:00:00	133	13:00:00	145	18:00:00	217	23:00:00	226
3:15:00	141	8:15:00	137	13:15:00	145	18:15:00	209	23:15:00	232
3:30:00	141	8:30:00	137	13:30:00	148	18:30:00	195	23:30:00	229
3:45:00	141	8:45:00	137	13:45:00	150	18:45:00	198	23:45:00	217
4:00:00	141	9:00:00	137	14:00:00	150	19:00:00	188	24:00:00	193
4:15:00	141	9:15:00	133	14:15:00	150	19:15:00	180		
4:30:00	141	9:30:00	133	14:30:00	150	19:30:00	190		
4:45:00	133	9:45:00	133	14:45:00	152	19:45:00	209		
5:00:00	133	10:00:00	133	15:00:00	152	20:00:00	214		
APRIL 30, 1999 Mountain Daylight Time									
0:15:00	304	5:15:00	435	10:15:00	458	15:15:00	483	20:00:00	465
0:30:00	328	5:30:00	435	10:30:00	458	15:30:00	483	20:15:00	463
0:45:00	350	5:45:00	435	10:45:00	458	15:45:00	485	20:30:00	463
1:00:00	350	6:00:00	435	11:00:00	465	16:00:00	488	20:45:00	463
1:15:00	361	6:15:00	438	11:15:00	465	16:15:00	488	21:00:00	458
1:30:00	400	6:30:00	435	11:30:00	465	16:30:00	490	21:15:00	455
1:45:00	409	6:45:00	435	11:45:00	471	16:45:00	490	21:30:00	453
2:00:00	430	7:00:00	435	12:00:00	476	17:00:00	490	21:45:00	450
2:15:00	453	7:15:00	438	12:15:00	478	17:15:00	494	22:00:00	443
2:30:00	455	7:30:00	445	12:30:00	483	17:30:00	494	22:15:00	438
2:45:00	458	7:45:00	453	12:45:00	485	17:35:00	565	22:30:00	438
3:00:00	458	8:00:00	458	13:00:00	485	17:45:00	492	22:45:00	435
3:15:00	463	8:15:00	463	13:15:00	488	18:00:00	488	23:00:00	435
3:30:00	458	8:30:00	463	13:30:00	485	18:15:00	488	23:15:00	435
3:45:00	448	8:45:00	458	13:45:00	485	18:30:00	485	23:30:00	430
4:00:00	448	9:00:00	458	14:00:00	485	18:45:00	483	23:45:00	430
4:15:00	448	9:15:00	458	14:15:00	485	19:00:00	478	24:00:00	427
4:30:00	440	9:30:00	458	14:30:00	485	19:15:00	476		
4:45:00	435	9:45:00	458	14:45:00	485	19:30:00	471		
5:00:00	435	10:00:00	458	15:00:00	485	19:45:00	471		

continued on next page

Table B.2, continued from previous page

MAY 01, 1999 Mountain Daylight Time									
0:15:00	424	5:15:00	350	10:15:00	270	15:15:00	264	20:15:00	222
0:30:00	418	5:30:00	342	10:30:00	270	15:30:00	264	20:30:00	222
0:45:00	412	5:45:00	342	10:45:00	267	15:45:00	261	20:45:00	222
1:00:00	412	6:00:00	335	11:00:00	264	16:00:00	259	21:00:00	219
1:15:00	406	6:15:00	331	11:15:00	264	16:15:00	259	21:15:00	209
1:30:00	403	6:30:00	328	11:30:00	264	16:30:00	256	21:30:00	209
1:45:00	394	6:45:00	321	11:45:00	264	16:45:00	253	21:45:00	206
2:00:00	391	7:00:00	317	12:00:00	267	17:00:00	253	22:00:00	204
2:15:00	388	7:15:00	310	12:15:00	270	17:15:00	250	22:15:00	204
2:30:00	388	7:30:00	307	12:30:00	270	17:30:00	247	22:30:00	201
2:45:00	385	7:45:00	304	12:45:00	276	17:45:00	247	22:45:00	199
3:00:00	377	8:00:00	301	13:00:00	276	18:00:00	247	23:00:00	196
3:15:00	377	8:15:00	297	13:15:00	276	18:15:00	241	23:15:00	193
3:30:00	373	8:30:00	291	13:30:00	276	18:30:00	241	23:30:00	191
3:45:00	369	8:45:00	288	13:45:00	276	18:45:00	233	23:45:00	188
4:00:00	369	9:00:00	285	14:00:00	276	19:00:00	233	24:00:00	188
4:15:00	365	9:15:00	282	14:15:00	276	19:15:00	230		
4:30:00	361	9:30:00	276	14:30:00	273	19:30:00	227		
4:45:00	354	9:45:00	273	14:45:00	270	19:45:00	225		
5:00:00	350	10:00:00	273	15:00:00	267	20:00:00	225		
MAY 02, 1999 Mountain Daylight Time									
0:15:00	188	5:15:00	173	10:15:00	161	15:15:00	149	20:15:00	143
0:30:00	185	5:30:00	173	10:30:00	158	15:30:00	149	20:30:00	143
0:45:00	180	5:45:00	170	10:45:00	158	15:45:00	149	20:45:00	143
1:00:00	180	6:00:00	170	11:00:00	158	16:00:00	149	21:00:00	141
1:15:00	180	6:15:00	170	11:15:00	156	16:15:00	149	21:15:00	141
1:30:00	178	6:30:00	170	11:30:00	156	16:30:00	149	21:30:00	141
1:45:00	178	6:45:00	168	11:45:00	156	16:45:00	149	21:45:00	141
2:00:00	178	7:00:00	168	12:00:00	156	17:00:00	149	22:00:00	141
2:15:00	178	7:15:00	168	12:15:00	152	17:15:00	149	22:15:00	141
2:30:00	178	7:30:00	166	12:30:00	152	17:30:00	147	22:30:00	141
2:45:00	178	7:45:00	166	12:45:00	149	17:45:00	147	22:45:00	141
3:00:00	175	8:00:00	166	13:00:00	149	18:00:00	147	23:00:00	141
3:15:00	175	8:15:00	166	13:15:00	149	18:15:00	147	23:15:00	141
3:30:00	175	8:30:00	163	13:30:00	149	18:30:00	147	23:30:00	141
3:45:00	175	8:45:00	163	13:45:00	149	18:45:00	145	23:45:00	139
4:00:00	175	9:00:00	163	14:00:00	149	19:00:00	145	24:00:00	139
4:15:00	175	9:15:00	161	14:15:00	149	19:15:00	145		
4:30:00	175	9:30:00	161	14:30:00	149	19:30:00	145		
4:45:00	173	9:45:00	161	14:45:00	149	19:45:00	145		
5:00:00	173	10:00:00	161	15:00:00	149	20:00:00	145		

Table B.3: Discharge records for April 28–May 2, 1999, at USGS gauge 07105500.

UNITED STATES DEPARTMENT OF THE INTERIOR GEOLOGICAL SURVEY - COLORADO DISTRICT									
STATION NUMBER 07105500 FOUNTAIN CREEK AT COLORADO SPRINGS, CO. STREAM SOURCE AGENCY USGS LATITUDE 384859 LONGITUDE 1044920 DRAINAGE AREA 392.00 DATUM 5900.00 STATE 08 COUNTY 041 DISCHARGE FROM DCP, IN CFS COMPUTED UNIT VALUES (INSTANTANEOUS)									
APRIL 28, 1999 Mountain Daylight Time									
0:15:00	135	5:15:00	135	10:15:00	131	15:15:00	137	20:15:00	149
0:30:00	135	5:30:00	135	10:30:00	135	15:30:00	137	20:30:00	153
0:45:00	135	5:45:00	135	10:45:00	137	15:45:00	137	20:45:00	160
1:00:00	137	6:00:00	137	11:00:00	137	16:00:00	137	21:00:00	174
1:15:00	139	6:15:00	135	11:15:00	137	16:15:00	139	21:15:00	228
1:30:00	139	6:30:00	137	11:30:00	137	16:30:00	139	21:30:00	269
1:45:00	139	6:45:00	135	11:45:00	137	16:45:00	135	21:45:00	302
2:00:00	135	7:00:00	133	12:00:00	133	17:00:00	137	22:00:00	390
2:15:00	137	7:15:00	137	12:15:00	139	17:15:00	133	22:15:00	463
2:30:00	135	7:30:00	133	12:30:00	137	17:30:00	133	22:30:00	538
2:45:00	137	7:45:00	139	12:45:00	137	17:45:00	137	22:45:00	701
3:00:00	139	8:00:00	137	13:00:00	137	18:00:00	135	23:00:00	689
3:15:00	139	8:15:00	135	13:15:00	137	18:15:00	133	23:15:00	660
3:30:00	137	8:30:00	137	13:30:00	135	18:30:00	133	23:30:00	951
3:45:00	135	8:45:00	139	13:45:00	137	18:45:00	135	23:45:00	1120
4:00:00	135	9:00:00	135	14:00:00	137	19:00:00	137	24:00:00	1660
4:15:00	135	9:15:00	135	14:15:00	137	19:15:00	137		
4:30:00	135	9:30:00	135	14:30:00	137	19:30:00	137		
4:45:00	135	9:45:00	135	14:45:00	137	19:45:00	141		
5:00:00	137	10:00:00	135	15:00:00	135	20:00:00	143		

*continued on next page*

Table B.3, continued from previous page

APRIL 29, 1999 Mountain Daylight Time									
0:15:00	2560	5:15:00	3010	10:15:00	3020	15:15:00	4330	20:15:00	6120
0:30:00	2950	5:30:00	2920	10:30:00	2970	15:30:00	4300	20:30:00	6320
0:45:00	4050	5:45:00	2740	10:45:00	3100	15:45:00	4310	20:45:00	6510
1:00:00	4710	6:00:00	2690	11:00:00	2970	16:00:00	4250	21:00:00	6660
1:15:00	4720	6:15:00	2590	11:15:00	3000	16:15:00	4160	21:15:00	7130
1:30:00	4610	6:30:00	2600	11:30:00	3070	16:30:00	4170	21:30:00	7420
1:45:00	4350	6:45:00	2660	11:45:00	3140	16:45:00	4140	21:45:00	7450
2:00:00	4520	7:00:00	2670	12:00:00	3380	17:00:00	4260	22:00:00	7240
2:15:00	3750	7:15:00	2620	12:15:00	3680	17:15:00	4370	22:15:00	7130
2:30:00	3620	7:30:00	2780	12:30:00	3830	17:30:00	4580	22:30:00	7090
2:45:00	3480	7:45:00	2820	12:45:00	3920	17:45:00	4750	22:45:00	7060
3:00:00	3460	8:00:00	2840	13:00:00	4170	18:00:00	4960	23:00:00	7270
3:15:00	3330	8:15:00	2970	13:15:00	4220	18:15:00	4980	23:15:00	7230
3:30:00	3580	8:30:00	3100	13:30:00	4090	18:30:00	5000	23:30:00	7210
3:45:00	3730	8:45:00	3060	13:45:00	4060	18:45:00	5000	23:45:00	7140
4:00:00	3660	9:00:00	3110	14:00:00	3920	19:00:00	5060	24:00:00	7040
4:15:00	3640	9:15:00	3100	14:15:00	3950	19:15:00	5160		
4:30:00	3430	9:30:00	3120	14:30:00	3920	19:30:00	5330		
4:45:00	3360	9:45:00	3020	14:45:00	4000	19:45:00	5550		
5:00:00	3230	10:00:00	2990	15:00:00	4200	20:00:00	5830		
APRIL 30, 1999 Mountain Daylight Time									
0:15:00	7000	5:15:00	6510	10:15:00	8560	15:15:00	9260	20:15:00	6570
0:30:00	6900	5:30:00	6620	10:30:00	8300	15:30:00	9180	20:30:00	6550
0:45:00	6840	5:45:00	6800	10:45:00	8530	15:45:00	9000	20:45:00	6480
1:00:00	6690	6:00:00	6790	11:00:00	8580	16:00:00	9210	21:00:00	6360
1:15:00	6760	6:15:00	7000	11:15:00	8770	16:15:00	9310	21:15:00	6350
1:30:00	6660	6:30:00	6940	11:30:00	8800	16:30:00	9310	21:30:00	6160
1:45:00	6590	6:45:00	7090	11:45:00	8810	16:45:00	9100	21:45:00	6160
2:00:00	6590	7:00:00	7040	12:00:00	8910	17:00:00	9020	22:00:00	5970
2:15:00	6540	7:15:00	7370	12:15:00	9130	17:15:00	8700	22:15:00	6010
2:30:00	6400	7:30:00	7530	12:30:00	9180	17:30:00	8360	22:30:00	5870
2:45:00	6400	7:45:00	7620	12:45:00	9100	17:45:00	8000	22:45:00	5790
3:00:00	6390	8:00:00	7730	13:00:00	9390	18:00:00	7820	23:00:00	5680
3:15:00	6270	8:15:00	7940	13:15:00	9440	18:15:00	7620	23:15:00	5470
3:30:00	6200	8:30:00	8060	13:30:00	9340	18:30:00	7420	23:30:00	5360
3:45:00	6050	8:45:00	8100	13:45:00	9450	18:45:00	7190	23:45:00	5310
4:00:00	6080	9:00:00	8160	14:00:00	9360	19:00:00	7070	24:00:00	5260
4:15:00	6080	9:15:00	8270	14:15:00	9490	19:15:00	6930		
4:30:00	6170	9:30:00	8490	14:30:00	9390	19:30:00	6830		
4:45:00	6350	9:45:00	8580	14:45:00	9410	19:45:00	6760		
5:00:00	6570	10:00:00	8500	15:00:00	9340	20:00:00	6690		

continued on next page

Table B.3, continued from previous page

MAY 01, 1999 Mountain Daylight Time									
0:15:00	5160	5:15:00	4030	10:15:00	3490	15:15:00	4570	20:15:00	3680
0:30:00	5020	5:30:00	4020	10:30:00	3410	15:30:00	4560	20:30:00	3620
0:45:00	4970	5:45:00	4050	10:45:00	3460	15:45:00	4620	20:45:00	3590
1:00:00	4880	6:00:00	3950	11:00:00	3440	16:00:00	4460	21:00:00	3500
1:15:00	4830	6:15:00	3920	11:15:00	3440	16:15:00	4400	21:15:00	3460
1:30:00	4790	6:30:00	3870	11:30:00	3450	16:30:00	4360	21:30:00	3440
1:45:00	4740	6:45:00	3870	11:45:00	3530	16:45:00	4360	21:45:00	3330
2:00:00	4650	7:00:00	3840	12:00:00	3680	17:00:00	4400	22:00:00	3380
2:15:00	4570	7:15:00	3800	12:15:00	3770	17:15:00	4370	22:15:00	3220
2:30:00	4520	7:30:00	3760	12:30:00	3910	17:30:00	4270	22:30:00	3180
2:45:00	4470	7:45:00	3730	12:45:00	3990	17:45:00	4160	22:45:00	3130
3:00:00	4380	8:00:00	3680	13:00:00	4060	18:00:00	4070	23:00:00	3070
3:15:00	4320	8:15:00	3640	13:15:00	4130	18:15:00	4070	23:15:00	3010
3:30:00	4310	8:30:00	3600	13:30:00	4190	18:30:00	4060	23:30:00	3010
3:45:00	4260	8:45:00	3590	13:45:00	4290	18:45:00	4050	23:45:00	2990
4:00:00	4220	9:00:00	3620	14:00:00	4250	19:00:00	4000	24:00:00	2940
4:15:00	4190	9:15:00	3510	14:15:00	4420	19:15:00	3950		
4:30:00	4140	9:30:00	3510	14:30:00	4530	19:30:00	3870		
4:45:00	4140	9:45:00	3530	14:45:00	4610	19:45:00	3810		
5:00:00	4090	10:00:00	3490	15:00:00	4600	20:00:00	3760		
MAY 02, 1999 Mountain Daylight Time									
0:15:00	2890	5:15:00	2370	10:15:00	1700	15:15:00	1690	20:15:00	1550
0:30:00	2840	5:30:00	2300	10:30:00	1940	15:30:00	1660	20:30:00	1610
0:45:00	2840	5:45:00	2250	10:45:00	1880	15:45:00	1630	20:45:00	1540
1:00:00	2810	6:00:00	2280	11:00:00	1880	16:00:00	1620	21:00:00	1480
1:15:00	2730	6:15:00	2290	11:15:00	1840	16:15:00	1590	21:15:00	1490
1:30:00	2660	6:30:00	2220	11:30:00	1830	16:30:00	1580	21:30:00	1440
1:45:00	2660	6:45:00	2250	11:45:00	1880	16:45:00	1590	21:45:00	1430
2:00:00	2640	7:00:00	2130	12:00:00	1860	17:00:00	1590	22:00:00	1430
2:15:00	2610	7:15:00	2110	12:15:00	1730	17:15:00	1610	22:15:00	1390
2:30:00	2640	7:30:00	2030	12:30:00	1730	17:30:00	1570	22:30:00	1460
2:45:00	2610	7:45:00	2040	12:45:00	1740	17:45:00	1590	22:45:00	1390
3:00:00	2560	8:00:00	2000	13:00:00	1720	18:00:00	1590	23:00:00	1390
3:15:00	2550	8:15:00	1910	13:15:00	1680	18:15:00	1590	23:15:00	1380
3:30:00	2580	8:30:00	2070	13:30:00	1680	18:30:00	1630	23:30:00	1400
3:45:00	2550	8:45:00	1980	13:45:00	1770	18:45:00	1550	23:45:00	1390
4:00:00	2510	9:00:00	1890	14:00:00	1720	19:00:00	1530	24:00:00	1430
4:15:00	2520	9:15:00	1960	14:15:00	1700	19:15:00	1470		
4:30:00	2510	9:30:00	1990	14:30:00	1730	19:30:00	1490		
4:45:00	2450	9:45:00	1860	14:45:00	1660	19:45:00	1540		
5:00:00	2420	10:00:00	1630	15:00:00	1720	20:00:00	1550		

Table B.4: Discharge records for April 28–May 2, 1999, at USGS gauge 07105530.

UNITED STATES DEPARTMENT OF THE INTERIOR GEOLOGICAL SURVEY - COLORADO DISTRICT									
STATION NUMBER 07105530									
FOUNTAIN CR BL JANITELL RD BL COLO. SPRINGS, CO.									
STREAM SOURCE AGENCY USGS									
LATITUDE 384811 LONGITUDE 1044743 DRAINAGE AREA 413									
DATUM 5840 STATE 08 COUNTY 041									
DISCHARGE FROM DCP, IN CFS									
COMPUTED UNIT VALUES (INSTANTANEOUS)									
APRIL 28, 1999 Mountain Daylight Time									
0:15:00	174	5:15:00	131	10:15:00	209	15:15:00	181	20:15:00	212
0:30:00	169	5:30:00	131	10:30:00	200	15:30:00	176	20:30:00	221
0:45:00	166	5:45:00	133	10:45:00	198	15:45:00	179	20:45:00	218
1:00:00	166	6:00:00	133	11:00:00	189	16:00:00	181	21:00:00	230
1:15:00	162	6:15:00	133	11:15:00	187	16:15:00	176	21:15:00	243
1:30:00	162	6:30:00	137	11:30:00	184	16:30:00	139	21:30:00	277
1:45:00	155	6:45:00	137	11:45:00	189	16:45:00	203	21:45:00	340
2:00:00	152	7:00:00	144	12:00:00	195	17:00:00	200	22:00:00	493
2:15:00	148	7:15:00	144	12:15:00	198	17:15:00	203	22:15:00	540
2:30:00	148	7:30:00	144	12:30:00	198	17:30:00	206	22:30:00	645
2:45:00	148	7:45:00	150	12:45:00	189	17:45:00	203	22:45:00	773
3:00:00	146	8:00:00	166	13:00:00	184	18:00:00	203	23:00:00	958
3:15:00	141	8:15:00	162	13:15:00	184	18:15:00	200	23:15:00	987
3:30:00	139	8:30:00	164	13:30:00	187	18:30:00	198	23:30:00	968
3:45:00	137	8:45:00	189	13:45:00	184	18:45:00	198	23:45:00	1280
4:00:00	137	9:00:00	200	14:00:00	184	19:00:00	198	24:00:00	1580
4:15:00	131	9:15:00	209	14:15:00	187	19:15:00	198		
4:30:00	131	9:30:00	209	14:30:00	192	19:30:00	200		
4:45:00	131	9:45:00	209	14:45:00	198	19:45:00	206		
5:00:00	133	10:00:00	209	15:00:00	189	20:00:00	212		

*continued on next page*

Table B.4, continued from previous page

APRIL 29, 1999 Mountain Daylight Time									
0:15:00	2260	5:15:00	3250	10:15:00	2850	15:15:00	3630	20:15:00	6760
0:30:00	3320	5:30:00	3040	10:30:00	2860	15:30:00	3700	20:30:00	6970
0:45:00	3490	5:45:00	2760	10:45:00	2970	15:45:00	3650	20:45:00	7850
1:00:00	4820	6:00:00	2560	11:00:00	2980	16:00:00	3570	21:00:00	8440
1:15:00	5190	6:15:00	2370	11:15:00	2970	16:15:00	3560	21:15:00	9100
1:30:00	5540	6:30:00	2280	11:30:00	3020	16:30:00	3450	21:30:00	10100
1:45:00	5600	6:45:00	2250	11:45:00	3110	16:45:00	3430	21:45:00	10500
2:00:00	5190	7:00:00	2370	12:00:00	3160	17:00:00	3450	22:00:00	10700
2:15:00	5170	7:15:00	2390	12:15:00	3320	17:15:00	3540	22:15:00	10600
2:30:00	4900	7:30:00	2470	12:30:00	3560	17:30:00	3600	22:30:00	10500
2:45:00	4580	7:45:00	2580	12:45:00	3750	17:45:00	3730	22:45:00	10500
3:00:00	4510	8:00:00	2640	13:00:00	3780	18:00:00	3880	23:00:00	10800
3:15:00	4450	8:15:00	2540	13:15:00	3830	18:15:00	4050	23:15:00	10800
3:30:00	4270	8:30:00	2620	13:30:00	3760	18:30:00	4240	23:30:00	10800
3:45:00	4330	8:45:00	2800	13:45:00	3630	18:45:00	4380	23:45:00	10400
4:00:00	4290	9:00:00	2780	14:00:00	3590	19:00:00	4540	24:00:00	10000
4:15:00	4070	9:15:00	2780	14:15:00	3540	19:15:00	4840		
4:30:00	3760	9:30:00	2880	14:30:00	3510	19:30:00	5150		
4:45:00	3590	9:45:00	2830	14:45:00	3480	19:45:00	5540		
5:00:00	3360	10:00:00	2760	15:00:00	3570	20:00:00	5990		
APRIL 30, 1999 Mountain Daylight Time									
0:15:00	9360	5:15:00	7820	10:15:00	13100	15:15:00	13700	20:15:00	8910
0:30:00	8710	5:30:00	8310	10:30:00	13200	15:30:00	13500	20:30:00	8760
0:45:00	8610	5:45:00	8820	10:45:00	13100	15:45:00	13500	20:45:00	8620
1:00:00	8380	6:00:00	8950	11:00:00	13100	16:00:00	13400	21:00:00	8540
1:15:00	7970	6:15:00	9360	11:15:00	13200	16:15:00	13400	21:15:00	8330
1:30:00	7690	6:30:00	9690	11:30:00	13300	16:30:00	13300	21:30:00	8090
1:45:00	7470	6:45:00	10100	11:45:00	13200	16:45:00	13300	21:45:00	7940
2:00:00	7240	7:00:00	10500	12:00:00	13500	17:00:00	13200	22:00:00	7820
2:15:00	6910	7:15:00	10800	12:15:00	13500	17:15:00	12800	22:15:00	7530
2:30:00	6680	7:30:00	11000	12:30:00	13400	17:30:00	12400	22:30:00	7300
2:45:00	6540	7:45:00	11300	12:45:00	13600	17:45:00	11900	22:45:00	7120
3:00:00	6450	8:00:00	11700	13:00:00	13600	18:00:00	11400	23:00:00	6800
3:15:00	6380	8:15:00	11700	13:15:00	13600	18:15:00	11100	23:15:00	6550
3:30:00	6310	8:30:00	12000	13:30:00	13500	18:30:00	10500	23:30:00	6310
3:45:00	6150	8:45:00	12100	13:45:00	13500	18:45:00	10300	23:45:00	6130
4:00:00	5990	9:00:00	12100	14:00:00	13500	19:00:00	10100	24:00:00	5840
4:15:00	6170	9:15:00	12600	14:15:00	13600	19:15:00	9780		
4:30:00	6060	9:30:00	12600	14:30:00	13700	19:30:00	9520		
4:45:00	6430	9:45:00	12900	14:45:00	13700	19:45:00	9330		
5:00:00	7060	10:00:00	13000	15:00:00	13800	20:00:00	9150		

continued on next page

Table B.4, continued from previous page

MAY 01, 1999 Mountain Daylight Time									
0:15:00	5470	5:15:00	3310	10:15:00	2660	15:15:00	6610	20:15:00	3540
0:30:00	5370	5:30:00	3210	10:30:00	2640	15:30:00	6130	20:30:00	3430
0:45:00	5010	5:45:00	3180	10:45:00	2640	15:45:00	5750	20:45:00	3320
1:00:00	4780	6:00:00	3140	11:00:00	2640	16:00:00	5580	21:00:00	3270
1:15:00	4490	6:15:00	3070	11:15:00	2660	16:15:00	5270	21:15:00	3180
1:30:00	4400	6:30:00	3040	11:30:00	2730	16:30:00	5150	21:30:00	3070
1:45:00	4290	6:45:00	2980	11:45:00	2830	16:45:00	5170	21:45:00	3020
2:00:00	4240	7:00:00	2950	12:00:00	3000	17:00:00	5070	22:00:00	2980
2:15:00	4120	7:15:00	2910	12:15:00	3320	17:15:00	5050	22:15:00	2950
2:30:00	4030	7:30:00	2900	12:30:00	3620	17:30:00	4670	22:30:00	2910
2:45:00	3930	7:45:00	2860	12:45:00	3830	17:45:00	4330	22:45:00	2860
3:00:00	3830	8:00:00	2830	13:00:00	3980	18:00:00	4190	23:00:00	2860
3:15:00	3760	8:15:00	2780	13:15:00	4170	18:15:00	4000	23:15:00	2830
3:30:00	3680	8:30:00	2760	13:30:00	4330	18:30:00	4000	23:30:00	2800
3:45:00	3620	8:45:00	2760	13:45:00	4360	18:45:00	4010	23:45:00	2800
4:00:00	3570	9:00:00	2730	14:00:00	4620	19:00:00	3960	24:00:00	2750
4:15:00	3490	9:15:00	2720	14:15:00	4860	19:15:00	3880		
4:30:00	3450	9:30:00	2720	14:30:00	5860	19:30:00	3800		
4:45:00	3380	9:45:00	2700	14:45:00	6460	19:45:00	3680		
5:00:00	3360	10:00:00	2660	15:00:00	6650	20:00:00	3600		
MAY 02, 1999 Mountain Daylight Time									
0:15:00	2700	5:15:00	2560	10:15:00	2110	15:15:00	2060	20:15:00	2020
0:30:00	2720	5:30:00	2540	10:30:00	2110	15:30:00	2060	20:30:00	2020
0:45:00	2660	5:45:00	2500	10:45:00	2110	15:45:00	2060	20:45:00	2010
1:00:00	2680	6:00:00	2470	11:00:00	2110	16:00:00	2030	21:00:00	2010
1:15:00	2660	6:15:00	2430	11:15:00	2090	16:15:00	2030	21:15:00	2010
1:30:00	2660	6:30:00	2410	11:30:00	2110	16:30:00	2020	21:30:00	2010
1:45:00	2660	6:45:00	2370	11:45:00	2110	16:45:00	2010	21:45:00	2000
2:00:00	2660	7:00:00	2350	12:00:00	2110	17:00:00	2010	22:00:00	2000
2:15:00	2660	7:15:00	2280	12:15:00	2110	17:15:00	2010	22:15:00	1990
2:30:00	2700	7:30:00	2250	12:30:00	2090	17:30:00	2000	22:30:00	1990
2:45:00	2750	7:45:00	2230	12:45:00	2090	17:45:00	2020	22:45:00	1990
3:00:00	2760	8:00:00	2250	13:00:00	2080	18:00:00	2020	23:00:00	1970
3:15:00	2800	8:15:00	2190	13:15:00	2080	18:15:00	2030	23:15:00	1970
3:30:00	2750	8:30:00	2190	13:30:00	2080	18:30:00	2020	23:30:00	1970
3:45:00	2780	8:45:00	2160	13:45:00	2080	18:45:00	2000	23:45:00	1970
4:00:00	2750	9:00:00	2140	14:00:00	2060	19:00:00	2020	24:00:00	1970
4:15:00	2720	9:15:00	2130	14:15:00	2080	19:15:00	2020		
4:30:00	2680	9:30:00	2110	14:30:00	2060	19:30:00	2010		
4:45:00	2620	9:45:00	2110	14:45:00	2060	19:45:00	2020		
5:00:00	2600	10:00:00	2110	15:00:00	2080	20:00:00	2010		

## Appendix C

### SWMM RUNOFF SIMULATION FILES

An archive of SWMM RUNOFF input and output files employed for this thesis is available to researchers upon request. The reader is invited to contact the author or Prof.

L.A. Roesner for a copy of this archive. A list of the archive directories is given below.

#### Directory Contents

- Hx** SWMM RUNOFF input (*\*.dat*) and output (*\*.out*) files for simulations that relied on only hourly rainfall gauges in and near the modeled watershed. Partial file listings of only input sub-basin configurations (*\*.prn*) or only discharge results at locations of interest (*\*.txt*) are also included. For a description and tabulation of these results, the reader is referred to Section 4.1 of this thesis.
- HDx** SWMM RUNOFF input (*\*.dat*) and output (*\*.out*) files for simulations that relied on all existing hourly and daily rainfall gauges in and near the modeled watershed. Partial file listings of only input sub-basin configurations (*\*.prn*) or only discharge results at locations of interest (*\*.txt*) are also included. For a description and tabulation of these results, the reader is referred to Section 4.2 of this thesis.
- HDSabc** SWMM RUNOFF input (*\*.dat*) and output (*\*.out*) files for simulations that relied on existing hourly and daily rainfall gauges and derived supplemental gauge records. Partial file listings of only input sub-basin configurations (*\*.prn*) or only discharge results at locations of interest (*\*.txt*) are also included. For a description and tabulation of these results, the reader is referred to Section 4.3 of this thesis.
- HDSd** SWMM RUNOFF input (*\*.dat*) and output (*\*.out*) files for simulations that relied on existing hourly and daily rainfall gauges and supplemental gauge records as determined by iterative simulation methods. Directories containing individual zone-based simulation files are also included here. Partial file listings of only input sub-basin and channel configurations (*\*.prn*) or only discharge results at locations of interest (*\*.txt*) are also included. For a description and tabulation of these results, the reader is referred to Section 4.4 of this thesis.

## Appendix D

### U.S.–METRIC CONVERSION FACTORS

Table D.1: Factors for conversion from U.S. Customary units to Metric units.

#### Length

from: U.S. Customary Units	to: Metric Units	multiply by
inches (in)	centimeters (cm)	2.54
feet (ft)	meters (m)	0.3048
miles (mi)	kilometers (km)	1.609

#### Area

from: U.S. Customary Units	to: Metric Units	multiply by
acres (ac)	hectares (Ha)	0.4047
square miles (mi <sup>2</sup> )	hectares (Ha)	259.0
square miles (mi <sup>2</sup> )	km <sup>2</sup>	2.590

#### Volume

from: U.S. Customary Units	to: Metric Units	multiply by
ft <sup>3</sup> (cf)	liters (l)	28.317
acre-feet (ac-ft)	m <sup>3</sup>	1233.5

#### Rate

from: U.S. Customary Units	to: Metric Units	multiply by
ft <sup>3</sup> s <sup>-1</sup> (cfs)	liters/sec (l/s)	28.317
ft <sup>3</sup> s <sup>-1</sup> (cfs)	m <sup>3</sup> s <sup>-1</sup> (cms)	0.028317